STUDY OF CRUST AND MANTLE DIFFERENTIATION PROCESSES FROM VARIATIONS IN Nd, Sr, and Pb ISOTOPES

Thesis by

Stein Bjørnar Jacobsen

In Partial Fulfillment of the Requirements

for the Degree of

Doctor of Philosophy

California Institute of Technology

Pasadena, California

1980

(Submitted March 26, 1980)

ACKNOWLEDGMENTS

I wish to thank Professor G. J. Wasserburg for his continued interest and enthusiasm in, and edifying criticism of, this work. Special thanks go to Dimitri Papanastassiou for sharing much of his experience in high precision mass spectrometry with me.

I am grateful to Knut S. Heier of the Geological Survey of Norway for encouraging me to go to graduate school in the U.S.

During the tenure of this study, I have benefited from numerous discussions with James Chen, Bob Kelly, and Malcolm McCulloch.

I thank Evelyn Brown for her assistance and friendliness and Joanne Clark for indispensible help in preparing this manuscript.

Many people have contributed samples or valuable guidance with the field work, and I would especially like to thank H. Brueckner, N. Christensen, W. L. Griffin, K. S. Heier, B. T. Larsen, T. V. Segalstad, B. Sundvoll, E. Tveten, and H. Williams.

The hospitality and friendliness of my colleagues has been greatly appreciated. The first part of this work was done while I held a Rotary Foundation Fellowship. I am grateful to Lektor O. Halsen of the Drammen Rotary Club in Norway for his efforts in getting me the Rotary Fellowship and his continued interest in my work. This work has been supported by NSF Grant EAR 76-22494 and NASA Grant NGL 05-002-188.

I would also like to thank the Examining Committee, consisting of Professors L. T. Silver (Chairman), T. J. Ahrens, D. Anderson, K. Sieh, E. Stolper, H. P. Taylor, G. J. Wasserburg, and A. B. Thompson (guest), for good and thorough discussions during my thesis defense and for showing enthusiastic interest in my work.

ABSTRACT

This study discusses two simple transport models for the evolution of the mantle and the crust. In Model I, the continents grow by extraction of melts over the history of the earth from undepleted mantle; the residue forms a depleted mantle, which today is the source of mid-ocean ridge basalts. In Model II, new additions to the continents are derived from a mantle reservoir which becomes increasingly depleted through time by repeated extraction of melts. In developing these models, I solved the transport equations for stable, radioactive, and daughter isotopes for arbitrary crustal growth curves. For both models the isotopic composition and concentrations of trace elements reduce to simple mathematical expressions which readily permit calculations of basic evolutionary parameters from new and published data.

New measurements of $^{143}Nd/^{144}Nd$ in chondrites yield a range in values of 3.4 ε-units (0.511767 to 0.511845), which correlates with the variation of 2.6% in $^{147}Sm/^{144}Nd$ (0.1920 to 0.1969). From these data a new set of reference values for CHUR ("chondritic uniform reservoir") have been selected. The evolution of $^{143}Nd/^{144}Nd$ in CHUR can be described by a self-consistent set of present-day values of $(^{143}Nd/^{144}Nd)^{o}_{CHUR}$ = 0.511836 and $(^{147}Sm/^{144}Nd)^{o}_{CHUR}$ = 0.1967. Some terrestrial samples of Archean age show clear deviations from the new CHUR curve. If the CHUR curve is representative of undifferentiated mantle then it demonstrates that some Archean rocks were formed from depleted sources. This may indicate that the depleted source of present-day mid-ocean ridge basalts

(MORB) originated very early in the earth's history.

Two Sm-Nd internal isochrons for pyroxene-gabbros of the Bay of Islands Ophiolite Complex give well-defined ages of 508±6 m.y. and 501±13 m.y. with initial $^{143}Nd/^{144}Nd$ of $\varepsilon_{Nd} = +7.9\mp0.1$ and $\varepsilon_{Nd} = +7.7\mp0.2$, respectively. Total rock samples from pillow basalts, sheeted dikes, trondhjemites, hornblende gabbros, pyroxene gabbros, and an orthopyroxenite layer from the harzburgite give initial ε_{Nd} in the range from +6.7 to +8.3 with an average value of +7.8. However, the initial $^{87}Sr/^{86}Sr$ within the different phases of the complex is found to be highly variable (~ 52 ε-units) and shows the effect of seawater alteration. The magnitude of the initial ε_{Nd} values (+7.8) are somewhat smaller than for typical present-day mid-ocean ridge basalts (+10). This is most likely due to differential evolution over the past 0.5 AE of the oceanic mantle relative to the bulk earth.

Sm-Nd and Rb-Sr data for the Oslo Rift demonstrate that this province which is strongly enriched in large ion lithophile (LIL) elements is derived from depleted to undepleted mantle materials. A source with a long history of light rare earth (LREE) enrichment can clearly be ruled out.

Sm-Nd data for the Archean granulite and amphibolite facies migmatites of Langøy and Hinnøy in Vesterålen indicate that their protoliths formed ~ 2.6 AE ago. Rb and U loss during a granulite facies metamorphism at ~ 1.8 AE caused serious disturbance of total rock U-Pb and Rb-Sr systems. Therefore these systems do not provide any precise age information for the granulite facies migmatites. For the amphibolite facies migmatites of Vesterålen both Sm-Nd, Rb-Sr, and Pb-Pb total

rock systems give model ages of ~ 2.6 AE.

Sm-Nd and Rb-Sr isotopic data for continental crust, depleted and undepleted mantle, have been used to evaluate both models and yield young mean ages for the mass of the continental crust of 1.8 AE and 1.5 AE for Model I and Model II, respectively. Both models also suggest that the rate of growth of the continents for the last 0.5 AE is much less than the average growth rate. The young mean age of the continents implies either rapid refluxing of crustal materials to the mantle in the period from 4.5 AE to 3.6 AE or that very little early crust ever formed. Mass balance calculations for both models show that the continents were only formed from ~ 30% of the total mantle leaving 70% of the mantle as undepleted. The major difference in the two models lies in the difference in the compositions of newly derived crust. For Model I the trace element concentrations in new additions to the crust is constant and the isotopic values are those of the undepleted mantle reservoir in agreement with recent Nd isotopic studies. Model II implies that new additions to the continents have the isotopic characteristics of the depleted mantle and that the concentrations of Rb, U, Ba and other highly incompatible trace elements in newly added material have changed by a factor of ~ 10 through time. There is no evidence, however, for such a large change in the concentration of these elements with time.

TABLE OF CONTENTS

LIST OF SYMBOLS

i = species; $i = s$ = a stable isotope which is not affected by radioactive decay
$i = r$ = a radioactive isotope
$i = d$ = a stable daughter isotope which is the decay product of a radioactive isotope r

j = reservoir; $j = 1$ = undifferentiated mantle
$j = 2$ = depleted mantle
$j = 3$ = continental crust

τ = time; $\tau = 0$ at the time of initial chemical differentiation of the earth
$\tau = T_o$ today and T_o is the age of the earth

T = age; $T = T_o - \tau$

M_j = mass of reservoir j

N_{ij} = number of species i in reservoir j

C_{ij} = concentration of species i in reservoir j

J_{ijn} = flux of species i from reservoir j to reservoir n

F = degree of melting

D_i = effective partition coefficient for species i between the residue and the partial melt

$$\varepsilon_{d,j} \equiv \{[(N_{d,j}/N_{s,j})/(N_{d,1}/N_{s,1})] - 1\}\ 10^4$$

$$f_j^{r/s} \equiv [(N_{r,j}/N_{s,j})/(N_{r,1}/N_{s,1})] - 1$$

$$Q_d^*(\tau) \equiv 10^4 \lambda\ N_{r,1}(\tau)/N_{d,1}(\tau)$$

$$\varepsilon^*_{d,j}(\tau) = \varepsilon^*_{d,j}(T_o - T) \equiv \varepsilon_{d,j}(T)$$

$$Q_d^*(\tau) = Q_d^*(T_o - T) \equiv Q_d(T)$$

$\bar{t}_{i,j}$ = mean age of species i in reservoir j

$\bar{t}_{M,j}$ = mean age of the mass of reservoir j

$$\bar{t}_{r/s} \equiv \frac{1}{f_2^{r/s}(\tau)} \int_o^\tau f_2^{r/s}(\xi)\,d\xi$$

$d_i \equiv 1/[F + D_i\ (1-F)]$

$K_i \equiv [(d_i M_3(T_o)/(T_o M_2(0))]$

$\alpha_{r/s} \equiv (d_r - d_s) M_3(\tau)/M_2(0)$

$\alpha \equiv {}^{206}Pb/{}^{204}Pb$

$\beta \equiv {}^{208}Pb/{}^{204}Pb$

$\alpha \equiv {}^{208}Pb/{}^{204}Pb$

$\mu \equiv {}^{238}U/{}^{204}Pb$

INTRODUCTION

Inferences may be drawn about crust and mantle evolution from the observed regularities in initial isotopic composition of Nd in crustal rocks through geologic time and the modern values of Nd, Sr, and Pb isotopes in oceanic flood basalts. Over the past few years a substantial amount of new data have become available on the Sm-Nd and Rb-Sr isotope characteristics of mantle and crustal reservoirs. These data have been used to determine the times of additions of new continental crustal materials [McCulloch and Wasserburg, 1978c] and in discussions of the evolution of the mantle sources of modern continental and oceanic basalts. These studies have demonstrated that the mid-ocean ridge basalts (MORB) have been derived from a depleted mantle source [DePaolo and Wasserburg, 1976a,b; Richard et al., 1976] and that young continental flood basalts and new additions to the continents throughout most of the earth's history appear mainly to have been derived from undepleted mantle reservoirs [DePaolo and Wasserburg, 1976b, 1979b]. The continents are ancient heterogeneous bodies preserving rocks of up to ~ 3.8 AE while the oceanic crust is young. The young age and uniform isotopic composition of oceanic crust suggest that its isotopic character is representative of large volumes of the oceanic mantle which are convectively mixed on a short time scale.

New Nd and Sr isotope data on chondrites, the Bay of Islands Ophiolite, the Oslo Rift, granulite and amphibolite facies migmatites of Lofoten-Vesterålen and the garnet peridotites of southwest Norway will be presented. The data on the Bay of Islands ophiolite will permit an

estimate to be made of the isotopic composition of the oceanic mantle in the early paleozoic. The chondrite data are used to obtain reference values for the chondritic evolution of $^{143}Nd/^{144}Nd$, which were previously only inferred from achondrite data [Lugmair et al., 1975a,b]. The simplest model for explaining the observed isotopic heterogeneities in the mantle would be to assume that they formed in a single event [Brooks et al., 1976a,b; Brooks and Hart, 1978]. However, as discussed by O'Nions et al. [1978], Tatsumoto [1978], and in Appendix 2, available Pb, Nd, and Sr isotopic data on young basalts do not appear to fit such a single stage model and it is not compatible with our knowledge that the continental crust has evolved in many stages over geologic time [see for example Moorbath, 1978; O'Nions and Pankhurst, 1978; McCulloch and Wasserburg, 1978c]. Because of these considerations it is necessary to analyze the data in terms of continuous or multi-episodic mantle-crust transport models. As the depleted oceanic mantle most likely represents the residue left behind in the mantle after continental crust-forming events, it should reflect the time average characteristics of the evolution of the continental crust over the history of the earth.

An analysis of two simple transport models for trace elements is presented utilizing the isotopic abundance patterns that can be observed. The models presented here assume that the transport is solely from mantle to continental crust and for simplicity do not treat the flux back to the mantle of continental crustal material, but the treatment may be simply extended to include this. In the first model (Model I) the mechanism for crustal growth is by deriving melts over the age of the earth by equilibrium partial melting from undepleted mantle. In the

second model (Model II) melts that form new continental crust are being derived from a mantle reservoir that is continuously depleted through time. Although the models involve rather complicated algebra, they lead to exceedingly simple expressions for the isotopic ratios and trace element abundances in terms of the mass of continental crust and depleted mantle which are evolved. The models presented here apply to arbitrary crustal growth rates in contrast to previous transport models [Patterson, 1964; Patterson and Tatsumoto, 1964; Wasserburg, 1966; Armstrong, 1968; Hart and Brooks, 1970; Russell, 1972; Russell and Birnie, 1974; DePaolo, 1978; O'Nions et al., 1979]. This approach is a generalization of the treatment of nucleosynthetic time scales given by Schramm and Wasserburg [1970]. The results may be used directly to discuss earth models using available isotopic data and concentration data for mantle and crustal rocks. This treatment appears to give a deep and direct insight in the problems of mantle evolution.

CHAPTER I. BASIC PRINCIPLES

It is well established that the solid earth consists of three major geochemical reservoirs: the crust, the mantle, and the core. Differentiation from an initially homogeneous earth requires the segregation into reservoirs with complementary chemistry. If a homogeneous reservoir is differentiated into two reservoirs with different chemical compositions, then these two reservoirs may have different parent/ daughter ratios for the radioactive species of interest. Consequently these two reservoirs may subsequently develop different ratios of the radiogenic daughter isotopes relative to the stable isotopes of the same chemical elements. Thus radiogenic isotope data on samples of rocks derived from the earth's interior contain information about the degree to which the earth's interior has differentiated into distinct reservoirs. The isotopic data also put constraints on the element fractionation patterns in the interior of the earth and thus also the processes involved. An earth structure model based on Nd and Sr isotopic data has recently been presented by Wasserburg and DePaolo [1979]. The resulting structure that was inferred consists of a lower mantle that is still essentially undifferentiated, overlain by an upper mantle that is the residue of the original source from which the continents were derived. Radiogenic isotopes also contain information about the evolution through time of the reservoirs if the transport of material between reservoirs can be modeled. Transport of chemical species in the upper part of the earth crust, hydrosphere, and atmosphere have in general been more thoroughly studied than the processes within the lower crust and mantle

due to the fact that the reservoirs and their inputs and outputs can be more directly studied. Barth [1952] first used the concept of residence time in geochemistry in the analysis of box models for the oceans. Since that time increasingly complex box models have been applied with much success to describe exogenic processes. The use of box models and characteristic times to interpret endogenic processes have received much less attention. As the size and compositions of reservoirs within the solid earth and the processes relating them are being better understood, the data for the radiogenic isotopes of Nd, Sr, and Pb will be of increasing importance in determining the time evolution of reservoirs in the interior of the earth and in evaluating earth differentiation models, as for example the one of Anderson [1980].

1.1. TRANSPORT EQUATIONS

The differentiation of the earth into a number of different geochemical reservoirs may be described by a set of differential equations. Assume that the solid earth is made up of K different reservoirs. Consider the following species: (1) stable isotopes s which are not affected by radioactive decay, (2) radioactive isotopes r with decay constants λ_r depending on the species r, and (3) daughter isotopes d which are the decay product of some radioactive species r. Then for each isotope i = s,r,d in reservoir j we have the following transport equations:

$$\frac{dN_{ij}}{d\tau} = \sum_{n=1}^{K} J_{inj} - \sum_{n=1}^{K} J_{ijn} - \lambda_i N_{rj} \qquad \begin{pmatrix} \lambda_i = 0, & i = s \\ \lambda_i = \lambda_r, & i = r \\ \lambda_i = -\lambda_r, & i = d \end{pmatrix} \qquad (1.1)$$

$$(J_{inn} = 0)$$

where $N_{ij}(\tau)$ is the number of species i in j at time τ, and $J_{ijn}(\tau)$

is the flux of species i from reservoir j to reservoir n at time τ. Here $\sum_{n=1}^{K} J_{ijn}$ is the total flux of i into j and $\sum_{n=1}^{K} J_{ijn}$ is the total flux of i out of j. A complete description must also include differential equations for the total mass of each reservoir and equations for conservation of species and mass.

1.2. CHARACTERISTIC TIMES

It is useful to describe the rates of transport processes between various reservoirs in terms of the characteristic times of these processes. The content of a species i in a reservoir may have a well-defined age structure. Let $G_{ij}(\tau,\xi)$ be the amount of species i added per unit time to reservoir j at time ξ and remaining at time τ. Then the mean age ($\bar{t}_{ij}$) of species i in j is defined as the average age of species i subsequent to its addition to reservoir j of material still present in j. The total amount of species i in j at time τ is

$$N_{ij}(\tau) = \int_0^\tau G_{ij}(\tau,\xi)d\xi \tag{1.2}$$

The mean age is

$$\bar{t}_{ij} = \frac{1}{N_{ij}(\tau)} \int_0^\tau (\tau-\xi)\, G_{ij}\,(\tau,\xi)d\xi \tag{1.3}$$

The mean residence time of species i in j is defined as the mean age of the material leaving the reservoir. The mean residence time ($\bar{\tau}_{ij}$) can be calculated as the average of $-dG_{ij}(\tau,\xi)/d\tau$ since the only contribution to this derivative is the removal rate from the reservoir. The total flux of species i out of reservoir j at τ is calculated as

$$F_{ij}(\tau) = \int_0^{\tau} \left(- \frac{dG_{ij}(\tau,\xi)}{d\tau} \right) d\xi \qquad (1.4)$$

The mean residence time is

$$\bar{\tau}_{ij} = \frac{1}{F_{ij}(\tau)} \int_0^{\tau} (\tau-\xi) \left(- \frac{dG_{ij}(\tau,\xi)}{d\tau} \right) d\xi \qquad (1.5)$$

In general the mean age and the mean residence times are different.

1.3. PROCESSES

To be able to use equations such as (1.1) we need information about the material transfer processes from reservoir j to n. If for instance reservoir 2 is partially melted and the melt is transferred to reservoir 3 and the residue left in reservoir 2 then

$$J_{i23}(\tau) = d_i \frac{N_{i2}(\tau)}{M_2(\tau)} \left(\frac{dM_3}{d\tau} \right) \qquad (1.6)$$

where d_i is the enrichment factor of i in the melt relative to the source and M_j is the mass of reservoir j. If the mathematical form of all J_{inj} is known then these may be substituted into (1.1) and (1.1) may be integrated. In general for systems with more than 2 or 3 reservoirs the solutions get exceedingly complex. The values of the chemical enrichment factor d_i may be estimated from partial melting equations such as those of Shaw [1970] if the relevant mineral melt distribution coefficients are known. In chapter 2 these principles were used for two simple mantle-crust transport models with unidirectional transport.

1.4. DATA REPRESENTATION

The bulk earth reservoir used as a reference for the Sm-Nd system (CHUR) has a chondritic Sm/Nd ratio with $(^{147}Sm/^{144}Nd)^{o}_{CHUR} = 0.1967$ and $^{143}Nd/^{144}Nd$ ratio today of $I^{Nd}_{CHUR}(0) = 0.511836$ (see chapter 3.1). $^{143}Nd/^{144}Nd$ in CHUR at any time T in the past is given by

$$I^{Nd}_{CHUR}(T) = I^{Nd}_{CHUR}(0) - \left(\frac{^{147}Sm}{^{144}Nd}\right)^{o}_{CHUR} (e^{\lambda_{Sm}T} - 1) \qquad (1.7)$$

where $\lambda_{Sm} = 0.00654\ AE^{-1}$. The bulk earth reference reservoir for Rb-Sr (UR) is taken to have $(^{87}Rb/^{86}Sr)^{o}_{UR} = 0.0827$ and the value of $^{87}Sr/^{86}Sr$ in UR at any time T in the past is given by

$$I^{Sr}_{UR}(T) = I^{Sr}_{UR}(0) - \left(\frac{^{87}Rb}{^{86}Sr}\right)^{o}_{UR} (e^{\lambda_{Rb}T} - 1) \qquad (1.8)$$

where $I^{Sr}_{UR}(0) = 0.7045$ is the value in UR today [DePaolo and Wasserburg, 1976b] and $\lambda_{Rb} = 0.0142\ AE^{-1}$.

Following DePaolo and Wasserburg [1976a] the $^{143}Nd/^{144}Nd$ ratio in a reservoir j at time T is expressed as the fractional deviation in parts in 10^4 from that in CHUR at time T and denoted by $\varepsilon_{Nd,j}(\tau)$. Let $I^{Nd}_{j}(T)$ be the $^{143}Nd/^{144}Nd$ ratio in a reservoir j at time T, then we have

$$\varepsilon_{Nd,j}(\tau) = 10^4 \left[\frac{I^{Nd}_{j}(T)}{I^{Nd}_{CHUR}(T)} - 1 \right] \qquad (1.9)$$

Initial $^{143}Nd/^{144}Nd$ ratios for a rock may be expressed in ε-units relative to the CHUR curve using equation (1.9). Then $I^{Nd}_{j}(T)$ is the initial value determined by an internal isochron as calculated from the

present-day values of $^{143}Nd/^{144}Nd$ and $^{147}Sm/^{144}Nd$ of the rock and an independently determined age. The measured present-day values of $^{143}Nd/^{144}Nd$ in rock samples relative to $I^{Nd}_{CHUR}(0)$ are also often given in ε-units and are denoted $\varepsilon_{Nd}(0)$. The $^{147}Sm/^{144}Nd$ ratio in a reservoir j is expressed as the enrichment factor relative to CHUR

$$f_j^{Sm/Nd} = \frac{(^{147}Sm/^{144}Nd)_j}{(^{147}Sm/^{144}Nd)^o_{CHUR}} - 1 \qquad (1.10)$$

For Rb-Sr we will use similarly defined ε_{Sr} and $f^{Rb/Sr}$ values. This notation may also be extended to the U-Th-Pb system and the appropriate bulk earth reference values are given in chapter 4.

Model ages T^{Nd}_{CHUR} and T^{Sr}_{UR} can be calculated relative to these reference reservoirs [McCulloch and Wasserburg, 1978c] and date the time in the past at which $^{143}Nd/^{144}Nd$ and $^{87}Sr/^{86}Sr$ ratios in the samples were identical to those in the reference reservoirs CHUR and UR, respectively. The model ages are given by

$$T^{Nd}_{CHUR} = \frac{1}{\lambda_{Sm}} \ln \left[1 + \frac{I^{Nd}_{CHUR}(0) - (^{143}Nd/^{144}Nd)_M}{(^{147}Sm/^{144}Nd)^o_{CHUR} - (^{147}Sm/^{144}Nd)_M} \right] \qquad (1.11)$$

$$T^{Sr}_{UR} = \frac{1}{\lambda_{Rb}} \ln \left[1 + \frac{I^{Sr}_{UR}(0) - (^{87}Sr/^{86}Sr)_M}{(^{87}Rb/^{86}Sr)^o_{UR} - (^{87}Rb/^{86}Sr)_M} \right] \qquad (1.12)$$

where the subscript M denotes the ratio measured in the rock today.

CHAPTER 2. MANTLE-CRUST TRANSPORT MODELS

2.1. MODEL I

Consider first a model of crustal growth from an undifferentiated mantle reservoir (reservoir 1) with a given segment of the mantle being differentiated to form two reservoirs: a depleted mantle (2) and a continental crust (3). The model is shown schematically in Fig. 2.1. Define M_j, $N_{i,j}$, and $C_{i,j}$ to be the total mass of reservoir j, number of atoms of species i in reservoir j, and the concentration of species i in reservoir j respectively. Differential masses added to or subtracted from the total reservoir j are denoted by δM_j. The number of species i and the concentration of i in the differential mass δM_j are denoted by $\delta N_{i,j}$ and $c_{i,j}$ respectively. Let us assume that a mass δM_1 is removed from reservoir 1 and a partially melted fraction F is extracted from this differential mass to form new crust with added mass δM_3 and a new residual mass δM_2 is added to the depleted mantle. This gives $\delta M_3/\delta M_1 = F$ and $\delta M_2/\delta M_1 = 1 - F$. It is imagined that mantle reservoir is diminished in amount by mass δM_1. The mantle reservoir is diminished in amount by mass δM_1. The mass δM_2 is added to the depleted mantle which is assumed to be otherwise isolated from the remaining undifferentiated reservoir (1).

The number of atoms of species i in each differential mass j in this unit process are $\delta N_{i,j}$ which gives

$$\delta N_{i,1} = \delta N_{i,2} + \delta N_{i,3} \tag{2.1}$$

Figure 2.1. Cartoon showing the processes in Model I and Model II. Model I is a three layer model consisting of undepleted mantle (1), depleted mantle (2), and continental crust (1) as indicated under the final state. In Model I a given segment (the differentiating layer δM_1) of undepleted mantle (1) is being differentiated by equilibrium partial melting and added to two reservoirs: a depleted mantle (2) and a continental crust (3). It is assumed that a differential mass δM_1 is removed from reservoir 1 and a partially melted fraction F is extracted from this differential mass to form new crust with added mass δM_3 and that a new residual mass δM_2 is added to the depleted mantle. In this differentiation process the masses of reservoirs 1, 2, and 3 are conserved. The masses of the depleted mantle and the crust increase with time and the undepleted mantle decreases with time. The upper boundary of the undepleted mantle is thus lowered and the volumes of both depleted mantle and crust increased. These stages are shown in the second and third columns. In Model II the crust grows from an initially undifferentiated mantle reservoir (2) which is depleted at all times subsequent to the initial chemical differentiation as a result of continuing crustal growth. This reservoir may make up all or part of the mantle. Layers 2 and 3 are thus the only active regions in this model. The remaining undifferentiated mantle is passive and is still indicated as layer 1. In this model it is assumed that a differential mass δM^* of reservoir 2 is being differentiated into a melt δM_3 which is

added to the continental crust and a residue δM_R^* . The degree of melting F is taken as finite. The residue after removal of a melt fraction from reservoir 2 is assumed to be homogenized instantaneously with the remaining part of the depleted mantle. The total mass of reservoirs 2 and 3 is conserved; the continental crust increases in mass with time and the depleted mantle decreases in mass with time. In both models the depleted mantle is taken to include the basaltic part of the oceanic crust since it is derived from the depleted mantle and is subducted back to the depleted mantle at a short timescale (< 0.2 AE).

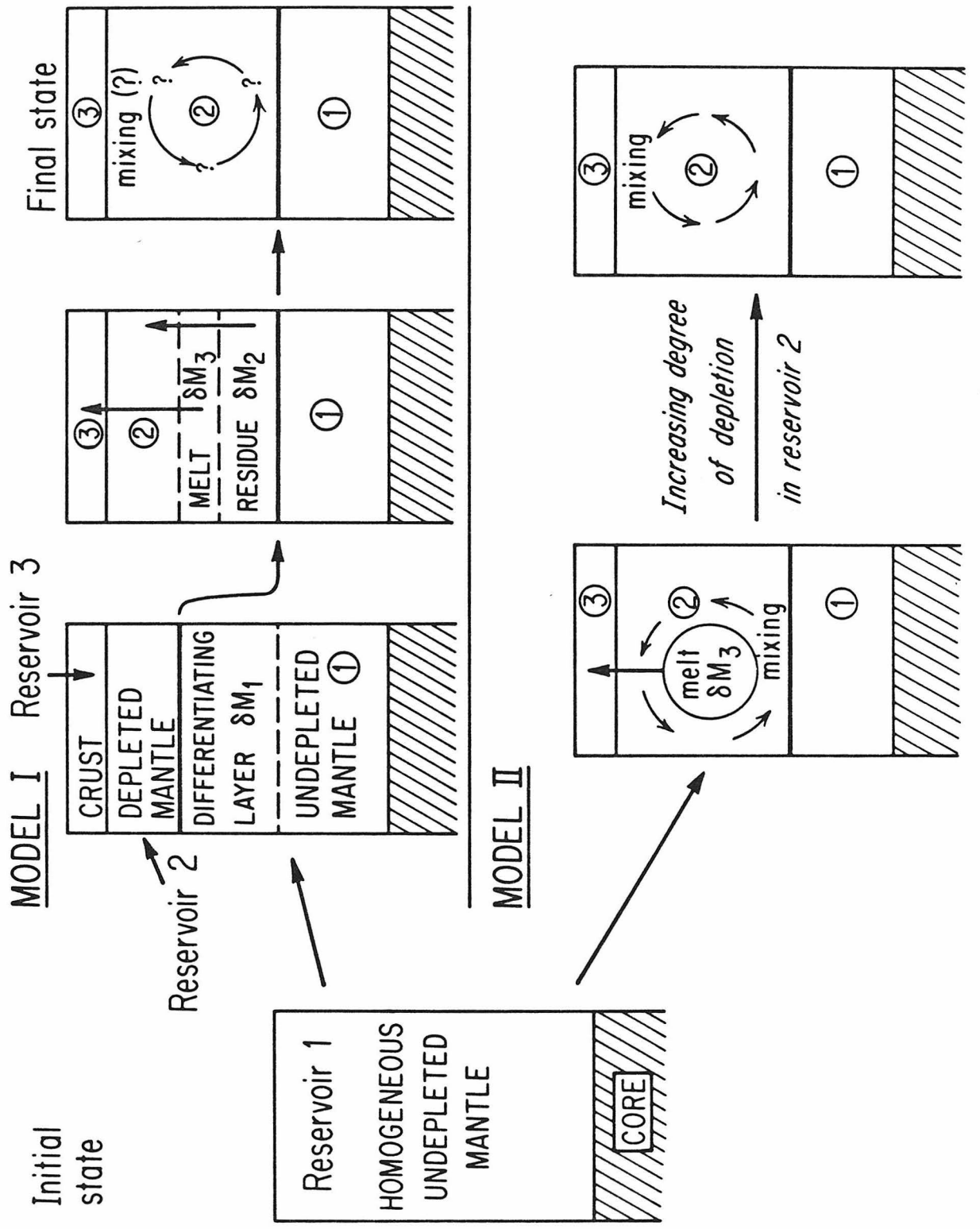
Initial state
Reservoir 1
HOMOGENEOUS UNDEPLETED MANTLE
CORE
Reservoir 2
MODEL I
Reservoir 3
CRUST
DEPLETED MANTLE
DIFFERENTIATING LAYER δM1
UNDEPLETED MANTLE ①
③
②
MELT δM3
RESIDUE δM2
①
Final state
③
mixing (?)
? ? ? ?
②
①
MODEL II
③
melt δM3
②
mixing
①
Increasing degree of depletion in reservoir 2
③
mixing
②
①

Fig. 2.1

The number of species i in the differential mass δM_j may be written $\delta N_{i,j} = c_{i,j}\delta M_j$. Conservation of species and mass gives

$$c_{i,1} = c_{i,2}(1-F) + c_{i,3}F \tag{2.2}$$

Trace elements are fractionated between melts and residue with an effective partition coefficient. The effective partition coefficient D_i for element i between the residue (δM_2) and the partial melt (δM_3) is defined by $D_i \equiv c_{i,2}/c_{i,3}$. The concentration in δM_3 is

$$c_{i,3} = \frac{c_{i,1}}{F + D_i(1-F)} = \frac{c_{i,2}}{D_i} \tag{2.3}$$

The number of species i in the differential masses j may thus be expressed in terms of their masses δM_j and the concentration in reservoir 1 since $c_{i,1} = C_{i,1}$.

$$\delta N_{i,j} = \frac{D_{i,j}C_{i,1}}{F + D_i(1-F)}\,\delta M_j \quad \begin{cases} D_{i,j}=D_i\,, j = 2 \\ D_{i,j}=1\,, j = 3 \end{cases} \tag{2.4}$$

Consider the following species: (A) a stable index isotope s of an element which is not affected by radioactive decay; (B) a radioactive isotope r with decay constant λ; and (C) a daughter isotope d which is the decay product of r and of the same chemical element as s.

The transport equations for the total reservoir j containing the number $N_{i,j}$ of each isotope i = s,r,d are:

$$\frac{dN_{i,j}(\tau)}{d\tau} = \frac{\delta N_{i,j}}{\delta \tau} - \lambda_i N_{r,j}(\tau) \quad \begin{cases} \lambda_i = 0\,, i = s \\ \lambda_i = \lambda\,, i = r \\ \lambda_i = -\lambda, i = d \end{cases} \tag{2.5}$$

where $dN_{i,j}/d\tau$ is the time derivative and $\delta N_{i,j}/\delta\tau$ is the flux of species

i into reservoir j. In this treatment $\delta\tau$ is the time over which mass δM_1 is differentiated at time τ. For simplicity we have chosen to ignore transport between 2 and 3. Using the expressions for $\delta N_{i,j}$ in terms of $C_{i,1}$ and δM_j and calling $\delta M_j/\delta\tau \equiv M_j'(\tau)$, which is the rate of mass growth of reservoir j, the basic transport equation for Model I is obtained,

$$\frac{dN_{i,j}}{d\tau} = \frac{D_{i,j}C_{i,1}(\tau)}{F + D_i(1-F)} M_j'(\tau) - \lambda_i N_{r,j}(\tau) \tag{2.6}$$

where $D_{i,j}$ and λ_i are defined as in (2.4) and (2.5). The first term on the right hand side of (2.6) is the transport-term and the second term is due to either radioactive decay or production. The general solution of equation (2.6) for a stable index isotope is:

$$N_{s,j}(\tau) = \frac{D_{s,j}}{F + D_s(1-F)} \int_0^\tau C_{s,1}(\xi)\, M_j'(\xi)d\xi \tag{2.7}$$

The equation was integrated with the assumption that the time $\tau = 0$ at the time of initial chemical differentiation of the earth and $N_{s,j}(0) = 0$. The earth is taken to be initially homogeneous.

The undifferentiated reservoir is characterized by a closed system behavior for intensive quantities so that the concentration for species s, r, and d are:

$$C_{s,1}(\tau) = C_{s,1}(0) \tag{2.8}$$

$$C_{r,1}(\tau) = C_{r,1}(0)\, e^{-\lambda\tau} \tag{2.9}$$

$$C_{d,1}(\tau) = C_{d,1}(0) + C_{r,1}(0)\, [1 - e^{-\lambda\tau}] \tag{2.10}$$

The relationship between the masses of reservoirs 2 and 3 is given by $M_3(\tau) = [F/(1-F)]M_2(\tau)$. Substituting (2.8) into (2.7) gives the following general solutions for stable isotopes in reservoirs 2 and 3:

$$N_{s,2}(\tau) = \frac{D_s C_{s,1}(0)}{F + D_s(1-F)} M_2(\tau) \tag{2.11}$$

$$N_{s,3}(\tau) = \frac{C_{s,1}(0)}{F + D_s(1-F)} M_3(\tau) \tag{2.12}$$

The above equation for a stable isotope in the crust may also be written as $C_{s,3}(\tau) = C_{s,1}(0)/[F + D_s(1-F)]$ which is equivalent to the equation for equilibrium partial melting derived by Consolmagno and Drake [1976] which showed that previous equations given by Shaw [1970], Schilling [1971], and O'Nions and Clarke [1972] all reduce to this general form.

The solutions of (2.6) for radioactive isotopes and daughter isotopes are

$$N_{r,2}(\tau) = \frac{D_r e^{-\lambda\tau} C_{r,1}(0)}{F + D_r(1-F)} M_2(\tau) \tag{2.13}$$

$$N_{r,3}(\tau) = \frac{e^{-\lambda\tau} C_{r,1}(0)}{F + D_r(1-F)} M_3(\tau) \tag{2.14}$$

$$N_{d,2}(\tau) = \frac{D_d\left\{C_{d,1}(\tau)M_2(\tau) + \lambda C_{r,1}(0)\left[\frac{F+D_d(1-F)}{F+D_r(1-F)}\left(\frac{D_r}{D_d}\right)-1\right]\int_o^\tau M_2(\xi)\exp[-\lambda\xi]d\xi\right\}}{F + D_d(1-F)} \tag{2.15}$$

$$N_{d,3}(\tau) = \frac{C_{d,1}(\tau)M_3(\tau) + \lambda C_{r,1}(0)\left[\frac{F+D_d(1-F)}{F+D_r(1-F)}-1\right]\int_o^\tau M_3(\xi)\exp[-\lambda\xi]d\xi}{F + D_d(1-F)} \tag{2.16}$$

where $D_s = D_d$ since d and s are isotopes of the same element and $C_{d,1}(\tau)$ is given by equation (2.10).

The enrichment factor of the ratio of a radioactive isotope to a stable isotope in a reservoir j relative to that in reservoir 1 is called $f_j^{r/s}$. This enrichment factor is the same both for new additions to j and for the total reservoir j and it is defined by

$$f_j^{r/s} \equiv \frac{N_{r,j}(\tau)/N_{s,j}(\tau)}{N_{r,1}(\tau)/N_{s,1}(\tau)} - 1 \tag{2.17}$$

For this model the enrichment factor is independent of time and is given by

$$f_2^{r/s} + 1 = \left(\frac{D_r}{D_s}\right) \frac{F + D_s(1-F)}{F + D_r(1-F)} = \left(\frac{D_r}{D_s}\right) (f_3^{r/s} + 1) \tag{2.18}$$

As $D_s = D_d$, the ratio of a daughter isotope to a stable reference isotope of the same element (with no parent) in each reservoir is given by:

$$\frac{N_{d,j}(\tau)}{N_{s,j}(\tau)} = \frac{N_{d,1}(\tau)}{N_{s,1}(\tau)} + \frac{N_{r,1}(\tau)}{N_{s,1}(\tau)} \frac{f_j^{r/s}\lambda}{M_j(\tau)} \int_o^{\tau} M_j(\xi)\exp[\lambda(\tau-\xi)]d\xi \tag{2.19}$$

In terms of deviations $\varepsilon^*_{d,j}(\tau)$ in parts in 10^4 from the ratios in the undifferentiated reference reservoir we obtain the final equations to be used in calculations for this model for arbitrary rates of growth of the crust and mantle

$$\varepsilon^*_{d,j}(\tau) = \frac{Q^*_d(\tau)\ f_j^{r/s}}{M_j(\tau)} \int_o^{\tau} M_j(\xi)\ \exp[\lambda(\tau-\xi)]d\xi \tag{2.20a}$$

and

$$\frac{\varepsilon^*_{d,3}(\tau)}{\varepsilon^*_{d,2}(\tau)} = \frac{f_3^{r/s}}{f_2^{r/s}} \tag{2.20b}$$

where

$$Q_d^*(\tau) \equiv \frac{10^4\lambda\left(\frac{N_{r,1}(\tau)}{N_{s,1}(\tau)}\right)}{\left(\frac{N_{d,1}(\tau)}{N_{s,1}(\tau)}\right)} \qquad (2.20c)$$

The time parameter τ is the time running forward from the initial state [cf. equation (2.7)] and the time measured backward from the present will as usual be called T [see Fig. 2.2]. Here $\varepsilon^*_{d,j}(\tau) = \varepsilon^*_{d,j}(T_o - T) \equiv \varepsilon_{d,j}(T)$ where $T = T_o - \tau$ and T_o is the age of the earth today and $\varepsilon_{d,j}(T)$ correspond to ε_{Nd} and ε_{Sr} as defined by DePaolo and Wasserburg [1976a,1977]. The asterisks denote the functional form of the deviations "ε," relative to a time variable with an origin at the time of formation of the earth. Similarly define $Q^*_d(\tau) = Q^*_d(T_o - T) \equiv Q_d(T)$ and note that $Q_d(0)$ is equal to the constants Q_{Nd} and Q_{Sr} used by DePaolo and Wasserburg [1976a, 1979a] for the Sm/Nd and Rb/Sr systems respectively. If $\lambda\tau \ll 1$ then we have a good approximation that $Q^*_d(\tau) = Q_d(0)$. Note that the values of $\varepsilon^*_{d,j}$ are the average values in each reservoir. Insofar as each new added segment was isolated, the added segment would follow its own evolutionary path governed by its initial state. This model has the property that new crustal and new mantle material would at the time of addition have the isotopic values of the undifferentiated reservoir (1). Magmas derived from subsequent melting of the crust or the depleted mantle would have distinctive characteristics at a given time. For a constant rate of crustal growth equation (2.20a) takes the following form

$$\varepsilon^*_{d,j}(\tau) = \frac{Q^*_d(\tau)\ f_j^{r/s}}{\lambda}\left[\frac{e^{\lambda\tau} - 1}{\lambda\tau} - 1\right] \qquad (2.21a)$$

and if $\lambda\tau \ll 1$ this equation reduces to

$$\varepsilon^{*}_{d,j}(\tau) = Q^{*}_{d}\, f_{j}^{r/s}\, \frac{\tau}{2} \qquad (2.21b)$$

The average time of residence ($\bar{\mathcal{t}}$) of a stable atom (s), which is not produced by radioactive decay, in reservoir j (j = 2 or 3) at a time τ is, using equations 11 and 12:

$$\bar{\mathcal{t}}_{s,j} \equiv \langle (\tau-\xi)\ \delta N_{s,j}(\xi)/N_{s,j}(\tau)\rangle = \frac{1}{N_{s,j}(\tau)} \int_{o}^{\tau} (\tau-\xi) \left(\frac{\delta N_{s,j}}{\delta \xi}\right) d\xi$$

$$= \frac{1}{M_j(\tau)} \int_{o}^{\tau} (\tau-\xi) M_j'(\xi)\, d\xi = \frac{1}{M_j(\tau)} \int_{o}^{\tau} M_j(\xi)\, d\xi \qquad (2.22)$$

It is here assumed that there was initially no crust or depleted mantle so that $N_{s,j}(0) = M_j(0) = 0$. Expression (2.22) is equivalent to the average age as measured today of continental crustal material if $\tau = T_o$, the age of the earth, otherwise it is the average age as measured $T = T_o - \tau$ years ago. Note that for this model $\bar{\mathcal{t}}_{s,j}$ is the same as the average age of the crust or depleted mantle and is independent of the species or of the reservoir. The subscripts on $\bar{\mathcal{t}}$ may therefore be dropped for this model.

Defining

$$\langle \mathcal{t}^{n} \rangle \equiv \frac{1}{M_j(\tau)} \int_{o}^{\tau} (\tau-\xi)^{n} \left(\frac{dM_j}{d\xi}\right) d\xi = \frac{n}{M_j(\tau)} \int_{o}^{\tau} (\tau-\xi)^{n-1} M_j(\xi)\, d\xi \qquad (2.23)$$

where n is an integer, then the integral in (2.20) can be written in the following form

$$I_j(\tau) \equiv \frac{1}{M_j(\tau)} \int_{o}^{\tau} M_j(\xi) \exp[\lambda(\tau-\xi)]\, d\xi = \frac{1}{M_j(\tau)} \int_{o}^{\tau} \sum_{n=0}^{\infty} \frac{\lambda^{n}}{n!} (\tau-\xi)^{n} M_j(\xi)\, d\xi$$

$$= \sum_{n=1}^{\infty} \frac{\lambda^{n-1}}{n!} \langle \mathcal{t}^{n} \rangle \qquad (2.24)$$

Then it follows from equation (2.20) that

$$\varepsilon^*_{d,j}(\tau) = Q^*_d(\tau)\ f_j^{r/s} \sum_{n=1}^{\infty} \frac{\lambda^{n-1}}{n!} \langle t^n \rangle \tag{2.25}$$

$$= Q^*_d(\tau)\ f_j^{r/s}\ \langle t^1 \rangle \left[1 + \frac{\lambda\langle t^2\rangle}{2\langle t^1\rangle} + \frac{\lambda^2\langle t^3\rangle}{6\langle t^1\rangle} + - - - -\right]$$

Note that for long-lived isotopes with $\lambda\tau \ll 1$ we get to a good approximation that

$$\varepsilon^*_{d,j}(\tau) = Q^*_d(\tau)\ f_j^{r/s}\ \bar{t}$$

or (2.26)

$$\varepsilon_{d,j}(T) = Q_d(T)\ f_j^{r/s}\ \bar{t}$$

as $\bar{t} = \langle t^1 \rangle$.

If we can measure $\varepsilon^*_{d,j}(\tau)$ and $f_j^{r/s}$ for a very long-lived isotope at $T = T_o - \tau$ years ago, then the only information we can obtain is the <u>mean age</u> of reservoir j as measured $T = T_o - \tau$ years ago. The resulting mean age is independent of which very long-lived species is used. This is independent of the rate of growth of the mass of reservoir j or the rate of transport of species i. This general treatment gives an integral which resembles a Laplace transform of $M_j(\tau)$ with a transform variable λ. This would permit a unique inversion for $M_j(\tau)$ if the transform was known for all values of λ. Insofar as there is only a limited number of decay schemes, a unique inversion is not possible although a substantial amount of information may be deduced. $I_j(\tau)$ have been calculated for a constant rate of crustal growth for various parent-daughter systems (Table 2.1) for $\tau = 4.55$ AE and thus a mean age of the mass of j of 2.275 AE. The isotopes

^{147}Sm, ^{87}Rb, ^{187}Re, ^{176}Lu, and ^{232}Th all have mean lives that are sufficiently long so that $I_j(\tau) \approx \bar{t}$ as shown in Table 2.1. The concordant results obtained for Rb-Sr and Sm-Nd single stage ages for the oceanic mantle in Appendix 2 clearly do not represent a unique time event but an average age and the concordance for Model I is a consequence of the long mean lives of both ^{147}Sm and ^{87}Rb. Inspection of Table 2.1 shows that ^{238}U has a significant deviation from the case with $\lambda = 0$ and ^{40}K and ^{235}U are greatly different from this case. These species have sufficiently short mean lives that the higher order terms become important and the equations are no longer redundant. From this result it is clear that the detailed history of the early earth must be derived from the latter two decay schemes. These different decay schemes when taken together yield information on the detailed time evolution by measurement at a single point in time.

The mean age $\bar{t}$ shows the relationship

$$\frac{d\bar{t}}{d\tau} = 1 - \frac{\bar{t}}{M}\left(\frac{dM}{d\tau}\right) = 1 - \bar{t}\left(\frac{d\ln M}{d\tau}\right) \qquad (2.27)$$

so that for $(dM/d\tau) > 0$, $(d\bar{t}/d\tau) < 1$. When $(dM/d\tau) = 0$ it follows that $(d\bar{t}/d\tau) = 1$. We also note that $(d\ell n\bar{t}/d\tau) \geq -(d\ln M/d\tau)$ and that $(d\bar{t}/d\tau) \leq 0$ if $(d\ln M/d\tau) \geq (1/\bar{t})$. This is shown schematically in Fig. 2.2. It follows from equation (2.27) that a similar relationship must hold for the ε-value for all systems involving very long-lived isotopes. If we know $\bar{t}$ as a function of time and the mass of the crust today then we may calculate the mass of the continents as a function of time from the following equation

Table 2.1. Values of $I_j(\tau)$ at τ = 4.55 AE for various parent/daughter systems for a constant rate of crustal growth with a mean age of $\bar{\tau}$ = 2.275 AE.

Radioactive parent	Decay constant (AE^{-1})	$I_j(\tau)$(AE)
-	0	2.275
^{147}Sm	0.00654	2.30
^{87}Rb	0.0142	2.32
^{187}Re	0.0161	2.33
^{176}Lu	0.0198	2.34
^{232}Th	0.049475	2.45
^{238}U	0.155125	2.92
^{40}K	0.5543	6.39
^{235}U	0.98485	18.77
^{244}Pu	8.48	1.44×10^{15}

Figure 2.2. Cartoon showing the relationship between a mean age $\bar{\tau}$ and the corresponding mass growth curve $M_3(\tau)$ for the crust. Two time variables are shown where τ is the time measured from the origin of the earth and T is the time measured backward from today. The vertical dashed line is shown for a time $\tau = t$ years after the origin of the earth which corresponds to a time $T_o - t$ years ago. Curve A shows the mean age of the mass of the crust $\bar{\tau}_{M,3}$ versus time τ. The breaks in curve A correspond to the breaks in $M_3(\tau)$. Rapid addition of new material implies a rapid decrease in $\bar{\tau}_{M,3}$ of the continental crust. For periods where no significant new mass is added $(d\bar{\tau}/d\tau) = 1$. This is valid for any model. For models as Model I where the concentration of stable isotopes does not vary with time $\bar{\tau}_{M,3}$ is also the mean age of any stable isotope $\bar{\tau}_{s,3}$ in the crust. For parent-daughter systems with $\lambda\tau \ll 1$, $\bar{\tau}_{M,3}$ is also the mean age of the parent and daughter isotopes in the crust (i.e., $\bar{\tau}_{M,3} = \bar{\tau}_{d,3} = \bar{\tau}_{r,3}$). Curve B shows the case where a stable isotope is strongly enriched in the crust earlier in time and the concentration in the bulk crust decreases monotonically with time. This weights the older material more strongly and raises the value of $\bar{\tau}_{s,3}$ above $\bar{\tau}_{M,3}$ (curve A). The curve $\bar{\tau}_{s,3}$ for Model II has a more subdued behavior compared to Model I for more recent additions. Similarly, if a long-lived parent is much more strongly enriched than the daughter in the crust then the factor $\bar{\tau}_{r/s}$ shows a behavior like that of curve B. Subsequent to $\tau = t$ no mass is added so $(d\bar{\tau}/d\tau) = 1$ for both curves for the time interval $\tau = t$ to $\tau = T_o$. The difference between the two curves is given by equation (2.66).

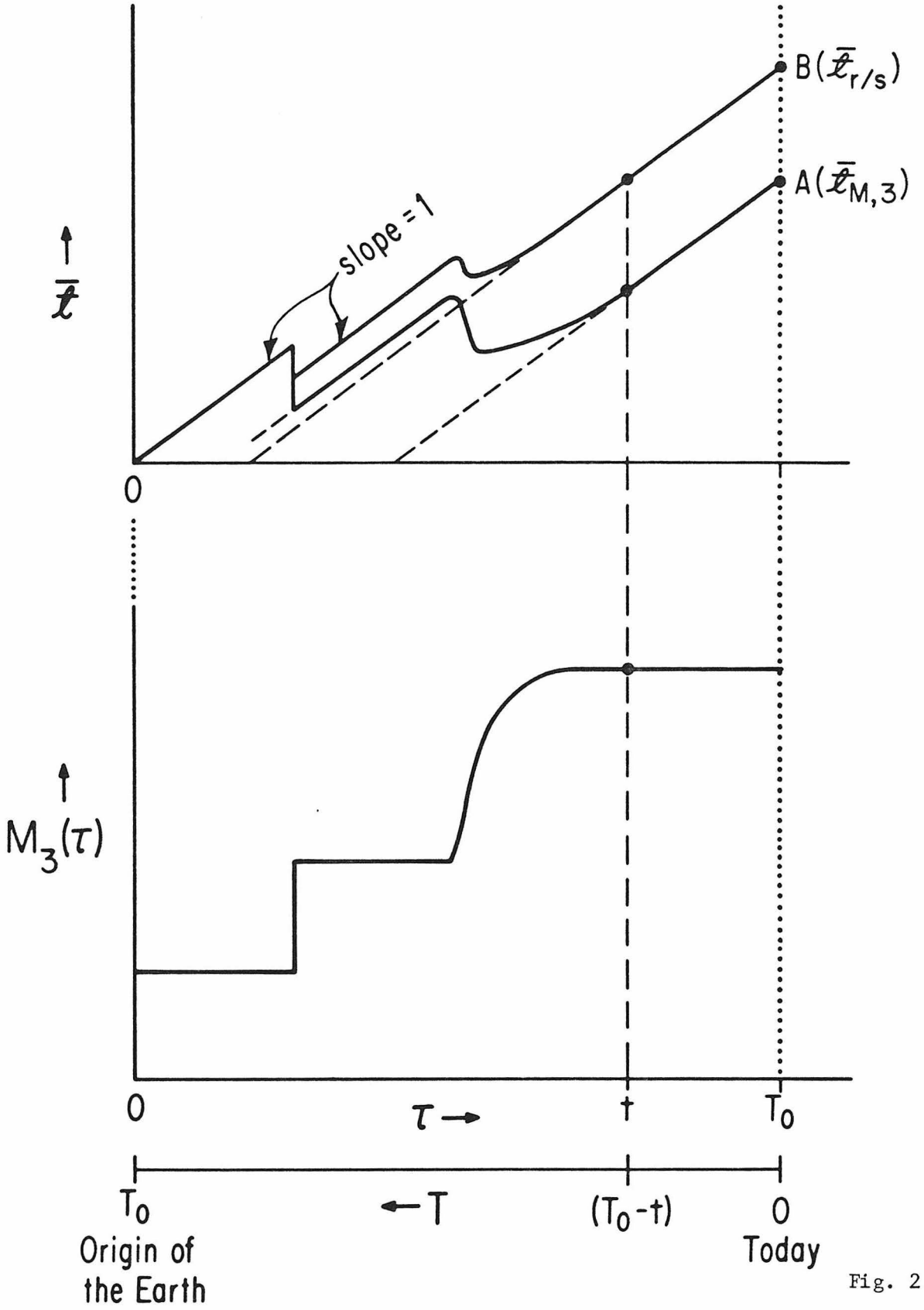
B($\bar{\mathcal{E}}_{r/s}$)
A($\bar{\mathcal{E}}_{M,3}$)
slope = 1
$\bar{\mathcal{E}}$
0
$M_3(\tau)$
0
$\tau \rightarrow$
t
T_0
T_0
$\leftarrow T$
$(T_0 - t)$
0
Origin of the Earth
Today

Fig. 2.2

$$M_3(\tau) = M_3(T_o) \frac{\overline{\mathcal{L}}(T_o)}{\overline{\mathcal{L}}(\tau)} \exp \left[- \int_{\tau}^{T_o} \frac{d\xi}{\overline{\mathcal{L}}(\xi)} \right] \tag{2.28}$$

where T_o is the age of the earth as measured today.

2.2. GEOMETRICAL CONSTRAINTS FOR MODEL I

The mechanism for crustal growth in this model is by deriving melts from undepleted mantle. The mass transfer from a deep-seated undepleted reservoir may occur through rising blobs. At shallow levels in the mantle the blobs may intersect the solidus and be partially melted (Fig. 2.3). However, only a fraction β of the blobs may rise underneath the continental crust and contribute to crustal growth. The remaining fraction of the blobs $(1 - \beta)$ rise underneath the oceanic crust and may contribute to oceanic volcanism. However, these may be mixed back into the mantle with a short time scale (< 0.2 AE) owing to the rapid turnover in the oceanic mantle implied by seafloor spreading and not become attached to the continents. This would correspond to adding undifferentiated mantle to the depleted mantle. The possibility that undifferentiated mantle in this way gets mixed with depleted mantle may easily be incorporated in the equations for Model I. It is assumed that a differential mass δM_1, is derived from reservoir 1 and adds a differential mass δM_O^* to blobs underneath the oceans and δM_C^* to blobs rising underneath the continental crust. Then we have that $\delta M_C^*/\delta M_1 = \beta$ and $\delta M_O^*/\delta M_1 = 1 - \beta$ where β is the probability that a mass taken from reservoir 1 is directed toward a continental segment. The blobs underneath the continental crust are partially melted to a degree F and thus the differential mass added to the crust is $\delta M_3 = F\delta M_C^*$ and the corresponding residue R of $\delta M_R^* = (1-F)\delta M_C^*$ is left in the mantle and remixed. The blobs δM_O^* which rise in the oceanic regions will also differentiate but

Figure 2.3. Cartoon of the mechanism for crustal growth in Model I. The mass transfer from a deepseated undepleted reservoir may occur through rising blobs. At shallow levels in the mantle the blobs intersect the solidus and may be partially melted. The density of dots in each reservoir reflects the concentration of LIL elements.

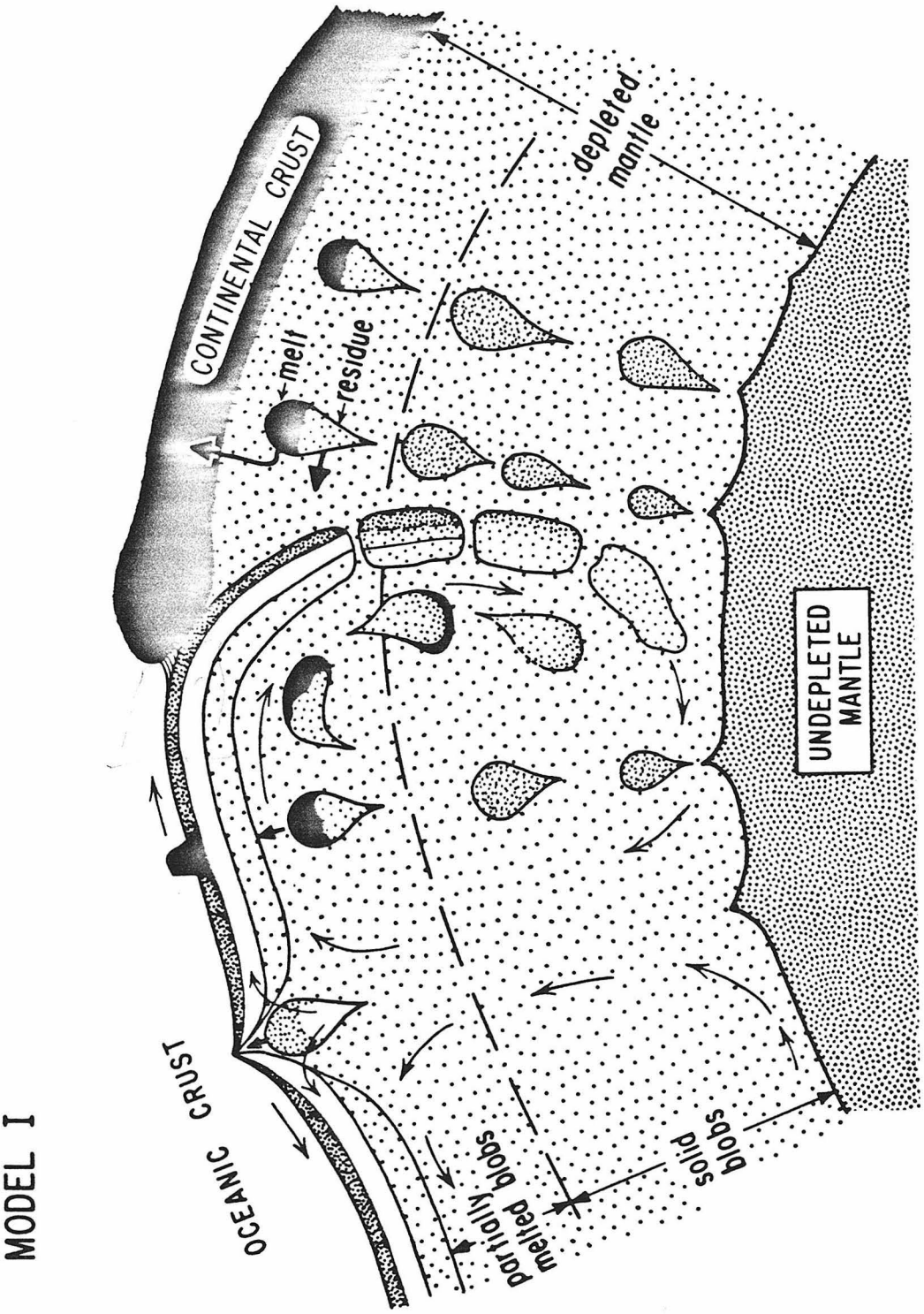
MODEL I
CONTINENTAL CRUST
melt
residue
depleted mantle
UNDEPLETED MANTLE
OCEANIC CRUST
partially melted blobs
solid blobs

Fig. 2.3

are not isolated and are taken to be remixed consistent with the general scheme of model I. The contributions of δM_0^* to reservoir 2 are thus not depleted. In this process a mass $\delta M_2 = \delta M_0^* + \delta M_R^*$ is added to reservoir 2. Conservation of mass and species imply that the concentration of i in the crust $c_{i,3}$ is given by $C_{i,1} = c_{1,3}[F + D_i(1-F]$ as before (equation 2.3). However, the relationship between the rates of growth of the crust and depleted mantle and the composition of the depleted mantle will be changed. The relationship between the masses of reservoirs 2 and 3 is given by

$$M_3(\tau) = M_2(\tau)\left[\frac{\beta F}{1 - \beta F}\right] \tag{2.29}$$

In this case we have from mass and species conservation that $C_{i,1} = c_{i,3}\beta F + \tilde{c}_{i,2}(1 - \beta F)$ where $\tilde{c}_{i,2}$ is the effective concentration in the total material added to layer 2 in masses δM_0^* and δM_R^*. The concentration of species i in reservoir 2 is given by

$$\frac{\tilde{c}_{i,2}}{C_{1,1}} = \frac{F(1-\beta) + D_i(1-F)}{(1-F\beta)[F + D_i(1-F)]} \tag{2.30}$$

where $(\tilde{c}_{i,2}/C_{i,1}) > D_i/[F + D_i(1-F)]$. This version of Model I changes equations (2.3), (2.4), and (2.6) for reservoir 2 and gives $(\delta N_{i,2}/\delta\tau) = \tilde{c}_{i,2}(\delta M_2/\delta\tau)$ in equation (2.5). All the equations for the continental crust will be the same as those derived previously. For reservoir 2 the transport equation corresponding to (2.6) is

$$\frac{dN_{i,2}}{d\tau} = \frac{F(1-\beta) + D_i(1-F)}{(1-F\beta)[F+D_i(1-F)]} C_{i,1}(\tau)M_2'(\tau) - \lambda_i N_{r,2}(\tau) \tag{2.31}$$

The solution of (2.31) for a stable isotope is

$$N_{s,2}(\tau) = \frac{F(1-\beta) + D_s(1-F)}{(1-\beta F)[F+D_s(1-F)]} C_{s,1}(0)M_2(\tau) \tag{2.32}$$

and corresponding changes for radioactive and daughter isotopes have to be made in (2.13) and (2.15) given previously. The enrichment factor as defined in (2.17) is then given for reservoir 2 by

$$f_2^{r/s} = \left[\frac{F(1-\beta) + D_r(1-F)}{F(1-\beta) + D_s(1-F)}\right]\left[\frac{F + D_s(1-F)}{F + D_r(1-F)}\right] - 1 \tag{2.33}$$

and this value should be used in equation (2.19) and (2.20), respectively. From the mass and species conservation equations given previously for this case written for radioactive and stable species it may be shown that

$$D_s = \left\{\frac{(\beta-1)f_2^{r/s} + \beta\left[1-\left(\frac{C_{r,3}}{C_{r,1}}\right)F\right]}{\left(\frac{C_{r,3}}{C_{r,1}}\right)F\beta + f_2^{r/s}}\right\} \quad \frac{F}{1-F} > 0 \tag{2.34}$$

Since $0 < F(C_{r,3}/C_{r,1}) < 1$, it follows from (2.34) that for $f_2^{r/s} < 0$ and $0 < D_r < D_s < 1$ that

$$\beta > \left(\frac{C_{r,3}}{C_{r,1}}\right)F\beta > - f_2^{r/s} \tag{2.35}$$

and for $f_2^{r/s} > 0$ and $0 < D_s < D_r < 1$ we have that

$$\beta > \frac{f_2^{r/s}}{f_2^{r/s} + 1} \tag{2.36}$$

Thus given a value for $f_2^{r/s}$ this may put serious constraints on the value of β. If for example the continents always occupied 1/3 of the surface area and if the continents only grew from rising material

by this geometrical consideration then β would be 1/3. Were it possible to show that β is very different from this, then this would indicate that the geometrical considerations were not controlling the rate of continental growth and some sweeping or disaggregation process was required. Note that the case with $\beta < 1$ has many similarities with models involving refluxing of material from the crust to the depleted mantle. If a fraction $1 - \beta$ of new additions to the crust is always immediately subducted back to the depleted mantle, then the exact solution of this problem is also given by (2.29) to (2.36) above. Similarly, these equations also describe the case where a fraction $1 - \beta$ of the melt is always trapped in the residual solid. The conceptual pictures in Fig. 2.1 and the descriptions of Model I in the text does not fully describe the variety of physical circumstances which are represented by the equations derived for Model I.

2.3. MODEL II

Consider a model where the continental crust (3) grows from an initially undifferentiated mantle reservoir (2) which is depleted at all times subsequent to $\tau = 0$ as a result of crustal growth. This reservoir (2) may make up all or part of the mantle.

Define a reference reservoir (1) which corresponds to the total of reservoirs 2 and 3. Initially the whole mantle is supposed to be homogeneous and undifferentiated. A remaining portion of the mantle which is not involved in crust formation may remain isolated and undifferentiated. This reservoir will follow the isotopic evolution of the reference reservoir (1) but otherwise has nothing to do with the model. The model is shown in Fig.2.1. Let us assume that a differential mass is removed from reservoir 2 as a partial melt to form new crust and increases the mass of the crust by δM_3 and decreases the mass of reservoir 2 by $\delta M_2 = -\delta M_3$. The concentration of an element i in the partial melt at time τ is $c_{i,3}(\tau)$.

There are two different cases of this model that merit discussion. A) Assume that the differential melt δM_3 equilibrates with all of reservoir 2. Then the mass of the residue is all of reservoir 2 and the degree of melting $F = \delta M_3/M_2$ must be a differential. This means that for an element i with bulk distribution coefficient $D_i = 0$ all of the element would be transported into the crust as soon as any differential melt formed from reservoir 2. This does not seem physically realistic. B) Assume that a differential mass δM^* of reservoir 2 is differentiated into a melt δM_3 and a residue δM_R^* with the degree of melting F being finite. Case B seems physically more realistic than A.

For case B, we have that $\delta M_3/\delta M^* = F$ and $\delta M_R^*/\delta M^* = 1-F$. The residue after removal of a melt fraction from reservoir 2 is assumed to be homogenized instantaneously with the remaining part of the depleted mantle. Conservation of species and mass gives $C_{i,2}(\tau)\delta M^* = c_{i,3}(\tau)\delta M_3 + c_{i,R}(\tau)\delta M_R^*$ and since $c_{i,R}(\tau)/c_{i,3}(\tau) \equiv D_i$ it follows that $c_{i,3}(\tau) = d_i\, C_{i,2}(\tau)$ where

$$d_i \equiv \frac{1}{F + D_i(1-F)} \tag{2.37}$$

This case thus corresponds to the melting law in Model I. The difference is that in Model II the residue always has to be homogenized with the remaining part of the mantle reservoir it is derived from and this reservoir is continuously depleted. Case B will be used in the following discussion.

The number of species i in the differential melt (δM_3) that is added to the crust is given by

$$\delta N_{i,3}(\tau) = c_{i,3}(\tau)\ \delta M_3 = d_i \frac{\delta M_3}{M_2(\tau)} N_{i,2}(\tau) \tag{2.38}$$

If $\delta\tau$ is the time over which the mass δM_3 is added to the continental crust, then the transport equations for reservoirs j = 2,3 are

$$\frac{dN_{i,j}(\tau)}{d\tau} = (-1)^{j+1}\left(\frac{\delta N_{i,3}}{\delta\tau}\right) - \lambda_i N_{r,j}(\tau) \quad \left\{\begin{array}{l} \lambda_i = 0 \ , \ i = s \\ \lambda_i = \lambda_r \ , \ i = r \\ \lambda_i = -\lambda_r, \ i = d \end{array}\right\} \tag{2.39}$$

For simplicity mass transport from 3 to 2 is again ignored. Using the expression for $\delta N_{i,3}$ and calling $\delta M_3/\delta\tau \equiv M_3'(\tau)$ the following basic transport equations for Model II are obtained:

$$\frac{dN_{i,j}(\tau)}{d\tau} = (-1)^{j+1}\, d_i\, \frac{M_3'(\tau)}{M_2(\tau)}\, N_{i,2}(\tau) - \lambda_i\, N_{r,j}(\tau) \qquad (2.40)$$

The masses of the total reservoirs 2 and 3 must satisfy

$$M_2(\tau) + M_3(\tau) = M_2(0) \quad ; \quad M_2'(\tau) = - M_3'(\tau) \qquad (2.41)$$

The integrals of the transport equations for a stable species s in reservoirs 2 and 3 are

$$N_{s,2}(\tau) = N_{s,2}(0) \left[\frac{M_2(\tau)}{M_2(0)}\right]^{d_s} \qquad (2.42)$$

$$N_{s,3}(\tau) = N_{s,2}(0) - N_{s,2}(\tau) \qquad (2.43)$$

Equation (2.42) for a stable isotope in reservoir 2 may be written in the following form

$$C_{s,2}(\tau) = C_{s,2}(0) \left[1 - \frac{M_3(\tau)}{M_2(0)}\right]^{(d_s - 1)}$$

This expression has the same general form as the equation of Shaw [1970] for the solid residue after modal fractional (Rayleigh) melting, however d_s takes the place of the inverse bulk distribution coefficient and the degree of crust formation $M_3(\tau)/M_2(0)$ takes the place of the degree of melting.

The solutions of equation (2.40) for radioactive and daughter isotopes are

$$N_{r,2}(\tau) = N_{r,2}(0)\, e^{-\lambda\tau} \left[\frac{M_2(\tau)}{M_2(0)}\right]^{d_r} \qquad (2.44)$$

$$N_{r,3}(\tau) = N_{r,2}(0)\, e^{-\lambda\tau} - N_{r,2}(\tau) \tag{2.45}$$

$$N_{d,2}(\tau) = \left[N_{d,2}(0) + N_{r,2}(0)\lambda \int_o^\tau \left[\frac{M_2(\xi)}{M_2(0)}\right]^{(d_r-d_s)} \exp\,[-\lambda\xi]d\xi\right]\left[\frac{M_2(\tau)}{M_2(0)}\right]^{d_s} \tag{2.46}$$

$$N_{d,3}(\tau) = N_{d,2}(0) + N_{r,2}(0)[1 - e^{-\lambda\tau}] - N_{d,2}(\tau) \tag{2.47}$$

where $d_s = d_d$ since d and s are isotopes of the same element. The ratios of a radiogenic isotope to a stable isotope for the two reservoirs are

$$\frac{N_{d,2}(\tau)}{N_{s,2}(\tau)} = \frac{N_{d,1}(\tau)}{N_{s,1}(\tau)} - \lambda \frac{N_{r,1}(\tau)}{N_{s,1}(\tau)} \int_o^\tau \left\{1 - \left[\frac{M_2(\xi)}{M_2(0)}\right]^{(d_r-d_s)}\right\} \exp[\lambda(\tau-\xi)]d\xi \tag{2.48}$$

$$\frac{N_{d,3}(\tau)}{N_{s,3}(\tau)} = \frac{N_{d,1}(\tau)}{N_{s,1}(\tau)} - \lambda \frac{N_{r,1}(\tau)}{N_{s,1}(\tau)} \left[\frac{\int_o^\tau \left\{1 - \left[\frac{M_2(\xi)}{M_2(0)}\right]^{(d_r-d_s)}\right\}\exp[\lambda(\tau-\xi)]d\xi}{1 - \left[\frac{M_2(\tau)}{M_2(0)}\right]^{(-d_s)}}\right] \tag{2.49}$$

From equations (2.17) and (2.42) to (2.45) the enrichment factors of the ratio of a radioactive isotope to a stable isotope in the total reservoirs 2 and 3 relative to that in reservoir 1 are given by

$$f_2^{r/s}(\tau) = \left[\frac{M_2(\tau)}{M_2(0)}\right]^{(d_r-d_s)} - 1 \approx \exp\left[-(d_r-d_s)\,\frac{M_3(\tau)}{M_2(0)}\right] - 1 \tag{2.50}$$

$$\frac{f_2^{r/s}(\tau)}{f_3^{r/s}(\tau)} = 1 - \left[\frac{M_2(\tau)}{M_2(0)}\right]^{(-d_s)} \approx 1 - \exp\left[d_s\,\frac{M_3(\tau)}{M_2(0)}\right] \tag{2.51}$$

where the approximations hold for the mass of the crust much smaller than that of the depleted mantle $[(M_3(\tau)/M_2(0)) \ll 1]$. Equations (2.48) and (2.49) may be written in terms of deviations in parts in 10^4 from the reference reservoir 1:

$$\varepsilon^*_{d,2}(\tau) = Q^*_d(\tau) \int_o^\tau f_2^{r/s}(\xi) \exp[\lambda(\tau-\xi)]d\xi \tag{2.52}$$

$$\varepsilon^*_{d,3}(\tau) = \varepsilon^*_{d,2}(\tau) \frac{f_3^{r/s}(\tau)}{f_2^{r/s}(\tau)} \tag{2.53}$$

where $Q^*_d(\tau)$ is defined by equation (2.20). Equations (2.50) to (2.53) in conjunction with (2.37) are the basic equations for calculations with this model for arbitrary rates of crustal growth. In this class of models the average enrichment factors are a function of the time and correspond to a time dependent chemical evolution. For $\lambda\tau \ll 1$ the deviations $\varepsilon^*_{d,j}$ are then proportional to the weighted time average of the enrichment factors $\langle f_j^{r/s} \rangle$ and given by

$$\varepsilon^*_{d,2}(\tau) = Q^*_d(\tau) \langle f_2^{r/s}(\tau) \rangle_\tau \tag{2.54}$$

$$\varepsilon^*_{d,3}(\tau) = Q^*_d(\tau) \frac{f_3^{r/s}(\tau)}{f_2^{r/s}(\tau)} \langle f_2^{r/s}(\tau) \rangle_\tau \tag{2.55}$$

This means that the simple species independent time averages which govern the ε function for models of type I no longer apply and an average age is not directly applicable to reservoir 2.

In this model the depleted mantle is assumed to always be homogeneous. For the crust the equations give the average values. If

each new addition to the crust is isolated, then the new individual segments follow their own evolutionary path. The initial state of new additions to 3 at time τ' are given by

$$f_{new}^{r/s}(\tau') = \frac{d_r}{d_s}\,[f_2^{r/s}(\tau') + 1] - 1 \tag{2.56}$$

$$\varepsilon^*_{d,new}(\tau') = \varepsilon^*_{d,2}(\tau') \tag{2.57}$$

and subsequent evolution will follow

$$\varepsilon^*_{d,new}(\tau) = \varepsilon^*_{d,3}(\tau') + \frac{Q^*_d(\tau)}{\lambda}\, f_{new}^{r/s}(\tau')\left\{\exp[\lambda(\tau-\tau')] - 1\right\} \tag{2.58}$$

This model has the property that new crust would at the time of addition have the isotopic values of depleted mantle (2) and the interpretation of T^{Nd}_{CHUR} model ages [McCulloch and Wasserburg, 1978c] of new crust would depend on the detailed history of reservoir 2.

For this model we may again define the mean age of species s in the crust (3) by

$$\bar{\tau}_{s,3} = \frac{1}{N_{s,3}(\tau)} \int_o^\tau (\tau-\xi)\,\frac{dN_{s,3}}{d\xi}\,d\xi = \frac{1}{N_{s,3}(\tau)} \int_o^\tau N_{s,3}(\xi)d\xi \tag{2.59}$$

and the mean age of the mass M_3 by

$$\bar{\tau}_{M,3} = \frac{1}{M_3(\tau)} \int_o^\tau (\tau-\xi)\, M_3'(\xi)d\xi = \frac{1}{M_3(\tau)} \int_o^\tau M_3(\xi)d\xi \tag{2.60}$$

The mean age of the depleted mantle reservoir (2) may not be defined in the same manner. Note that for model II, $N_{s,3}(\tau)/M_3(\tau)$ is not a constant independent of τ so that $\bar{\tau}_{s,3} \neq \bar{\tau}_{M,3}$. The result of this is distinct from Model I and is shown schematically in Fig. 2.2. Using

equations (2.43) and (2.59) we may write

$$\bar{\tau}_{s,3} = \frac{1}{1 - \left[1 - \frac{M_3(\tau)}{M_2(0)}\right]^{d_s}} \int_0^{\tau} \left\{1 - \left[1 - \frac{M_3(\xi)}{M_2(0)}\right]^{d_s}\right\} d\xi$$

$$\approx \frac{1}{1 - \exp\left[-\frac{d_s M_3(\tau)}{M_2(0)}\right]} \int_0^{\tau} \left\{1 - \exp\left[-d_s \frac{M_3(\xi)}{M_2(0)}\right]\right\} d\xi \qquad (2.61)$$

assuming that $(M_3(\tau)/M_2(0)) \ll 1$ in the second expression. In the case that $[d_s M_3(\tau)/M_2(0)] \ll 1$ then $\bar{\tau}_{s,3} \approx \bar{\tau}_{M,3}$. If $[d_s M_3(\tau)/M_2(0)] \gg 1$ for $\tau \geq \tau^*$ then $\bar{\tau}_{s,3} \approx$ const + $(\tau - \tau^*)$ for $\tau \geq \tau^*$ and $(d\bar{\tau}_{s,3}/d\tau) = 1$. This corresponds to the bulk of the species s being transported into the crust by time τ^* after the formation of the earth. The mass transfer is then subsequently decoupled from addition of the trace element s and the average age of the mass $\bar{\tau}_{M,3}$ may be substantially younger than $\bar{\tau}_{s,3}$ as the different trace element abundances of the crust change with time. The difference between $\bar{\tau}_{s,3}$ and $\bar{\tau}_{M,3}$ is of interest and may be evaluated quantitatively. We have

$$\bar{\tau}_{s,3} - \bar{\tau}_{M,3} = \frac{\int_0^{\tau} \left\{M_3(\tau) - M_3(\xi) + M_3(\xi)\exp\left[-d_s \frac{M_3(\tau)}{M_2(0)}\right] - M_3(\tau)\exp\left[-d_s \frac{M_3(\xi)}{M_2(0)}\right]\right\} d\xi}{\left\{1 - \exp\left[-d_s \frac{M_3(\tau)}{M_2(0)}\right]\right\} M_3(\tau)} \qquad (2.62a)$$

$$= \frac{\left[\frac{d_s}{M_2(0)}\right]^2 \int_0^{\tau} M_3(\xi) \left\{\sum_{n=2}^{\infty} \frac{(-1)^n}{n!} \left[M_3(\tau)\left(\frac{d_s M_3(\tau)}{M_2(0)}\right)^{n-2} - M_3(\xi)\left(\frac{d_s M_3(\xi)}{M_2(0)}\right)^{n-2}\right]\right\} d\xi}{\left\{1 - \exp\left[-d_s \frac{M_3(\tau)}{M_2(0)}\right]\right\}}$$

If $d_s < 0$ it may be seen that $\bar{t}_{s,3}-\bar{t}_{M,3} < 0$. This expression converges rather well even for large values of $d_s[M_3(\tau)/M_2(0)]$ ($\leqslant 2$). In the limit for small $d_s/M_2(0)$ we have rather precisely

$$\frac{\bar{t}_{s,3}-\bar{t}_{M,3}}{\left(\frac{d_s}{M_2(0)}\right)} \approx \frac{1}{2M_3(\tau)} \int_o^\tau M_3(\xi)[M_3(\tau) - M_3(\xi)]d\xi \qquad (2.62b)$$

so in this approximation $\bar{t}_{s,3}-\bar{t}_{M,3} > 0$ for $d_s > 0$. For a model of a constant rate of crustal growth we obtain

$$\bar{t}_{s,3} - \bar{t}_{M,3} \approx \frac{d_s\, M_3(\tau)}{12\, M_2(0)}\, \tau \qquad (2.62c)$$

which gives a difference of 0.65 AE for $d_s = 100$ with $M_3(\tau)/M_2(0) = 0.0174$. It follows that for $d_s \leqslant 10$ there are only small differences in the mean ages.

Note that the expressions for ϵ^* (2.52, 2.53) may be written in a form analogous to that for Model I. Inspection of equations (2.61) and (2.52) show that $\epsilon^*_{d,2}$ may be written as

$$\epsilon^*_{d,2}(\tau) = Q^*_d(\tau)\, f_2^{r/s}(\tau)\, \bar{t}_{r/s} \qquad (2.63)$$

where

$$\bar{t}_{r/s} \equiv \frac{1}{f_2^{r/s}(\tau)} \int_o^\tau f_2^{r/s}(\xi)d\xi = \frac{\tau\, \langle f_2^{r/s}(\tau)\rangle}{f_2^{r/s}(\tau)} \qquad (2.64)$$

The factor $\bar{t}_{r/s}$ is the time weighted average of $f_2^{r/s}$ for reservoir 2. If $d_r-d_s > 0$, this is equivalent to the mean age of an element r/s with a distribution coefficient $d_{r/s} = d_r-d_s$ and an enrichment factor $f_2^{r/s}$. Note

that $\bar{t}_{r/s}$ is explicitly dependent on the particular parent daughter system as distinct from the case for Model I. If the differentiation took place in only a single event, then $\bar{t}_{r/s} = \bar{t}_{M,3}$. More generally there will be a difference between $\bar{t}_{r/s}$ and $\bar{t}_{M,3}$ which may be calculated from

$$\bar{t}_{r/s} - \bar{t}_{M,3} \approx \frac{d_r - d_s}{2M_3(\tau)M_2(0)} \int_0^\tau M_3(\xi)[M_3(\tau) - M_3(\xi)]d\xi \tag{2.65}$$

The derivation of expression (2.65) follows that given previously for $\bar{t}_{s,3} - \bar{t}_{M,3}$. For a model of constant rate of crustal growth we have

$$\bar{t}_{r/s} - \bar{t}_{M,3} = \frac{(d_r - d_s)M_3(\tau)}{12\ M_2(0)}\ \tau \tag{2.66}$$

If $|(d_r-d_s)M_3(\tau)/M_2(0)| \ll 1$, then equations (2.50) and (2.52) may for very long-lived isotopes be approximated by

$$\varepsilon^*_{d,2}(\tau) \approx -\ (d_r-d_s)\ \frac{Q^*_d(\tau)M_3(\tau)}{M_2(0)}\ \bar{t}_{M,3} \tag{2.67}$$

and

$$f_2^{r/s}(\tau) \approx -\ (d_r-d_s)\ \frac{M_3(\tau)}{M_2(0)} \tag{2.68}$$

If it also holds that $[d_sM_3(\tau)/M_2(0)] \ll 1$, then

$$f_3^{r/s}(\tau) \approx \frac{d_r}{d_s} - 1 \tag{2.69}$$

and

$$\varepsilon^*_{d,3}(\tau) \approx Q^*_d(\tau)\left[\frac{d_r}{d_s} - 1\right]\bar{t}_{M,3} \tag{2.70}$$

An important special case is when $(dM_3/d\tau)$ is a constant. In this case $M_3(\tau) = [M_3(T_o)/T_o]\tau$ and defining $K_i \equiv [(d_i M_3(T_o))/(T_o M_2(0))]$ then for very long-lived isotopes

$$\varepsilon^*_{d,2}(\tau) = -Q^*_d(\tau)\left\{\tau - \frac{1-\exp[-(K_r-K_s)\tau]}{(K_r-K_s)}\right\} \tag{2.71}$$

$$f_2^{r/s}(\tau) = \exp[-(K_r-K_s)\tau] - 1 \tag{2.72}$$

$$\frac{f_2^{r/s}(\tau)}{f_3^{r/s}(\tau)} = 1 - \exp(K_s\tau) \tag{2.73}$$

$$\varepsilon^*_{d,3}(\tau) = \frac{\varepsilon^*_{d,2}(\tau)}{1-\exp(K_s\tau)} \tag{2.74}$$

There are two different classes of solutions depending on whether (d_r-d_s) is negative (as for Sm-Nd) or positive (as for Rb-Sr). Examples are shown for Rb-Sr and Sm-Nd in Fig. 2.4 and 2.5, respectively. For short times we have in both cases that $\varepsilon^*_{d,2} \propto \tau^2$ and $\varepsilon^*_{d,3} \propto \tau$. For long times we get $\varepsilon^*_{Sr,2} \approx -Q^*_{Sr}(\tau-\tau^\dagger)$ where $\tau^\dagger = 1/(K_{Rb}-K_{Sr}) = 2$ AE and $\varepsilon^*_{Nd,2} \propto \exp[-(K_{Sm}-K_{Nd})\tau]$ for the depleted mantle. The curves for the crust go to an extremum and then asymptotically approach zero. The inclusion of the term $\exp[\lambda(\tau-\xi)]$ for shorter-lived isotopes in the exact integral of (2.52) will, of course, quantitatively alter the nature of these results. The curve for $\varepsilon^*_{Sr,3}$ has a maximum at $\tau = 7.5$ AE and for much longer times $\varepsilon^*_{Sr,3} \propto \exp[-K_{Sr}\tau]$. Similarly the $\varepsilon_{Nd,3}$ curve for the crust has a minimum at $\tau = 21$ AE and $\varepsilon_{Nd,3} \propto -\exp[-K_{Nd}\tau]$ for much longer times. These solutions enable us to qualitatively understand the nature of the results for more general cases of crustal growth with time. From these results we may

Figure 2.4. $\varepsilon^*_{Sr,j}$ - curves for the bulk depleted mantle (2) and the bulk crust (3) as a function of time τ for a constant rate of growth of the crust. Curves that give the same present-day ε^*_{Sr} values are shown for both Model I and Model II and are identified by the symbols I and II respectively. Note the marked difference in behavior for ε^*_{Sr} as a function of time τ for the two models. Model I is a straight line for both reservoirs and Model II starts out as nearly a straight line for the crust but with a significantly different slope. The curves for Model II are constrained to give $f_2^{Rb/Sr} = -0.9$ and $f_3^{Rb/Sr} = +2.18$ today. The implied values of $K_{Rb}-K_{Sr}$ and K_{Sr} are given. The systematics shown are valid for decay systems with $\lambda\tau \ll 1$ and $(d_r - d_s) > 0$.

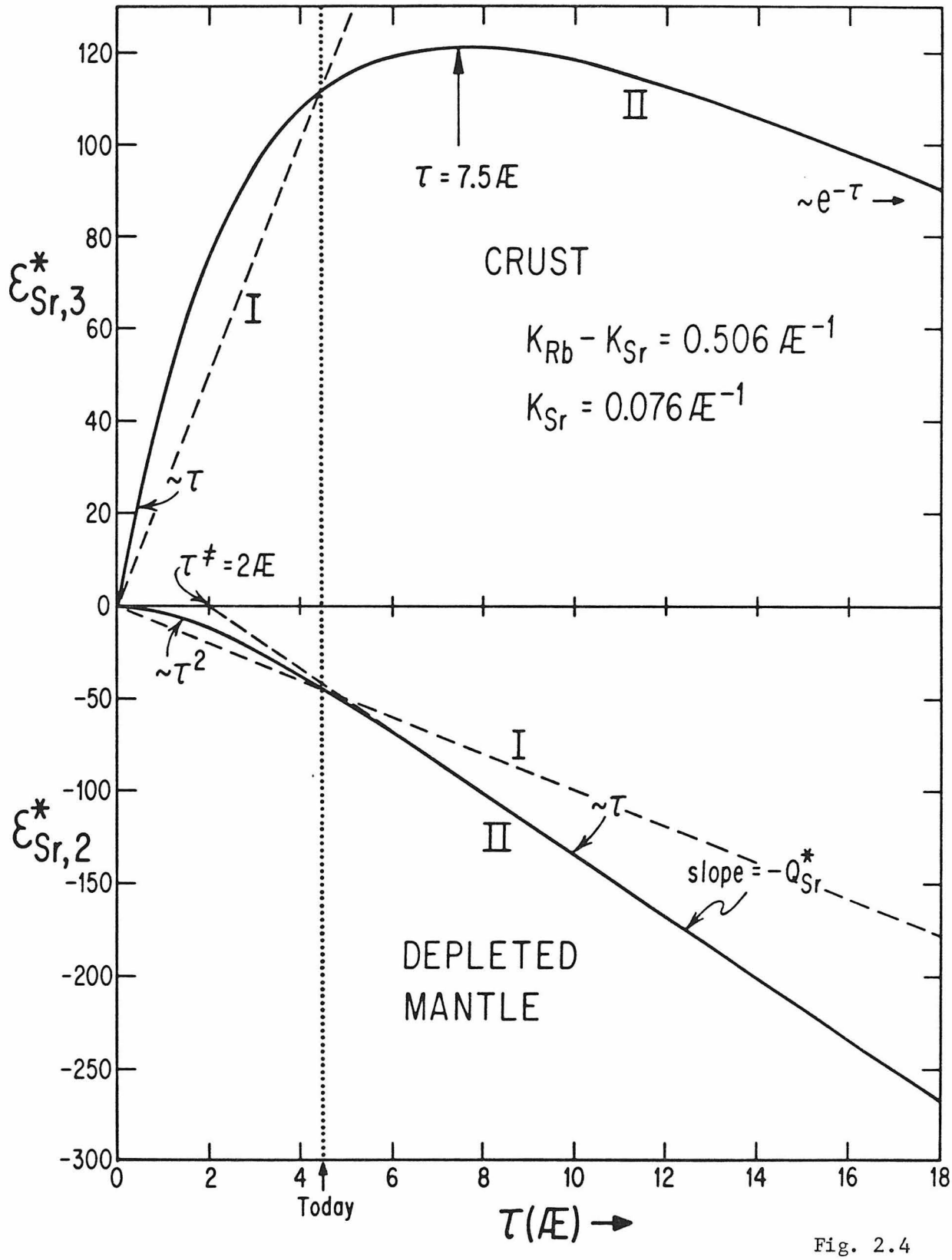
120
100
80
60
40
20
0
-50
-100
-150
-200
-250
-300
$\varepsilon^*_{Sr,3}$
$\varepsilon^*_{Sr,2}$
I
II
$\tau = 7.5$ Æ
$\sim e^{-\tau}$
CRUST
$K_{Rb} - K_{Sr} = 0.506$ Æ$^{-1}$
$K_{Sr} = 0.076$ Æ$^{-1}$
$\sim\tau$
$\tau^{\neq} = 2$ Æ
$\sim\tau^2$
$\sim\tau$
slope $= -Q^*_{Sr}$
DEPLETED
MANTLE
0
2
4
6
8
10
12
14
16
18
Today
τ(Æ) →

Fig. 2.4

Figure 2.5. $\varepsilon^*_{Nd,j}$ - curves for bulk depleted mantle (2) and bulk crust (3) as a function of time τ for a constant rate of growth of the crust. The notation is the same as in Fig. 2.4. The curves for Model II are constrained to give $f_2^{Sm/Nd} = +0.225$ and $f_3^{Sm/Nd} = -0.4$ today. The implied values of $K_{Sm}-K_{Nd}$ and K_{Nd} are shown. Note that the curves are reversed from those in Fig. 2.4 due to the change in sign of $K_r - K_s$. The systematics shown are valid for decay systems with $\lambda\tau \ll 1$ and $(d_r - d_s) < 0$.

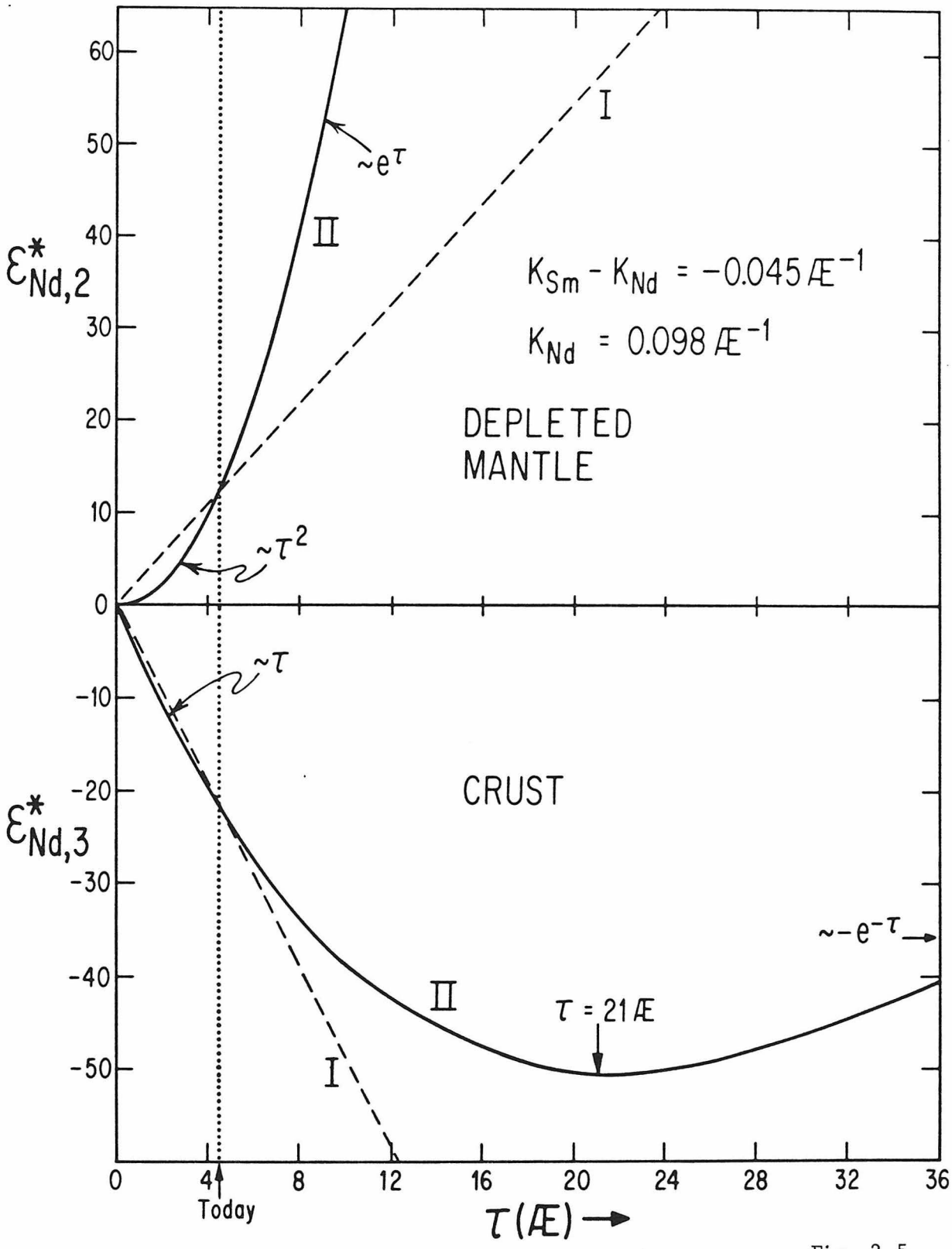
60
50
40
30
20
10
0
-10
-20
-30
-40
-50
$\varepsilon^*_{Nd,2}$
$\varepsilon^*_{Nd,3}$
I
II
$\sim e^{\tau}$
$\sim \tau^2$
$K_{Sm} - K_{Nd} = -0.045\,Æ^{-1}$
$K_{Nd} = 0.098\,Æ^{-1}$
DEPLETED MANTLE
CRUST
$\sim \tau$
$\sim -e^{-\tau}$
$\tau = 21\,Æ$
0
4
8
12
16
20
24
28
32
36
Today
$\tau\,(Æ) \rightarrow$

Fig. 2.5

infer that for any continuous or multiepisodic mass growth of the crust, the basic isotopic systematics for long-lived isotopes must follow those outlined in Fig. 2.4 and 2.5. Note that for the case of episodic mass growth $\varepsilon^*_{d,3}$ will be discontinuous due to the factor $f_3^{r/s}/f_2^{r/s}$ outside of the integral in equation (2.53). The value of $\varepsilon^*_{d,2}$ for the depleted mantle will still be continuous but will show changes in slope corresponding to the discontinuities in the mass growth curve. The general case for arbitrary mass transport is of course included in the exact basic equations (2.50) to (2.53).

Calculations with Model II are more complex than with Model I where the average age ($\bar{\tau}$) is independent of species. For the mantle the following exact results have been obtained:

$$\varepsilon^*_{d,2} = Q^*_d(\tau)\ \langle f_2^{r/s}\rangle_\tau = Q^*_d(\tau)\ f_2^{r/s}(\tau)\bar{\tau}_{r/s} \qquad (2.75)$$

It follows that if $\varepsilon^*_{d,2}(\tau)$ is known at τ then $\langle f_2^{r/s}\rangle$ is determined. If $\varepsilon^*_{d,2}$ and $f_2^{r/s}$ are known, then (d_r-d_s) is known from equation (2.50) and $\bar{\tau}_{r/s}$ is determined. $\bar{\tau}_{r/s}$ is the time required to generate $\varepsilon^*_{d,2}$ with the present value of $f_2^{r/s}$. As $f_2^{r/s}$ is monotonic in this model, $\bar{\tau}_{r/s}$ is the shortest time in which differentiation could have occurred (as a single stage process). All possible crustal mass growth laws $M_3(\tau)$ must satisfy the relationship between $f_2^{r/s}$ and M_3. The relationships are shown schematically in Fig. 2.6. If decay schemes with very long-lived parents have $|(d_r-d_s)M_3/M_2(0)| \ll 1$ then they will all yield the same values of $\bar{\tau}_{r/s}$ and no further information may be derived about the change of M_3 with time from the different systems at one time τ. If two systems have distinctive parameters (such as Rb-Sr and Sm-Nd) then they will have

Figure 2.6. Cartoon showing the relationship between the mean age of the mass of the crust $\overline{\tau}_{M,3}$, the mass growth curve of the crust M_3, the enrichment factor of the depleted mantle $f_2^{r/s}$, and the factor $\overline{\tau}_{r/s}$. The upper diagram shows a mass growth curve where the crust is formed in two stages with a mean age $\overline{\tau}_{M,3}$ at time τ. The middle diagram shows the corresponding change in $f_2^{r/s}$ with time if $(d_r - d_s) = 100$ and $[M_3(\tau)/M_2(0)] = 0.0174$. The difference between $\overline{\tau}_{r/s}$ and $\overline{\tau}_{M,3}$ is also indicated. If we know $\overline{\tau}_{r/s}$, $f_2^{r/s}$, and M_3 today there is insufficient information to determine a unique solution for $M_3(\xi)$ and $f_2^{r/s}(\xi)$. In the lower part of the diagram some other possible $f_2^{r/s}$ curves that give the same value for $\overline{\tau}_{r/s}$ are shown. For a given curve $f_2^{r/s}$ with knowledge of $(d_r - d_s)$ determines a corresponding M_3 curve from equation (2.50). The area underneath the $[f_2^{r/s}(\xi)/f_2^{r/s}(\tau)]$ curve must be the same for all M_3 curves with the same value for $\overline{\tau}_{r/s}$. $\overline{\tau}_{r/s}$ is the shortest time in which differentiation could have occurred as a single stage process and curve (a) shows such an evolution. Curve (b) shows a possible continuous curve. The dashed horizontal curve gives $[\langle f_2^{r/s} \rangle / f_2^{r/s}] = [\overline{\tau}_{r/s}/\tau]$. All of these curves in the lower figure are compatible with the $\overline{\tau}_{r/s}$ fixed by the assumed model with $M_3(\xi)$ as given in the top and the $f_2^{r/s}(\tau)$ value.

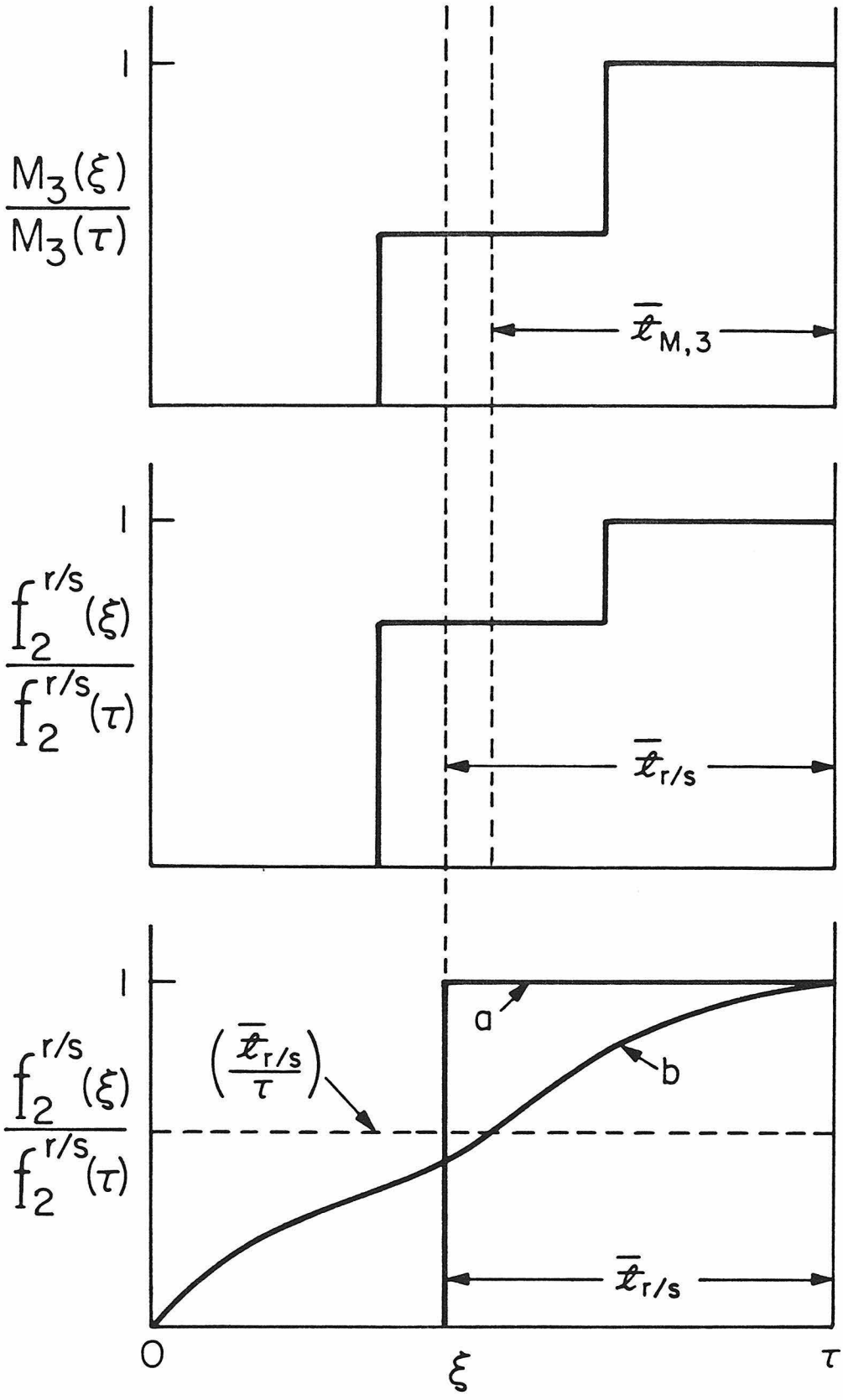
1
$\frac{M_3(\xi)}{M_3(\tau)}$
$\bar{t}_{M,3}$
1
$\frac{f_2^{r/s}(\xi)}{f_2^{r/s}(\tau)}$
$\bar{t}_{r/s}$
1
$\frac{f_2^{r/s}(\xi)}{f_2^{r/s}(\tau)}$
$\left(\frac{\bar{t}_{r/s}}{\tau}\right)$
a
b
$\bar{t}_{r/s}$
0
ξ
τ

Fig. 2.6

different values of $\overline{\mathcal{t}}_{r/s}$ which will give more information about $M_3(\tau)$. For N independent values of $\overline{\mathcal{t}}_{r/s}$ from N different decay schemes with $\lambda\tau \ll 1$, it is, in principle, possible to calculate models of multiple stage mass evolution with time. For example, for an n stage evolution we write

$$\overline{\mathcal{t}}_{r/s} = \sum_{i=1}^{n} \frac{\exp[-\alpha_{r/s} X_{i-1}] - 1}{\exp[-\alpha_{r/s}] - 1} (\tau_i - \tau_{i-1}) \tag{2.76}$$

where $\tau_o = 0$, $\tau_n = \tau$, $X_{n-1} = 1$, and $X_0 = 0$. The solutions for X_i may in general not be a unique description of earth evolution. Here $X_i - X_{i-1}$ is the fraction of $M_3(\tau)$ made at time τ_i and $\alpha_{r/s} = (d_r - d_s)M_3(\tau)/M_2(0)$. Such equations may be solved numerically for the X_i and τ_i which must provide simultaneous solutions for different $\overline{\mathcal{t}}_{r/s}$ values. In the degenerate case when $\alpha_{r/s} \ll 1$

$$\overline{\mathcal{t}}_{r/s} = \sum_{i=1}^{n} X_{i-1} (\tau_i - \tau_{i-1}) \tag{2.77}$$

which is independent of r/s.

CHAPTER 3. NEW DATA

3.1. CHONDRITES

Sm-Nd results for two carbonaceous chondrites (Murchison and Allende), three ordinary chondrites (Peace River, Guareña, and St. Severin), and one achondrite (Juvinas) will be presented. Murchison is classified as a CM2 chondrite which comprises the most abundant type of carbonaceous chondrites. Allende is a CV3 chondrite and is considered the petrologically most primitive class of carbonaceous chondrites. It contains inclusions of high-temperature condensates, some of which have the most primitive $^{87}Sr/^{86}Sr$ ratio so far found [Gray, Papanastassiou, and Wasserburg, 1973], and inclusions which are isotopically anomalous for Sm and Nd [McCulloch and Wasserburg, 1978a,b] as well as for other elements. Peace River is an L6 chondrite which is a class that constitutes the most abundant of ordinary chondrites. Guareña and St. Severin are H6 and LL6 chondrites, respectively, which have been extensively studied for Rb-Sr, U-Th-Pb, and I-Pu-Xe systematics because of their high content of whitlockite [Wasserburg, Papanastassiou, and Sanz, 1969; Wasserburg, Huneke, and Burnett, 1969; Lewis, 1975; Manhes, Minster and Allègre, 1978]. Finally, Juvinas is a basaltic achondrite which has a Sm/Nd ratio close to the average chondritic value and apparently crystallized early in the history of a basaltic achondrite parent body [Lugmair, 1974].

The long-lived isotope ^{147}Sm which decays to ^{143}Nd is an important tracer for chemical differentiation processes affecting the REE and other large ion lithophile (LIL) elements during planetary

evolution. The purpose here is to obtain an estimate of the average solar system values for $^{147}Sm/^{144}Nd$ and $^{143}Nd/^{144}Nd$ using chondrite samples. Our ability to determine the solar values depends on whether the solar nebula was initially isotopically homogeneous for the elements of interest and whether we have samples of material which is chemically unfractionated in Sm relative to Nd. Direct measurements of the abundances of Nd and Sm in the sun have recently been made by Maier and Whaling [1977] and Saffman and Whaling [1979] respectively. These studies give $\log (A_{Sm}/A_{Nd})_{\odot} = -0.46 \pm 0.25$ from which we calculate $(^{147}Sm/^{144}Nd)_{\odot} = 0.22$. From the summary of solar abundances by Ross and Aller [1976], we get $\log (A_{Sm}/A_{Nd})_{\odot} = -0.51 \pm 0.6$ from which we calculate $(^{147}Sm/^{144}Nd)_{\odot} = 0.19$. These values can serve as a guide in the subsequent discussion.

The first survey of REE in chondrites [Schmitt, Smith, Lasch, Mosen, Olehy, and Vasilevskis, 1963; Schmitt, Smith, and Olehy, 1964] demonstrated a reasonable degree of consistency in relative abundances of REE with an accuracy of about 10%. Later the isotope dilution technique was applied to REE in chondrites [Gast, Hubbard, and Weismann, 1970; Schnetzler and Bottino, 1971; Masuda, Nakamura, and Tanaka, 1973; Nakamura and Masuda, 1973; Nakamura, 1974; Evensen, Hamilton, and O'Nions, 1978] with the precision for individual REE considered to be 1 to 2%. The concentration levels of REE in chondrites are fairly low (~0.6 ppm Nd) and no measurements exist on chondrites for both $^{143}Nd/^{144}Nd$ and $^{147}Sm/^{144}Nd$ except for the very approximate data of Notsu and Mabuchi [1975]. A 1% error in the Sm/Nd ratio adds an error of 1.1 parts in 10^4 to the $^{143}Nd/^{144}Nd$ ratio over 4.5 AE. Therefore, it is necessary to

measure both the $^{147}Sm/^{144}Nd$ and $^{143}Nd/^{144}Nd$ ratios with high precision to establish a $^{143}Nd/^{144}Nd$ evolution curve. We are currently able to routinely measure the $^{147}Sm/^{144}Nd$ ratio with an accuracy of 0.5‰ and the error added to a $^{143}Nd/^{144}Nd$ evolution curve from the measurement of the Sm/Nd ratio is therefore insignificant (i.e., it is 6 parts in 10^6). The first serious meteorite measurements were made by Lugmair, Scheinin, and Marti [1975a], who chose a basaltic achondrite (Juvinas) which had a $^{147}Sm/^{144}Nd$ isotope ratio close to the average chondritic value. Therefore, if the source of Juvinas on the basaltic achondrite parent body (BACH) did not have a long pre-history as suggested by Rb-Sr and Sm-Nd internal isochrons for Juvinas [Allègre, Birck, Fourcade, and Semet, 1975; Lugmair, 1974], this should give close to the correct values. Lugmair et al. [1975b] used the Juvinas values as an approximation to chondritic Sm-Nd evolution.

3.1.1. Sm-Nd systematics of chondrites

The refractory lithophile elements Si, Mg, and Cr show a factor of two fractionation relative to Al between individual chondrite classes. This is most likely due to fractional condensation [Larimer, 1979]. The isotope dilution measurements of REE patterns in chondrites referred to above also indicate a large range of $^{147}Sm/^{144}Nd$ from 0.183 to 0.236; however, the averages of each class of chondrites show a smaller range in $^{147}Sm/^{144}Nd$. The averages of C, E, H, L, and LL chondrites are 0.196, 0.196, 0.195, 0.194, and 0.197, respectively. These values are all within error of each other and identical to the less precisely known solar value of $(^{147}Sm/^{144}Nd)_{\odot} = 0.2$. The extent to which fractional condensation processes have fractionated Sm relative to Nd of individual

chondrite classes relative to each other and the average solar system is not known. Clearly variation of a few percent in the Sm/Nd ratio can be allowed for from the data. Much of the variation between individual total rock samples must be due to sample heterogeneity rather than differences between the parent bodies as different total rock samples of a single meteorite may show a variation comparable to the range in chondrites.

The chemical abundances in CI1 carbonaceous chondrites have a special significance since they compare very closely with the abundances of the condensable elements which can be reliably measured from studies of the photospheric spectrum of the Sun. However, they are not pristine samples of solar system condensate as they show the highest degree of low-temperature alteration among the carbonaceous chondrites [McSween, 1979]. The average $^{147}Sm/^{144}Nd$ of CI1 chondrites is 0.197 [Nakamura, 1974; Evensen et al., 1978] and is close to that of other chondrite classes. They, however, do show a 6% range in $^{147}Sm/^{144}Nd$ (0.192 to 0.204) so it appears that a unique value cannot be obtained from these objects. Other classes of chondrites also show variable degrees of alteration and metamorphism. Thus only the consistency of results from a variety of meteorite classes can tell us how well we can estimate the average solar system values.

Some simple evolutionary histories of planetary objects that condensed and accreted from the solar nebula are shown schematically in Fig. 3.1. At T_C (about 4.6 AE ago) solid objects began condensing from the solar nebula (SN), from which the planets and meteorites are ultimately derived. The rate of growth of $^{143}Nd/^{144}Nd$ in these planetary

Fig. 3.1. Schematic representation of the evolution of $^{143}Nd/^{144}Nd$ with time for chondritic and achondritic parent bodies. Solid objects started to condense from the solar nebula (SN) at time T_C and accreted to parent bodies at time T_A. Subsequent to T_A a part of the parent bodies of achondrites may have differentiated at T_D into crust and depleted mantle. At times T_X subsequent to T_D, melts may be tapped from both depleted mantle (D1) and from previously undifferentiated material (D2).

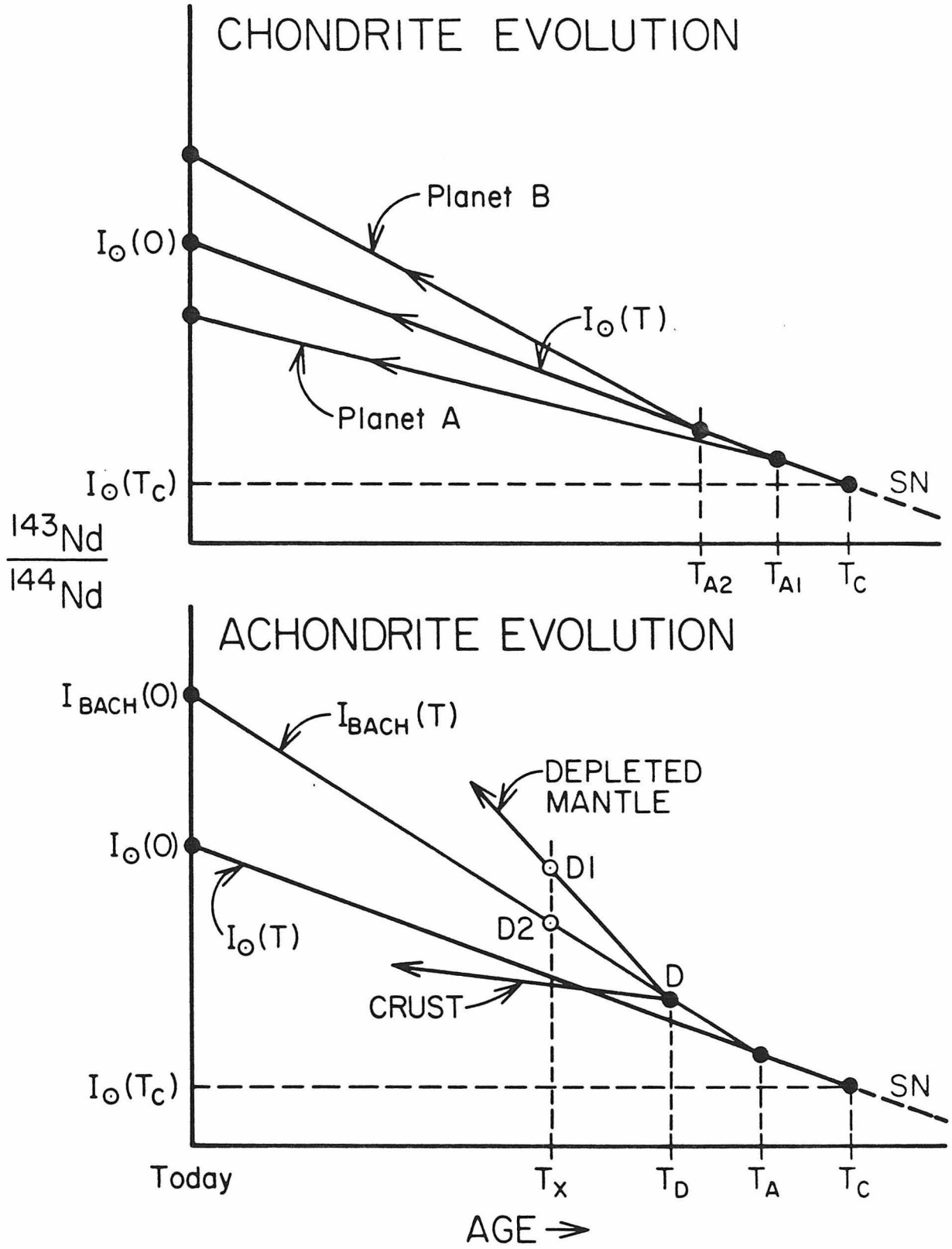
CHONDRITE EVOLUTION
Planet B
$I_\odot(0)$
$I_\odot(T)$
Planet A
$I_\odot(T_C)$
SN
$\frac{143Nd}{144Nd}$
T_{A2}
T_{A1}
T_C
ACHONDRITE EVOLUTION
$I_{BACH}(0)$
$I_{BACH}(T)$
DEPLETED MANTLE
$I_\odot(0)$
D1
D2
$I_\odot(T)$
D
CRUST
$I_\odot(T_C)$
SN
Today
T_X
T_D
T_A
T_C
AGE →

Fig. 3.1

objects may be different from the solar value due to variations in the relative chemical abundances of Sm and Nd during condensation and accretion. If a reservoir j is a closed system, then the evolution of $^{143}Nd/^{144}Nd$ as a function of time T is defined as $I_j^{Nd}(T)$ with $I_j^{Nd}(0)$ being the present-day value. The value of $^{143}Nd/^{144}Nd$ at any time in in the past in reservoir j is

$$I_j^{Nd}(T) = I_j^{Nd}(0) - \left(\frac{^{147}Sm}{^{144}Nd}\right)_j^o (\exp(\lambda T) - 1) \qquad (3.1)$$

where $(^{147}Sm/^{144}Nd)_j^o$ is the value in j today. Most meteorites come from small planetary objects and have ages within ~0.1 AE of the time of condensation from the solar nebula and provide important clues to the Sm/Nd isotopic evolution of the solar system. The objects of interest include meteorites which formed by melting processes on parent planets such as achondrites and the more primitive chondrites which appear to be aggregates of high- and low-temperature condensates from the solar nebula. DePaolo and Wasserburg [1976a] introduced the acronym CHUR ("chondritic uniform reservoir") for a bulk planet with $^{147}Sm/^{144}Nd$ and $^{143}Nd/^{144}Nd$ isotopic ratios the same as in average chondrites.

The evolution of chondritic meteorite parent bodies is shown schematically in Fig. 3.1; Planet A accretes at time T_{A1} with an Sm/Nd ratio lower than the solar value and Planet B accretes at time T_{A2} with Sm/Nd higher than the solar value.

In contrast to chondrites, achondrites are fragments of planetary crusts that began to form by partial melting at the time of early chemical differentiation of a parent body (T_D) subsequent to the time of

condensation and will show an evolution as is illustrated schematically in Fig. 3.1. Magmatic rocks formed subsequent to T_D at T_X may be derived from depleted mantle. There could be a 0.1 AE time difference between planet formation and melting, which for a source region having an enrichment factor $f^{Sm/Nd} = +0.2$ would give 1.0 ε-units difference from the solar value of the $^{143}Nd/^{144}Nd$ growth curve at the time of melting.

3.1.2. Results

The Sm-Nd results are given in Tables 3.1 and 3.2 and Fig. 3.2. Note that all non-radiogenic isotope ratios are within error of the grand mean of terrestrial normals and lunar samples measured in this laboratory [Papanastassiou et al., 1977]. There are thus no widespread isotopic anomalies in Nd for bulk chondrite samples to within ±0.5 ε-units. For Sm we routinely measured all isotopes except ^{150}Sm and ^{144}Sm and confirmed that $^{149}Sm/^{154}Sm$ and $^{152}Sm/^{154}Sm$ are within error (±1.0 ε-units) the same as the terrestrial values. The absence of any neutron capture effects on ^{149}Sm is consistent with the short exposure ages of these meteorites [Eugster et al., 1970; Russ et al., 1971]. This justifies the use of $^{143}Nd/^{144}Nd$ and $^{147}Sm/^{144}Nd$ isotope ratios calculated from spiked runs using the grand mean values of terrestrial normals for Sm and Nd isotopic compositions.

The data in Table 3.1 are shown on a Sm-Nd evolution diagram relative to a reference line with a slope corresponding to an age of ~4.6 AE. A variety of chondrites and the achondrite Juvinas lie within ±0.5 ε-units of the reference line shown. This conclusion is insensitive to the particular choice of age in a plausible neighborhood of 4.6 AE. The present-day range in these chondrites is, however, only

Table 3.1. Sm-Nd isotopic results.[c] [a]

Sample	Weight[d] (grams)	Nd(ppm)	Sm(ppm)	$\frac{^{147}Sm}{^{144}Nd}$	$\frac{^{143}Nd}{^{144}Nd}$	
I. Murchison (CM2)						
#1-ALIQ-1	0.51	0.63495	0.20671	0.19693	-	a
ALIQ-2		-	-	-	0.511845±29	b
ALIQ-3		0.63506	0.20672	0.19691	0.511816±25	a
#2	0.44	0.67034	0.21409	0.19320	0.511738±34	a
II. Allende (CV3)						
ALIQ-1	2.61	0.86957	0.28230	0.19639	-	a
ALIQ-2		-	-	-	0.511809±26	b
ALIQ-2		-	-	-	0.511839±25	b
III. Guareña (H6)						
	2.52	0.90208	0.29031	0.19468	0.511769±24	a
IV. Peace River (L6)						
ALIQ-1	2.97	0.69854	0.22615	0.19584	-	a
ALIQ-2		-	-	-	0.511831±32	b
V. St. Severin (LL6)						
Light	2.86	1.38562	0.43972	0.19197	0.511673±25	a
VI. Juvinas						
ALIQ-1	1.24	5.5245	1.7848	0.19543	0.511804±19	a

[a]Sample spiked with ^{150}Nd and ^{147}Sm tracers. Data normalized to $^{146}Nd/^{142}Nd = 0.636151$ and $^{148}Sm/^{154}Sm = 0.49419$. Concentrations calculated using $^{142}Nd/^{144}Nd = 1.138266$, $^{145}Nd/^{144}Nd = 0.348968$, $^{146}Nd/^{144}Nd = 0.724109$, $^{148}Nd/^{144}Nd = 0.243079$, $^{150}Nd/^{144}Nd = 0.238581$ (McCulloch and Wasserburg, 1978a) and an atomic weight of 144.24 for Nd. For Sm we used an atomic weight of 150.35 and the isotopic composition reported by Russ et al. (1971) and Russ (1974); $^{144}Sm/^{154}Sm = 0.13516$, $^{147}Sm/^{154}Sm = 0.65918$, $^{149}Sm/^{154}Sm = 0.60750$, $^{150}Sm/^{154}Sm = 0.32440$, $^{152}Sm/^{154}Sm = 1.17537$. [b]Unspiked samples normalized to $^{150}Nd/^{142}Nd = 0.2096$. [c]Reported errors are 2σ of the mean. [d]Weight of dissolved sample.

Table 3.2. Results for non-radiogenic Nd isotopes.[a]

Sample	ε_{142}	ε_{145}	ε_{146}	ε_{148}
I. Murchison				
#1-ALIQ-2	-0.4±0.4	+0.6±0.7	+0.5±0.7	-0.7±1.1
ALIQ-3	-0.5±0.4	-0.8±0.6	-	-1.0±0.7
#2	-0.2±0.5	+0.5±0.9	-	-0.4±1.6
II. Allende				
ALIQ-2	0.0±0.4	+0.4±0.5	0.0±0.5	+0.5±1.0
ALIQ-2	+0.1±0.6	+0.1±0.5	0.0±0.5	+0.7±0.6
III. Guareña				
	+0.3±0.4	-0.9±0.6	-	-0.3±0.9
IV. Peace River				
ALIQ-2	+0.4±0.4	+0.1±0.7	-0.6±0.7	-0.1±1.0
V. St. Severin				
Light	-0.2±0.4	+0.3±0.5	-	+0.2±1.1
VI. Juvinas				
ALIQ-1	-0.1±0.4	+0.1±0.5	-	+0.1±0.8

[a] ε-values are given as deviations in parts in 10^4 relative to the grand mean of terrestrial normals given in Table 1. Reported errors are 2σ of the mean.

Fig. 3.2. Sm-Nd evolution diagram for chondrite samples and Juvinas. A reference line with a slope of 4.6 AE is shown. The dashed lines represent the new values selected for average chondrites (CHUR).

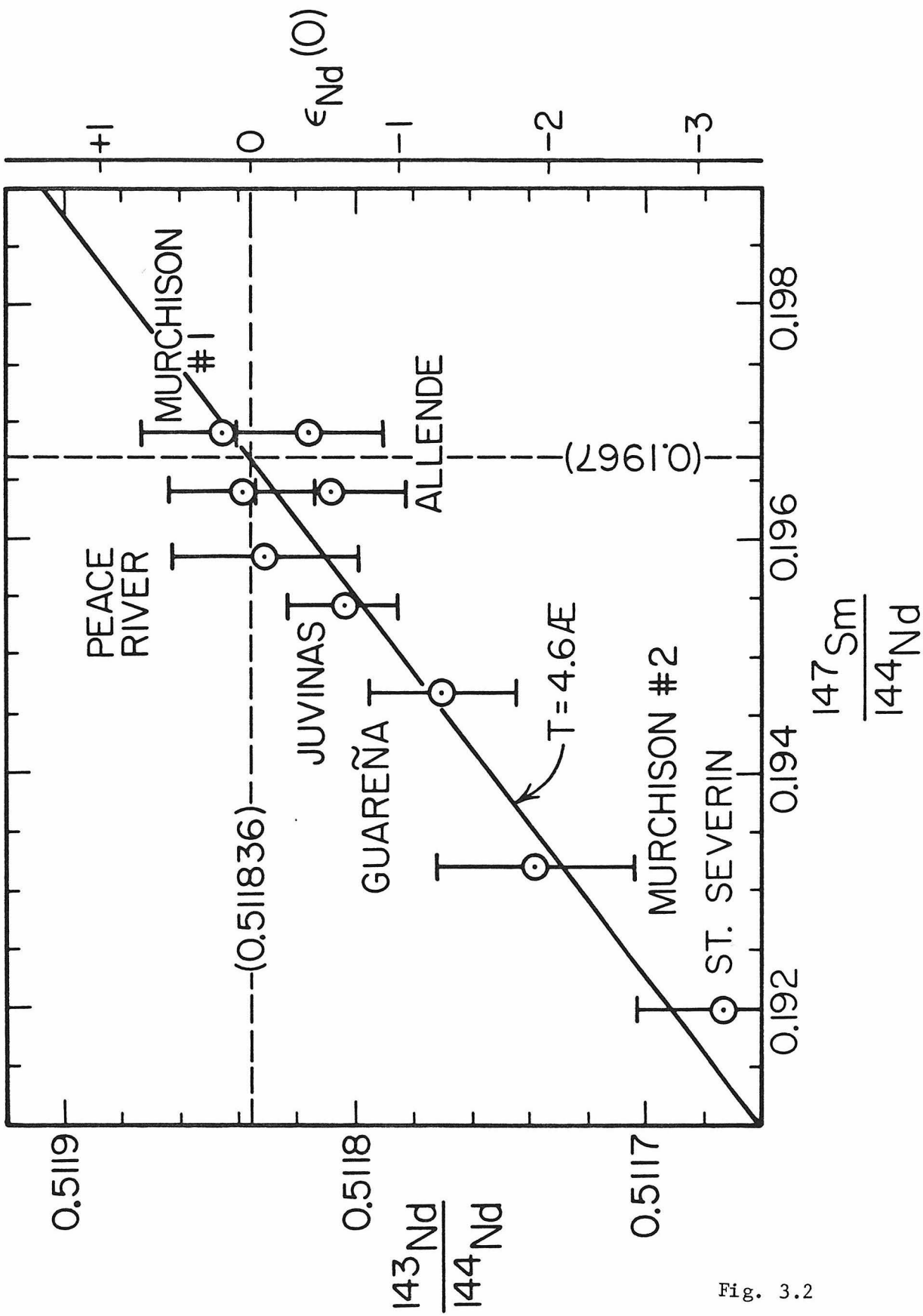
+1
0
−1
−2
−3
$\epsilon_{Nd}(0)$
MURCHISON #1
ALLENDE
PEACE RIVER
JUVINAS
GUAREÑA
T=4.6Æ
MURCHISON #2
ST. SEVERIN
(0.511836)
(0.1967)
0.5119
0.5118
0.5117
$\frac{143Nd}{144Nd}$
0.192
0.194
0.196
0.198
$\frac{147Sm}{144Nd}$

Fig. 3.2

3.4 ε-units in $^{143}Nd/^{144}Nd$ and 2.6% in $^{147}Sm/^{144}Nd$ and there is no evidence of large variations. If all chondrites are isochronous and from an isotopically uniform source, they should today lie on a line with a slope of 4.6 AE in a Sm-Nd evolution diagram. Insofar as there is variation in the Sm/Nd ratio between chondrite samples, there is no unique way of picking a set of values for $^{143}Nd/^{144}Nd$ and $^{147}Sm/^{144}Nd$ as representing the true solar ratio. The best we can do from the data is to pick a single set of reference values for $^{143}Nd/^{144}Nd$ and $^{147}Sm/^{144}Nd$ today that are consistent with the data array in Fig. 3.2. The approach used here will be to define the best present-day "solar" reference values rather than initial value $I_j^{Nd}(T_C)$ since the initial state is not well constrained. This follows the view adopted by DePaolo and Wasserburg [1976a] who referred evolution curves to determinations of the modern values rather than the derived initial values. For simplicity the approach we have chosen is the modern value for $^{143}Nd/^{144}Nd = 0.511836$, which is the currently used value for CHUR, as this will cause the least shift in the data representations and is fully consistent with the chondritic values. The corresponding $^{147}Sm/^{144}Nd$ ratio on the reference isochron is 0.1967 and lies between the data for Allende and one of the Murchison samples. This is also very close to the average $^{147}Sm/^{144}Nd$ of chondrites discussed earlier. Including the new data in Table 3.1 there are now 61 determinations of $^{147}Sm/^{144}Nd$ in bulk chondrite samples by isotope dilution. All these data are shown in a histogram in Fig. 3.3. As shown the value we have chosen lies close to the peak of the histogram. The previously published data are not accurate to better than about ±2% and most of the data

Fig. 3.3. Histogram showing all available $^{147}Sm/^{144}Nd$ ratios (N = 61) for chondritic meteorites determined by isotope dilution methods. The ratios from previously published REE studies on chondrites [Tanaka and Masuda, 1973; Masuda et al., 1973; Nakamura, 1974; Notsu and Mabuchi, 1975; Schnetzler and Bottino, 1971; Gast et al., 1970; Evensen et al., 1978] are probably accurate to ~2%. Chondritic meteorites show a large range in $^{147}Sm/^{144}Nd$, with most of the data in the range from 0.188 to 0.206. The value selected for average chondrites of 0.1967 is close to the peak of the histogram and is shown by the arrow. The $\varepsilon_{Nd}(0)$ value calculated assuming T_C = 4.6 AE is shown on the top of the figure. It is evident from these data that a total rock isochron for chondrites may be determined.

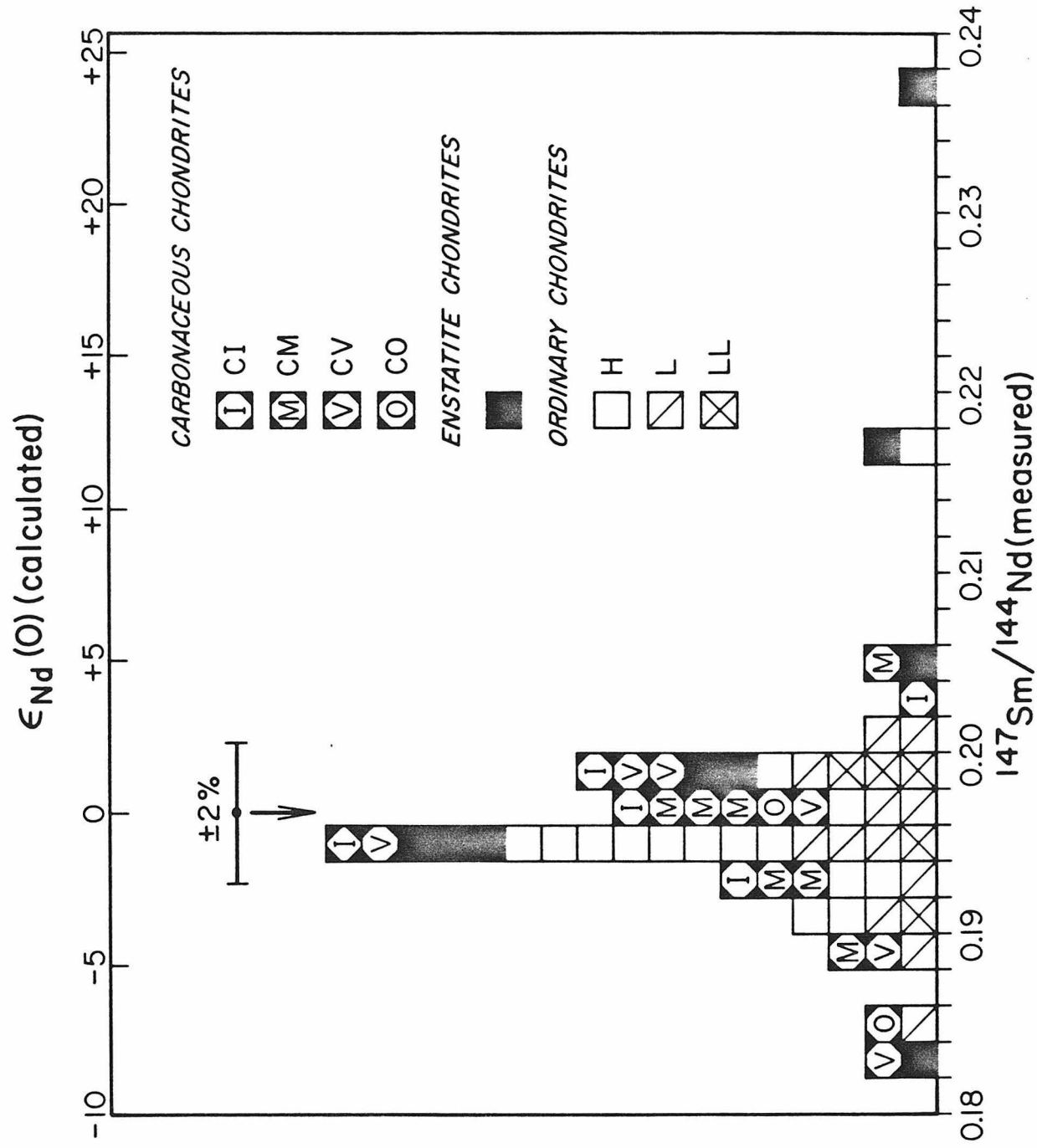
ϵ_{Nd} (0) (calculated)
+25
+20
+15
+10
+5
0
-5
-10
0.24
0.23
0.22
0.21
0.20
0.19
0.18
$^{147}Sm/^{144}Nd$(measured)
±2%
CARBONACEOUS CHONDRITES
CI
CM
CV
CO
ENSTATITE CHONDRITES
ORDINARY CHONDRITES
H
L
LL

Fig. 3.3

actually are within 2% of the average value chosen for chondrites. However, clear exceptions occur especially for the E-chondrites which show a variation in $^{147}Sm/^{144}Nd$ from 0.183 to 0.236. In general, the $^{143}Nd/^{144}Nd$ chosen here is close to that of Lugmair, Marti, Kurtz, and Scheinin [1976] for Juvinas, however the Sm/Nd ratio is 1.6% higher.

3.1.3. Comparison with previously published data

Previously published data on basaltic achondrites that fall in the neighborhood of our chondrite data are shown (Fig. 3.4) together with our new data on chondrites and Juvinas. The isochrons of ADOR and Moama are also shown, although all the data for these meteorites plot far outside the diagram. Let us first compare the Juvinas total rock data from various laboratories. The first report was by Notsu, Mabuchi, Yoshioku, Matsuda, and Ozima [1973] who presented some rather approximate data. The first high-precision data were published by Lugmair [1974] and Lugmair, Scheinin, and Marti [1975a]. The total rock value used by Lugmair, Scheinin, and Marti [1975b] (L1) is about 3.8 ε-units above our 4.6 AE reference line. A revised value (L2) with the same Sm/Nd ratio was reported by Lugmair et al. [1976] and is still 1.9 ε-units above our reference line. Lugmair and Carlson [1978] reported a 1.4 ε-unit reduction in the measured $^{143}Nd/^{144}Nd$ ratio for their laboratory standard. They chose, however, to correct their new data such that they were compatible with their previously published data. Their currently measured Juvinas value (L3) should thus be 1.4 ε-unit lower and as shown in Fig. 3.4 this value is within error of our 4.6 AE reference line. The values obtained by Nakamura, Tatsumoto, Nunes, Unruh, Schwab, and Wildeman [1976] for Juvinas plot distinctly higher.

Fig. 3.4. Sm-Nd evolution diagram comparing new chondrite data (black dots) and the Juvinas value with previously published data for achondrites. The points labelled L1, L2, and L3 represent three successive versions of the Juvinas total rock value by Lugmair et al. [1975, 1976] and Lugmair and Carlson [1978].

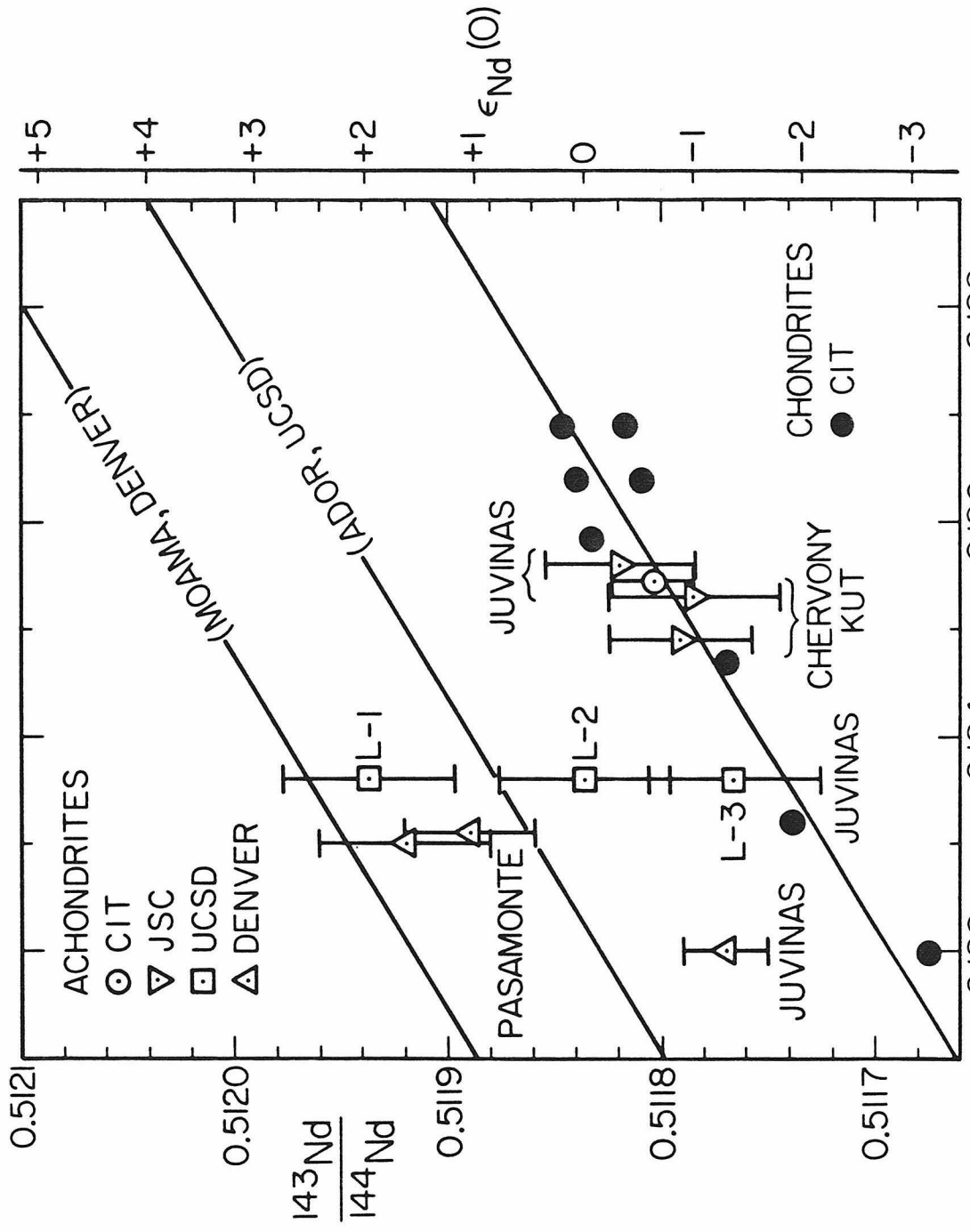
+5
+4
+3
+2
+1
0
-1
-2
-3
$\epsilon_{Nd}(0)$
0.5121
0.5120
0.5119
0.5118
0.5117
$\frac{143Nd}{144Nd}$
0.192
0.194
0.196
0.198
$\frac{147Sm}{144Nd}$
(MOAMA, DENVER)
(ADOR, UCSD)
ACHONDRITES
CIT
JSC
UCSD
DENVER
L-1
L-2
L-3
PASAMONTE
JUVINAS
JUVINAS
JUVINAS
CHERVONY KUT
CHONDRITES
CIT

Fig. 3.4

Their value is the same as L3 for $^{143}Nd/^{144}Nd$ but has a lower Sm/Nd ratio. Recently Nyquist, Shih, Wooden, Bansal, and Wiesman [1979] published data on Juvinas which agree with the measured (not corrected) $^{143}Nd/^{144}Nd$ L3 ratio by Lugmair and the value by Nakamura et al. [1976] but with a significantly higher $^{147}Sm/^{144}Nd$ ratio. Data on Juvinas by Nyquist et al. [1979] and the data obtained independently here agree to within 1‰ for $^{147}Sm/^{144}Nd$ and 0.3 ε-units for $^{143}Nd/^{144}Nd$. It would appear that the Juvinas data of Nakamura et al. [1976] and the revised data (L3) of Lugmair and Carlson [1978] are consistent with the $^{143}Nd/^{144}Nd$ obtained by Nyquist et al. [1979] and the data presented here, but their $^{147}Sm/^{144}Nd$ ratios are significantly lower and suggest an error in tracer calibrations by these workers. The data for Pasamonte [Unruh, Nakamura, and Tatsumoto, 1977], Moama [Hamet, Nakamura, Unruh, and Tatsumoto, 1978], and ADOR [Lugmair and Marti, 1977] also lie significantly above the 4.6 AE reference line (Fig. 3.4). Comparison between the results of Nyquist et al. [1979] and the data presented here on achondrites seems to be confirmatory. Note, however, that Nyquist et al. [1979] obtained metals for tracer calibration from the same source that this laboratory has been using (Ames Laboratory, Iowa), so both laboratories could have the same systematic errors in tracer calibrations. The normal values measured for $^{142}Nd/^{144}Nd$, $^{150}Nd/^{144}Nd$ reported by Nyquist et al. [1979] differ significantly from the values obtained in this laboratory while the remaining isotope ratios show good agreement. Thus the results from these two laboratories are not as consistent as might be believed. It is apparent that the actual cause of all the above discrepancies must be resolved before any progress can be made in interlaboratory comparisons. Using two different mass

spectrometers in this laboratory for hundreds of Nd analyses, no shift has been observed in the values of the nonradiogenic Nd isotopes over the past five years. In the same period, three different Nd and three different Sm tracer calibrations show no discrepancies exceeding 1‰. Nd was measured as NdO^+ so if the oxygen isotope composition used to reduce the data is incorrect then our data will be systematically biased [Papanastassiou et al., 1977]. Unless this procedure is subject to serious problems, it is considered that the measurements presented here are reliable and provide reasonable and consistent values for the chondritic $^{143}Nd/^{144}Nd$ and $^{147}Sm/^{144}Nd$ today and may be used as the basis for calculating the CHUR curve.

3.1.4. Initial values

The $^{143}Nd/^{144}Nd$ in CHUR as a function of time in the neighborhood of 4.5 AE is shown in Fig. 3.5. Assuming that a meteorite formed from this reservoir at T = 4.6 AE, it should have an initial $^{143}Nd/^{144}Nd$ value of 0.505829. Note that $^{143}Nd/^{144}Nd$ changes by 1 ε-unit in 39 m.y. The timescale for condensation and chemical fractionation from the solar nebula is probably on the order of only a few million years as suggested by the presence of ^{26}Al [Lee, Papanastassiou, and Wasserburg, 1976, 1977]. If the ^{26}Al is the cause of widespread heating and differentiation of small parent bodies, then these planets must have accreted within ~2 m.y. of the time of condensation from the solar nebula [Wasserburg et al., 1977]. Chondrites (e.g., Allende) exist that appear to preserve direct early condensates from the solar nebula which are only partly affected by later metamorphism. A reliable value for the solar system initial Nd value may be gotten if it is possible to obtain precise ages (±10 m.y.) and initial values to ±0.3 ε-units on such

Fig. 3.5. The $^{143}Nd/^{144}Nd$ value in CHUR is shown as a function of age in the neighborhood of 4.6 AE. If a solid object condensed from the solar nebula at 4.6 AE ago, it would have an initial $^{143}Nd/^{144}Nd$ ratio of 0.505829. Note the shift in $^{143}Nd/^{144}Nd$ for a change in choice of age.

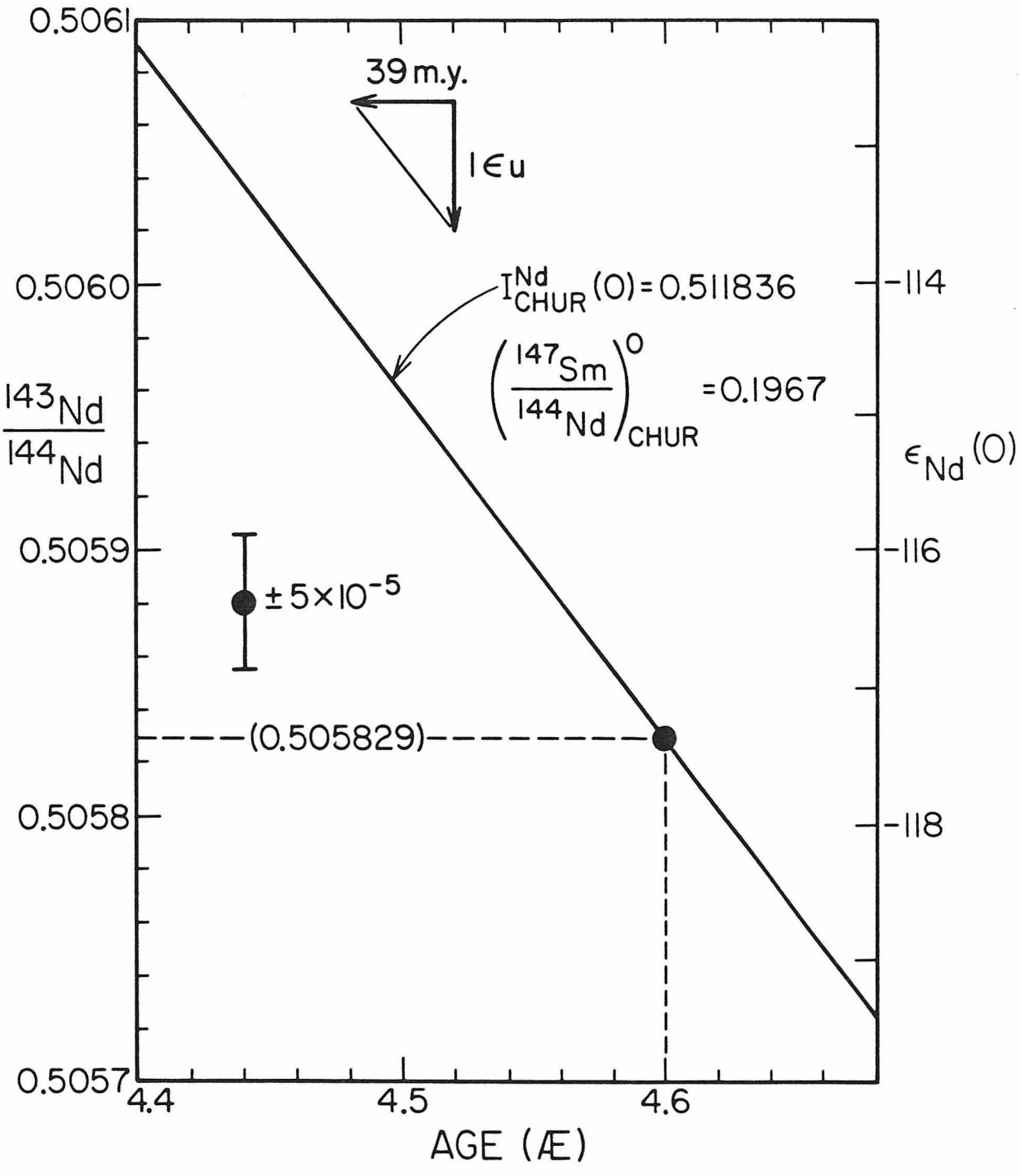
0.5061
0.5060
0.5059
0.5058
0.5057
143Nd/144Nd
39 m.y.
1εu
I^Nd_CHUR(0)=0.511836
(147Sm/144Nd)^0_CHUR =0.1967
±5×10^-5
(0.505829)
-114
-116
-118
εNd(0)
4.4
4.5
4.6
AGE (Æ)

Fig. 3.5

samples with an internal mineral isochron. If large planetary objects took 10^8 years to form as suggested by Safronov [1969], Tera and Wasserburg [1974], and Gancarz and Wasserburg [1977], then the initial $^{143}Nd/^{144}Nd$ could be 2.5 ε-units higher than that from the early condensates from the solar nebula. Although the initial state is not well known, one may in principle pick any set of self-consistent initial $^{143}Nd/^{144}Nd$, age and Sm/Nd ratio that plot on the CHUR curve as reference values to describe the CHUR evolution curve instead of the present-day values we are using. In absence of directly measured initial solar values [i.e., $T_C, I_{\odot}^{Nd}(T_C)$], it is important to pick a set of reference values which the solar system is believed to have passed through and that is prior to planetary differentiation processes. Model ages [cf. Wasserburg and Papanastassiou, 1975] may be calculated relative to such a chosen initial Nd value ($I^{Nd}(T_C)$) for the solar system

$$T_M^{Nd} = \frac{1}{\lambda} \ln \left[1 + \frac{(^{143}Nd/^{144}Nd)_{MEAS} - I_{\odot}^{Nd}(T_C)}{(^{147}Sm/^{144}Nd)_{MEAS}} \right] \qquad (3.2)$$

and should be compared to the corresponding initial time T_C on the CHUR curve. The values may be picked as shown in Fig. 3.5 as T_C = 4.6 AE and $I_{\odot}(T_C)$ = 0.505829. Samples which have T_M^{Nd} close to T_C may represent ancient materials with a simple history. If $T_M^{Nd} \gg T_C$ or $T_M^{Nd} \ll T_C$, then this demonstrates open system behavior at times less than 4.6 AE. The model age T_M^{Nd} is a strict upper limit to the last time of disturbance of the system. As chemical fractionation for Sm relative to Nd is often small for total rocks, the T_M^{Nd} model ages are currently of far less utility than corresponding model ages for the Rb-Sr system

where large chemical fractionations are common.

Hamilton, O'Nions, Evensen, Bridgwater, and Allaart [1978] have chosen an initial state using the initial Nd from ADOR and the age of ADOR together with average Sm/Nd determined from REE-studies of chondrites by Evensen et al. [1978] as a reference value for the CHUR curve. This selection is inconsistent with the new CHUR curve presented here due to the fact that the ADOR initial value does not plot on it.

3.1.5. Conclusions

From the data presented it is concluded that a self-consistent set of average present-day values for chondritic meteorites are $^{143}Nd/^{144}Nd$ = 0.511836 and $^{147}Sm/^{144}Nd$ = 0.1967. $^{143}Nd/^{144}Nd$ changes by 1 ε-unit in 39 m.y. in CHUR so the uncertainty in the initial time makes it difficult at present to know the initial solar value for $^{143}Nd/^{144}Nd$ precisely. These values are not consistent with most previously published achondrite data, but are consistent with achondrite data presented here and those reported by Nyquist et al. [1979]. The presence of inter-laboratory discrepancies in meteorite data is evident and may be due to errors in Sm and Nd spike calibrations or to measurement of isotopic abundances.

3.2. THE BAY OF ISLANDS OPHIOLITE

Most geologists now agree upon an oceanic origin for the ophiolites found in many mountain belts. Ophiolites are believed to be pieces of oceanic crust and mantle emplaced on the continent during the early stages of orogenesis resulting from plate collision. Studies of thickness, structure, seismic wave velocities, and geochemistry of

ophiolite suites indicate a close analogy between ophiolites and oceanic crust and mantle formed at midocean ridges [for a review see Coleman, 1977]. Spreading plate margins occur also in small ocean basins and these are of considerable importance as proposed origins of ophiolite complexes [Dewey and Bird, 1971; Karson and Dewey, 1978]. A Nd and Sr isotopic study of an early Paleozoic ophiolite, the Bay of Islands Complex, has therefore been carried out in order to:

(1) characterize the source of magmas which formed this ophiolite,

(2) determine if these magmas were derived from a mantle reservoir similar to that of MORB,

(3) determine the age by the internal Sm-Nd mineral isochron method and establish whether or not a Sm-Nd whole rock isochron exists for the complex.

3.2.1. Enrichment factors for Rb/Sr and Sm/Nd

For the interpretation of Nd and Sr isotopic data on MOR basalts and ophiolites, it is of importance to have good estimates of $f^{Rb/Sr}$ and $f^{Sm/Nd}$ in their sources. The average values for the oceanic crust may presumably be taken as the average value for the present day MORB source. The average of individual ophiolites may be taken as estimates for their sources. This should be a good approximation as the harzburgite residue left in the mantle after production of MOR tholeiite magmas contains insignificant amounts of LIL elements [see Appendix 2]. Oceanic gabbros and ophiolitic gabbros give an average $f^{Rb/Sr} = -0.95 \pm 0.05$ [Kay et al., 1970; Spooner et al., 1977; this work, Table 3.3]. The average value for unaltered normal MORB is $f^{Rb/Sr} = -0.8 \pm 0.1$. The average Sr

concentration is about 100 ppm in both the upper (basalt and dolerite) and the lower (gabbro) oceanic crust which as a final result gives an average value for oceanic crust of $f^{Rb/Sr} = -0.9^{+0.1}_{-0.05}$. From the data in Table 3.3 this f-value also seems to apply to the Bay of Islands Complex. The average of 30 normal MOR basalts gives $f^{Sm/Nd} = +0.12$ and Nd = 6.5 ppm [Kay et al., 1970; O'Nions et al., 1977; Carlson et al., 1978] and the average of 6 oceanic gabbros [Masuda and Jibiki, 1973; Kay et al., 1970] gives $f^{Sm/Nd} = +0.42$ and Nd = 3.3 ppm. Similar estimates are indicated from data on ophiolites [Montigny et al., 1973; Kay and Senechal, 1976]. The average for the Bay of Islands Complex appears to be $f^{Sm/Nd} \approx +0.2$ from the data in Table 3.3 and the REE patterns of Malpas [1978]. Assuming that the lower half of the oceanic crust is made of gabbro this gives $f^{Sm/Nd} = +0.22$ and (Sr/Nd) ≈ 22 for the average oceanic crust.

3.2.2. Age and initial Nd and Sr

Using the ^{147}Sm-^{143}Nd method on two unaltered gabbro samples BMD-2A and BMD-7, an attempt has been made to determine the crystallization age. The difficulty of obtaining precise dates on old terrestrial mafic and ultramafic rocks is well known. Other methods (K-Ar, Rb-Sr, U-Th-Pb) are much more susceptible to element redistribution subsequent to the time of crystallization and in many cases give a metamorphic age or intermediate ages of doubtful meaning rather than the time of crystallization. Using these methods it is often necessary to use minor phases and/or associated differentiated rocks whose relationship to the mafic/ultramafic rocks is difficult to establish unequivocally.

However, with the Sm-Nd method, it is possible to directly determine the crystallization age of major mafic/ultramafic igneous rocks. Sufficiently large differences in Sm/Nd ratios exist between plagioclase and pyroxene, which are the most common phases in gabbroic rocks, such that the Sm-Nd system can be used to obtain precise ages for most gabbroic rocks.

The Sm-Nd data for BMD-2A and BMD-7 are given in Appendix 2. The data for BMD-2A define an age of 508±6 m.y. and initial $^{143}Nd/^{144}Nd$ of $\varepsilon_{Nd} = +7.9\mp0.1$ but only show a relatively small range in $^{143}Nd/^{144}Nd$ of ~ 6 ε-units. The small uncertainty given by a York [1966] fit is due to the fact that the three data points are centered on the isochron to within 0.1 ε-units. The total rock points have higher concentration of Nd than both the pyroxene and plagioclase so it seems unlikely that the line is a two component mixing line. To confirm this age a second pyroxene gabbro was analyzed. The plagioclase and the pyroxene show a much larger spread in $^{147}Sm/^{144}Nd$ (0.099-0.31) than that of BMD-2A. BMD-7 yield an age of 501±13 m.y. and an initial $\varepsilon_{Nd} = 7.7\mp0.2$. The large range of ~ 14 ε-units permits this precise age determination. The concordant Sm/Nd ages for the two pyroxene gabbros strongly indicate that this is the time of crystallization. Insofar as the mobility of Sm and Nd during metamorphism and weathering is negligible and since the data were obtained on primary magmatic phases, these ages are interpreted to be the crystallization age of the gabbro at the time of its emplacement in the oceanic crust. A nominal age of 505 m.y. is assigned to both samples. An internal isochron is used here, since ages obtained by total rock isochrons depend on the assumption that all

the rocks had the same initial isotopic composition and age. This would not be expected to be a problem for minerals from a single total rock sample. The internal isochron has the disadvantage that later metamorphism is more likely to cause isotopic equilibration on the scale of minerals than on the scale of total rocks. Therefore data from several other total rock samples are compared with the internal isochron (Fig. 3.6). One two-pyroxene gabbro plots off the isochron by ~ 1.1 ε-units and must represent a distinctly different age or initial value. The other samples plot on the mineral isochron. The harzburgite BMD-18A is compatible with the mineral isochron, but the $^{143}Nd/^{144}Nd$ ratio is much less precise as it was measured on 1 ng of Nd and no firm conclusion can be drawn, other than that it is not grossly aberrant.

The initial ε_{Nd} values for all samples are given for a nominal age of 505 m.y. in Table 3.3. The initial ε_{Nd} is in the range from +7.2 to +8.3 for metagabbro, trondhjemite, and metadolerite samples. The pillow basalt sample has a $^{147}Sm/^{144}Nd$ ratio which is very near to chondritic so the initial value for this sample relative to the CHUR evolution line can be established as $\varepsilon_{Nd} = +7.8\pm0.3$, essentially independent of its age. The orthopyroxenite layer (BMD-17) from the harzburgite has a similar value of $\varepsilon_{Nd} = +7.6\pm0.8$. This indicates that the harzburgite is cogenetic with the remaining part of the ophiolite and supports the hypothesis that the harzburgite represents residual mantle remaining from the partial melting which produced the rest of the ophiolite. If it is assumed that BOI-62B has the same age, we obtain a distinctly lower initial value of $\varepsilon_{Nd} = +6.7\pm0.4$. The observed

Table 3.3. Evolutionary parameters for Nd and Sr.[a]

Sample	$f^{Rb/Sr}$	ε_{Sr}	$f^{Sm/Nd}$	ε_{Nd}
I. Pillow lavas				
BMD-24-TR	-0.7625	+6.2±0.3	-0.0173	+7.8±0.3
II. Sheeted dikes				
BMD-10-TR	-0.6670	+15.4±0.4	+0.0321	+8.3±0.5
BMD-12A-TR	-0.7971	+17.1±0.3	+0.0276	+8.3±0.5
III. Trondhjemite				
BMD-14	-0.4892	+32.5±0.6	-0.0969	+7.2±0.5
IV. Gabbros				
BMD-8	-0.8497	+23.0±0.4	+0.0682	+7.9±0.5
	-	-	-	+7.4±0.3
BMD-2A-TR	-0.9817	-19.6±0.7	+0.3585	+7.9±0.6
BMD-2A-CPX	-0.9677	-19.1±0.6	+0.4232	+7.9±0.3
BMD-2A-PLAG	-0.9919	-19.3±0.3	-0.0729	+7.9±0.7
BOI-62B-TR-A	-0.9634	-10.7±0.6	+0.3911	+6.7±0.4
	-	-	-	+6.7±0.4
BOI-62B-TR-B	-	-	+0.3899	+6.9±0.5
BMD-7-CPX	-0.7920	-16.7±0.4	+0.5641	+7.5±0.4
	-	-	-	+7.6±0.6
BMD-7-PLAG	-0.9512	-16.8±0.3	-0.4960	+7.7±0.5
	-	-	-	+7.7±0.4
V. Harzburgite				
BMD-17-TR	+6.057	-0.9±0.6	-0.0517	+7.6±0.8
BMD-18A-TR	+65.32	-171.6±16.0	-0.1371	+3.4±11.7

[a] ε-values calculated for an age of 505 m.y.

inhomogeneity in initial Nd in this complex obviously makes precise age determinations by whole-rock measurements difficult. Although field and petrologic evidence may suggest that all the samples appear to be differentiation products of the same magma, the data require that the parent magma was isotopically inhomogeneous due to contamination or that the complex is the result of multiple injection from mantle sources with variable Nd isotopic composition.

The Rb-Sr data are also given in Appendix 2 and the ε_{Sr}-values are given for a nominal age of 505 m.y. in Table 3.3. The data for the gabbros, dolerites, and pillow-basalts are shown in Fig. 3.7. They all have very low $^{87}Rb/^{86}Sr$ ratios (< 0.02) and would not have changed their $^{87}Sr/^{86}Sr$ due to <u>in situ</u> decay of ^{87}Rb by any substantial amount. It is clear that the different total rock samples show a wide scatter on the Rb-Sr evolution diagram. Samples of minerals and total rock from the fresh gabbro BMD-2A give measured $^{87}Sr/^{86}Sr$ ratios which are all the same within error. The clinopyroxene has the highest $^{87}Rb/^{86}Sr$ ratio of 0.0027. The total evolution in $^{87}Sr/^{86}Sr$ for this phase in 505 m.y. is 0.3 ε-units, so an estimate of the age cannot be obtained from these data. The initial $^{87}Sr/^{86}Sr$ value is 0.70254±2 or $\varepsilon_{Sr} = -19.3\pm0.3$. For BMD-7 both clinopyroxene and plagioclase give the same initial $^{87}Sr/^{86}Sr$ ratios of 0.70272±2 or $\varepsilon_{Sr} = -16.8\pm0.3$. Since the minerals would have different susceptibilities to Sr migration and have the same ε_{Sr}, this is good evidence that we are measuring the Sr isotope composition of these rocks at the time of crystallization. The two-pyroxene gabbro BOI-62B also has a very low $^{87}Rb/^{86}Sr$ ratio of ~ 0.003

and gives an initial $^{87}Sr/^{86}Sr$ of 0.70315±4. This is higher than that of BMD-2A and BMD-7, and since the sample shows only minor signs of alteration we take this to indicate a significantly different initial Sr value from the two other samples. The difference in $^{87}Sr/^{86}Sr$ cannot be due to an age difference. It appears that the three pyroxene gabbros show significant differences in initial Sr. BOI-62B also shows a significantly different initial Nd from those of BMD-7 and BMD-2A.

Sr analyses were carried out also on samples of metagabbro, trondhjemite, metadolerite, and pillow basalt which had obviously been subject to hydrothermal metamorphism. These samples give a wide spread in ε_{Sr} from +6.2 to +32.5 which is very different from the tightly clustered ε_{Nd} data. Note that the ε_{Sr}-values in general show an increase with the degree of metamorphism and alteration. This further demonstrates the much larger mobility of Rb-Sr compared to Sm and Nd during hydrothermal and metamorphic processes as has been evident from previous studies. This is most likely due to the lower solubility of REE in aqueous solutions and the difference in diffusivity in the solid phases, as compared to Rb-Sr.

3.2.3. Strontium isotope contamination

Isotopic studies of ocean-floor basalts and of young ophiolites have clearly demonstrated that $^{87}Sr/^{86}Sr$ in altered samples generally has been increased due to interaction with seawater [Dasch *et al.*, 1973; Hart *et al.*, 1974; Spooner *et al.*, 1977; McCulloch *et al.*, 1980].

Rocks from the Bay of Islands Ophiolite have a range of 1.6 ε-units in initial Nd while the initial ε_{Sr} values show a range of

Fig. 3.6. Sm-Nd evolution diagram showing the data for whole-rock samples of pillow basalt, sheeted dikes, trondhjemite, gabbros, and an orthopyroxenite layer in the harzburgite. The 508 m.y. mineral isochron for BMD-2A is shown for reference. All the data do not fit the isochron. Note that BOI-62B does not lie on the mineral isochron and indicates a distinctive initial value. The data point for the orthopyroxenite BMD-17 indicates that the harzburgite is cogenetic with the upper mafic part of the ophiolite.

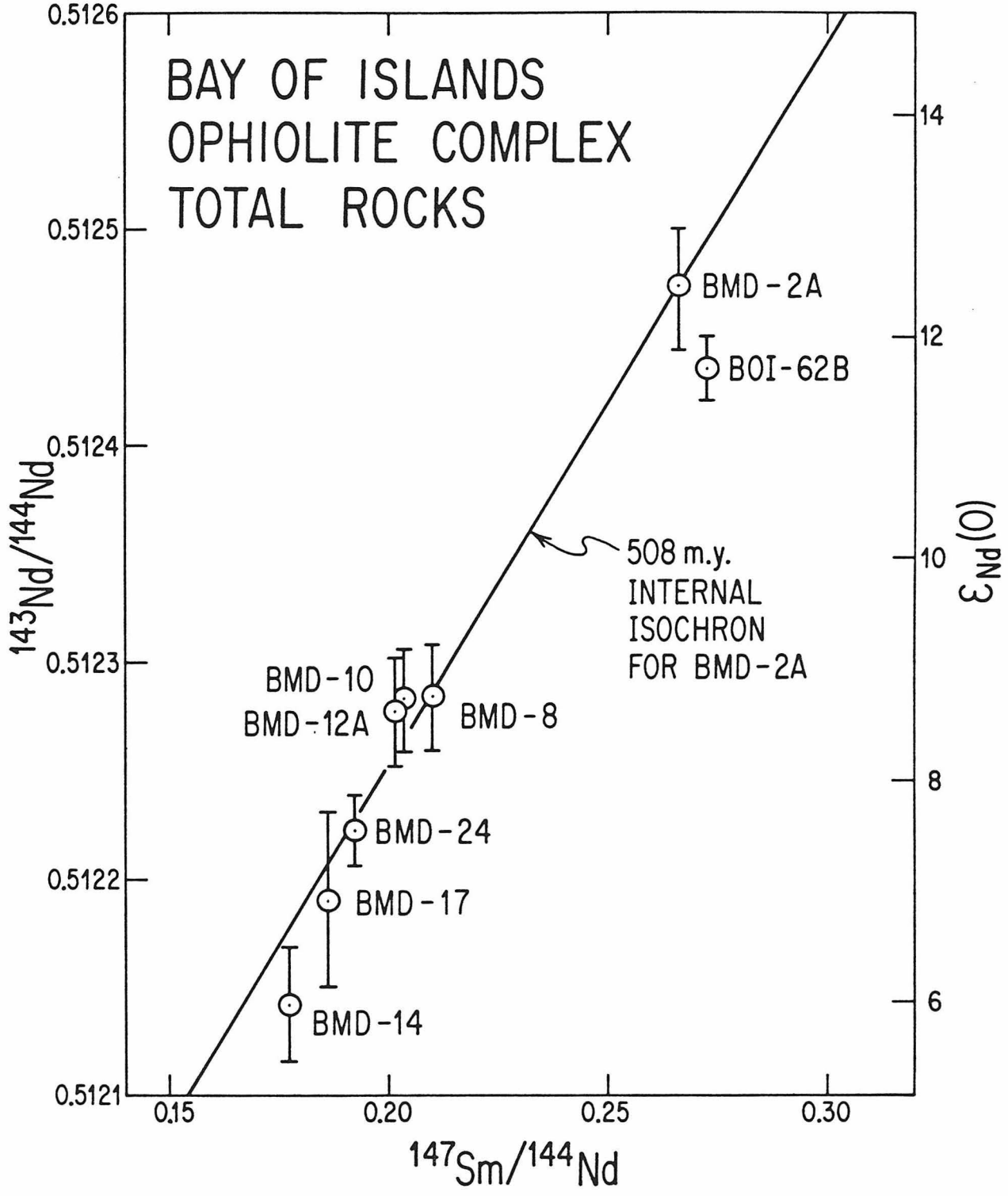
BAY OF ISLANDS
OPHIOLITE COMPLEX
TOTAL ROCKS
BMD-2A
BOI-62B
508 m.y.
INTERNAL
ISOCHRON
FOR BMD-2A
BMD-10
BMD-12A
BMD-8
BMD-24
BMD-17
BMD-14
0.5126
0.5125
0.5124
0.5123
0.5122
0.5121
0.15
0.20
0.25
0.30
14
12
10
8
6
$^{143}Nd/^{144}Nd$
$^{147}Sm/^{144}Nd$
$\varepsilon_{Nd}(0)$

Fig. 3.6

Fig. 3.7. Rb-Sr evolution diagram showing the mineral and total rock data for samples from the Blow-Me-Down massif. Reference lines with slopes corresponding to the Sm/Nd age are shown. Note the wide range in initial $^{87}Sr/^{86}Sr$ for different samples and the implied range in initial strontium.

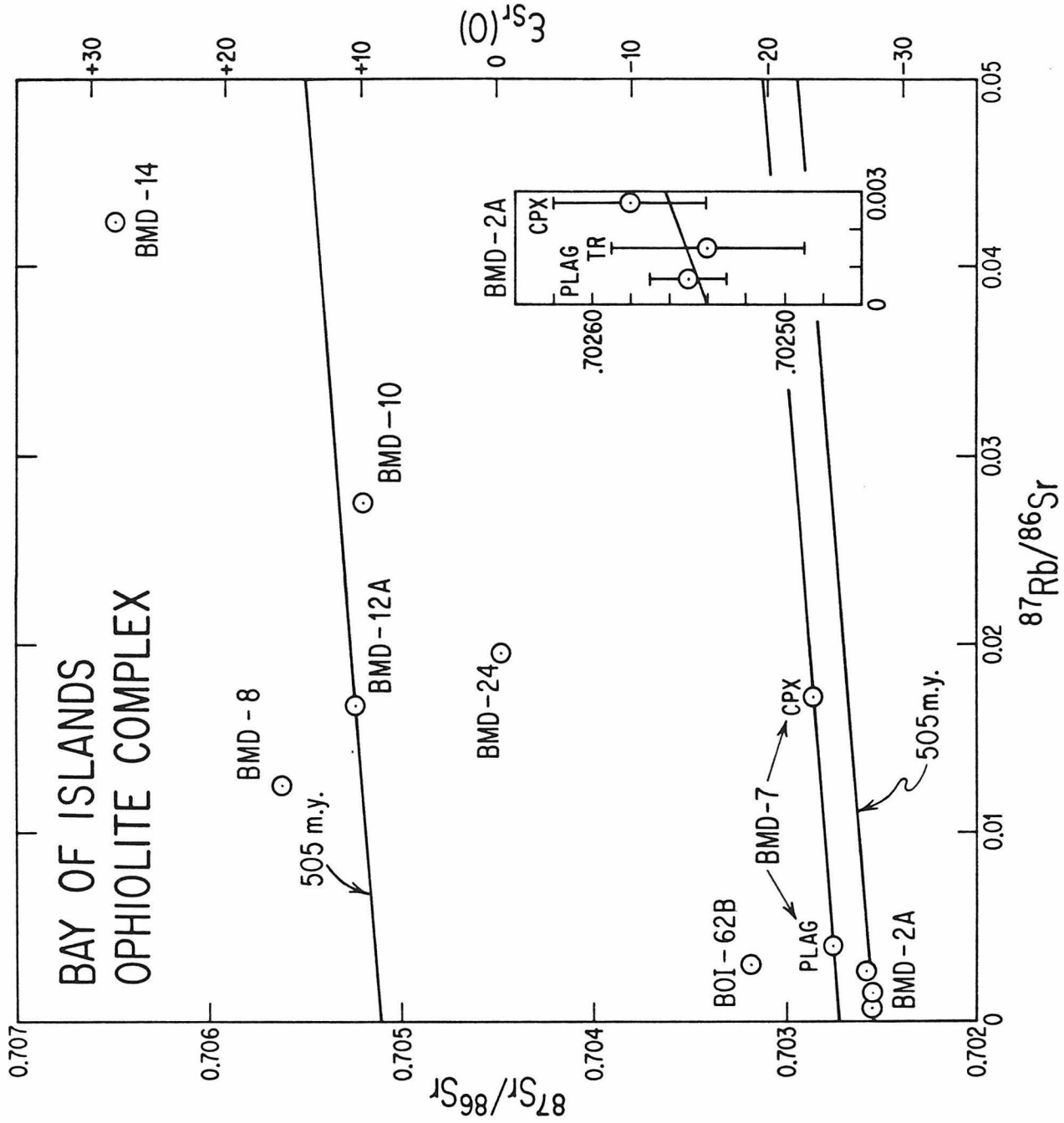
BAY OF ISLANDS
OPHIOLITE COMPLEX
BMD-14
BMD-8
505 m.y.
BMD-12A
BMD-10
BMD-24
BMD-2A
CPX
PLAG
TR
BOI-62B
BMD-7
CPX
PLAG
505m.y.
BMD-2A
$\varepsilon_{Sr}(0)$
$^{87}Sr/^{86}Sr$
$^{87}Rb/^{86}Sr$

Fig. 3.7

52 ε-units. The initial magmatic $^{87}Sr/^{86}Sr$ is in the range ε_{Sr} = -19.3 to -10.7 on fresh gabbro samples. Higher ε_{Sr} values are associated with hydrothermally metamorphosed samples. Since there is a general increase in the ε_{Sr}-value with the degree of alteration, these higher values are attributed to contamination by seawater. The magnitude of the ε_{Sr} shifts is similar to that observed in the much younger Troodos ophiolite [Spooner et al., 1977].

The amount of seawater needed for the observed ε_{Sr} shift may be calculated. The volumetric water/rock ratio (=W/R) is given by

$$\frac{W}{R} = \frac{\varepsilon_{Sr} - \varepsilon^{B}_{Sr}}{\varepsilon^{SW}_{Sr} - \varepsilon_{Sr}} \frac{Sr_B}{Sr_{SW}} \rho \qquad (3.3)$$

where B denotes the unaltered sample and SW denotes seawater. We use ε^{B}_{Sr} = -19.3 and ε^{SW}_{Sr} = +72 [estimated for Cambrian seawater; Veizer and Compston, 1974], $\rho \simeq 3$ g/cm^3, and a Sr concentration of 7.9 ppm in seawater [Holland, 1978]. This model assumes 100% efficiency in Sr exchange and therefore gives a minimum water/rock ratio. The bulk seawater rock ratio for the metagabbro is thus at least ~ 130:1 and for the pillow basalt at least ~ 23:1.

Using the above mentioned parameters for Sr and assuming that Cambrian seawater has ε_{Nd} = -5 and a concentration of Nd = 3 x 10^{-6} ppm, the mixing curve between an uncontaminated rock (Nd = 8 ppm and Sr = 120 ppm) and seawater may be calculated. The shape of the mixing curve depends on the parameter $K^{R-W}_{Sr/Nd} = (Sr/Nd)_{ROCK}/(Sr/Nd)_{SEAWATER}$ = 5.7 x 10^{-6}. The mixing line in the ε_{Nd}-ε_{Sr} diagram is horizontal

almost until it reaches the seawater value for ε_{Sr} (Fig. 3.9). The water/rock ratios shown on the mixing line in Fig. 3.9 assume 100% efficiency of exchange for Nd and Sr. In this case the ε_{Nd} value cannot change significantly before the water/rock ratio is ~ 10^5.

Oxygen and Sr isotope data and Fe_2O_3/FeO^* ratios together with other geological evidence strongly suggest that the pervasive hydrothermal metamorphism observed in the pillow lavas and sheeted dikes of ophiolites occurred in a subseafloor geothermal system at a spreading center [Spooner et al., 1974; Spooner et al., 1977]. The Bay of Islands data indicate that similar geothermal systems may have been active in Cambrian ocean ridges. The upper oceanic crust (pillow lavas and sheeted dikes) seem to have been a sink for Sr from seawater throughout the Phanerozoic. This can result in recycling of continental Sr into the mantle in subducted oceanic slabs. Nd and Sr isotopic studies of some young island arc tholeiites and dacites [DePaolo and Wasserburg, 1977; Hawkesworth et al., 1977] suggest that they may be derived from altered oceanic crust since they plot to the right of the MORB field in an ε_{Nd}- ε_{Sr} diagram as do altered oceanic basalts. The data presented here suggest that this may be a characteristic of island arc rocks back to Cambrian times if they were derived by melting subducted oceanic slabs.

3.2.4. Observed ε_{Nd}-ε_{Sr} and their correlation

A histogram of ε_{Nd} for young oceanic and continental basalts and for the Bay of Islands Complex is shown in Fig. 3.8. The initial ε_{Nd} values for the Bay of Islands samples are in the range from +6.7 to +8.3 and lie slightly lower than for typical present-day mid-ocean

ridge tholeiites and are thus clearly distinct from continental flood basalts (CFB). The Nd isotopic affinity with oceanic basalts can easily be seen. Richard et al. [1978] have reported $\varepsilon_{Nd}(0)$ and $\varepsilon_{Sr}(0)$ values for some young ophiolitic gabbros that also indicate their oceanic nature.

The Bay of Islands Ophiolite data are plotted on an ε_{Nd}-ε_{Sr} correlation diagram to determine whether the regularities observed for young oceanic samples also apply to old samples (Fig. 3.9). Previous studies have shown that ε_{Nd} and ε_{Sr} correlate well, especially for ocean ridge and oceanic island basalts. This regularity does not appear to be valid for island arcs due to Sr contamination by seawater [DePaolo and Wasserburg, 1976b, 1977; Hawkesworth et al., 1977]. Mid-ocean ridge basalts have the highest ε_{Nd} and lowest ε_{Sr} and a restricted range of values. Ocean islands have somewhat lower ε_{Nd} and higher ε_{Sr}. The correlation is also valid for selected continental basalts. The CFB have ε_{Nd} in the neighborhood of zero but tend to spread out to very high ε_{Sr}-values and negative ε_{Nd} resulting from crustal contamination [DePaolo and Wasserburg, 1976b, 1979]. Fig. 3.9 shows the fields of various types of young basaltic rocks. The data for the pyroxene gabbros plot in the upper part of the oceanic island field and near the lower end of the MORB field. The field of island arc tholeiites also includes these data points. However, the structure and geochemistry of the Bay of Islands Complex strongly suggest that it formed at a chemically normal mid-ocean ridge. Total rock samples of pillow basalts, dolerites, hornblende gabbros, and trondhjemites have high ε_{Sr} values and plot to the right of the island arc field due to submarine hydrothermal

Figure 3.8. Histogram comparing initial ε_{Nd} values from the Bay of Islands Complex with values for young basalts. Data are from DePaolo and Wasserburg [1976a,b, 1977], Richard et al. [1976], O'Nions et al. [1977], Hawkesworth et al. [1977], and Carlson et al. [1978]. The Bay of Islands Complex clearly has an oceanic affinity. The average value (+7.8) is, however, somewhat smaller than the average value of MORB (+10). This is most likely due to differential evolution of the oceanic mantle relative to the bulk earth over the past 0.5 AE.

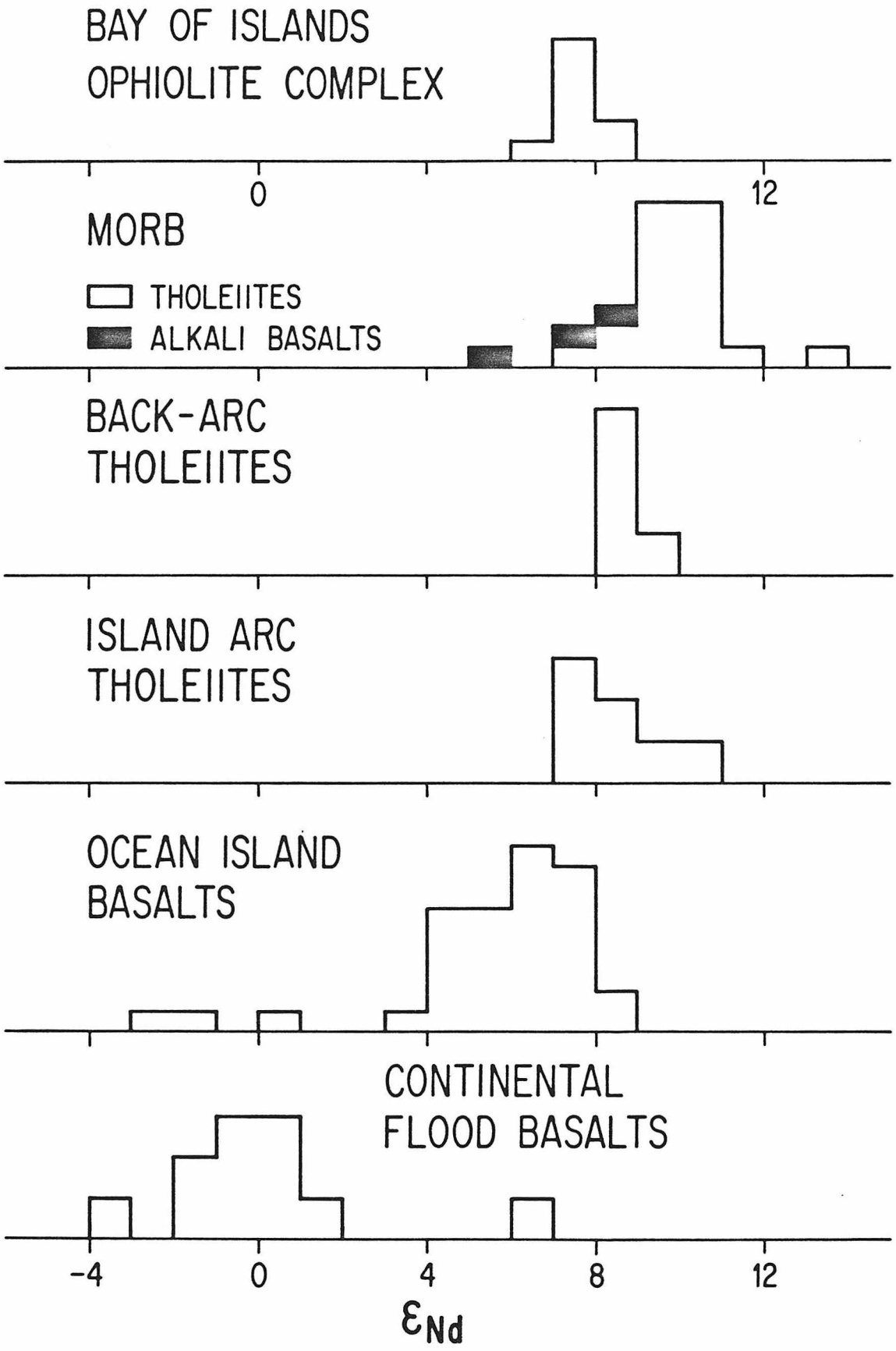
BAY OF ISLANDS
OPHIOLITE COMPLEX
0
12
MORB
THOLEIITES
ALKALI BASALTS
BACK-ARC
THOLEIITES
ISLAND ARC
THOLEIITES
OCEAN ISLAND
BASALTS
CONTINENTAL
FLOOD BASALTS
-4
0
4
8
12
εNd

Fig. 3.8

Figure 3.9. ε_{Nd}-ε_{Sr} diagram showing the data for the Bay of Islands samples. The cross represents average modern MOR tholeiites. The line through this cross and $\varepsilon_{Nd} = \varepsilon_{Sr} = 0$ represents the main correlation in young basaltic rocks ($\varepsilon_{Nd} = -0.37\ \varepsilon_{Sr}$) which is called the Mantle Array. The fields of young MOR tholeiites, island arc tholeiites, and ocean island basalts are shown. The ε_{Nd} and ε_{Sr} values of the unaltered pyroxene gabbros plot on the Mantle Array and show that mantle sources of the early Paleozoic follow a similar pattern to that found in present day mantle sources. The large dispersion in ε_{Sr} and an almost constant ε_{Nd} is due to interaction with Cambrian seawater. A mixing curve between seawater and the inferred composition of uncontaminated samples is given with the tick marks giving the volumetric water (W/R) to rock ratio and show that $W/R > 10^5$ before ε_{Nd} values are affected.

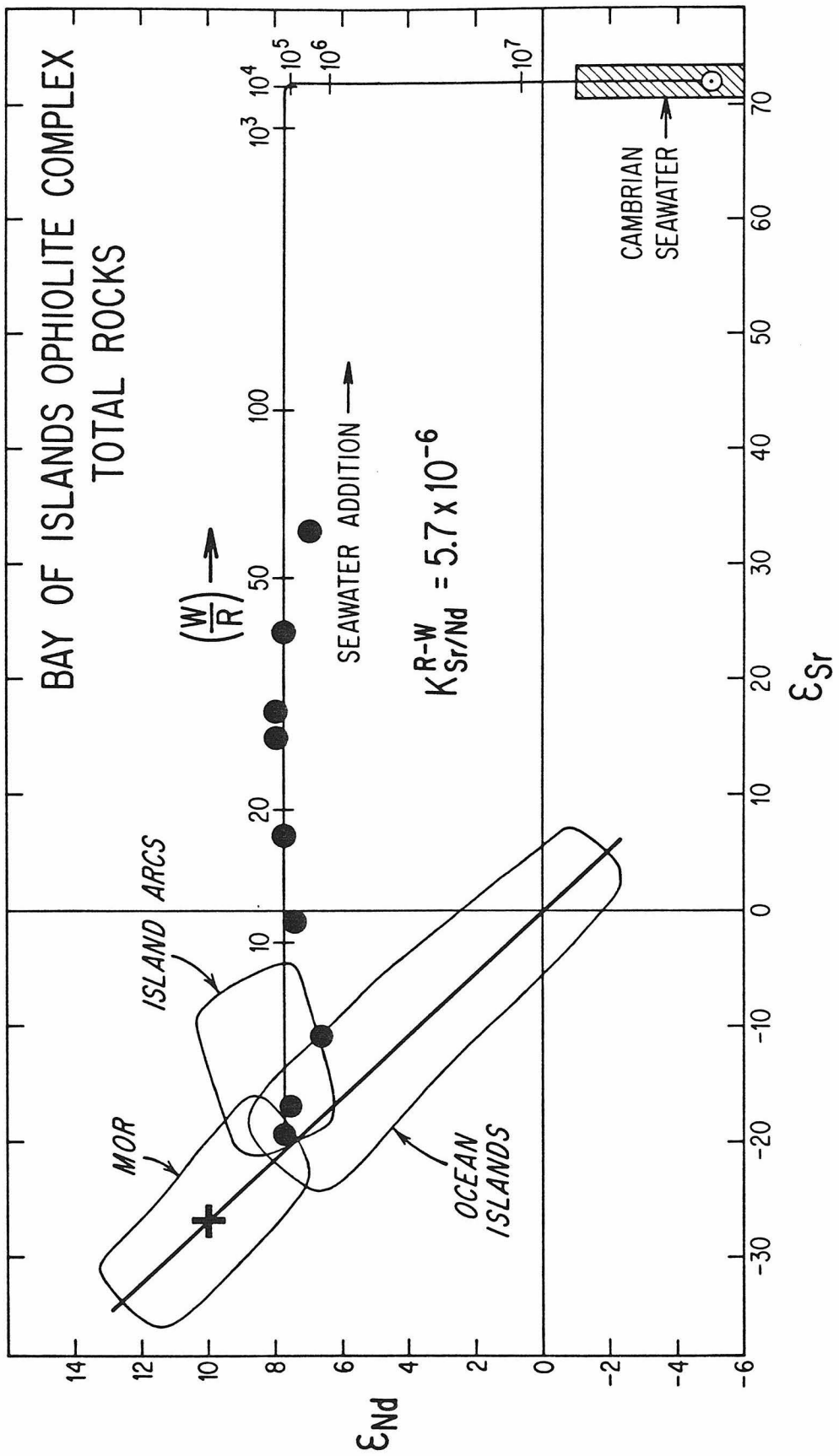
BAY OF ISLANDS OPHIOLITE COMPLEX
TOTAL ROCKS
$\left(\frac{W}{R}\right)$
SEAWATER ADDITION
$K^{R-W}_{Sr/Nd} = 5.7 \times 10^{-6}$
CAMBRIAN SEAWATER
ISLAND ARCS
MOR
OCEAN ISLANDS
ε_{Nd}
ε_{Sr}

Fig. 3.9

metamorphism. This behavior of Bay of Islands samples with shifts to the right is similar to that found for altered ocean floor basalts [O'Nions et al., 1977, 1978a]. It is concluded from the data presented here that the primary magmatic ε_{Nd} and ε_{Sr} for the Bay of Islands Complex lie on the correlation line for young volcanic rocks and exhibit clear oceanic affinity. It follows that the mantle sources of early Paleozoic oceanic rocks follow a similar pattern to that found in young oceanic rocks. However, typical ε_{Nd} and ε_{Sr} values for young normal ridge segments are +10 and -27 respectively (Fig. 3.8 and 3.9). Therefore, ε_{Nd} values for the Bay of Islands Complex are displaced down along the correlation line by ~ 2 to 3 ε-units from typical present-day MORB. It is concluded from the data that the average initial Nd value for the Bay of Islands is $\varepsilon_{Nd} = +7.8$ and for average initial Sr it is assumed that $\varepsilon_{Sr} = -19.3$ as for BMD-2A since this value makes it plot on the correlation line. A shift towards lower ε_{Nd} values and higher ε_{Sr} values is expected for old oceanic samples since $f^{Sm/Nd} > 0$ and $f^{Rb/Sr} < 0$ for the MORB source. However, in order to predict where the MORB field in Fig. 3.9 should be for old samples, it is necessary to utilize specific models of mantle evolution.

This 0.5 AE old ophiolite has characteristic oceanic ε_{Nd}-values which have been preserved both for altered and unaltered samples. This shows that the Nd isotopic signature may be used as a method to trace remnants of obducted oceanic crust in the Appalachian-Caledonian mountain chain in places where later tectonism and metamorphism have destroyed other geologic evidence.

3.2.5. Conclusions

The time of crystallization of the Bay of Islands Complex has been determined as 508±6 m.y. and 501±13 m.y. by two Sm-Nd mineral isochrons on the pyroxene gabbros from the Blow-Me-Down massif. This time refers to the time of crystallization as a part of the Iapetus oceanic crust.

The oceanic nature of the complex was previously demonstrated by its structure and petrology. The LIL element patterns (see Appendix 2, pp. 203-205) and isotopic data presented here are clearly in agreement with this interpretation. The origin of many early Paleozoic greenstone sequences, gabbros, and ultramafics is uncertain due to the fact that later metamorphism and tectonism have obliterated evidence for their oceanic or continental nature. It appears that the distinctive ε_{Nd} values of oceanic crust may now be used to identify ancient obducted oceanic lithosphere.

A small range in initial Nd of ε_{Nd} = +6.7 to +8.3 is observed for different rocks within the complex including an orthopyroxenite layer from the harzburgite, whereas the initial Sr on the same samples show a large range of ε_{Sr} from -19 to +33. The observed change in ε_{Nd} from +7.8 to +10 for the oceanic mantle over the last 0.5 AE is quantitatively expectable for a simple single stage model of mantle evolution. The large range observed in ε-values cannot be explained by mantle evolution. The wide range in ε_{Sr} with an almost constant ε_{Nd} is due to major interaction with seawater and thus shows that the early Paleozoic ocean floors were also important sinks for radiogenic crustal Sr.

3.3. THE OSLO RIFT

Radiogenic isotope studies have in the past few years contributed much to our understanding of the origin of continental alkaline rocks that typically occur in continental rifts [for a review see Powell and Bell, 1974]. Commonly mixing relationships or pseudo-isochrons are observed. The main problem is to decide whether the isotopic variations are due to (a) long term mantle heterogeneity, or (b) recent mantle-crust mixing. If (a) is the case, then we may perhaps be able to date mantle events, or in case (b) we may in favorable cases calculate the amount of crustal versus mantle material that is involved. Recent developments in Nd-Sr systematics may provide a powerful tool for looking into these problems.

This chapter presents further work in this direction in that it attempts to characterize magma sources of continental rifts utilizing data from the Permian Oslo Rift. The Oslo Rift was chosen for this study because of its great variety of well-exposed unaltered volcanic and plutonic rocks, and because it is one of the best-studied continental rifts. The Oslo Rift was in Permian time the site of extensive magmatic activity in the interior of a continent resulting in a wide variety of volcanic and plutonic rocks. The less differentiated rocks are petrologically similar to those of oceanic islands; however, the dominance of intermediate and felsic rocks in this rift is a clear difference from alkaline rocks in oceanic islands.

A likely source for most of the magmatic rocks in the rift is a body of dense material extending along the entire length of the Oslo Rift

at the base of the crust [Ramberg, 1976]. While the major part of this lower crustal body may be gabbro, the block probably also includes significant amounts of ultramafic rocks. The presence of a large gabbroic magma chamber would probably also cause significant melting of the lower crust. Ramberg has interpreted this deep crustal magma chamber to be due to the rapid development and rise of a hot asthenospheric diapir and discharge of basaltic material into the base of a gradually thinned crust.

Measurements of initial $^{143}Nd/^{144}Nd$ and $^{87}Sr/^{86}Sr$ on volcanic and plutonic rocks from the Permian Oslo Rift are reported to evaluate models of magma genesis in this continental riftzone. In addition, data on the Paleozoic shales in the Oslo rift and the local Precambrian basement are reported in order to decide whether this could be the source for any of the Oslo igneous rocks and to evaluate effects of crustal contamination or mixing with anatectic melts.

Previous workers who have studied the variation of initial Sr in the volcanic and plutonic rocks of the Oslo Rift [Heier and Compston, 1969b; Sundvoll, 1977] have concluded that these can be explained without postulating any contamination by country rock, and that an observed increase in initial Sr in the more differentiated products can be accounted for by an increase in Rb/Sr ratio with time in a fractionating magma chamber. They further conclude that the magma source is restricted to the upper mantle or the lower crust.

3.3.1 Geology and samples

The Permian Oslo Rift is a mildly alkaline sodic province where alkaline silica-undersaturated rocks and peralkaline silicic rocks are found in close association with subalkaline granites and undersaturated alkaline and peralkaline rocks. The relative areal distribution of the most important rock types in the province can be seen from Fig. 3.10 and is given by Barth [1945]. Unlike younger rift provinces, in the Oslo Rift most of these rock types are found as a plutonic series (~72%). Recent reviews of the existing geological, geochemical, and geophysical data on the Oslo Rift may be found in Dons and Larsen [1978].

Below the lava series there is up to 100 m of sedimentary rocks with Early Permian fossils and they unconformably overlie lower Palaeozoic folded sediments. The igneous rocks of the Oslo Rift have been dated by the Rb/Sr whole-rock method [Heier and Compston, 1969b; Jacobsen and Raade, 1975]. A detailed Rb/Sr study is in progress by Sundvoll and some preliminary reports have already been published [Sundvoll, 1977, 1978] and his work establishes a minimum time span from 288 m.y. to 242 m.y. for the development of the Oslo igneous complex. The lower Palaeozoic rocks again unconformably overlie the Precambrian medium to high-grade metamorphic terrain surrounding the Oslo Rift. The age of the Precambrian gneisses are mainly ~1.5-1.6 AE [Jacobsen and Heier, 1978]. To evaluate the effect of contamination with these gneisses on the isotopic composition of the Oslo igneous rocks a composite sample of quarzo-feldspathic gneisses have been made up from the Precambrian basement east and south of the Oslo Rift.

The volcanic products of the rift (~28%) can broadly be

Fig. 3.10. Geological sketch map of the Oslo Rift [Ramberg and Larsen, 1978]. Small circles show the localities of the analyzed samples.

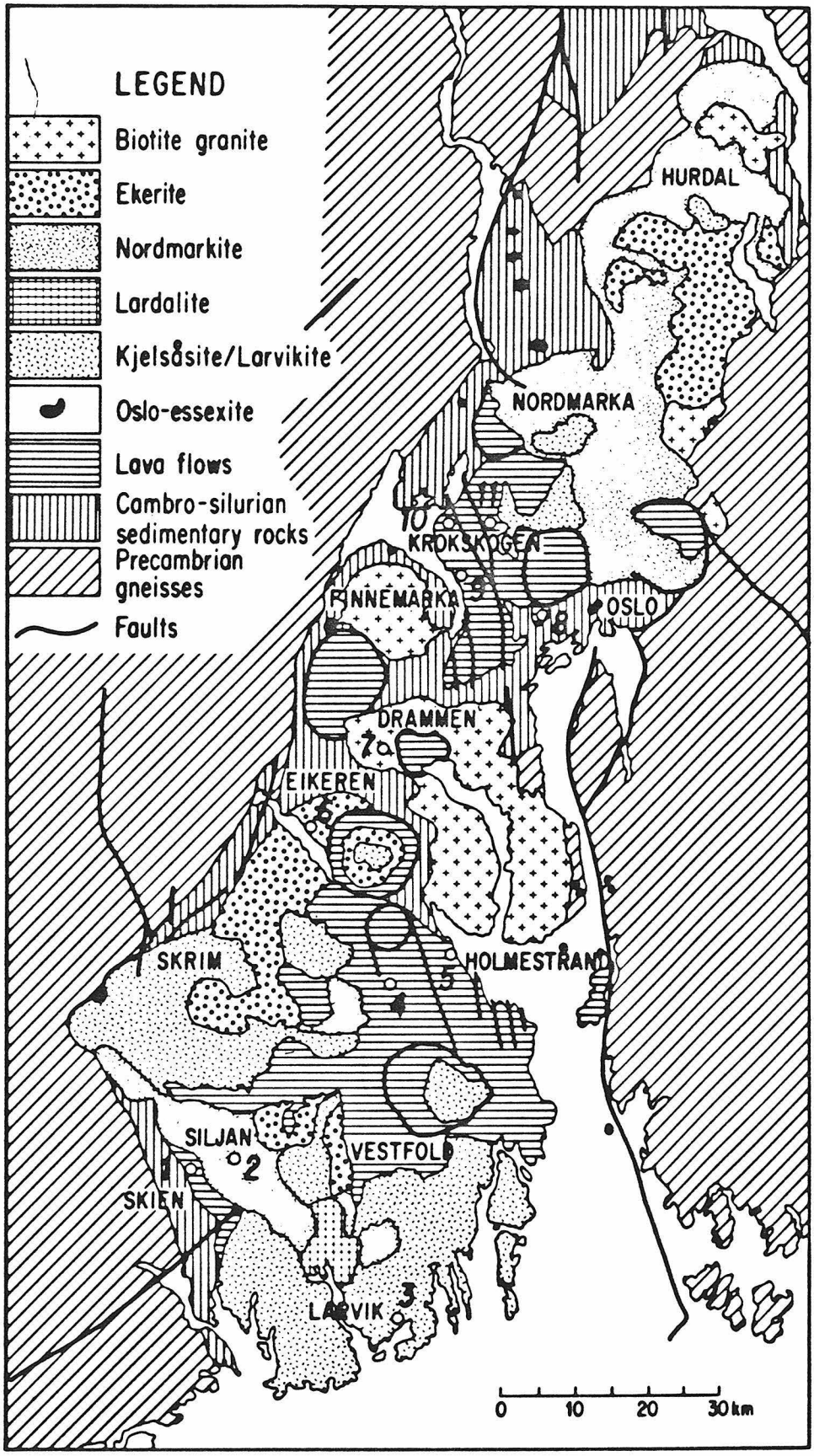
LEGEND
Biotite granite
Ekerite
Nordmarkite
Lardalite
Kjelsåsite/Larvikite
Oslo-essexite
Lava flows
Cambro-silurian sedimentary rocks
Precambrian gneisses
Faults
HURDAL
NORDMARKA
10
KROKSKOGEN
FINNEMARKA
OSLO
DRAMMEN
7a
EIKEREN
SKRIM
HOLMESTRAND
5
4
SILJAN
2
VESTFOLD
SKIEN
LARVIK
3
0
10
20
30 km

Fig. 3.10

classified as basaltic (B_1 ~25%), intermediate (rhomb porphyries (Rp), ~60%), and felsic (trachytes (T) and alkali rhyolites (R), ~15%). Ramberg and Larsen [1978] divided the eruptions into three phases: (1) initial basaltic (B_1) volcanism, (2) rhomb porphyry fissure eruptions, and (3) central volcano and cauldron stage.

The volcanism in the Oslo Rift started with basaltic eruptions. These basalts are the volumetrically most important basalts and have been given the designation B_1. Chemically the B_1 basalts change in composition from south to north [Weigand, 1975; Segalstad, 1979; Ramberg and Larsen, 1978]. The Skien basalt series (> 2000 m thick) is a trap series of basalts in the far south consisting of ankaramites (~8% normative nepheline), nephelinites, and basanites. The B_1 lavas are also found in the Krokskogen and Vestfold lava plateaus in the central and southern parts of the Oslo Rift, respectively. The Vestfold B_1 basalt is ~130 m thick with 10-15 flows of mildly undersaturated alkali olivine basalts and ankaramites with ~2.5% normative Ne. At Krokskogen the B_1 basalt consists of a single aphyric flow of quartz tholeiite. From the B_1 unit we selected six samples: one ankaramite and one nephelinite from Skien, two ankaramites from Vestfold, and two tholeiite samples from Krokskogen. The two tholeiite samples are separated by ~20 km in the field. The difference in major element chemistry between these three groups of basaltic rocks is clearly shown in an $Na_2O + K_2O$ versus SiO_2 diagram (Fig. 3.11).

Above B_1 there are at least 26 rhomb porphyry units (Rp_1-Rp_{26}) alternating with occasional basaltic and felsic lavas. They are often up to 100 m or more thick, quite extensive, and commonly composed of a

Fig. 3.11. ($Na_2O + K_2O$) - SiO_2 diagram for the Oslo Rift B_1 basalts [after Weigand, 1975]. Hawaii dividing line after MacDonald and Katsura [1964]. Additional data for the Skien basalts may be found in Segalstad [1979].

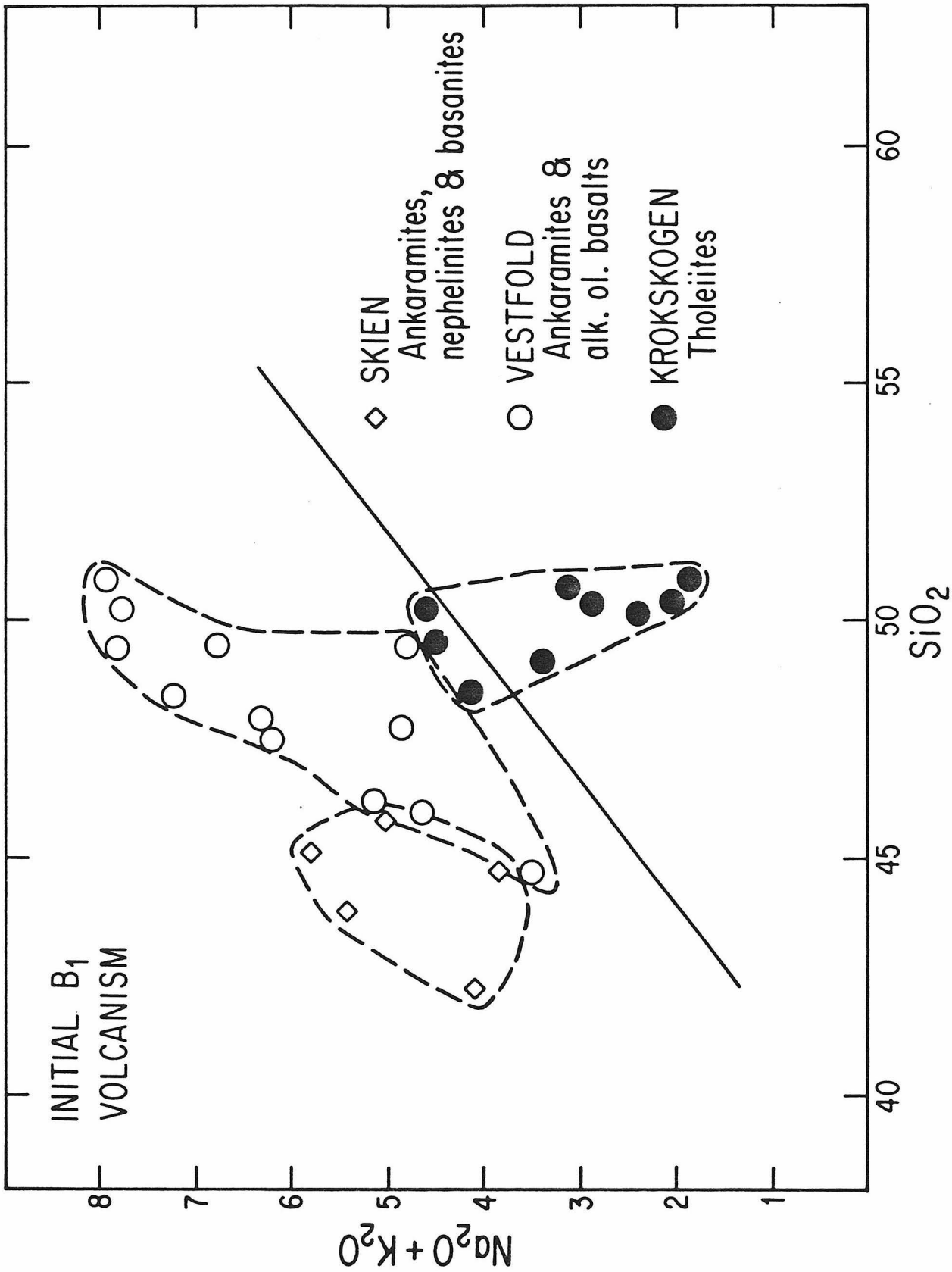
INITIAL B1
VOLCANISM
SKIEN
Ankaramites,
nephelinites & basanites
VESTFOLD
Ankaramites &
alk. ol. basalts
KROKSKOGEN
Tholeiites
Na2O + K2O
SiO2
40
45
50
55
60
1
2
3
4
5
6
7
8

Fig. 3.11

smaller number of individual flows. The units can be distinguished mainly by the amount, shape, and size of phenocrysts (anorthoclase-plagioclase). The rhomb porphyries are of broadly trachyandesitic to latitic composition and appear to define a unique rock group on a worldwide scale occurring in the Oslo Rift, East Africa, and Antarctica (Ross Island) [Ramberg, 1976]. Chemically they are very homogeneous, both in major and trace elements [Ramberg and Larsen, 1978]. Two rhombporphyry samples from the Krokskogen lava plateau have been selected: one sample from the lowest unit (Rp_1) and one from about the middle of the series (Rp_{11}).

The Vestfold and Krokskogen lava plateaus and the Skien basalt area represent mainly the stratigraphically lower part of the volcanic sequence whereas the cauldrons indicated on Fig. 3.10 include higher parts of the volcanic series. The cauldrons contain predominantly basalts (B_3), presumably representing the central volcanic stage, and felsic volcanics (trachytes and alkali rhyolites), representing the subsidence and caldera filling stage. A sample from the trachyte unit T_1 in Vestfold has been selected. This unit wedges out to the south and is thickest in the north, close to the Hillestad cauldron. Oftedahl and Petersen [1978] conclude that it flowed out of the Hillestad volcano before or during the caldera formation.

The plutonic rocks are found in three batholithic complexes and a large number of subvolcanic necks (Oslo-essexites). The subvolcanic necks make up only ~ 0.3% of surface area of plutonic rocks but contain rocks of generally ultramafic and alkali- and tholeiitic-gabbro composition. The emplacement of two major composite batholiths

consisting of monzonitic, syenitic, and granitic rocks has partly obliterated many of the earlier features of the volcanic series. The northern batholith (the Nordmarka-Hurdalen batholith) is largely syenitic, whereas the southern Larvik-Skrim batholith is dominantly monzonitic. Rocks of monzonitic composition (kjelsåsites, larvikites) make up ~ 37% of the plutonic series. Barth [1945] suggested that the more evolved plutonic rocks are related to the kjelsåsites and larvikites through fractional crystallization of feldspar + clinopyroxene ± amphibole to form the principal rock series: kjelsåsite → larvikite → nordmarkite (28%) → ekerite (16%) with larvikite → lardalite (1.3%) as a subordinate branch. One sample from each of the three major rock types in the southern Larvik-Skrim batholith have been selected.

The two composite batholiths are completely separated from the Finnemarka-Drammen batholith, which consists nearly entirely of biotite granite, by Cambro-Silurian sediments and underlying Precambrian gneisses. The biotite granites make up about 17% of the plutonic rocks and they are not supposed to be related to the other magmatic rocks. One sample from the Drammen granite which is the largest biotite granite in the Oslo Rift has been selected.

3.3.2. Mixing equations

A major problem in the interpretation of variations in initial Sr, Pb, and Nd data has been to decide whether the variations are due to long-term heterogeneities in the mantle sources or recent mixing of crustal and mantle material. Measurements of young basaltic rocks from oceanic and continental regions have shown that ε_{Nd} and ε_{Sr} are strongly correlated for samples with $\varepsilon_{Sr} < +10$ [DePaolo and Wasserburg, 1976b;

O'Nions et al., 1977]. This correlation (called the Mantle Array) appears to be characteristic of mantle reservoirs and may provide a reference line against which effects due to crust-mantle mixing processes can be evaluated and separated from the variations due to longterm mantle heterogeneity (Fig. 3.12). The shape of a data array caused by recent mixing depends on the $^{144}Nd/^{86}Sr$ ratios of the end members. If we mix two reservoirs A and B in various proportions then the mixing curve is given by

$$\frac{\varepsilon_{Nd} - \varepsilon^{A}_{Nd}}{\varepsilon_{Nd} - \varepsilon^{B}_{Nd}} = K^{A-B}_{Sr/Nd} \frac{\varepsilon_{Sr} - \varepsilon^{A}_{Sr}}{\varepsilon_{Sr} - \varepsilon^{B}_{Sr}} \tag{3.4}$$

where

$$K^{A-B}_{Sr/Nd} = \frac{(^{86}Sr/^{144}Nd)_A}{(^{86}Sr/^{144}Nd)_B} \cong \frac{(Sr/Nd)_A}{(Sr/Nd)_B} \tag{3.5}$$

and the subscripts refer to the values of the endmembers [DePaolo and Wasserburg, 1979b]. The mass fraction of A (X_A) in the mixture may be calculated from

$$\varepsilon_{Nd} = \frac{X_A\, \varepsilon^{A}_{Nd}(^{144}Nd_A/^{144}Nd_B) + (1 - X_A)\, \varepsilon^{B}_{Nd}}{X_A\, (^{144}Nd_A/^{144}Nd_B) + (1 - X_A)} \tag{3.6}$$

where $X_A = M_A/M_A + M_B$ and M_A, M_B are the masses of A and B in the mixture, respectively. Similarly for Sr we have that

$$\varepsilon_{Sr} = \frac{X_A\, \varepsilon^{A}_{Sr}\, (^{86}Sr_A/^{86}Sr_B) + (1 - X_A)\, \varepsilon^{B}_{Sr}}{X_A\, (^{86}Sr_A/^{86}Sr_B) + (1 - X_A)} \tag{3.7}$$

Fig. 3.12. The figure shows a hypothetical example where a magma is derived from the mantle with ε_{Nd} and ε_{Sr} on the Mantle Array, and then contaminated with typical continental crustal material which is expected to have negative ε_{Nd} and positive ε_{Sr} while the majority of basaltic magmas are expected to have positive ε_{Nd} and negative ε_{Sr}. Mixing lines for different values of $K_{Sr/Nd}$, the ratio of Sr/Nd in the endmembers, are shown and the equation used to calculate these mixing lines.

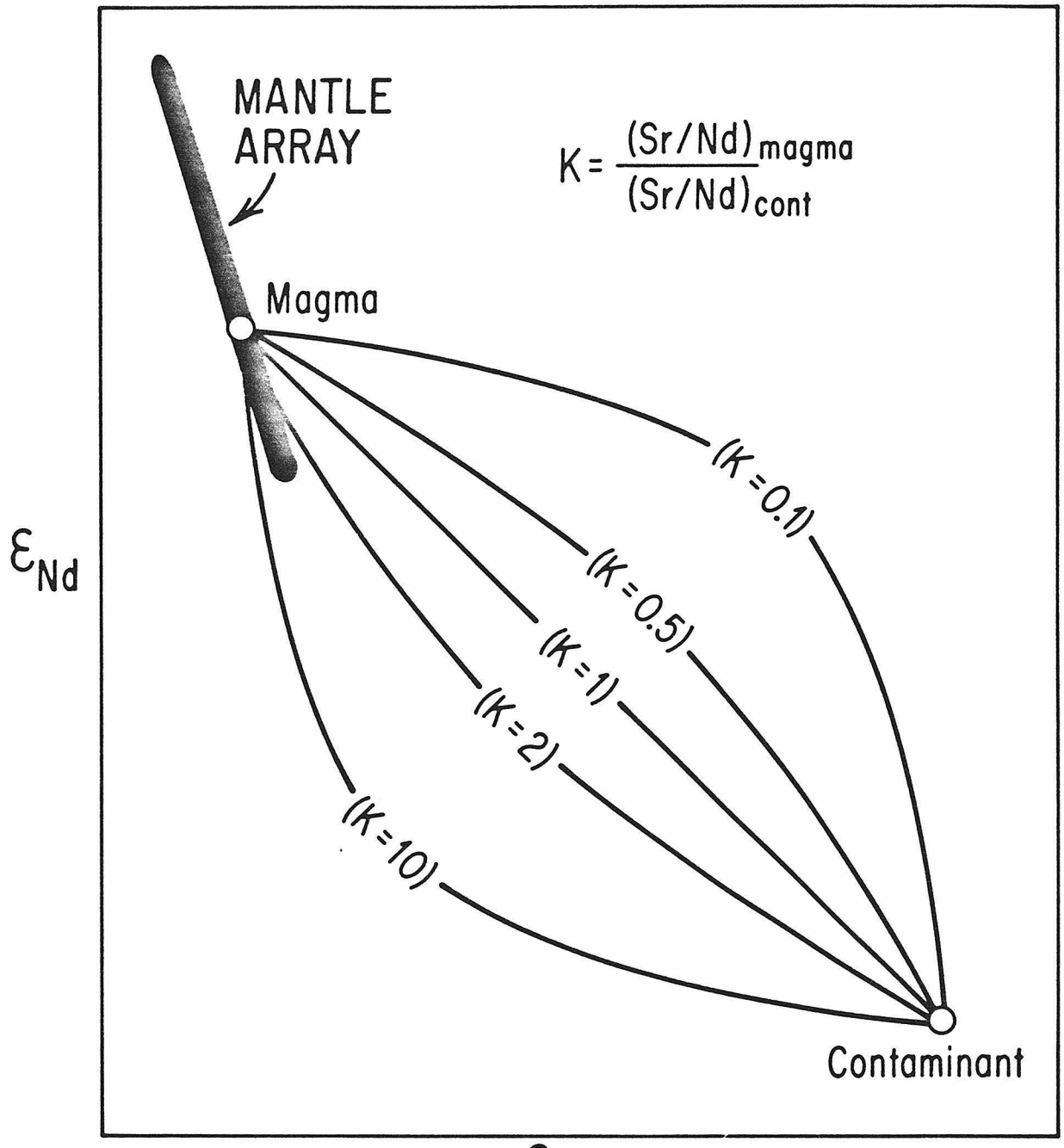

$$\frac{\varepsilon_{Nd} - \varepsilon_{Nd}^{magma}}{\varepsilon_{Nd} - \varepsilon_{Nd}^{cont}} = K \frac{\varepsilon_{Sr} - \varepsilon_{Sr}^{magma}}{\varepsilon_{Sr} - \varepsilon_{Sr}^{cont}}$$

Fig. 3.12

3.3.3. Results

Trace element and Nd and Sr isotopic data are given in Tables 3.4 and 3.5. The initial ε_{Nd} and ε_{Sr} values are given in Table 3.6. Trace element concentrations and ε-values for possible contaminants are given in Table 3.7. The initial ε_{Nd} values on thirteen Oslo Rift samples are compared with those of various types of modern basalts in Fig. 3.13. All samples have initial ε_{Nd} lying in the relatively narrow range from -1 to +4. These values are distinct from the bulk of the MOR basalts, ocean island basalts, and island arc rocks, but overlap with the bulk of continental flood basalts and fill in the gap between ocean island basalts and continental flood basalts. The Oslo Rift is a mildly alkaline province with sodic alkaline rocks. The ε_{Nd} values are very different from those of potassic alkaline rocks (Fig. 3.13). From the ε_{Nd} data we conclude that the source materials of these rocks must have time integrated REE-patterns that range from approximately chondritic to slightly LREE-depleted. The strong LREE-enrichment observed in these alkaline rocks by Neumann et al. [1977] must therefore result from fractionation during magmatic processes in Permian time or enrichment events in the mantle that occurred shortly prior to the time of magma genesis. It is clear from the ε_{Nd} data that none of the rocks could have formed by anatexis of either upper or lower continental crustal materials as the average crust surrounding the rift had $\varepsilon_{Nd} = -10$ in Permian time. This includes felsic rocks as syenite, trachyte, biotite granite, and peralkaline granite.

3.3.4. Basaltic rocks

The data obtained for the initial B_1 volcanism is shown in a

Table 3.4. Trace element (ppm) and potassium (wt %) concentrations

Sample[a]	K(%)	Rb	Sr	Ba	Nd	Sm	Rb/Sr	Sm/Nd	K/Rb	K/Ba	Sr/Nd	Ba/Nd
OB-62-TR	1.87	32.7	1203	790	60.4	9.58	0.027	0.159	572	24	19.9	13.1
S-36-77-TR	1.02	27.3	1508	934	128	20.5	0.018	0.160	374	11	11.8	7.3
OB-99-77-TR	1.91	43.9	734	604	65.0	11.8	0.060	0.182	435	32	11.3	9.3
OB-101-TR	0.918	14.5	2393	1139	57.8	9.47	0.0061	0.164	633	8.1	41.4	19.7
OB-78-TR	0.839	27.1	691	397	34.2	7.67	0.039	0.224	310	21	20.2	11.6
OB-8B-TR	0.583	12.8	374	280	31.0	7.12	0.034	0.230	455	21	12.1	9.1
K-1714-TR	4.17	167	1896	912	133	20.3	0.088	0.153	250	46	14.3	6.9
K-1516-TR	3.45	154	864	708	88.3	15.7	0.178	0.178	224	49	9.78	8.0
OT-1-TR	4.58	152	186	1208	79.8	14.7	0.817	0.184	301	38	2.33	15.1
OML-3-TR	3.78	102	713	1072	97.2	15.3	0.143	0.157	371	35	7.34	11.0
OSN-1-TR	5.18	116	27.4	87.4	92.8	15.1	4.23	0.163	447	593	0.295	0.94
OSN-1-CPX	0.251	3.06	2.89	-	-	-	1.06	-	820	-	-	-
OGE-1-TR	4.93	242	18.7	28.9	31.2	7.14	12.9	0.229	204	1706	0.599	0.92
OGE-1-AM	1.64	82.9	37.8	-	-	-	2.19	-	198	-	-	-
OGD-1-TR	4.53	249	82.6	347	26.5	4.41	3.01	0.166	182	131	3.12	13.1
OGD-1-PLAG	1.14	50.1	309	186	-	-	0.162	-	228	61	-	-

[a]TR = total rock, CPX = clinopyroxene, AM = amphibole, PLAG = plagioclase.

Table 3.5. Rb-Sr and Sm-Nd isotopic results

Sample[a]	$^{87}Rb/^{86}Sr$[b]	$^{87}Sr/^{86}Sr$[c]	$^{147}Sm/^{144}Nd$[d]	$^{143}Nd/^{144}Nd$[e]
OB-62-TR	0.0786	0.70358±3	0.0963	0.511723±22
S-36-77-TR	0.0523	0.70329±3	0.0970	0.511725±22
OB-99-77-TR	0.1733	0.70496±2	0.1106	0.511851±23
OB-101-TR	0.0175	0.70571±7	0.0995	0.511813±15
OB-78-TR	0.114	0.70591±3	0.1363	0.511691±19
OB-8B-TR	0.0922	0.70572±4	0.1395	0.511688±16
K-1714-TR	0.255	0.70472±3	0.0929	0.511799±16
K-1516-TR	0.518	0.70655±4	0.1077	0.511778±18
OT-1-TR	2.37	0.71630±4	0.1119	0.511638±16
OML-3-TR	0.423	0.70552±5	0.0955	0.511843±16
OSN-1-TR	12.4	0.75338±15	0.0987	0.511792±18
OSN-1-CPX	3.069	0.72048±5	-	-
OGE-1-TR	37.6	0.84932±5	0.1389	0.511887±18
OGE-1-AM	5.75	0.72851±5	-	-
OGD-1-TR	8.72	0.73883±4	0.1010	0.511671±18
OGD-1-PLAG	0.463	0.70730±3	-	-

[a] TR = total rock, CPX - clinopyroxene, AM = amphibole, PLAG = plagioclase. [b] Uncertainty ±1.0%. [c] Normalized to $^{86}Sr/^{88}Sr = 0.1194$, errors are 2σ mean. [d] Uncertainty ±0.5%. [e] Normalized to $^{150}Nd/^{142}Nd = 0.2096$ for unspiked runs or $^{146}Nd/^{142}Nd = 0.636151$ for spiked runs, errors are 2σ mean.

Table 3.6. Evolutionary parameters for Nd and Sr

Sample	Rock type	Stratigraphic Name	Locality[c]	Age(m.y.)	$f^{Sm/Nd}$	ε_{Nd}	$f^{Rb/Sr}$	ε_{Sr}
I. Volcanic rocks								
OB-62	Ankaramite	B_1	1	288[a]	-0.510	+1.5±0.4	-0.050	-12.8±0.4
S-36-77	Nephelinite	B_1	1	288[a]	-0.507	+1.5±0.4	-0.368	-15.4±0.4
OB-99	Ankaramite	B_1	5	288[a]	-0.438	+3.5±0.5	+1.096	+1.3±0.3
OB-101	Ankaramite	B_1	5	288[a]	-0.494	+3.1±0.3	-0.788	+21.0±1.0
OB-78	Tholeiite	B_1	10	288[a]	-0.307	-0.6±0.4	+0.378	+18.2±0.4
OB-8B	Tholeiite	B_1	8	288[a]	-0.291	-0.8±0.3	+0.115	+16.8±0.6
K-1714	Rhomb porphyry	Rp_1	9	288[a]	-0.528	+3.1±0.3	+2.08	-6.9±0.4
K-1516	Rhomb porphyry	Rp_{11}	11	288[a]	-0.452	+2.1±0.4	+5.26	+3.8±0.6
OT-1	Trachyte	T_1	4	288[a]	-0.431	-0.7±0.3	+27.7	+34.5±0.6
II. Plutonic rocks								
OML	Larvikite	-	3	279±5[b]	-0.486	+3.8±0.3	+4.11	-4.7±1.1
OSN-1	Nordmarkite	-	2	248±5	-0.498	+2.2±0.4	+148.9	+77.4±3.8
OGE-1	Ekerite	-	6	267±4	-0.294	+3.3±0.4	+453.7	+35.7±5.3
OGD-1	Biotite granite	-	7	268±4	-0.487	+0.1±0.4	+104.4	+19.1±0.8

[a]Three age determinations exist for the volcanic rocks. Rb-Sr ages of 286±8 m.y. and 288±5 m.y. have been obtained for the B_1 tholeiite and the rhomb porphyries respectively [Sundvoll, 1978]. A K-Ar age for alkalibasalt from locality 5 gives 290 m.y. [Neumann, 1960]. [b]Rb-Sr whole rock age from Sundvoll [1978]. [c]Locality numbers shown in Fig. 3.10.

Table 3.7. Trace element and isotopic values in possible contaminants

Sample	Rb(ppm)	Sr(ppm)	Nd(ppm)	Sm(ppm)	ε_{Nd}[a]	ε_{Sr}[a]
I. Paleozoic shales						
1d - Cambrian shale	18	44	32	5.4	-10	+500
4Cα - Ordovician shale	231	145	18	3.2	-10	+180
8ab - Silurian shale	131	237	29	5.2	-10	+140
II. Precambrian basement gneisses						
UC - Upper crust[b]	41	160	34	6.4	-10	+160
LC - Lower crust[b]	16	160	34	6.4	-10	+60

[a] ε-values for an age of 280 m.y.

[b] The values are based on the measurement of a composite sample of quartzo-feldspathic gneisses and the data of Jacobsen and Heier [1978].

Fig. 3.13. Histogram of initial ε_{Nd} values for the igneous rocks in the Oslo rift compared with histograms of ε_{Nd} values for young basalt samples and inferred REE pattern of their parental reservoirs. Also shown is the ε_{Nd} value measured today of a composite sample of the Precambrian basement in the Oslo Rift ($\varepsilon_{Nd}(0) = -12$). Data on continental flood basalts (CFB), oceanic island basalts, mid-ocean ridge basalts (MORB), island arcs (ARCS) and continental potassic alkaline rocks from DePaolo and Wasserburg [1976a,b, 1977], O'Nions et al. [1977], Richard et al. [1976], and Carter et al. [1978].

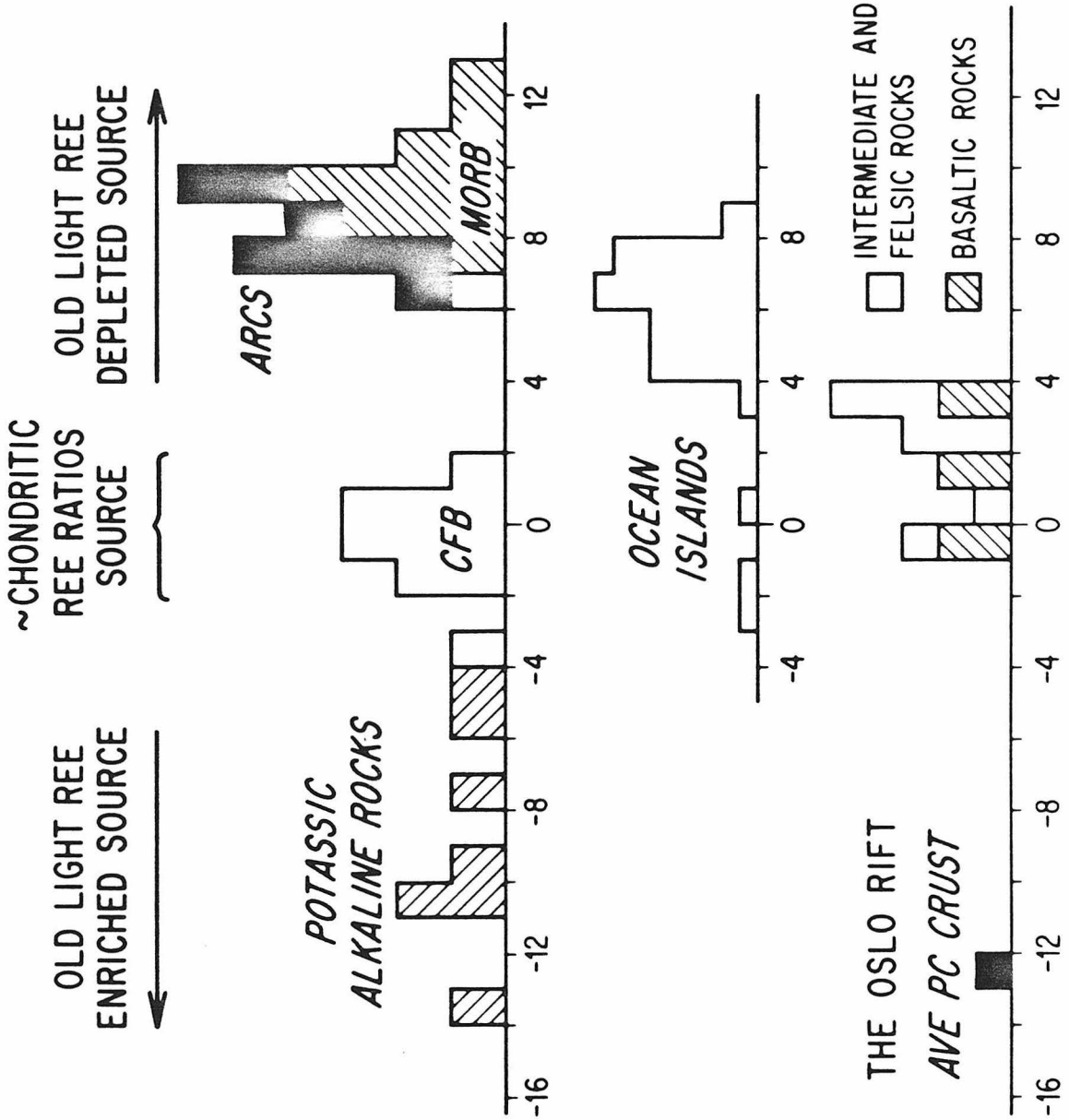
OLD LIGHT REE ENRICHED SOURCE
~CHONDRITIC REE RATIOS SOURCE
OLD LIGHT REE DEPLETED SOURCE
POTASSIC ALKALINE ROCKS
CFB
ARCS
MORB
OCEAN ISLANDS
THE OSLO RIFT
AVE PC CRUST
INTERMEDIATE AND FELSIC ROCKS
BASALTIC ROCKS
-16
-12
-8
-4
0
4
8
12
ϵ_{Nd}

Fig. 3.13

ε_{Nd}-ε_{Sr} diagram (Fig. 3.14). Two samples from the Skien basalt series of ankaramites, nephelinites, and basanites that represent the earliest volcanism in the rift have ε_{Nd} = +1.5 and ε_{Sr} ~ -15. They plot far to the left of the ε_{Nd}-ε_{Sr} correlation line. One explanation for this may be interaction with old lower crustal materials as low-SiO_2 magmas seem to have a very strong tendency to interact with the quartz-bearing crustal rocks [Turi and Taylor, 1976]. However, this would require an extremely Rb-depleted lower crust with an unusually low Sr/Nd ratio. Further, the bulk composition of the melanite-nephelinite (S-36-77) is similar to that of melillitite magmas [Segalstad, 1979] and it seems unlikely that it is contaminated significantly with continental crustal material. Alternatively these rocks may be derived from some special mantle reservoir. Menzies and Murthy [1979] have shown that kaersutite megacrysts also plot far to the left of the mantle array and they suggest these megacrysts may be derived from special metosomatized mantle source regions. Thus these strongly undersaturated magmas may be derived from a metozomatized mantle.

Two ankaramite samples from the subsequent alkali-olivine basalt volcanism further north (Vestfold) have ε_{Nd} = +3 and ε_{Sr} ~ +5 to +20. These represent the most primitive B_1 basalts since they have the highest mg values and Ni concentrations. This was followed by tholeiitic volcanism in the northern part of the rift (Krokskogen) and two samples give ε_{Nd} = -0.7 and ε_{Sr} ~ +18. They thus plot on a trend typical for some continental tholeiitic flood basalts [DePaolo and Wasserburg, 1977]. This trend extrapolates back to the correlation line at $\varepsilon_{Nd} \approx 0$ and $\varepsilon_{Sr} \approx 0$ and thus indicates a chondritic source with respect to the REE elements. This trend has been interpreted by DePaolo and Wasserburg [1977] to be due

Figure 3.14. ε_{Nd}-ε_{Sr} diagram for the initial basaltic volcanism (B_1) in the Oslo Rift. The Mantle Array [DePaolo and Wasserburg, 1976b, O'Nions et al., 1977] is also shown.

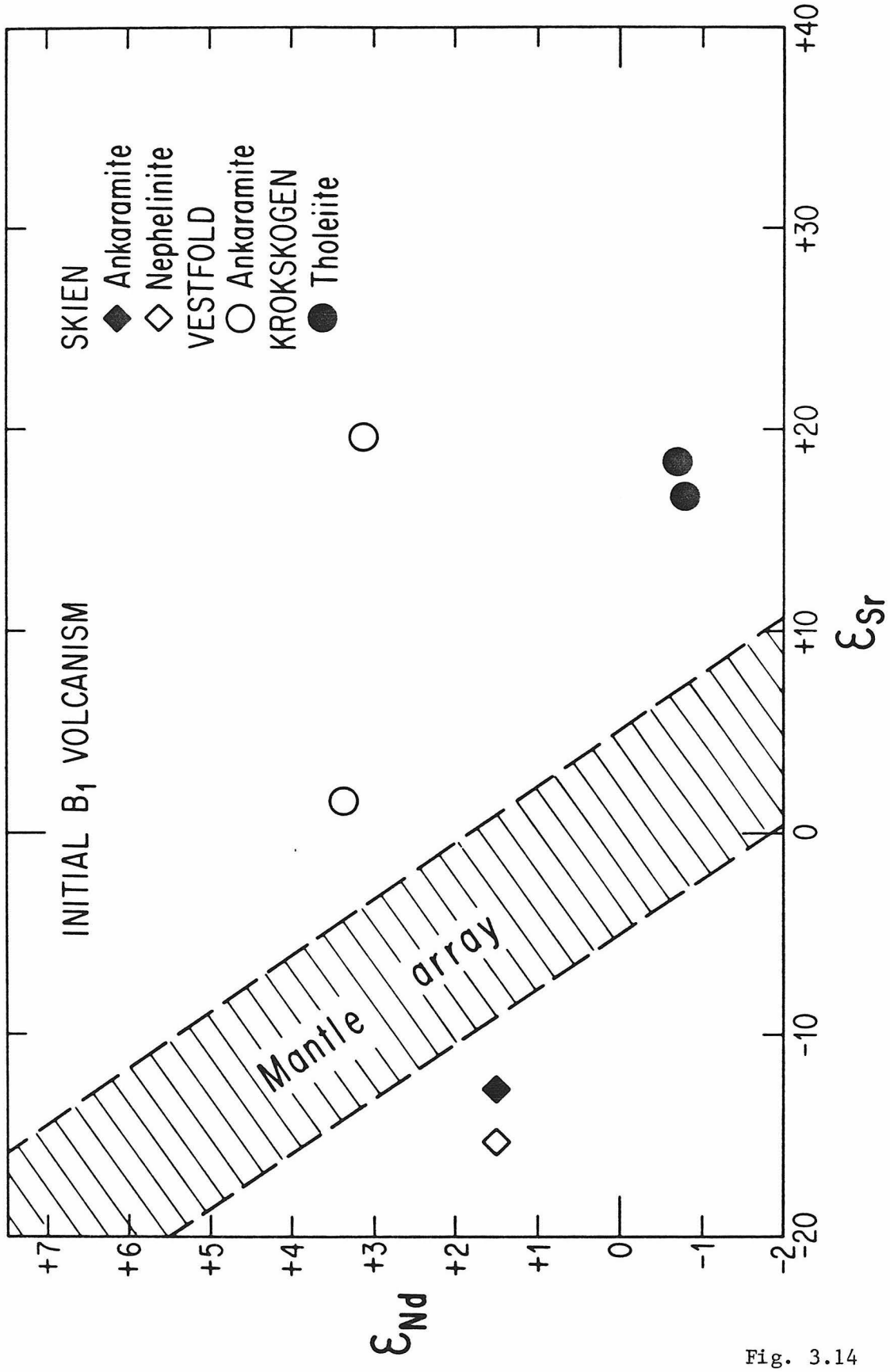
INITIAL B1 VOLCANISM
SKIEN
Ankaramite
Nephelinite
VESTFOLD
Ankaramite
KROKSKOGEN
Tholeiite
Mantle array
εNd
εSr
+7
+6
+5
+4
+3
+2
+1
0
-1
-2
-20
-10
0
+10
+20
+30
+40

Fig. 3.14

to contamination of tholeiitic magmas to varying degree at shallow levels in the crust.

The B_1 samples show a relatively small range in ε_{Nd} from -0.7 to +3.5. The ε_{Sr} values on the same samples show a much larger range from -15 to +33. The data plot on both sides of the ε_{Nd}-ε_{Sr} correlation line and show no immediate relation to it. Although we have only two ε_{Nd}-ε_{Sr} data points for each of the groups of B_1 basalts shown in Fig. 3.12, the data plotted in an ε_{Nd}-ε_{Sr} diagram (Fig. 3.14) suggest that each of these groups are derived from distinct source reservoirs or mixtures of source reservoirs.

3.3.5. Intermediate and felsic rocks

The intermediate magmas in the rift can be derived by fractional crystallization from alkali-basalts as the Vestfold ankaramites at pressures between about 7 and 10 kb, that is in the lower part of the crust [Neumann, 1979]. This is supported by the ε_{Nd} values which for both groups of samples lie in the range from +3 to +4; however, intermediate magmas have $\varepsilon_{Sr} \approx -7$ to -5 while the Vestfold alkali basalts show a range from +1 to +21 (Table 3.6). The felsic rocks have somewhat lower ε_{Nd} (+3 to -1) and higher ε_{Sr} (0 to +33) than the intermediate rocks. They all plot to the right of the Mantle Array and this suggests that small amounts of crustal contamination may be important in the genesis of these rocks. The composition of the local Precambrian basement in Permian time was $\varepsilon_{Nd} \approx -10$ and $\varepsilon_{Sr} \approx +160$. The paloeozoic shales also had $\varepsilon_{Nd} \approx -10$ in Permian time but they had highly variable ε_{Sr} from +140 to +500. Variable contamination with these contaminants could probably in part account for the great variety of differentiation trends observed from major and

Fig. 3.15. ε_{Nd}-ε_{Sr} diagram for the intermediate and felsic volcanic and plutonic rocks. The figure also shows the B_1 basalts and the Mantle Array.

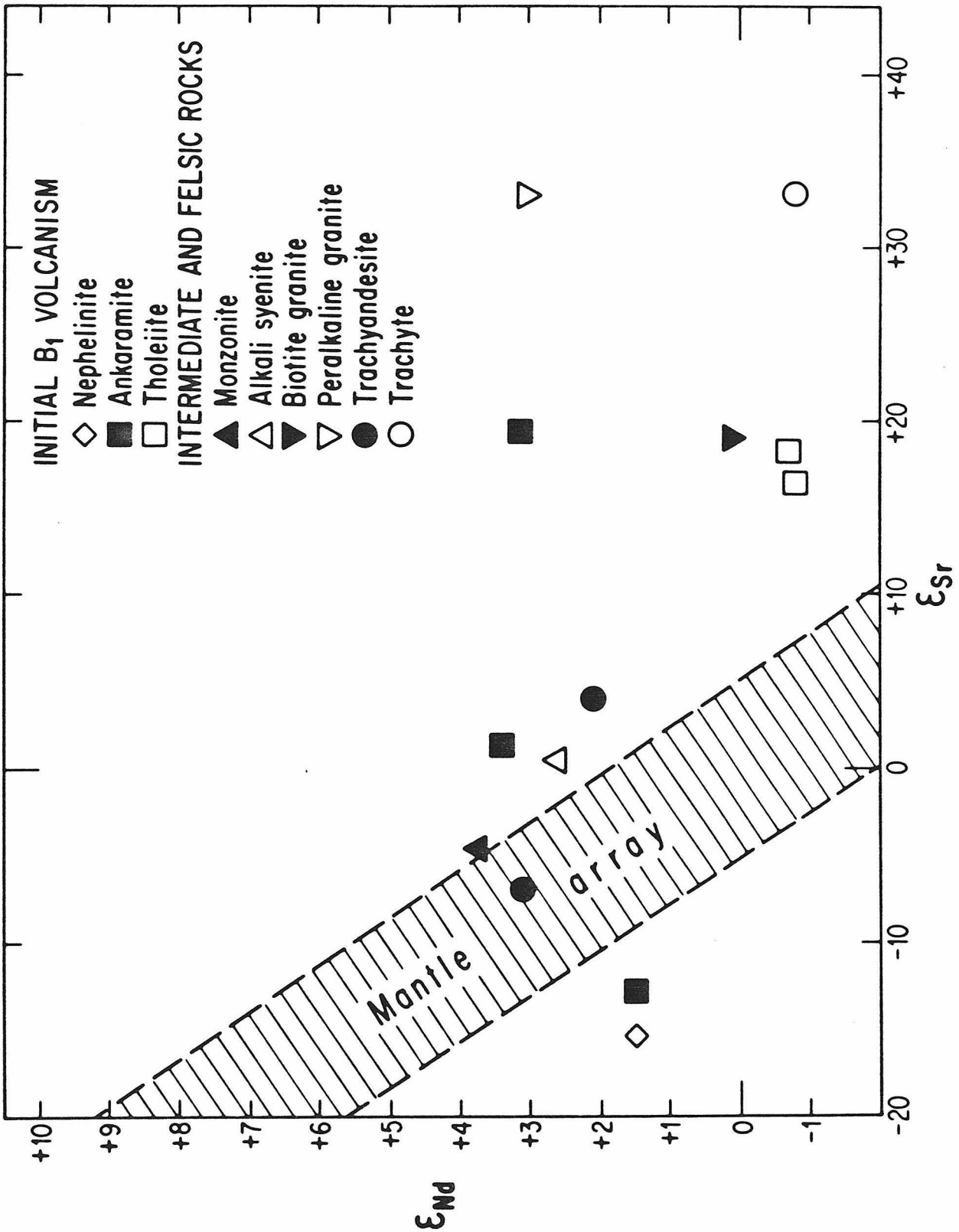
INITIAL B1 VOLCANISM
Nephelinite
Ankaramite
Tholeiite
INTERMEDIATE AND FELSIC ROCKS
Monzonite
Alkali syenite
Biotite granite
Peralkaline granite
Trachyandesite
Trachyte
Mantle array
εNd
εSr
+10
+9
+8
+7
+6
+5
+4
+3
+2
+1
0
-1
-20
-10
0
+10
+20
+30
+40

Fig. 3.15

trace element studies of these rocks [Neumann, 1976, 1978]. If crustal contamination is the reason for the variability in the Sr and Nd isotopic composition for the intermediate and felsic rocks, then the uncontaminated parent magmas must have had $\varepsilon_{Nd} > +4$ and $\varepsilon_{Sr} < -10$. To show the effects of contamination we have chosen a composition that plots on the Mantle Array for a hypothetical uncontaminated magma. The positions of various contaminants are shown in an ε_{Nd}-ε_{Sr} diagram (Fig. 3.16).

Mixing curves calculated from equations 3.4 to 3.7 between the hypothetical uncontaminated magma and the shale ld are shown. The lower mixing curve represents mixing between larvikite and the ld ($K_{Sr/Nd} \approx 7.3$) and the upper mixing curve represents mixing between ekerite and ld ($K_{Sr/Nd} \approx 0.44$). Similar mixing curves may be calculated with the other contaminants and will shift the ε_{Sr}-value of the contaminant. As shown in Fig. 3.16 the field of the intermediate and felsic rocks may be explained as mixtures between differentiation products of an uncontaminated magma with $\varepsilon_{Nd} = +4.4$, $\varepsilon_{Sr} = -12$, and variable amounts of the contaminants shown.

3.3.6. Discussion

The large variability in ε_{Nd} and ε_{Sr} values presented here show that current magma models for this rift zone are oversimplifications. It appears that the intermediate rocks in the Oslo Rift must have been derived from a mantle source with $\varepsilon_{Nd} > +4$. The depleted oceanic mantle would be expected to have $\varepsilon_{Nd} \approx +8.8$ in Permian time. Thus the most voluminous magmas in the rift must in part have been derived from a depleted mantle source. The reason that we never see a value of $\varepsilon_{Nd} \approx +8$ could be due to the fact that the source represents a mixture of a deep mantle plume

Fig. 3.16. Mixing curves calculated using data from Table 3.7 for possible contaminating crustal rocks (LC, UC, ld, 8ab, 4Cα). Tick marks give weight percentage of the crustal rock in the mixture. The field of the intermediate felsic rocks is indicated in the diagram. Black squares represent estimates of average lower crust (LC) and average upper crust (UC) based on data from the local Precambrian basement (Table 3.7). The solid line represents the Mantle Array. The average compositions of MORB (mid-ocean ridge basalts), OIB (ocean island basalts), and CFB (continental flood basalts) are also shown. The lower mixing curve represents mixing between larvikite and the Cambrian shale ld ($K_{Sr/Nd} \approx 7.3$). The upper mixing curve represents mixing between ekerite and ld ($K_{Sr/Nd} \approx 0.44$). Similar mixing curves may be calculated with the other contaminant but are omitted from the figure for clarity. The uncontaminated magma is assumed to plot on the mantle array and have $\varepsilon_{Nd} = +4.4$ and $\varepsilon_{Sr} = -12$. As shown the field of the intermediate and felsic rocks may be explained as mixtures between differentiation products of such a magma and variable amounts of the contaminants shown.

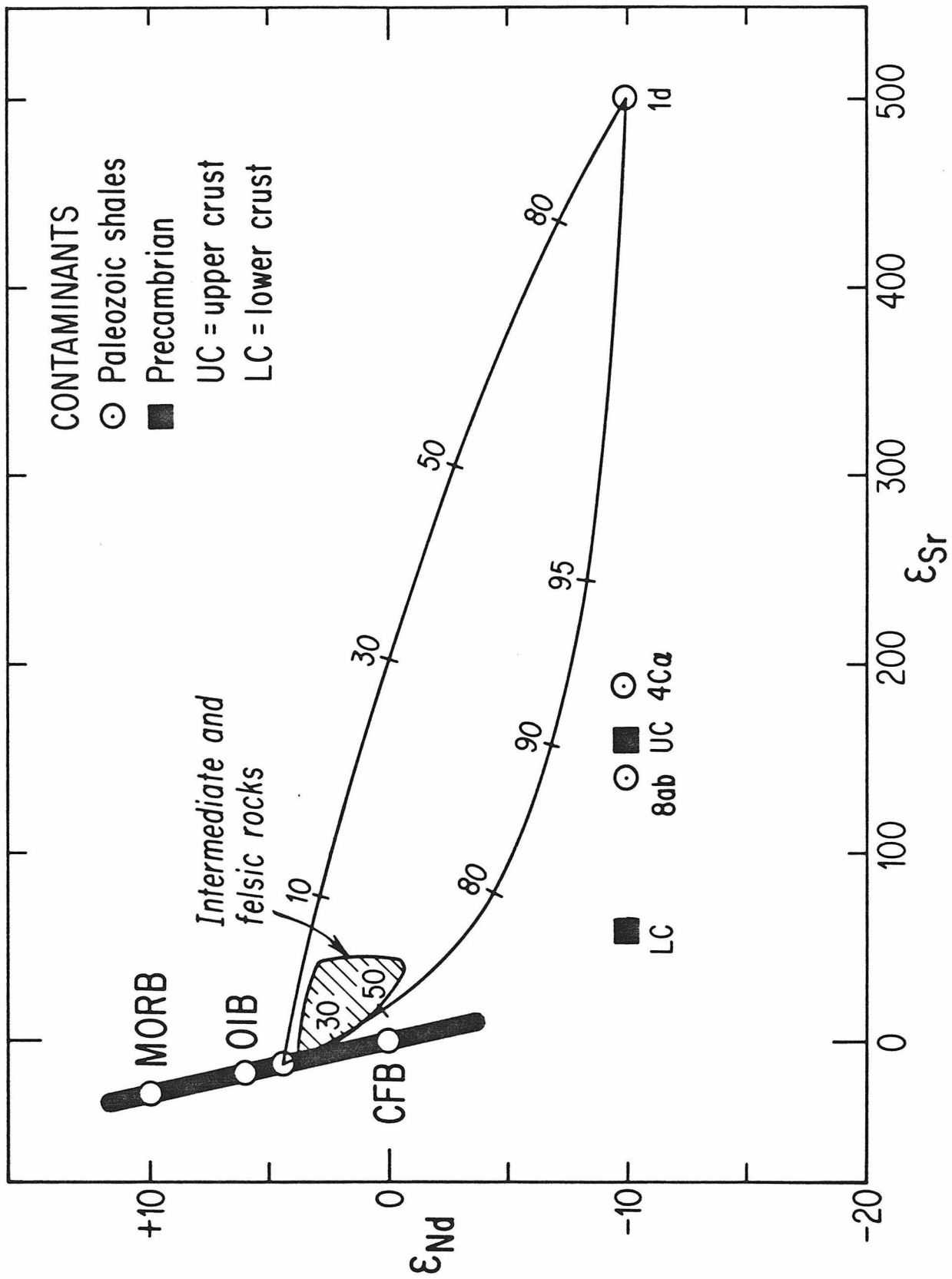
CONTAMINANTS
Paleozoic shales
Precambrian
UC = upper crust
LC = lower crust
MORB
OIB
CFB
Intermediate and
felsic rocks
10
30
50
80
90
95
1d
LC
8ab UC 4Ca
+10
0
-10
-20
ε_{Nd}
0
100
200
300
400
500
ε_{Sr}

Fig. 3.16

(ε_{Nd} = 0) and the upper depleted mantle (ε_{Nd} = +8.8) as in the model of Wasserburg and DePaolo [1979] or due to large amounts of crustal contamination even in the intermediate magmas. Crustal contamination appears to have the largest effect on the ε_{Sr} and ε_{Nd} values in the most differentiated rocks. The possibility that much of the variation in the isotopic parameters is due to crustal contamination makes it difficult to put detailed constraints on the mantle sources of these rocks. However, the data suggest that three different sources should be considered: (1) one that is the source of alkali-olivine basalts and intermediate to felsic rocks that represents a mixture of depleted and undepleted mantle, (2) one that is the source of nephelinites and ankaramites of the Skien area that may represent metasomatized depleted mantle (a large fraction of depleted mantle must be involved since the rocks have $\varepsilon_{Sr} \approx -15$ to -12), (3) one that is the source of the tholeiitic basalts which must be derived from essentially undepleted mantle. Essentially all rocks in this rift show strong LREE-enrichment ($f^{Sm/Nd} = -0.5$). It is clear, however, that none of the samples could be derived from a mantle with an ancient LREE enrichment. Carter et al. [1979] have shown that many of the basalts erupted during the opening of the North Atlantic ~ 60 m.y. ago have ε_{Nd},ε_{Sr} values similar to those of the depleted oceanic mantle. They claimed that there was no evidence for undepleted sources under the continent at that time. In contrast, the Oslo Rift appears to show evidence for both depleted and undepleted sources underneath the North Atlantic continent in Permian time. A major problem in studies like this is to sort out effects from crustal contamination from those due to variations or mixing in the mantle source regions.

3.4. LOFOTEN-VESTERÅLEN

The purpose of this study is to discuss constraints on the time of crust formation in Lofoten-Vesterålen, Norway, and parent-daughter fractionation of Sm-Nd, Rb-Sr, and U-Pb during the subsequent granulite facies metamorphism. This region exposes an unusually deep section through the continental crust. Taylor [1975] proposed that some of the oldest terrestrial rocks occur in this area. The geologically oldest rocks in Lofoten-Vesterålen are migmatitic granulite and amphibolite facies gneisses of generally intermediate composition [Griffin, Taylor, Hakkinen, Heier, Iden, Krogh, Malm, Olsen, Ormaasen, and Tveten, 1978]. The migmatite complex occur over large areas of the islands of Langøy, Hinnøy, and Moskenesøy. The migmatites are interpreted by Griffin et al. [1978] as having formed by in situ partial melting of volcanic rocks, accompanied by folding and boudinage, but without significant injection of any juvenile igneous component. Heier [1964] and Heier and Adams [1965] demonstrated for the first time that granulite facies rocks from this area are usually depleted in Rb and U.

A Rb-Sr whole-rock study by Heier and Compston [1969a] demonstrated a complex thermal history with events at ~ 2.8 AE and ~ 1.8 AE. Green, Brunfelt, and Heier [1969, 1972] showed that adjacent amphibolite facies gneisses have REE distribution patterns similar to the granulite facies gneisses, and Heier and Thoresen [1971] in a more extensive study of both major and trace elements in these rocks demonstrated that the granulite facies rocks have been depleted in Rb, U, and Th relative to the amphibolite facies rocks. Taylor [1975] reported a Pb-Pb two-stage model whole rock "isochron" age of 3.41±0.07

AE and a Rb-Sr whole-rock "isochron" of 2.25±0.15 AE with a high initial $^{87}Sr/^{86}Sr$ of 0.7126 for the migmatites at Vikan on the island of Langøy. He interpreted the inferred Pb-Pb age as the time of migmatite formation and the Rb-Sr age as the time of a granulite facies metamorphism resulting in Rb-depletion and argued that the U-Pb system was not disturbed during granulite facies metamorphism. From previous studies [Heier and Compston, 1969a; Griffin et al., 1978] it seems firmly established that a period of granulite facies metamorphism took place ~ 1.8 AE ago and that the granulite facies assemblages were superimposed on rocks that had already been migmatized.

3.4.1. Present results

The Sm-Nd data are shown in Fig. 3.17. It is clear from Fig. 3.17 that all the data do not define an isochron. All the Langøy (granulite facies) and Hinnøy (amphibolite facies) data, excluding GS-5, define a good linear array in the Sm-Nd isochron diagram. GS-5 is a petrographically untypical sample from Vikan (see Appendix 1). These five samples represent major lithologic units on Langøy and Hinnøy and have a rather small range of $^{147}Sm/^{144}Nd$ ratios from ~ 0.07 to 0.09. Therefore a best fit slope gives a rather imprecise age of 2.60±0.36 AE and an initial ratio I_{Nd} = 0.50847±20 that is within error of the CHUR evolution line.

As shown in Table 3.8 these five samples have very consistent T^{Nd}_{CHUR} model ages of 2.5-2.6 AE with a mean model age of 2.58 AE. Since this is true for both amphibolite and granulite facies samples that represent major lithologies in the area, it follows that Sm-Nd did not fractionate during the much-later granulite facies metmorphism. If we

Table 3.8. Evolutionary parameters and model ages for Nd and Sr

Sample[a]	$f^{Rb/Sr}$	$\varepsilon_{Sr}(0)$	$f^{Sm/Nd}$	$\varepsilon_{Nd}(0)$	T^{Sr}_{UR}(AE)	T^{Nd}_{CHUR}(AE)
I. Langøy (Granulite facies)						
GS-5 (Dioritic granulite)	-0.5549	+62.5±1.1	-0.4745	-27.8±0.5	-7.10±0.11	2.31±0.04
GS-23 (Granitic granulite)	+23.37	+1217.3±0.8	-0.5627	-36.6±0.3	3.06±0.02	2.57±0.02
V-9 (Granodioritic granulite)	+2.386	+259.2±0.4	-0.5386	-35.1±0.4	6.23±0.05	2.57±0.03
V-34 (Tonalitic granulite)	+1.415	+73.7±0.8	-0.6399	-41.1±0.5	3.06±0.06	2.54±0.03
II. Hinnøy (Amphibolite facies)						
GUG-2 (Granitic gneiss)	+50.32	+2185.5±0.8	-0.5350	-35.1±0.3	2.56±0.01	2.59±0.02
AM-2 (Tonalitic gneiss)	+7.006	+295.0±0.4	-0.6261	-41.4±0.3	2.48±0.02	2.61±0.02
III. Moskenesøy (Granulite facies)						
TL-39 (Monzonitic granulite)	+0.6457	+31.8±0.6	-0.4540	-22.6±0.4	2.89±0.08	1.97±0.04

[a]GS-23, GS-5, and V-9 are from Vikan [loc. 1 in Griffin et al., 1978] SW Langøy, V-34 from Myhre NW Langøy GUG-2 from the W side of Gullesfjord, AM-6 from Kringlen quarry NW Hinnøy, and TL-39 from Reine (loc. 2 in Griffin et al., 1978].

Fig. 3.17. Sm-Nd systematics of Lofoten-Vesterålen migmatites compared to a T^{Nd}_{CHUR} = 2.6 AE reference isochron. Samples that were fractionated from a chondritic reservoir at this time should be within error of this line. Deviations from the reference isochron are clearly significant. For the Hinnøy data the errors are of the same size as the symbol used. The five samples that plot close to the 2.6 reference isochron all represent major lithologies on Langøy and Hinnøy. The Langøy sample that plots distinctly off from this reference isochron indicates that younger lithic components also occur in these rocks. The Moseknesøy migmatites give T^{Nd}_{CHUR} = 1.97±0.04 AE appear to be distinctly younger than the Langøy and Hinnøy migmatites.

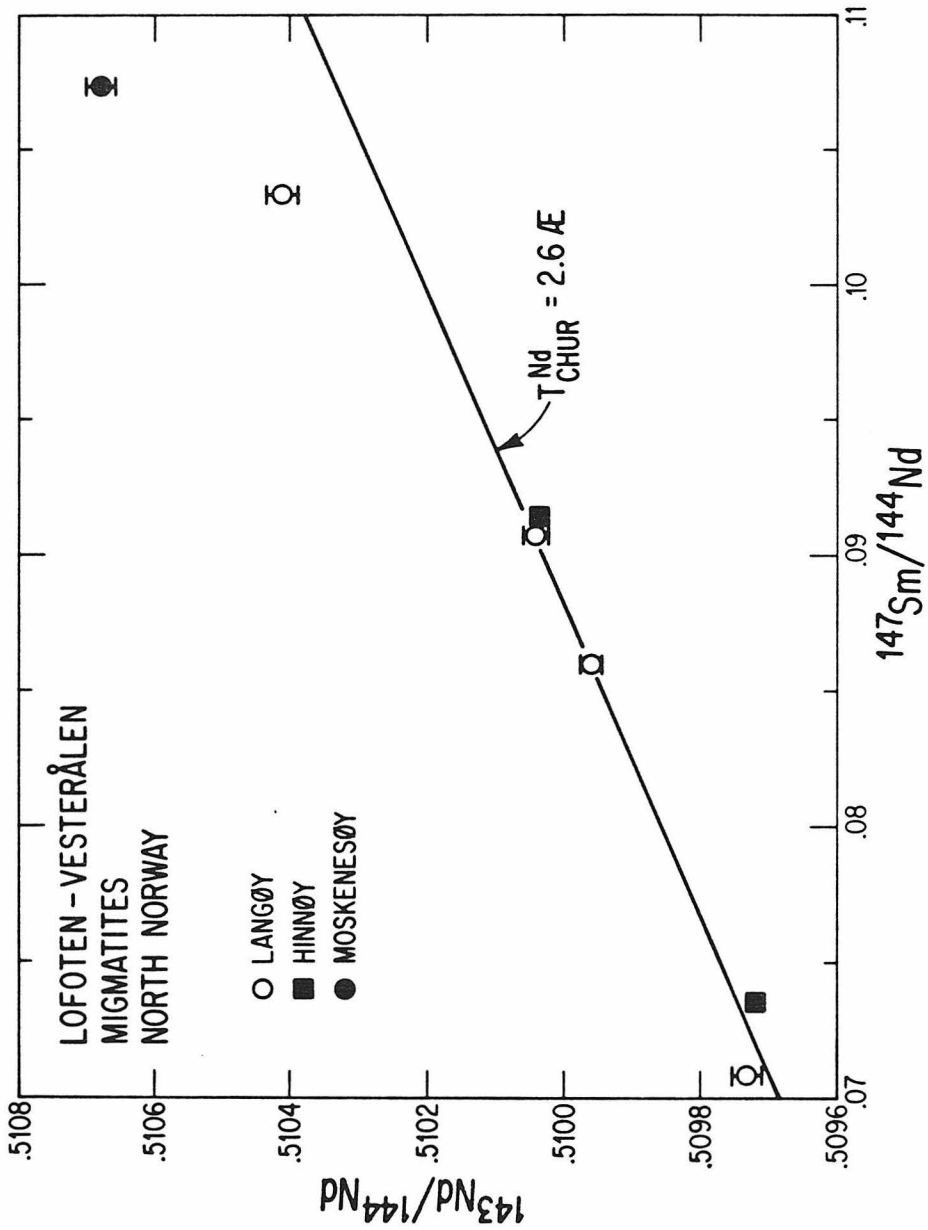
LOFOTEN-VESTERÅLEN
MIGMATITES
NORTH NORWAY
LANGØY
HINNØY
MOSKENESØY
T^{Nd}_{CHUR} = 2.6 Æ
$^{143}Nd/^{144}Nd$
$^{147}Sm/^{144}Nd$
.5108
.5106
.5104
.5102
.5100
.5098
.5096
.07
.08
.09
.10
.11

Fig. 3.17

look at the T^{Sr}_{UR} model ages in Table 3.8 it is clear that none of the T^{Sr}_{UR} model ages for the granulite facies samples agree with their T^{Nd}_{CHUR} model ages. Two granulite samples give geologically impossible ages. For the two amphibolite facies samples there is, however, a relatively good agreement between the T^{Nd}_{CHUR} and T^{Sr}_{UR} model ages. This demonstrates that the Rb-Sr total rock system was seriously disturbed during the much later granulite facies metamorphism. The mean T^{Nd}_{CHUR} model age of 2.58 AE is considered to provide the best estimate for the original time of formation of the protoliths of the Langøy and Hinnøy migmatites.

The sample TL-39 from Moskenesøy appears to be distinctly younger as it gives T^{Nd}_{CHUR} = 1.97±0.04 AE. This sample has a T^{Sr}_{UR} model age of 2.89±0.08 AE. However, the low measured $^{87}Sr/^{86}Sr$ ratio of 0.70674 makes this particularly sensitive to the assumptions involved in calculating the model age. The sample plots within error of a Rb-Sr total rock isochron giving T = 1.78±0.03 AE and I_{Sr} = 0.7037±3 reported by Heier and Compston [1969a] for the Lofoten granulites. This isochron included samples of the Moskenesøy granulites. It has been suggested that the Moskenesøy granulites are as old as the Langøy and Hinnøy migmatites but that they have been updated during the 1.8 AE event by essentially complete removal of radiogenic Sr [Heier and Compston, 1969a; Griffin et al., 1978; Griffin and Heier, 1969]. The distinctly younger T^{Nd}_{CHUR} model age indicates, however, that the protoliths of the Moskenesøy migmatites are distinctly younger and not related to the Langøy and Hinnøy migmatites.

3.4.2. Discussion of previous results

Taylor [1975] obtained a fairly good linear array of data points

in a Rb-Sr evolution diagram for the migmatites at Vikan; some scatter about the best-fit line, however, suggests a disturbed Rb-Sr system. Three additional analyses from the same locality are presented in Table 3.8. Two of these plot far from Taylor's Rb-Sr "isochron." Further, all the data from Vikan in Table 3.8 and Taylor's data plot to the left of a T^{Sr}_{UR} = 2.6 AE reference isochron which suggests Rb-depletion significantly later than the time of formation of the protoliths of the migmatites. This is still true for reference isochrons with any other reasonable choice of $^{87}Sr/^{86}Sr$ in the mantle at this time. Therefore the high initial Sr values indicated are due to Rb loss rather than remelting of older crust. This means that for all samples which have a higher Rb/Sr ratio than that of UR we get $T^{Sr}_{UR} > 2.6$ AE. Taylor excluded three data points from the Pb-Pb two-stage model "isochron" regression analysis and even then the analytical errors had to be expanded by a factor of seven for all the data to be within error of the best fit line. Thus the Pb-Pb and Rb-Sr data by Taylor [1975] and our Rb-Sr data for the migmatites at Vikan display significant scatter and neither age nor initial Sr or Pb isotopic ratios can be precisely determined from these data.

Although there is no evidence for Rb or U depletion in the amphibolite-facies migmatites, previously published Rb-Sr data [Heier and Compston, 1969a; Griffin et al., 1978] imply that the Rb-Sr whole rock systems have been significantly disturbed but still indicate an age of ~ 2.5 AE. The two amphibolite facies samples in Table 3.8 gives T^{Sr}_{UR} model ages of 2.48 and 2.56 AE that are very close to their T^{Nd}_{CHUR} ages of 2.59 AE and 2.61 AE. A Pb-Pb two-stage model total rock isochron for

the amphibolite facies migmatites also give a similar result of 2.69±0.07 AE [Griffin et al., 1978].

The major Sm/Nd fractionation most likely occurs during the formation of the protoliths of the migmatites. However, large fractionations of Rb/Sr and U/Pb are expected both during the formation of the protoliths of the migmatites and during the subsequent migmatization. The fact that all three decay systems give similar ages for the amphibolite facies migmatites implies that the timespan between these two events must have been short, on the order of less than 0.1-0.2 AE. Therefore, this stage can for practical purposes be ignored in the following model calculations.

3.4.3. U/Pb and Rb/Sr fractionation during granulite facies metamorphism

Taylor interpreted the linear Pb isotope array for the Vikan migmatites to give an age of 3.41 AE with a μ of 11.2 in the stage prior to this time and argued that the U-Pb system had essentially been left undisturbed from that time up to the present. For such a model his Pb-Pb data require μ's of 5 to 8 in the last stage for most of the samples and a total range of 3 to 12.

The average measured μ-values of the granulite facies rocks in this area calculated from the U-Pb data of Heier and Thoresen [1971] is 2.0. Such low measured μ-values are also typical of other granulite facies terrains [Gray and Oversby, 1972; Moorbath et al., 1969]. This shows that if Taylor's samples were at all representative of this rock complex it is not possible to explain the large range in measured $^{206}Pb/^{204}Pb$ and $^{207}Pb/^{204}Pb$ values in terms of his model. This interpretation is therefore rejected. Instead the T^{Nd}_{CHUR} model age obtained

from the Sm-Nd data is used and it will be shown that the Pb and Sr isotope data can then be well explained in terms of a model, with the time of formation of these crustal rocks at T_x = 2.6 AE and the time of granulite facies metamorphism at T_M = 1.8 AE.

A μ_1 value for time interval from T_x to T_M (stage 1) can then be calculated and a μ_2 value for the time interval T_M to 0 (stage 2) from the following equation ($\alpha = {}^{206}Pb/{}^{204}Pb$ and $\beta = {}^{207}Pb/{}^{204}Pb$):

$$\alpha_m = \alpha_I(T_x) + \mu_1(e^{\lambda T_x} - e^{\lambda T_M}) + \mu_2(e^{\lambda T_M} - 1) \qquad (3.8)$$

$$\beta_m = \beta_1(T_x) + \frac{\mu_1}{137.8}(e^{\lambda' T_x} - e^{\lambda' T_M}) + \frac{\mu_2}{137.8}(e^{\lambda' T_M} - 1) \qquad (3.9)$$

where the subscript m denotes the ratio measured in the rock today. The μ_1 values calculated from Taylor's Pb data are in the range from 2 to 38 with an average of ~ 13. The highest values are found in the granitic rocks. Most of the calculated μ_2 values are in the range from 1 to 4, the total range is from 0.4 to 14 and the average is 3.0. The U/Pb fractionation factor at T_M is then given by $F_{U/Pb} = \mu_2/\mu_1$ and we calculate an average $F_{U/Pb} \sim 0.25$, which compares well with the average μ_G/μ_A of ~ 0.33 (G = granulite facies, A = amphibolite facies) calculated from the U-Pb data of Heier and Thoresen [1971] for these migmatites. The very low μ-values of the granulite facies gneisses today, indicated both by these calculations and the U-Pb data of Heier and Thoresen [1971], imply that their Pb isotope composition has changed much less since 1.8 AE than in the time interval from 2.6 to 1.8 AE when the μ-values averaged ~ 13. Thus the isochron that was produced in the

time interval from 2.6 to 1.8 AE has generally been preserved and has only been slightly shifted to the right in a α-β diagram. This interpretation of the Pb data is shown in Fig. 3.18. The dashed line in this figure is the T = 3.41 AE two-stage model Pb-Pb isochron of Taylor.

Similarly, we can calculate an average Rb/Sr fractionation factor $F_{Rb/Sr} = (Rb/Sr)_2/(Rb/Sr)_1$ at T_M of ~ 0.46 from the equation

$$(^{87}Sr/^{86}Sr)_m = I^{Sr}_{UR}(T_x) + (^{87}Rb/^{86}Sr)_1(e^{\lambda_{Rb}T_x} - e^{\lambda_{Rb}T_M}) + (^{87}Rb/^{86}Sr)_2(e^{\lambda_{Rb}T_M} - 1) \quad (3.10)$$

where $(^{87}Rb/^{86}Sr)_2$ is the ratio measured today. We may compare the Rb-depletion indicated by the model calculations with that indicated by concentration data on the granulite facies relative to the amphibolite facies migmatites. From the concentration data of Heier and Thoresen, we obtain $(K/Rb)_A/(K/Rb)_G \sim 0.47$. It thus appears that both concentration data and isotopic data are well explained by assuming a bulk loss of U and Rb from the granulite facies gneisses. If this model is approximately correct, then the isotopic data require this loss to have occurred at ~ 1.8 AE. This is one of the rather rare cases where granulite facies metamorphism postdates rock formation by as much as 0.8 AE.

Note also that the average $F_{U/Pb}$ and $F_{Rb/Sr}$ calculated from the isotopic data discussed above vary systematically with the mineralogy or major element composition of the gneisses at Vikan:

	$F_{U/Pb}$	$F_{Rb/Sr}$
Granitic granulites	0.15	0.7
Granodioritic-Tonalitic granulites	0.4	0.25
Dioritic granulites	0.5	0.15

Fig. 3.18. Lead isotopic data on total rocks from Vikan [Taylor, 1975]. The parameters for the growth curve shown are given in the text. The Sm-Nd data indicate that the protoliths of the Vikan migmatites formed 2.6 AE ago. Note that none of the total rock leads are less radiogenic than expected for this age. Two reference isochrons are shown. If the protoliths formed at 2.6 AE with initial lead on the growth curve and lost all their U during the granulite facies metamorphism at T = 1.8 AE then all the total rocks should plot on the line labeled T = 2.6-1.8 AE. If they instead evolved from 2.6 to present without any disturbance of the U-Pb system, they should all plot on the line labeled T = 2.6-0 AE. Most of the samples plot in the wedge between these two reference lines. This is expected if they were depleted in U relative to Pb at T = 1.8 AE. Only two points plot to the right of this line and this requires that U was enriched relative to Pb at T = 1.8 AE for these samples in terms of an episodic model. The three least radiogenic samples plot on the T = 2.6-0 reference line giving further evidence that 2.6 AE is the time of formation of the protoliths. The dashed line shows Taylor's [1975] two-stage model Pb-Pb "isochron" that gives T = 3.41 AE and requires a very high μ-value of 11.2 in the stage from 4.45 AE to 3.41 AE.

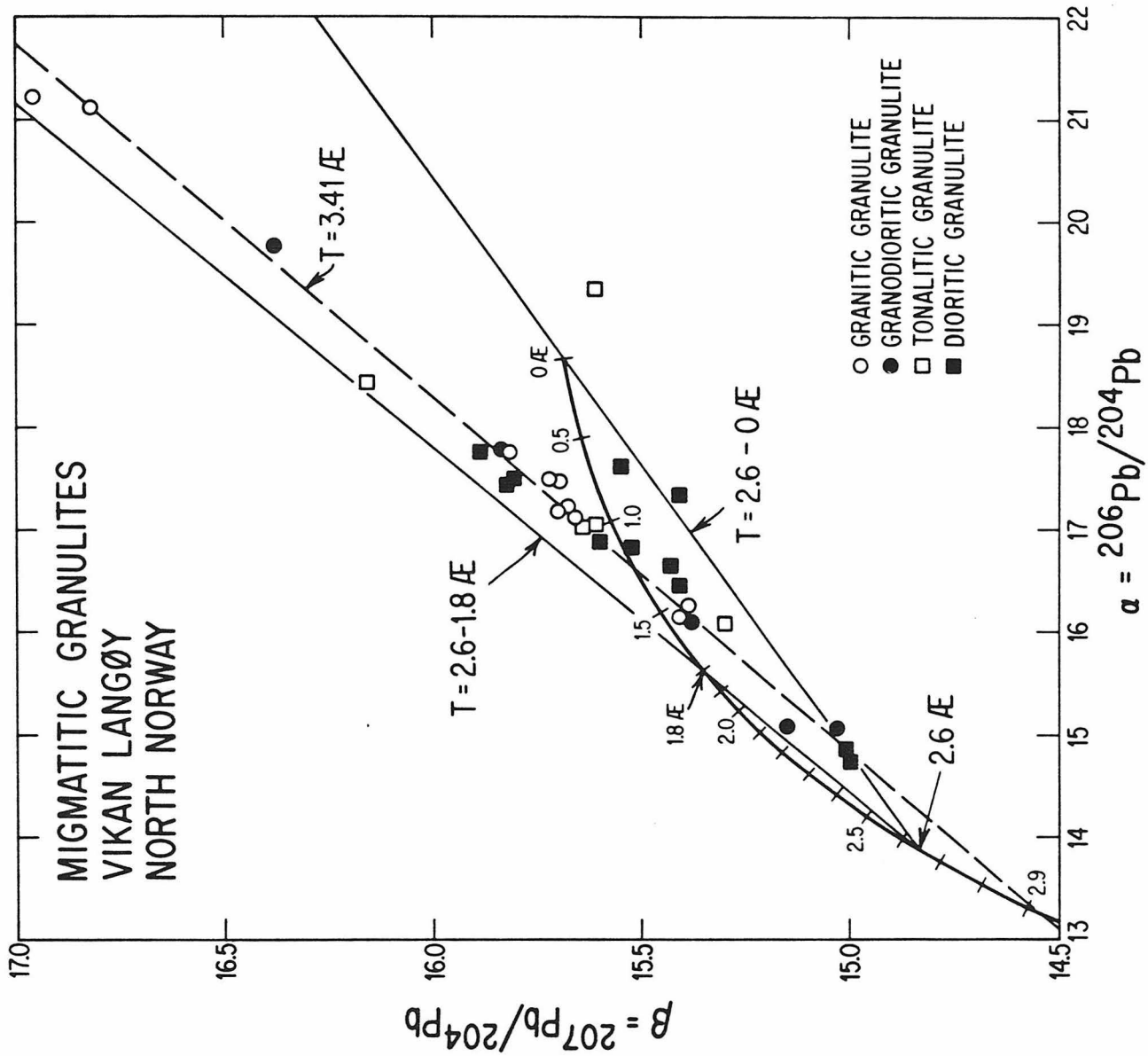
MIGMATITIC GRANULITES
VIKAN LANGØY
NORTH NORWAY
T = 3.41 Æ
T = 2.6-1.8 Æ
T = 2.6 - 0 Æ
2.6 Æ
0 Æ
0.5
1.0
1.5
1.8 Æ
2.0
2.5
2.9
GRANITIC GRANULITE
GRANODIORITIC GRANULITE
TONALITIC GRANULITE
DIORITIC GRANULITE
β = 207Pb/204Pb
α = 206Pb/204Pb
17.0
16.5
16.0
15.5
15.0
14.5
13
14
15
16
17
18
19
20
21
22

Fig. 3.18

This most likely reflects the difference in mineralogic changes with major element composition for the amphibolite-granulite transition.

3.4.4. Conclusions

The results strongly suggest that total rock Rb-Sr and Pb-Pb data have to be interpreted with great care for granulite facies gneisses. Complex Rb-Sr and U-Pb systematics displayed by granulite facies gneisses may, however, be resolved by ages obtained with independent methods and can be used to trace U/Pb and Rb/Sr fractionation during high-grade metamorphism. For migmatite complexes T^{Nd}_{CHUR} model ages appear to provide the best time constraints for the formation of the protoliths as the dominating REE-fractionation will be associated with this event rather than with subsequent metamorphic events. For the Vesterålen amphibolite facies migmatites Sm-Nd, Rb-Sr, and Pb-Pb give model ages of ~ 2.6 AE. However, for the granulite facies migmatites only the Sm-Nd system gives this age while the Rb-Sr and U-Pb total rock systems do not provide any precise age information. If a granulite facies metamorphism occurred long after the time of crust formation, then in general we may expect $T^{Sr}_{UR} > T^{Nd}_{CHUR}$, except in more basic rocks where the measured Rb/Sr ratio may be lower than that of UR.

It is concluded that the interpretation presented by Taylor [1975] for a very ancient crustal component in the Archean terrane of Vesterålen is not valid. Instead this terrane appears to be part of the worldwide crustal forming event at 2.6 AE. The possibility that very ancient crustal segments may really be present in other areas of the Fennoscandian Shield must remain the subject of future investigations.

The approach used in this work suggests that Sm-Nd model ages

as well as total rock isochrons may be very valuable in identifying time equivalent lithic units in complex metamorphic terranes. The coordinated use of different isotopic systems which have different susceptibilities to metamorphism gives a much deeper insight into both the times and mechanisms of chemical fractionation.

3.5. THE NORWEGIAN GARNET PERIDOTITES

Nd isotopic data suggest that the continental crust has been mainly derived by partial melting of undepleted mantle through time. The mass transfer from a deep-seated undepleted reservoir may occur through rising diapirs as discussed in Chapter 2.2. At shallow levels in the mantle the diapirs may intersect the solidus and be partially melted and the melt partly separated. The separated melt is added to the continental crust and the depleted residue is added to the depleted upper mantle. However, a minor amount of the residual fraction of these diapirs may be welded onto the base of the continental crust or occasionally (during collisions) overthrust. The peridotite massifs observed in orogenic belts are candidates for this residual material. These massifs consist mainly of lherzolite, harzburgite, and dunite, but also contain "magmatic" layers that may represent high pressure cumulates.

New Nd and Sr isotopic data on the oldest known terrestrial garnet peridotite massifs that occur in Norway are presented here. Eclogite facies assemblages of two types occur within the "Basal Gneiss Complex" of southern Norway [Eskola, 1921], namely eclogites associated with peridotite bodies, and eclogites directly enclosed in amphibolite to high pressure granulite facies gneisses (often termed "country rock" eclogites). Rb-Sr whole-rock isochron studies and U-Pb on zircons

[Pidgeon and Råheim, 1972; Lappin et al., 1979] give ages of the country rocks of 1.5-1.7 AE. K-Ar and Rb-Sr mineral analyses generally give consistent ages around 0.4 AE [Brueckner, 1972]. The distribution of eclogitic rocks is shown in Fig. 3.19.

Eclogite facies assemblages of the first type comprise rare lenses (up to ~ 100 meters) of garnet lherzolite, garnet wehrlite, garnet websterite, and rarely bimineralic eclogite within garnet free peridotite or dunite bodies. These ultramafic rocks are unusually fresh and only minor serpentinization occurs. There are three large (1-4 km) masses of dunite-peridotite at Otrøy, Tafjord, and Almklovdalen and one small at Sandvik that contain layers and lenses of garnet periodotite and garnet pyroxenite. It has been argued [Carswell 1968a, 1968b] that such assemblages were probably developed in the upper mantle prior to the tectonic emplacement of these peridotite bodies into their present position. Clinopyroxenes from these garnet-peridotites have been reported to have some of the lowest $^{87}Sr/^{86}Sr$ ratios ever measured on terrestrial rocks ~ 0.7010 to 0.7029 [Brueckner, 1974].

Clinopyroxene and garnet from a garnet-websterite layer of the Almklovdalen peridotite give a 1.12% spread in $^{143}Nd/^{144}Nd$ (Table 3.9) and this yields an age of 1477±7 m.y. and an initial $^{143}Nd/^{144}Nd$ = 0.509879±17 (initial ε_{Nd} = -0.9±0.2). The peridotite massif is emplaced into country rocks of 1.5-1.7 AE age that were later metamorphosed under eclogite facies conditions. The mineral isochron of the garnet websterite most likely date the eclogite facies metamorphism. Garnet lherzolites have $f^{Sm/Nd}$ in the range from +0.2 to +0.4 and have clearly been depleted in LREE. However, the initial ε_{Nd} value of ~ 0 suggests

Fig. 3.19. Simplified geologic map of the Basal Gneiss Complex of southwestern Norway showing distribution of ultramafic rocks (circle) and country rock eclogites (x's) [Brueckner, 1977].

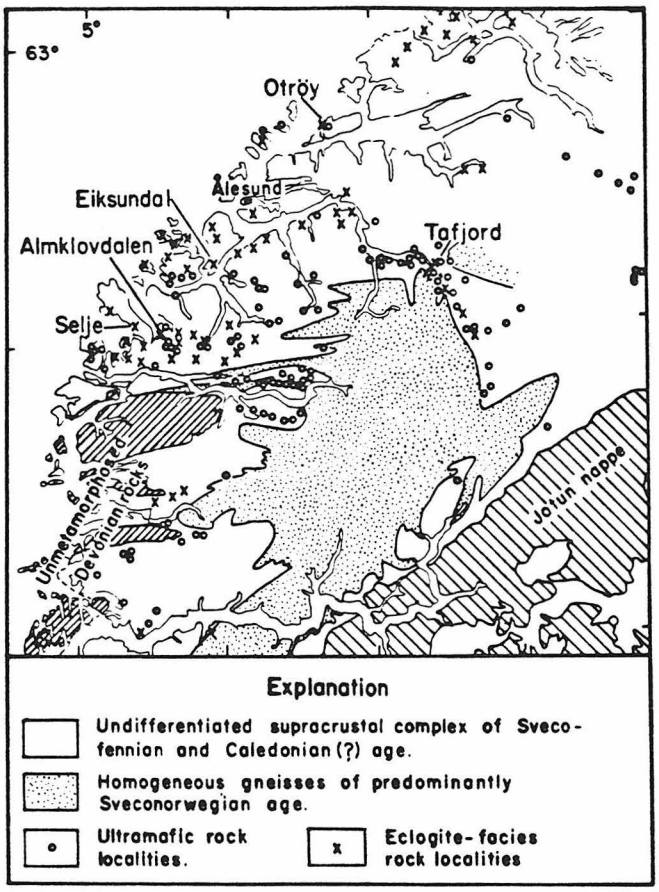
5°
63°
Otröy
Ålesund
Eiksundal
Almklovdalen
Tafjord
Selje
Unmetamorphosed Devonian rocks
Jotun nappe
Explanation
Undifferentiated supracrustal complex of Svecofennian and Caledonian (?) age.
Homogeneous gneisses of predominantly Sveconorwegian age.
Ultramafic rock localities.
Eclogite-facies rock localities

Fig. 3.19

that this LREE depletion occurred simultaneously with the main crust forming event in this area. The measured $^{87}Sr/^{86}Sr$ on the garnet websterite is very primitive (0.7017). The initial ε_{Sr} value is -15 which suggests that a Rb depletion occurred at least 2.4 AE ago in this peridotite massif. Brueckner [1974] reported a measured $^{87}Sr/^{86}Sr$ = 0.7011 on clinopyroxene from a garnet wherlite of the same locality. The more precise data obtained here on the same clinopyroxene mineral separate (Ah-6) give $^{87}Sr/^{86}Sr$ = 0.701980±38 and do not confirm the extremely low value of Brueckner [1974]. The Nd and Sr isotope data suggest that the peridotites massif may represent residual material that has been involved in several stages of continental crust formation.

Table 3.9. Analytical data for samples from Helgehornsvannet, Almklovdalen peridotite

Sample	Sr(ppm)	$\frac{^{87}Rb}{^{86}Sr}$	$\frac{^{87}Sr}{^{86}Sr}$	Nd(ppm)	$\frac{^{147}Sm}{^{144}Nd}$	$\frac{^{143}Nd}{^{144}Nd}$
Garnet websterite:						
Garnet	-	-	-	0.287	0.7110	0.516780±35
Clinopyroxene	165	0.000379	0.701697±17 0.701768±45 0.701745±53	9.97	0.1190	0.511034±22
Garnet wehrlite[a]:						
Clinopyroxene	124	0.00023	0.701980±38	-	-	-

[a]Sample Ah-6 from Brueckner [1974]. He obtained $^{87}Sr/^{86}Sr$ = 0.7011±2, 0.7013±1, and 0.7010±3 for three individual mass spectrometer runs on the same clinopyroxene separate.

CHAPTER 4. BOUNDARY CONDITIONS FOR THE MODELS

The parameters involved for both models described in chapter 2 are the initial and final concentrations and isotopic compositions for each reservoir j, the solid/melt distribution coefficients, and the mass of reservoir j as a function of time. All these parameters need not be specified and in the following the parameters believed to be the best known will be used to make estimates of others.

The total mass of the mantle and the crust is 403.4×10^{25} grams. In both models the depleted mantle is taken to include the basaltic part of the oceanic crust since it is derived from the depleted mantle and is subducted back to the depleted mantle at short time scale (< 0.2 AE). The total mass of the continental crust (2.256×10^{25} grams) is taken as the total amount of continental materials including Layer 1 of the oceanic crust which is considered to be mainly sediments derived from weathering of continental crust.

4.1. BULK EARTH VALUES

The bulk earth (reservoir 1) values used for the Rb-Sr, Sm-Nd, and U-Th-Pb systems are given in Table 4.1. The values for Sm-Nd are those for average chondrites presented in chapter 3. The new bulk earth values for U-Th-Pb in Table 4.1 were derived from the data in Table 4.2. Model calculations for Rb-Sr and Sm-Nd systems are insensitive to the choice of age of the earth in the neighborhood of 4.5 AE. A value of 4.55 AE which is the age of the oldest meteorites is used here. Pb isotope models are, however, very sensitive to the choice of age of the earth because of the short half-life of ^{235}U. The age of the earth determined from the single

Table 4.1. Bulk earth values for Nd, Sr, and Pb isotopes

Decay system (r-d)	Decay constant ($10^{-9}yr^{-1}$)	Stable reference isotope (s)	$\frac{N_{d,1}(0)}{N_{s,1}(0)}$	$\frac{N_{d,1}(T_o)}{N_{s,1}(T_o)}$	$\frac{N_{r,1}(T_o)}{N_{s,1}(T_o)}$	"Age of the earth" (T_o, AE)	$Q_d^*(T_o)$ (AE^{-1})	Reference
^{87}Rb-^{87}Sr	0.0142	^{86}Sr	0.69898	0.7045	0.0827	4.55	16.70	1,2,3
^{147}Sm-^{143}Nd	0.00654	^{144}Nd	0.505895	0.511836	0.1967	4.55	25.13	4
^{238}U-^{206}Pb	0.155125	^{204}Pb	9.307	18.55	9.353	4.43	782.1	5,6
^{235}U-^{207}Pb	0.98485	^{204}Pb	10.294	15.55	0.06784	4.43	42.97	5,6
^{232}Th-^{208}Pb	0.049475	^{204}Pb	29.476	38.34	36.17	4.43	466.7	5,6

References are 1, Papanastassiou and Wasserburg [1969]; 2, DePaolo and Wasserburg [1976b]; 3, O'Nions et al. [1977]; 4, This work, chapter 3; 5, Tatsumoto et al. [1973]; 6, This work, Table 4.2.

Table 4.2. Average Pb isotope values for various reservoirs in the earth

	$\alpha = \frac{^{206}Pb}{^{204}Pb}$	$\beta = \frac{^{207}Pb}{^{204}Pb}$	$\gamma = \frac{^{208}Pb}{^{204}Pb}$
Continental crust[a]	18.86	15.62	38.83
Depleted mantle[b]	18.12	15.46	37.66
Bulk earth[c]	18.55	15.55	38.34

[a]Doe and Zartman [1979]. These are their average values for a present-day orogene. They are very similar to the average values for oceanic sediments, manganese nodules, California metamorphics, and continental sediments (Mesozoic/Cenozoic) given by Stacey and Kramers [1975].

[b]Average value for mid-ocean ridge tholeiites [Stacey and Kramers, 1975].

[c]Bulk earth values are the intersections of the geochrons with the tielines between the continental crust and the depleted mantle. The age of the earth is assumed to be 4.43 AE.

stage Pb growth curve is 4.43 AE [Doe and Stacey, 1974] which is ~ 0.1 AE younger than the age of the oldest meteorites. The only detailed study of initial Pb on early archean rocks give 4.47±0.05 AE for the age of the earth and confirm this value [Gancarz and Wasserburg, 1977]. This young model age of the earth will be used here and could be due to either core formation at this time or late accretion of the earth.

The silicate portion of the earth is assumed to be initially chemically homogeneous and the core is assumed to have insignificant amounts of the lithophile elements considered here. The concentrations of these elements in the silicate portion of the earth are thus 1.48 times their concentrations in the total earth. It is known that the earth is depleted in volatile elements relative to chondrites [Gast, 1960]. However, the ratios of refractory elements in the earth appear to be equal to those in chondrites both from isotopic studies [DePaolo and Wasserburg, 1976a] and chemical studies [Sun and Nesbitt, 1977]. It has been concluded elsewhere that the concentrations of the refractory lithophile elements Ca, Al, U, Th, Ba, Sr, and REE in the mantle are about 2.0±0.5 those in ordinary chondrites [Frey and Green, 1974; Loubet et al., 1975; Sun and Nesbitt, 1977]. A value two times ordinary chondrites will thus be used for the refractory lithophile elements in the crust plus mantle. Estimates for the Rb and K concentrations in the silicate portion of the earth can then be estimated from the bulk earth Rb/Sr ratio of 0.029 [DePaolo and Wasserburg, 1976b] and the bulk earth K/U ratio. Previous estimates of the K/U ratio of the earth [Heier and Rogers, 1963; Wasserburg et al., 1964] were based mainly on upper crustal rocks and are very close to 10^4. This is most likely a lower limit since

Table 4.3. Concentrations of trace elements

	Bulk earth (crust + mantle) (ppm)	Continental crust (ppm)
K	⩾ 260	15000
Rb	0.63	33
Sr	22	370
Ba	7.6	500
Sm	0.406	5
Nd	1.26	26
U	0.026	0.7
Th	0.098[a]	2.8
^{204}Pb	0.00238[a]	0.093[b]

For sources of K, Rb, Sr, Sm, Nd, and U data see Appendix 3.

[a]Based on U = 0.026 ppm and the bulk earth values in Table 3.

[b]Taylor [1977].

lower crustal granulites have (K/U) > 10^4 [Lambert and Heier, 1968b]. Estimates of the concentrations of K, U, Ba, Rb, Sr, Sm, and Nd in the crust plus mantle are given in Table 4.3.

4.2. THE CONTINENTAL CRUST

Estimates of the ε and f-values are given in Table 4.4. The ε-values for $^{206}Pb/^{204}Pb$, $^{207}Pb/^{204}Pb$, and $^{208}Pb/^{204}Pb$ are denoted ε_α, ε_β and ε_γ respectively. In general the continental crust is chemically exceedingly heterogeneous. Most of the ε and f values show a large range and good average values are difficult to obtain. A notable exception may be the $f^{Sm/Nd}$ value of -0.4 ± 0.1 for the continental crust. As discussed in Table 4.2 average crustal values for Pb isotopes also appear to be relatively well defined.

Extensive work has established that the upper crustal composition is close to that of grandiorite [Poldervaart, 1955; Shaw et al., 1967; Eade and Fahrig, 1971]. It is well known from the heatflow data that the upper crustal concentrations of K, U, and Th cannot extend to a depth of more than 10-15 km, so that the lower crust must be depleted in these elements [Heier, 1965, 1973]. This has led to the hypothesis that the lower crust is made up of dry granulite facies rocks and related igneous rocks since they show the necessary depletions in U and Th [Heier, 1965] and they also show Rb depletions and generally low Rb/Sr ratios [Heier, 1964]. Extensive geochemical studies of granulite facies rocks with particular emphasis on the distribution of heat producing elements have been carried out in Australia and Norway [Heier and Adams, 1965; Lambert and Heier, 1967, 1968a,b; Heier and Thoresen, 1971]. Lambert and Heier [1968b] used estimates of the heat producing elements in upper and lower

crustal materials together with constraints from heatflow to calculate concentration profiles of K, U, and Th through the continental crust. They estimated total crust concentrations of K = 1.5 wt % and U = 0.7 ppm for Precambrian shields. A set of average concentrations in the continental crust for the elements of interest here is given in Table 4.3. Since the average composition of the continental crust may be somewhat differentiated relative to primary mantle derived basalts, it is likely that large amounts of ultramafic cumulates from primary melts are retained in the mantle. Thus the D-values in the equations in chapter 2 are not necessarily equilibrium distribution coefficients. They may rather be effective distribution coefficients between the final melt added to the crust and the residue and cumulates retained in the mantle.

4.3. THE DEPLETED MANTLE

In contrast to the continental crust the isotopic composition of normal mid-ocean ridge basalts appear to be rather uniform and well-defined average values have been obtained (Table 4.4). Note also that $f^{Rb/Sr} = -0.9$ and is close to its limit of -1. Therefore the strongest constraint on any model must come from the Rb-Sr data on the depleted mantle. No attempts have been made to estimate the f-values directly for U-Th-Pb or the concentrations of the elements of interest in the depleted mantle. These parameters will be calculated in the next chapter.

Table 4.4. Ranges of parameters based on directly observed values

	Continental crust (today)	Depleted mantle (today)	Depleted mantle (0.5 AE ago)
$f^{Rb/Sr}$	+1 to +10	$-0.9^{+0.1}_{-0.05}$	-0.9
ε_{Sr}	+60 to +250	-27±5	-19.3
$f^{Sm/Nd}$	-0.4±0.1	$+0.22^{+0.08}_{-0.07}$	~ +0.2
ε_{Nd}	-10 to -25	+10±2	+7.8
ε_{α}	+167	-230	-
ε_{β}	+45	-58	-
ε_{γ}	+128	-177	-

The values for Rb-Sr and Sm-Nd are the estimates given in Appendix 3, where the estimates for the depleted mantle 0.5 AE ago are based on data from the Bay of Islands Complex. The ε-values for the U-Th-Pb system are calculated from the data in Table 4.2.

CHAPTER 5. RESULTS OF MODEL CALCULATIONS

5.1. MODEL I

The parameters of this model will now be evaluated for Rb-Sr, Sm-Nd, and U-Th-Pb by first only considering estimates from observed ε-values and f-values for Sm-Nd and Rb-Sr (Table 4.4) using equation (2.26). These parameters are more directly known than the concentrations in the various reservoirs. The enrichment factor for Rb-Sr in the depleted mantle is estimated to be $f^{Rb/Sr} = -0.9$ and the mean ε_{Sr} value is -27. These values give a reliable estimate of the mean age of the depleted mantle today ($\bar{t} = 1.8$ AE) which must also be the mean age of the continental crust. If the rate of production of crust was constant over 4.5 AE, then $\bar{t} = T_o/2 = 2.3$ AE. As $\bar{t}$ is much less than 2.3 AE this shows that if Model I is valid, the rate of crustal and mantle formation was much greater in the time subsequent to 1.8 AE as compared to the rate between 1.8 AE and 4.55 AE. It is of interest to note that for a uniform rate of crustal formation, we calculate $T_o = 3.6$ AE the age of the oldest known terrestrial rocks. This model suggests a low initial rate of crustal formation. A self-consistent set of the remaining f and ε values for Rb-Sr and Sm-Nd may then be estimated using this mean age of 1.8 AE as discussed in detail in Appendix 3.

Assuming that the Bay of Islands data are a proper representation of the MORB source of 0.5 AE ago (Table 4.4), we may calculate the various model parameters at that time. For Rb-Sr using $f_2^{Rb/Sr} = -0.9$ from Table 5.1 and the observed $\varepsilon_{Sr,2} = -19.3$, we obtain $\bar{t} = 1.3$ AE at 0.5 AE ago. Similarly for Sm-Nd using the observed $\varepsilon_{Nd,2} = +7.8$ and the parameters in Table 5.1 we get $\bar{t} = 1.4$ AE. Equation (2.27) gives

the variation of the mean age with time. Since $d\bar{\tau}/d\tau = 1 - \bar{\tau}(d\ln M/d\tau) \leq 1$, it follows that $\bar{\tau}$ (today) - $\bar{\tau}$ (0.5 AE ago) ≤ 0.5. For Rb/Sr this difference is 0.5 implying $dM/d\tau \cong 0$ for the last 500 m.y. For Sm/Nd this difference is 0.4 implying $(d\ln M/d\tau) = 0.11\ AE^{-1}$ for the last 500 m.y. which is half of the average growth rate of the crust $[(1/T_o) = 0.22\ AE^{-1}]$. However, if the mean age measured 0.5 AE ago was 1.5 AE instead of 1.3 or 1.4 AE, then $(dM/d\tau)$ for the last 0.5 AE would be equal to the average growth rate of the crust. Thus the value for $(dM/d\tau)$ during the last 0.5 AE is very sensitive to small differences in the mean ages. No firm conclusion can be drawn but the data suggest that the average growth rate of the continents and the rate of differentiation of the mantle for the last 0.5 AE is much less than the average value over the history of the earth.

The concentrations of Rb, Sr, Nd, and Sm and the masses of the various reservoirs will now be estimated. The concentrations used for the undepleted mantle and the crust are those from Table 4.3, except for the Rb concentration in the crust which will be calculated in the following. These parameters are given in Table 5.1. Mass and species conservation leads to the following equation that relates the masses of reservoirs 2 and 3 to the f-values of 2 and 3 and the concentrations of the stable isotope in 1 and 3.

$$\frac{M_3(\tau)}{M_2(\tau) + M_3(\tau)} = \frac{f_2^{r/s}(\tau)\ C_{s,1}(\tau)}{[f_2^{r/s}(\tau) - f_3^{r/s}(\tau)]\ C_{s,3}(\tau)} \qquad (5.1)$$

This equation holds for any model as long as reservoirs 2 and 3 are derived from the reference reservoir 1. For Model I the left-hand

side of equation (5.1) must be equal to the degree of melting $F = M_3(\tau)/[M_2(\tau)+M_3(\tau)]$. The degree of melting must be the same for all species so (5.1) gives us a relation between the f-values for the Rb/Sr and the Sm/Nd system. From the values of $f_2^{Sm/Nd}$, $f_3^{Sm/Nd}$, $C_{Nd,1}$, and $C_{Nd,3}$ in Table 5.1, it follows that $F = 0.0174$. The mass of the total continental crust is 2.256×10^{25} gram which implies that the mass of the depleted mantle today is 127×10^{25} gram. This corresponds to approximately the upper 650 km of the mantle or ~ 1/3 of the mass of the mantle. As noted previously the values of $f_3^{Rb/Sr}$ and $C_{Rb,3}$ are not well known. We therefore use equation (5.1), the values of $f_2^{Rb/Sr}$, $C_{Sr,1}$, and $C_{Sr,2}$ from Table 5.1, and $F = 0.0174$ as estimated above to calculate $f_3^{Rb/Sr} = 2.18$ and $C_{Rb,3} = 33.7$. This gives $\varepsilon_{Sr,3}(0) = +65.5$ if $\bar{\tau} = 1.8$ AE.

The constraints $F = 0.0174$ and $\bar{\tau} = 1.8$ AE obtained from the Rb-Sr and Sm-Nd data will now be used for the U-Th-Pb system. The decay constants are sufficiently large, however, so the integral $I_j(\tau)$ (equation 2.24) does not have the same value as $\bar{\tau}$. The simplest model is to assume a uniform growth of the crust over the past 3.6 AE. We then get values of 2.19 AE, 8.62 AE, and 1.91 AE for $I_j(\tau)$ for ^{206}Pb, ^{207}Pb, and ^{208}Pb, respectively. These values are used with (2.24). Using $\varepsilon_{\alpha,2} = -230$ (Table 4.4) then gives $f^{U/Pb} = -0.134$. This value of $f^{U/Pb}$ then implies $\varepsilon_{\beta,2} = -50$ which is in good agreement with the measured average value of -58 (Table 4.4). Using $\varepsilon_{\gamma,2} = -177$ gives $f^{Th/Pb} = -0.199$. A complete set of selfconsistent parameters can now be obtained using $F = 0.0174$ following the same principles as outlined above. The results are given in Table 5.1. Using the bulk earth

Table 5.1. Self-consistent sets of parameters for the models

	Depleted mantle (2)		Continental crust (3)	
	Model I	Model II	Model I	Model II
Rb	0.044	0.041	33.7	29.4
Sr	15.8	14.5	370	370
$f^{Rb/Sr}$	-0.9	-0.9	+2.18	+1.78
ε_{Sr}	-27	-27	+65.5	+53.4
Sm	0.32	0.29	5.0	5.0
Nd	0.82	0.74	26	26
$f^{Sm/Nd}$	+0.225	+0.281	-0.4	-0.4
ε_{Nd}	+10	+10	-17.8	-14.3
U	0.00964	-	0.949	-
Th	0.0336	-	3.73	-
^{204}Pb	0.00102	-	0.0792	-
$f^{U/Pb}$	-0.134	-	+0.0975	-
$f^{Th/Pb}$	-0.199	-	+0.145	-
ε_{α}	-230	-	+167	-
ε_{β}	-50	-	+36	-
ε_{γ}	-177	-	+129	-
$\bar{t}_{M,3}$(AE)	1.8	1.5	1.8	1.5
M_j(grams)	127.4×10^{25}	110.5×10^{25}	2.256×10^{25}	2.256×10^{25}

concentration of ^{204}Pb from Table 4.3 crustal concentrations of U,Th and ^{204}Pb (Table 5.1) are obtained that are in reasonable agreement with the observed average values given in Table 4.3.

The possibility that undifferentiated material is being mixed with the depleted mantle by the mechanism described by equations (2.29) to (2.33) will now be considered. In this case $\beta F = M_3(\tau)/(M_2(\tau)+M_3(\tau))$. From the value of $f_2^{Rb/Sr} = -0.9$ from Table 5.1 we get from (2.35) that $\beta > 0.9$. This means that the amount of undifferentiated material that may be mixed with the depleted mantle is less than 10%. Considering only the surface area covered by continents and oceans today, we would expect $\beta = 0.42$ using the surface areas given by Ronov and Yaroshevskiy [1976]. This suggests that if Model I is valid there must be some mechanism for efficient addition to continents of melt fractions from undifferentiated material that differentiates beneath oceans.

As discussed in chapter 2 the case with $\beta < 1$ is analogous to refluxing of crust to depleted mantle in a generalized version of Model I. This shows that only 10% of the total amount of material added to the crust may have been subducted back to the depleted mantle.

5.2. MODEL II

We now evaluate the present-day parameters for this model. As for Model I we again start out with the most reliable values given in Table 4.4. Substituting $\varepsilon_{Sr,2} = -27$ and $f_2^{Rb/Sr} = -0.9$ into equation (2.63) gives $\bar{t}_{Rb/Sr} = 1.8$ AE. As discussed in detail in Appendix 3 for this model we get $M_3(T_o)/M_2(0) = 0.020\pm0.003$ and this gives $M_2(T_o) = 110.5 \times 10^{25}$ gram which is 28% of the mantle. Using this value in equation (5.1) together with $C_{Nd,1} = 1.26$ ppm, $C_{Nd,3} = 26$ ppm, and

$f_3^{Sm/Nd} = -0.4$ gives $f_2^{Sm/Nd} = +0.281$ and thus $\alpha_{Sm/Nd} = -0.248$. From equation (2.63) it now follows that $\bar{t}_{Sm/Nd} = 1.44$ AE which together with $f_3^{Sm/Nd} = -0.4$ gives $\varepsilon_{Nd,3} = -14.3$. Similarly using equation (5.1) for Rb-Sr with $f_2^{Rb/Sr} = -0.9$, $[M_3(T_o)/M_2(0)] = 0.02$, $C_{Sr,1} = 22$ ppm, and $C_{Sr,3} = 370$ ppm, we get $f_3^{Rb/Sr} = +1.78$, $C_{Rb,3} = 29.4$ ppm, and since $\bar{t}_{Rb/Sr} = 1.8$ AE it also follows that $\varepsilon_{Sr,3} = +53.4$.

A selfconsistent set of f and ε-values for Model II is now determined and is given in Table 5.1. From the values $f_2^{r/s}$ and $f_3^{r/s}$ for Sm/Nd and Rb/Sr together with $[M_3(T_o)/M_2(0)] = 0.02$ we can by using (2.51) and (2.52) determine all the d-values. Since $D_{Rb} > 0$ it follows from the value calculated for $d_{Rb} = 135.5$ that $F < 0.0076$. Choosing $D_{Rb} = 0.0025$ gives $F = 0.005$. From the calculated d-values listed in Appendix 3 and the concentrations of the undepleted reservoir we may now calculate the concentrations of these elements in the depleted reservoir. The complete set of self-consistent parameters for Model II for Rb, Sr, Sm, and Nd is given in Table 5.1. The parameters for Rb imply that the concentation of Rb in new additions to the crust has changed from 86 ppm initially to 6 ppm today giving an average concentration today of ~ 30 ppm. This large change of Rb concentration in the crust over geologic time does not appear supportable from the existing data. The magnitude of this time dependence is not changed by any choice of parameters so long as $f^{Rb/Sr}$ for the depleted mantle is close to its lower limit of -1.

Attention is now turned to what the data can tell us about the time-evolution of the continental crust. The simplest growth model would be $(dM_3/d\tau)$ = constant over the history of the earth. Using this assumption we get $\bar{t}_{Sm/Nd} - \bar{t}_{M,3} = -0.09$ AE from equation (2.66) with

τ = 4.5 AE and $\alpha_{Sm/Nd}$ = -0.248 so since $\bar{t}_{Sm/Nd}$ = 1.44 AE it follows that $\bar{t}_{M,3} \approx$ 1.5 AE. However, since $\bar{t}_{M,3} \leq \bar{t}_{Rb/Sr}$ = 1.8 AE < $(T_o/2)$ this would require that the crust started to form late. The longest time compatible with a uniform growth may be determined from equations (2.71) and (2.72). For Rb-Sr we get 2.7 AE and for Sm-Nd we get 3.0 AE for the longest time compatible with a constant growth rate of the crust using the f and ε values for reservoir 2 given in Table 4.4. These are both unrealistically low values so we must conclude that a uniform growth rate can hardly explain the data. Since the mean mass age of the crust is substantially less than $(T_o/2)$ = 2.3 AE for this model too, it is clear that the dominant parts of the continents have formed late in the earth's history.

CHAPTER 6. DISCUSSION AND CONCLUSIONS

6.1. MANTLE-CRUST TRANSPORT MODELS

The basic transport equations for the unidirectional earth differentiation models shown in Fig. 2.1 give simple results when solved for arbitrary mass growth curves $M_j(\tau)$ for the continental crust ($j = 3$) and the depleted mantle ($j = 2$). The solution for Model I is:

$$\varepsilon^*_{d,j}(\tau) = \frac{Q^*_d(\tau) f_j^{r/s}}{M_j(\tau)} \int_o^\tau M_j(\xi)\exp[\lambda(\tau-\xi)]d\xi$$

where $Q^*_d(\tau) = 10^4\lambda\left[\frac{N_{r,1}(\tau)}{N_{d,1}(\tau)}\right]$ and $f_j^{r/s}$ is the enrichment factor which is constant for all time. The mean age $\bar{\tau}_{s,j}$ of stable isotopes is equal to the mean age of the mass of j; $\bar{\tau}_{M,j} = \int_o^\tau [M_j(\xi)/M_j(\tau)]d\xi$. For longlived isotopes ($\lambda^{-1} \gg 4.5$ AE) $\varepsilon^*_{d,j} = Q^*_d\, f_j^{r/s}\, \bar{\tau}_{M,j}$ and $Q^*_d \simeq$ constant. Knowledge of $\varepsilon^*_{d,j}$ and $f_j^{r/s}$ at a single time fixes $\bar{\tau}_{M,j}$. The mean age shows the relationship $(d\bar{\tau}/d\tau) = 1 - \bar{\tau}(d\ln M_j/d\tau)$ so if $M_j(\tau)$ and $f_j^{r/s}$ are known, then $\bar{\tau}_{M,j}$ and $\varepsilon^*_{d,j}(\tau)$ are known.

For Model II which has continuous fractionation in the source reservoir, the concentrations are functions of time and we get

$$\varepsilon^*_{d,2}(\tau) = Q^*_d(\tau) \int_o^\tau f_2^{r/s}(\xi)\exp[\lambda(\tau-\xi)]d\xi$$

$$\varepsilon^*_{d,3}(\tau) = \varepsilon^*_{d,2}(\tau)\,\frac{f_3^{r/s}(\tau)}{f_2^{r/s}(\tau)}$$

$$f_2^{r/s}(\tau) = \left[\frac{M_2(\tau)}{M_2(0)}\right]^{(d_r-d_s)}$$

$$\frac{f_2^{r/s}(\tau)}{f_3^{r/s}(\tau)} = 1 - \left[\frac{M_2(\tau)}{M_2(0)}\right]^{(-d_s)}$$

Define $\bar{\tau}_{r/s} \equiv \int_o^\tau [f_2^{r/s}(\xi)/f_2^{r/s}(\tau)]d\xi$, then for long-lived isotopes we have $\varepsilon^*_{d,j}(\tau) = Q^*_d\, f_j^{r/s}(\tau)\, \bar{\tau}_{r/s}$ where $\bar{\tau}_{r/s}$ is the time required to generate $\varepsilon^*_{d,j}$ with the present value of $f_j^{r/s}$. Note that $\bar{\tau}_{r/s}$ depends on the parent-daughter system and is in general different from $\bar{\tau}_{M,3}$. The difference is given by

$$\bar{\tau}_{r/s} - \bar{\tau}_{M,3} \approx \frac{(d_r - d_s)}{2M_3(\tau)M_2(0)} \int_o^\tau M_3(\xi)[M_3(\tau) - M_3(\xi)]d\xi$$

for small $[(d_r - d_s)/M_2(0)]$. Decay systems with small $(d_r - d_s)$ may be used to estimate $\bar{\tau}_{M,3}$. These simple expressions may be used to calculate earth models with great facility without requiring a computer calculation.

6.2. THE Nd EVOLUTION CURVE FOR THE EARTH

The old CHUR curve was shown to be a good representation of the terrestrial values, although there are clear discrepancies. Consider therefore the data on Archean rocks where the claim has been made that most of the data fit the CHUR curve. All available Archean data are shown in Fig. 6.1. The small shifts in the CHUR evolution curve reported here do not alter the basic conclusions by other workers that the isotopic composition of Nd in a variety of crustal rocks follows the evolution of a reservoir with chondritic Sm/Nd. However, the more refined results reported here make it evident that more stringent tests are needed. The

Fig. 6.1. Fractional deviations in parts in 10^4 of initial $^{143}Nd/^{144}Nd$ of Archean rocks, from evolution in the CHUR reservoir. Data for Stillwater, Great Dyke, Louis Lake batholith, Preissac Lacorne batholith, Fiskenaesset anorthosite, and Amitsoq gneiss from DePaolo and Wasserburg [1976a,b, 1979]; Duffer dacite and Uivak gneiss from McCulloch [1979]; Rhodesian Greenstones, Lewisian granulite and amphibolite facies gneisses, Onweracht volcanics, and Isua volcanics, from Hamilton et al. [1977, 1978, 1979a,b].

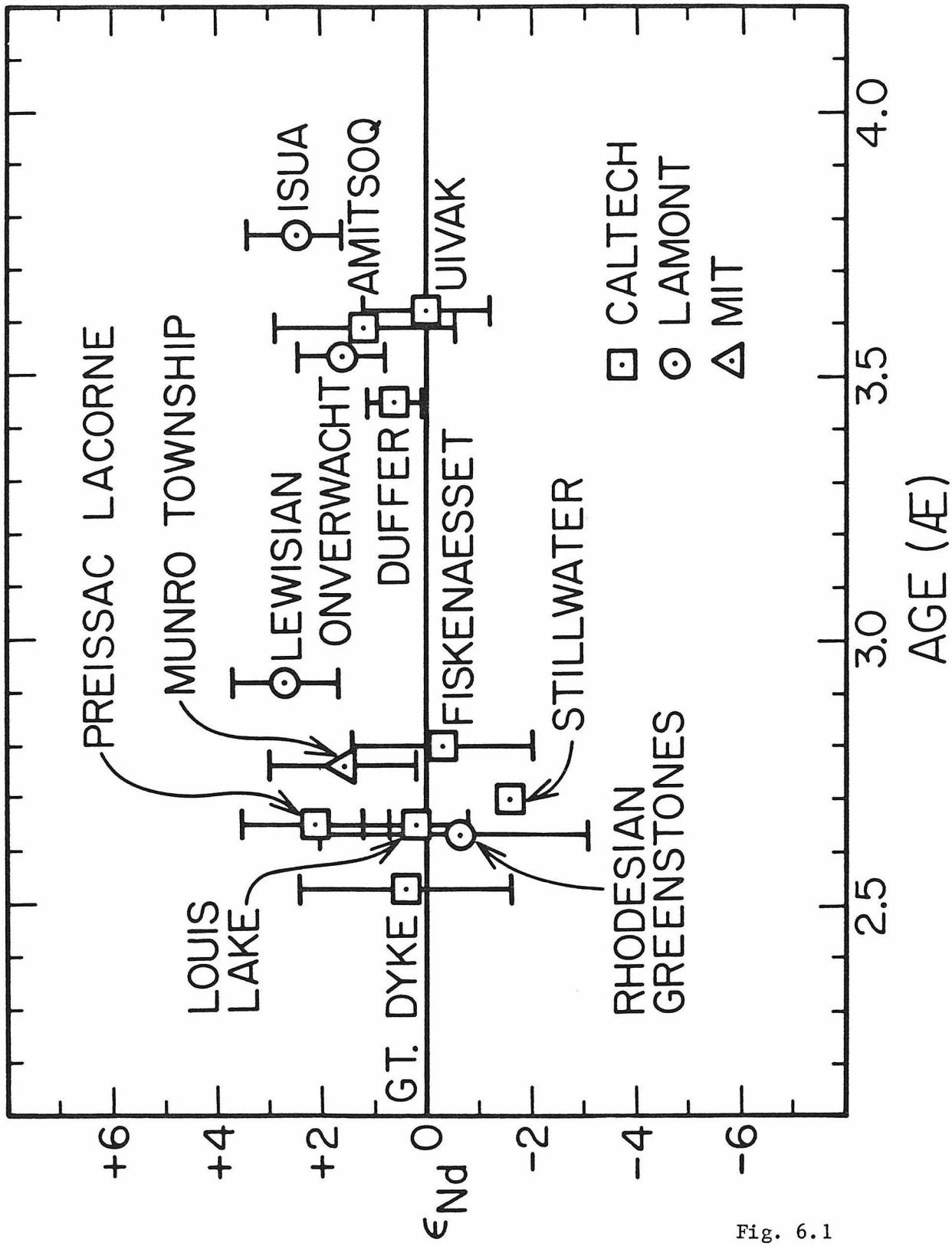
PREISSAC LACORNE
MUNRO TOWNSHIP
LEWISIAN
ONVERWACHT
DUFFER
ISUA
AMITSOQ
UIVAK
FISKENAESSET
STILLWATER
LOUIS LAKE
GT. DYKE
RHODESIAN GREENSTONES
CALTECH
LAMONT
MIT
+6
+4
+2
0
-2
-4
-6
ϵ_{Nd}
2.5
3.0
3.5
4.0
AGE (AE)

Fig. 6.1

data on the Lewisian rocks (2.9 AE) and the Isua volcanics (3.8 AE) now plot ~2.5 ε-units above the curve. These positive ε_{Nd} values indicate the presence of a depleted layer in the mantle throughout the Archean. Such a layer may represent the early evolution of the source of the present-day mid-ocean ridge basalts which today have $\varepsilon_{Nd} \approx +10$. This implies that the source of the Isua volcanics was residual mantle material that was involved in crust-forming events at least 4.2 AE ago. Most of the other data are still within error of the CHUR curve; however, they are subject to rather large uncertainties. The only precise data point is for the Stillwater [DePaolo and Wasserburg, 1979] which plots distinctly below the curve. The apparent deviations from the CHUR curve in this time region are rather large and comparable with the modern variations considering the shortened time scale. For a detailed understanding of the evolution of the Archean mantle, it will be necessary to obtain much more precise initial values and ages for Archean samples than are currently available.

Note that it is not possible to define the present-day $^{143}Nd/^{144}Nd$ in chondrites uniquely due to variability of their Sm/Nd ratio. It is possible that this is a sampling problem and that all planets formed with exactly the same values. Alternatively, bulk planets could be fractionated by 1 to 2% from the solar Sm/Nd ratio. It is well established that $\varepsilon_{Nd}(0) \approx +10$ for mid-ocean ridge basalts which clearly must sample a depleted mantle (DM). The only major enriched reservoir in the earth is the continental crust (CC) which has $\varepsilon_{Nd} \approx -18$ and is complementary to the depleted mantle. The bulk earth value has to be somewhere in between these two values. A logical choice is $\varepsilon_{Nd}(0) \approx 0$ for the bulk earth.

Currently we would assign some special significance to young rocks that cluster in the range between A and B on Fig. 6.2, namely that they are derived from a chondritic undifferentiated reservoir. However, if $\varepsilon_{Nd}^{\oplus}(0) = +2$ as shown schematically in Fig. 6.2, then undifferentiated mantle materials would have this value and basalts with a value of $\varepsilon_{Nd}(0) \approx 0$ would then be assumed to represent mixtures of magmas derived from depleted mantle and old continental crust. If many terrestrial samples plotted precisely on a curve close or identical to the CHUR curve back through time, then this would be strong evidence that these rocks were derived through time from undifferentiated mantle materials. As discussed previously at present the terrestrial data do not precisely define a curve back through time. This makes it difficult to decide whether the data are sufficient evidence for an undifferentiated reservoir in the earth or whether the terrestrial data that roughly follow the CHUR curve represent mixtures of depleted mantle and old continental crust back through time. In the absence of a very well-defined curve based on terrestrial samples the CHUR curve will be used as an approximation to the bulk earth. For typical continental crustal rocks with $f^{Sm/Nd} \approx -0.4$, the new model parameters will only cause small changes in the previously published T^{Nd}_{CHUR} model ages.

6.3. THE MANTLE ARRAY

It is of special interest here to look in detail at the data base for present-day MORB. Fig. 6.3 shows existing data for normal and chemically anomalous MOR tholeiites. The data for anomalous MORB [O'Nions *et al.*, 1977; Richard *et al.*, 1976] are mainly from the geochemical transition zone south of the Azores and have trace element and isotopic

Fig. 6.2. Hypothetical evolution of $^{143}Nd/^{144}Nd$ for the earth (⊕) and CHUR. DM represents the average $\varepsilon_{Nd}(0)$ value for depleted mantle as determined from mid-ocean ridge basalts, and CC the average $\varepsilon_{Nd}(0)$ value for the continental crust. T_C is the time of condensation and T_A the time of accretion. The figure shows the hypothetical case where the bulk earth gets a 1.7% higher Sm/Nd ratio than that of CHUR during accretion. This results in an $\varepsilon_{Nd}(0)$ value of +2 for the bulk earth today. As discussed in the text if this is the case then it may change our interpretation of data that follows the CHUR curve.

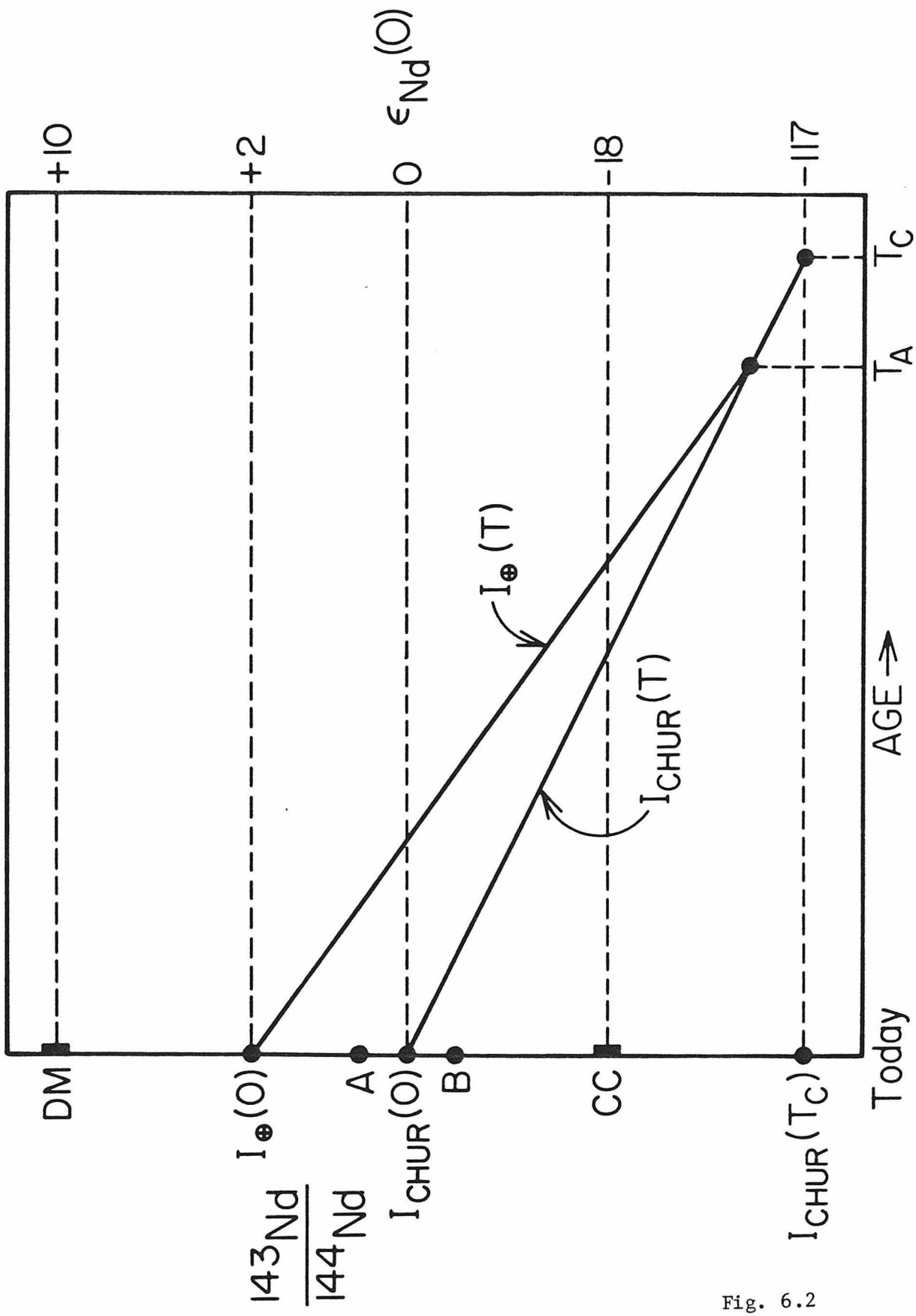
+10
+2
0
-18
-117
$\epsilon_{Nd}(0)$
T_C
T_A
$I_\oplus(T)$
$I_{CHUR}(T)$
AGE ⇒
DM
$I_\oplus(0)$
A
$I_{CHUR}(0)$
B
CC
$I_{CHUR}(T_C)$
Today
$\frac{143Nd}{144Nd}$

Fig. 6.2

characteristics intermediate between the Azores platform and normal ridge tholeiites [White and Shilling, 1978]. One sample [O'Nions et al., 1977] is from the geochemical gradient observed along the Reykjanes Ridge south of Iceland [Schilling, 1973; Sun et al., 1975]. The data for normal MORB spread out along the Mantle Array as shown in Fig. 6.3 and the data cannot be explained as samples of different reservoirs with different f values formed at one time since they do not follow the steep part of any constant time curve. The diagram rather indicates that the source of the normal MORB formed as residue after melting over a time interval from ~ 2.3 AE to 1.5 AE ago with a relatively constant degree of melting of F = 0.025 to 0.04 to form the continents. The MORB may of course represent an arbitrary degree of melting which is not directly related to the values of F given here. The average MORB represented by the cross in Fig. 6.1 indicates that the mean value for the time of differentiation is 1.9 AE for the MORB source today. The anomalous MORB are displaced toward somewhat lower ε-values along the Mantle Array. Younger differentiation ages are thus indicated for the source of anomalous MORB in the range from 1.7 to 1.0 AE ago. The oceanic island magmas mainly cluster around $\varepsilon_{Nd} = +6$ but spread out along the correlation line to $\varepsilon_{Nd} \sim 0$ and this may indicate even younger differentiation ages for their sources. It is concluded that while it is possible to explain the MORB data alone by partial melting of a reservoir formed in a unique event, it is not possible to explain the anomalous MORB or the Mantle Array by such a single stage model. It is possible that one may have a variety of depleted mantle reservoirs formed at different times due to partial melting events with relatively constant

Figure 6.3. ε_{Nd}-ε_{Sr} diagram showing data for young MOR tholeiites and the 505 m.y. old Bay of Islands pyroxene gabbros. Constant time of differentiation curves for a single stage model are shown for a range of ages from 1 to 2.5 AE and were calculated using the partial melting model discussed in Appendix 2. Constant degree of melting curves are also shown. Typical values for the Bay of Islands source are inferred to be ε_{Nd} = +7.8 and ε_{Sr} = -19.3 identical to the values for one of the pyroxene gabbros (BMD-2A). This corresponds to F = 0.03 and a time of differentiation of 1.35 AE prior to the time of crystallization which corresponds to an isolation of the source 1.85 AE ago. The expected value for the Bay of Islands source if sampled today is shown by the open square and is close to the average value for modern MOR tholeiites (cross).

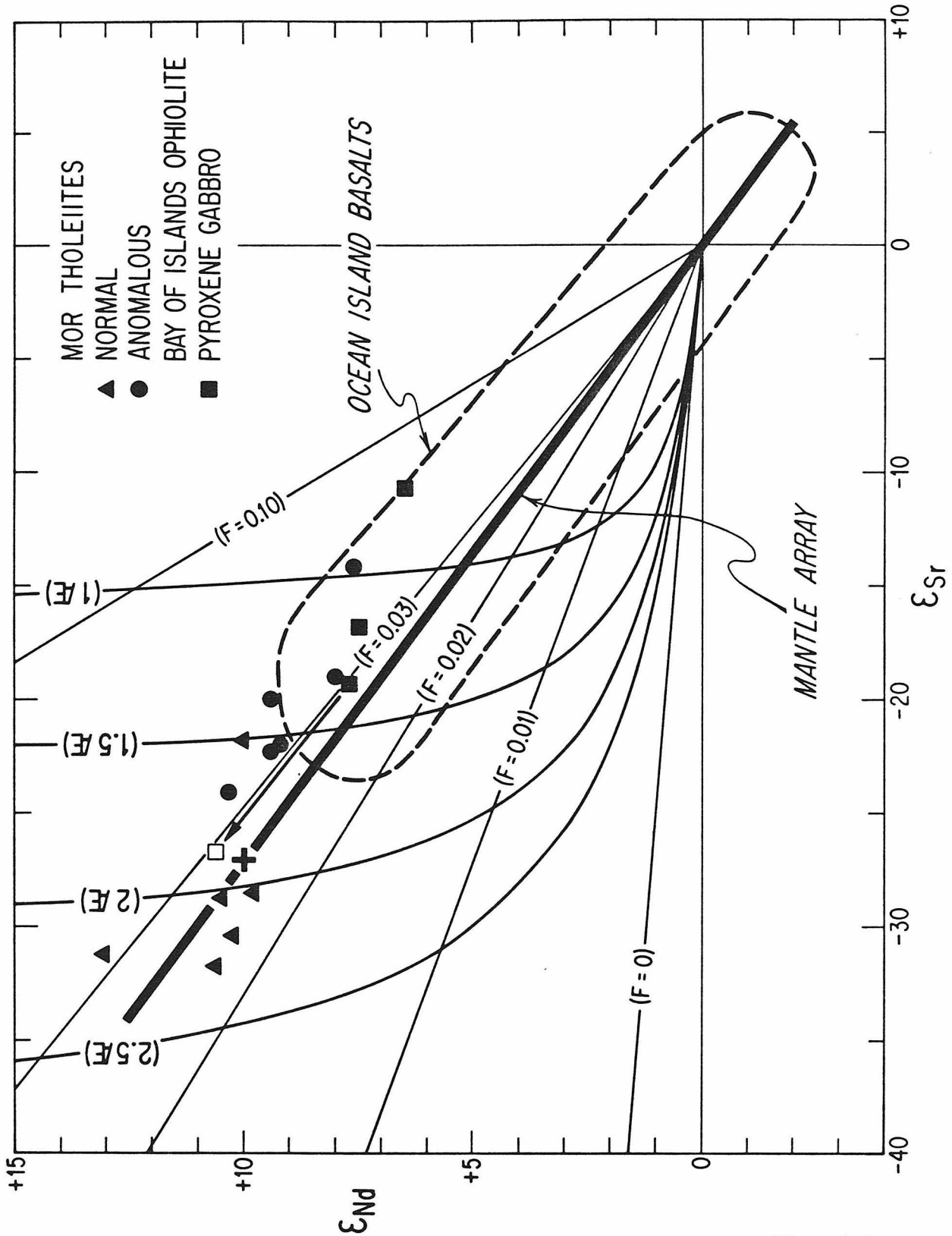
MOR THOLEIITES
NORMAL
ANOMALOUS
BAY OF ISLANDS OPHIOLITE
PYROXENE GABBRO
OCEAN ISLAND BASALTS
MANTLE ARRAY
(F=0.10)
(F=0.03)
(F=0.02)
(F=0.01)
(F=0)
(1 E)
(1.5 E)
(2 E)
(2.5 E)
+15
+10
+5
0
-40
-30
-20
-10
0
+10
εNd
εSr

Fig. 6.3

degree of melting. The set of all such reservoirs would if sampled today plot on a line. One may thus get the Mantle Array by having layers of different times of differentiation and with the degree of melting in the range from ~ 0.02 to 0.04 as indicated in Fig. 6.3. Today this would give the isotopic characteristics of basalts which lie on the correlation line. Mixtures of such reservoirs formed at different times would then also always lie on the correlation line. The simplest choice is to have only two reservoirs and the samples with isotopic characteristics intermediate between these two reservoirs would be blends of these two sources. The simplest choice of endmembers is the endpoints of the Mantle Array. Thus the source of normal MORB for the LIL depleted endmember and the origin (CHUR,UR) as the undepleted endmember is chosen. The age of the undepleted reservoir is 4.55 AE; while the age of the depleted reservoir is probably on the order of 3.6 AE as discussed in chapter 5 and its mean age is ~ 1.8 AE.

Interpretation of the Mantle Array as a mixing line is basically in agreement with the interpretations by Schilling [1973], Sun et al. [1975], and White and Schilling [1978] that anomalous MORB magmas are derived by mantle plume mixing with a LIL depleted asthenosphere. It is concluded that the Mantle Array may be most simply explained as a result of mixing of the MORB source and an undifferentiated mantle source [DePaolo and Wasserburg, 1976b; Hawkesworth et al., 1978; DePaolo and Wasserburg, 1979a; DePaolo, 1979]. This is not compatible with most of the Pb isotope data array on oceanic islands [for a review, see Tatsumoto, 1978] since this data array does not pass through the bulk earth values. Many of the oceanic islands have $^{206}Pb/^{204}Pb$ ratios that are much more radiogenic

than the bulk earth. Thus for lead an old enriched component of the mantle also appears to be involved. This may be true also for Sr and Nd, however the ratios of Sr/Nd and Sr/Pb in the various components may be such that for Nd and Sr the mixture is dominated by contribution from depleted and undepleted mantle.

6.4. MIXING IN THE DEPLETED MANTLE

The average $f^{Sm/Nd}$ value for the depleted mantle is +0.22 so we should see a range of ε_{Nd} values from 0 to +20 for depleted mantle formed over a timespan of 3.6 AE if no mixing occurred in the depleted mantle. Instead the normal oceanic mantle shows a rather limited range today from +8 to +12 implying relatively rapid mixing in the depleted mantle. The average $f^{Sm/Nd}$ = +0.12 for the upper oceanic crust and is +0.42 for the lower oceanic crust. If large blocks of the oceanic crust made up of these different materials were preserved then heterogeneities of ~ 4 ε_{Nd}-units should develop on a timescale of 0.5 AE unless these units get well mixed after being subducted back to the oceanic mantle. As the total range in ε_{Nd} today is ~ 4ε units and the Bay of Islands Complex gives an ε_{Nd} value consistent with the mean $f^{Sm/Nd}$ value for the MORB source, it is therefore inferred that rapid mixing must have occurred in the oceanic mantle for at least the last 1.0 AE.

If mixing has been going on continuously in the depleted mantle, then the degree of homogenieity in various radiogenic isotopes will depend on the decay constants. Daughter products of long-lived isotopes should all be homogenized to the same degree. However, variations in an isotope as ^{207}Pb produced from ^{235}U would have been erased to a much larger degree since these could only have been produced early in the earth's

history. The fact that the oceanic lead isotope array [Tatsumoto, 1978] has a shallower slope than the bulk earth-MORB tieline in a $^{207}Pb/^{204}Pb$-$^{206}Pb/^{204}Pb$ diagram may be due to this.

6.5. MANTLE AND CRUST DIFFERENTIATION

The results from Models I and II (Table 5.1) are first compared. The mean age of the crust is 1.8 AE for Model I and 1.5 AE for Model II so a young mean age of the crust is confirmed by both models. Similarly both models indicate that the rate of growth over the last 0.5 AE is much less than the average rate of growth. Therefore, most of the crust probably formed in the time interval from ~ 0.5 AE to ~ 3 AE ago. The Pb isotope data are also consistent with a relatively uniform growth of the crust over the past 3.6 AE. Both models also require the depleted mantle complementary to the continental crust to make up about 1/3 of the mantle which corresponds approximately to the upper 650 km of the mantle. This does not seem to be compatible with whole mantle convection as discussed by Hager and O'Connell [1979], but is more in agreement with convection in discrete layers as discussed by Richter [1979]. The present day ε and f values and the concentration in each reservoir are fairly similar for both models as shown in Table 5.1. Insofar as the mantle consists of an undepleted reservoir and a depleted reservoir that is complementary to the crust, the above conclusions are basically model independent. Model I indicates a larger degree of melting (1.7%) than Model II (0.5%). At the present time both of these values seem to be plausible estimates of the average degree of melting through time. The major difference in the results for the two models is in the composition of new additions to continental crust. Model I predicts that $\varepsilon_{Nd} = \varepsilon_{Sr} = 0$ for new

additions to the continental crust and Model II predicts that the ε_{Sr} and ε_{Nd} of new additions are those of the source of mid-ocean ridge basalts. The fact that island arcs have bulk composition and REE abundances similar to average continental crust and that they usually are found at or near continental margins has led to the hypothesis that the continents grow by accreting island arcs along their margins [Taylor and White, 1965; Ringwood, 1975]. If this is the case then the Nd isotopic studies reported by DePaolo and Wasserburg [1977] and Hawkesworth et al. [1977] show that new continental material should have ε_{Nd}-values similar to MORB and are thus derived from depleted mantle. This mechanism for continental growth is thus described by Model II. However, this model cannot explain why typically most continental crustal materials have $\varepsilon_{Nd} \approx 0$ throughout the earth's history. While values of $\varepsilon \approx 0$ may be obtained at early times for both models, it is not possible to continue production of such materials in more recent geologic time for Model II.

In Model I the concentrations of stable isotopes in new additions to the crust are the same for all time; however, in Model II the concentrations may decrease by over a factor of 10 for highly incompatible elements as K, Rb, Ba, and U. There is no evidence for such drastic changes with time. It is therefore concluded that Model I best describes crust and mantle evolution. Some additions to the continents during the last 1.5 AE have $\varepsilon_{Nd} > 0$ [DePaolo and Wasserburg, 1976a,b] so some new additions to the crust may follow Model II. A modified version of Model I where it is allowed for mixing of undepleted mantle with depleted mantle shows that this contribution must be less than 10%. This model also shows that less than 10% of the total continental crust has been refluxed

back to the depleted mantle. It is concluded that Nd,Sr and Pb isotope data are broadly consistent with a unidirectional transport model to form the earth crust by partial melting of the mantle throughout the earth's history.

Considering the young mean ages derived for the continents there is very little evidence of crust forming very early in the earth's history. Search for old crustal rocks by direct dating has established a low abundance of ~ 3.6 AE old crustal rocks and the apparent absence of much older rocks at the surface of the earth. An alternative way of looking for old crust is to look at the residue in the mantle after crust formation. If the pre-3.6 AE old crust were buried in the lower crust, then we would still expect to see it in the isotopic systematics of the depleted mantle. The depleted mantle gives a young mean age of ~ 1.8 AE and this implies either that very little early crust ever formed or that the early crust was destroyed by rapid refluxing into the mantle in the period from 4.5 AE to 3.6 AE ago. If the latter is the case then this would have caused early degassing of the earth's AR as suggested by $^{40}Ar/^{36}Ar$ ratios in the mantle [Ozima, 1975]. The detailed history of this time period must be derived from data for ^{40}K and ^{235}U and perhaps also ^{244}Pu and the extinct ^{129}I.

REFERENCES

Allègre, C. J., J. L. Birck, S. Fourcade, and M. Semet, $^{87}Rb/^{87}Sr$ age of the Juvinas achondrite and early igneous activity of the solar system, Science, 187, 436-438, 1975.

Anderson, D. L., Irreversible differentiation of the earth and plate tectonics, Science (in press, 1980).

Armstrong, R. L., A model for the evolution of strontium and lead isotopes in a dynamic Earth, Rev. Geophys. Space Phys., 6, 175-199, 1968.

Barth, T. F. W., Studies on the igneous rock complex of the Oslo Region II. Systematic petrography of the plutonic rocks. Skr. Norske Vidensk.-Akad. i Oslo, I. Mat.-Naturv. KL. 1944, No. 9, 104 pp., 1945.

Barth, T. F. W., Theoretical Petrology, Wiley, New York, 387 pp. 1952.

Brooks, C., and S. R. Hart, Rb-Sr mantle isochrons and variations in the chemistry of Gondwanaland's lithosphere, Nature, 271, 220-223, 1978.

Brooks, C., D. E. James, and S. R. Hart, Ancient lithosphere: Its role in young continental volcanism, Science, 193, 1086-1094, 1976.

Brooks, C., S. R. Hart, A. Hoffman, and D. E. James, Rb-Sr mantle isochrons from oceanic regions, Earth Planet. Sci. Lett., 32, 51-61, 1976.

Brueckner, H. K., Interpretation of Rb-Sr ages from the Precambrian and Paleozoic rocks of southern Norway, Am. J. Sci., 272, 334-358, 1972.

Brueckner, H. K., "Mantle" Rb/Sr and $^{87}Sr/^{86}Sr$ ratios for clinopyroxenes from Norwegian garnet peridotites and pyroxenites, Earth Planet. Sci. Lett., 24, 26-32, 1974.

Brueckner, H. K., A crustal origin for eclogites and a mantle origin for garnet peridotites: Strontium isotopic evidence from clinopyroxenes, Contr. Mineral. and Petrol., 60, 1-15, 1977.

Carlson, R. W., J. D. MacDougall, and G. W. Lugmair, Differential Sm/Nd evolution in oceanic basalts, Geophys. Res. Letts., 5, 229-232, 1978.

Carswell, D. A., Picritic magma-residual dunite relationships in garnet peridotite at Kalskaret near Tafjord, south Norway, Contr. Mineral. and Petrol., 19, 97-124, 1968a.

Carswell, D. A., Possible primary upper mantle periodotite in Norwegian basal gneiss, Lithos, 1, 322-355, 1968b.

Carter, S. R., N. M. Evensen, P. J. Hamilton, and R. K. O'Nions, Continental volcanics derived from enriched and depleted source regions: Nd- and Sr-isotope evidence, Earth and Planetary Science Letters, 37, 401-408, 1978.

Carter, S. R., N. M. Evensen, P. J. Hamilton, and R. K. O'Nions, Basalt magma sources during the opening of the North Atlantic, Nature, 281, 28-30, 1979.

Coleman, R. G., Ophiolites, Springer-Verlag, 1977.

Consolmagno, G. J., and M. J. Drake, Equivalence of equations describing trace element distribution during equilibrium partial melting, Geochim. Cosmochim. Acta, 40, 1421-1422, 1976.

Dasch, E. J., C. E. Hedge, and J. Dymond, Effect of sea water interaction on strontium isotope composition of deep-sea basalts, Earth Planet. Sci. Lett., 19, 177-183, 1973.

DePaolo, D. J., Study of magma sources, mantle structure and the differentiation of the earth using variations of $^{143}Nd/^{144}Nd$ in igneous rocks, Ph.D. Thesis, Calif. Inst. of Technol., Pasadena, 1978.

DePaolo, D. J., Implications of correlated Nd and Sr isotopic variations for the chemical evolution of the crust and mantle, Earth Planet. Sci. Lett., 43, 201-211, 1979.

DePaolo, D. J., and G. J. Wasserburg, Nd isotopic variations and petrogenetic models, Geophys. Res. Letts., 3, 249-252, 1976a.

DePaolo, D. J., and G. J. Wasserburg, Inferences about magma sources and mantle structure from variations of $^{143}Nd/^{144}Nd$, Geophys. Res. Letts., 3, 743-746, 1976b.

DePaolo, D. J., and G. J. Wasserburg, The sources of island arcs as indicated by Nd and Sr isotopic studies, Geophys. Res. Letts., 4, 465-468, 1977.

DePaolo, D. J., and G. J. Wasserburg, Sm-Nd age of the Stillwater Complex and the mantle evolution curve for Neodymium, Geochim. Cosmochim Acta, 43, 999-1008, 1979a.

DePaolo, D. J., and G. J. Wasserburg, Petrogenetic mixing models and Nd-Sr isotopic patterns, Geochim. Cosmochim. Acta, 43, 615-627, 1979b.

DePaolo, D. J., and G. J. Wasserburg, Nd isotopes in flood basalts from the Siberian Platform and inferences about their mantle sources, Proc. Nat. Acad. Sci. U.S., 76, 3056-3060, 1979c.

Dewey, J. F., and J. M. Bird, Origin and emplacement of the ophiolite suite: Appalachian ophiolites in Newfoundland, Journal of Geophysical Research, 76, 3179-3206, 1971.

Doe, B. R., and J. S. Stacey, The application of lead isotopes to the problem of ore genesis and ore prospect evaluation: a review, Econ. Geol., 69, 757-776, 1974.

Doe, B. R., and R. E. Zartman, Plumbotectonics, The Phanerozoic, In Geochemistry of Hydrothermal Ore Deposits, Sec. Ed., H. L. Barnes (ed.), John Wiley & Sons, New York, pp. 22-70, 1979.

Dons, J. A., and B. T. Larsen (eds.), The Oslo Paleorift, Norges Geologiske Undersøkelse, 1337, 199 pp., 1978.

Eade, K. E., and W. F. Fahrig, Chemical evolutionary trends of continental plates - a preliminary study of the Canadian shield, Bull. Geol. Surv. Can., 179, 51 pp., 1971.

Eskola, P., On the eclogites of Norway, Norsk Vidensk. Selsk. Skr., Mat. Nat. Kl., No. 8, 118 pp., 1921.

Eugster, O., F. Tera, D. S. Burnett, and G. J. Wasserburg, The isotopic composition of Gadolinium and neutron capture effects in some meteorites, J. Geophys. Res., 75, 2753-2768, 1970.

Evensen, N. M., P. J. Hamilton, and R. K. O'Nions, Rare-earth abundances in chondritic meteorites, Geochim. Cosmochim. Acta, 42, 1199-1212, 1978.

Frey, F. A., and D. H. Green, The mineralogy, geochemistry, and origin of lherzolite inclusions in victorian basanites, Geochim. Cosmochim. Acta, 38, 1023-1059, 1974.

Gancarz, A. J. and G. J. Wasserburg, Initial Pb of the Amitsoq gneiss, west Greenland, and implications for the age of the earth, Geochim. Cosmochim. Acta, 41, 1283-1301, 1977.

Gast, P. W., Limitations on the composition of the upper mantle, J. Geophys. Res., 65, 1287-1297, 1960.

Gast, P. W., N. J. Hubbard, and H. Weismann, Chemical composition and petrogenesis of basalts of Tranquility Base, In Proc. Apollo 11 Lunar Sci. Conf., pp. 1143-1163, Pergamon Press, New York, 1970.

Gray, C. M., and V. M. Oversby, The behaviour of lead isotopes during granulite facies metamorphism, Geochim. Cosmochim. Acta, 36, 939-952, 1972.

Gray, C. M., D. A. Papanastassiou, and G. J. Wasserburg, The identification of early condensates from the solar nebula, Icarus, 20, 213-239, 1973.

Green, T. H., A. O. Brunfelt, and K. S. Heier, Rare earth element distribution in anorthosites and associated high grade metamorphic rocks, Lofoten-Vesterålen, Norway, Earth Planet. Sci. Lett., 7, 93-98, 1969.

Green, T. H., A. O. Brunfelt, and K. S. Heier, Rare-earth element distribution and K/Rb ratios in granulites, mangerites and anorthosites, Lofoten-Vesterålen, Norway, Geochim. Cosmochim. Acta, 36, 241-257, 1972.

Griffin, W. L., and K. S. Heier, Parageneses of garnet in granulite-facies rocks, Lofoten-Vesterålen, Norway, Contr. Mineral. and Petrol., 23, 89-116, 1969.

Griffin, W. L., P. N. Taylor, J. W. Hakkinen, K. S. Heier, I. K. Iden, E. J. Krogh, O. Malm, K. I. Olsen, D. E. Ormaasen, and E. Tveten, Archean and Proterozoic crustal evolution in Lofoten-Vesterålen, Norway, Jour. Geol. Soc. London, 135, 629-647, 1978.

Hager, B. H., and R. J. O'Connell, Kinematic models of large-scale flow in the earth's mantle, J. Geophys. Res., 84, 1031-1048, 1979.

Hamet, J., N. Nakamura, D. M. Unruh, and M. Tatsumoto, Origin and history of the adcumulate eucrite, Moama as inferred from REE abundances, Sm-Nd and U-Pb systematics, Proc. Lunar Planet. Sci. Conf. 9th, p. 1115-1136, 1978.

Hamilton, P. J., R. K. O'Nions, and N. M. Evensen, Sm-Nd dating of Archean basic and ultrabasic volcanics, Earth Planet. Sci. Lett., 36, 263-268, 1977.

Hamilton, P. J., R. K. O'Nions, N. M. Evensen, D. Bridgwater, and J. Allaart, Sm-Nd isotopic investigations of the Isua supracrustals, West Greenland: implications for mantle evolution, Nature, 272, 41-43, 1978.

Hamilton, P. J., N. M. Evensen, R. K. O'Nions, and J. Tarney, Sm-Nd systematics of Lewisian gneisses: implications for the origin of granulites, Nature, 277, 25-28, 1979.

Hamilton, P. J., N. M. Evensen, R. K. O'Nions, H. S. Smith, and A. J. Erlank, Sm-Nd dating of Onverwacht Group Volcanics, southern Africa, Nature, 279, 298-300, 1979.

Hart, S. R., and Brooks, C., Rb-Sr mantle evolution models, Carnegie Inst. Wash. Yearbook, 69, 426-429, 1970.

Hart, S. R., A. J. Erlank, and E. J. D. Kable, Sea floor basalt alteration: some chemical and Sr isotopic effects, Contr. Mineral. and Petrol., 44, 219-230, 1974.

Hawkesworth, C. J., M. J. Norry, J. C. Roddick, and R. Vollmer, The significance of trace element modeling calculations for the evolution of Sr and Nd isotopes in the mantle, U.S. Geol. Survey Open-File Report, 78-701, 162-164, 1978.

Hawkesworth, C. J., R. K. O'Nions, R. J. Pankhurst, P. J. Hamilton, and N. M. Evensen, A geochemical study of island-arc and back-arc tholeiites from the Scotia Sea, Earth Planet. Sci. Letters, 36, 253-262, 1977.

Heier, K. S., Rubidium/Strontium and Strontium-87/Strontium 86 ratios in deep crustal material, Nature, 202, 477-478, 1964.

Heier, K. S., Radioactive elements in the continental crust, Nature, 208, 479-480, 1965.

Heier, K. S., A model for the composition of the deep continental crust, Fortschr. Mineral., 50, 174-187, 1973.

Heier, K. S., and J. A. S. Adams, Concentration of radioactive elements in deep crustal material, Geochim. Cosmochim. Acta, 29, 53-61, 1965.

Heier, K. S., and W. Compston, Interpretation of Rb-Sr age patterns in high-grade metamorphic rocks, North Norway, Norsk Geologisk Tidsskrift, 49, 257-283, 1969a.

Heier, K. S., and W. Compston, Rb-Sr isotopic studies of the plutonic rocks of the Oslo Region, Lithos, 2, 133-145, 1969b.

Heier, K. S., and J. J. Rogers, Radiometric determination of thorium, uranium and potassium in basalts and in two magmatic differentiation series, Geochim. Cosmochim. Acta, 27, 137-154, 1963.

Heier, K. S., and K. Thoresen, Geochemistry of high grade metamorphic rocks, Lofoten-Vesterålen, North Norway, Geochim. Cosmochim. Acta, 35, 89-99, 1971.

Holland, H., The Chemistry of the Atmosphere and Oceans, John Wiley & Sons, Inc., New York, 1978.

Jacobsen, S. B., and K. S. Heier, Rb-Sr isotope systematics in metamorphic rocks, Kongsberg sector, South Norway, Lithos, 11, 257-276, 1978.

Jacobsen, S. B., and G. Raade, Rb-Sr whole rock dating of the Nordagutu granite, Oslo Region, Norway, Norsk Geologisk Tidsskrift, 55, 171-178, 1975.

Karson, J., and J. F. Dewey, Coastal Complex, western Newfoundland: An Early Ordovician oceanic fracture zone, Geol. Soc. Am. Bull., 89, 1037-1049, 1978.

Kay, R. W., and R. G. Senechal, The rare earth chemistry of the Troodos ophiolite complex, J. Geophys. Res., 81, 964-970, 1976.

Kay, R., N. J. Hubbard, and P. W. Gast, Chemical characteristics and origin of oceanic ridge volcanic rocks, Journ. Geophys. Res., 75, 1585-1613, 1970.

Lambert, I. B., and K. S. Heier, The vertical distribution of uranium, thorium, and potassium in the continental crust, Geochim. Cosmochim. Acta, 31, 377-390, 1967.

Lambert, I. B., and K. S. Heier, Geochemical investigations of deep-seated rocks in the Australian shield, Lithos, 1, 30-53, 1968a.

Lambert, I. B., and K. S. Heier, Estimates of the crustal abundance of thorium, uranium and potassium, Chem. Geol., 3, 233-238, 1968b.

Lappin, M. A., R. T.Pidgeon, and O. Van Breemen, Geochronology of basal gneisses and mangerite syenites of Stadtlandet, west Norway, Norsk Geologisk Tidssknift, 59, 161-181, 1979.

Larimer, J. W., The condensation and fractionation of refractory lithophile elements, Icarus, 40, 446-454, 1979.

Lee, T., D. A. Papanastassiou, and G. J. Wasserburg, Demonstration of ^{26}Mg excess in Allende and evidence for ^{26}Al, Geophys. Res. Lett., 3, 109-112, 1976.

Lee, T., D. A. Papanastassiou, and G. J. Wasserburg, ^{26}Al in the early solar system: Fossil or fuel?, The Astrophysical J. Lett., 211, 107-110, 1977.

Lewis, R. S., Rare gases in separated whitlockite from St. Severin chondrite: xenon and krypton from fission of extinct ^{244}Pu, Geochim. Cosmochim. Acta, 39, 417-432, 1975.

Loubet, M., N. Shimizu, and C. J. Allègre Rare earth elements in alpine peridotites, Contrib. Mineral. Petrol., 53, 1-12, 1975.

Lugmair, G. W., Sm-Nd ages: a new dating method (abs.) Meteoritics, 9, 369, 1974.

Lugmair, G. W., N. B. Scheinin, and K. Marti, Search for extinct ^{146}Sm, 1. The isotopic abundance of ^{142}Nd in the Juvinas meteorite, Earth Planet. Sci. Lett., 27, 79-84, 1975a.

Lugmair, G. W., N. B. Scheinin, and K. Marti, Sm-Nd age and history of Apollo 17 basalt 75075: Evidence for early differentiation of the Lunar exterior, Proc. Lunar Sci. Conf. 6th, 1419-1429, 1975b.

Lugmair, G. W., K. Marti, J. P. Kurtz, and N. B. Scheinin, History and genesis of lunar troctolite 76535 or: How old is old? Proc. Lunar Sci. Conf. 7th, 2009-2033, 1976.

Lugmair, G. W., and K. Marti, Sm-Nd-Pu timepieces in the Angra dos Reis meteorite, Earth Planet. Sci. Lett., 35, 273-284, 1977.

Lugmair, G. W., and R. W. Carlson, The Sm-Nd history of KREEP, Proc. Lunar Sci. Conf. 9th, 689-704, 1978.

MacDonald, R., and T. Katsura, Chemical composition of Hawaiian lavas, Jour. of Petrology, 5, 82-133.

Maier, R. S. and W. Whaling, Transition probabilities in Nd (II) and the solar neodymium abundance, J. Quant. Spectrosc. Radiat. Transfer, 18, 501-507, 1977.

Malpas, J., Magma generation in the upper mantle, field evidence from ophiolite suites, and application to the generation of oceanic lithosphere, Phil. Trans. R. Soc. Lond., A.288, 527-546, 1978.

Manhes, G., J. F. Minster, and C. J. Allègre, Comparative uranium-thorium-lead and rubidium-strontium study of the Saint Sèverin amphoterite: consequences for early solar system chronology, Earth. Planet. Sci. Lett., 39, 14-24, 1978.

Masuda, A., and H. Jibiki, Rare-earth patterns of Mid-Atlantic Ridge gabbros: Continental nature?, Geochemical Journal, 7, 55-65, 1973.

Masuda, A., N. Nakamura, and T. Tanaka, Fine structures of mutually normalized rare-earth patterns of chondrites, Geochim. Cosmochim. Acta, 37, 239-248, 1973.

McCulloch, M. T. and G. J. Wasserburg, Barium and Neodymium isotopic anomalies in the Allende meteorite, The Astrophysical J., 220, L15-L19, 1978a.

McCulloch, M. T. and G. J. Wasserburg, More anomalies from the Allende meteorite: Samarium, Geophys. Res. Lett., 5, 599-602, 1978b.

McCulloch, M. T. and G. J. Wasserburg, Sm-Nd and Rb-Sr chronology of continental crust formation, Science, 200, 1003-1011, 1978c.

McCulloch, M. T., Part I. Sm-Nd and Rb-Sr chronology of crustal formation. Part II. Ba, Nd, and Sm isotopic anomalies in the Allende meteorite, Ph.D. Thesis, Calif. Instit. of Technol., Pasadena, 1979.

McCulloch, M. T., R. T. Gregory, G. J. Wasserburg, and H. P. Taylor, A neodymium, strontium, and oxygen isotopic study of the cretaceous Samail ophiolite and implications for the petrogenesis and seawater-hydrothermal alteration of oceanic crust, Earth Planet. Sci. Lett., 46, 201-211, 1980.

McSween, H. Y., Are carbonaceous chondrites primitive or processed? Rev. Geophys. Space Phys., 17, 1059-1078, 1979.

Menzies, M. A., and V. R. Murthy, Nd isotopic disequilibrium in metasomatized lherzolite nodules, Geol. Soc. of Am., Abstracts with programs, 11, 478, 1979.

Montigny, R., H. Bougault, Y. Bottinga, and C. J. Allégre, Trace element geochemistry and genesis of the Pindos ophiolite suite, Geochim. Cosmochim. Acta, 37, 2135-2147, 1973.

Moorbath, S., Age and isotope evidence for the evolution of continental crust, Phil. Trans. Roy. Soc. London, Ser. A, 288, 401-413, 1978.

Moorbath, S., H. Welke, and N. H. Gale, The significance of lead isotope studies in ancient, high-grade metamorphic basement complexes, as exemplified by the Lewisian rocks of Northwest Scotland, Earth Planet. Sci. Lett., 6, 245-256, 1969.

Nakamura, N., Determination of REE, Ba, Fe, Mg, Na, and K in carbonaceous and ordinary chondrites, Geochim. Cosmochim. Acta, 38, 757-775, 1974.

Nakamura, N. and A. Masuda, Chondrites with peculiar rare-earth element patterns, Earth Planet. Sci. Lett., 9, 359-364, 1973.

Nakamura, N., M. Tatsumoto, P. D. Nunes, D. M. Unruh, A. P. Schwab, and T. R. Wildeman, 4.4 b.y.-old clast in Boulder 7, Apollo 17: A comprehensive chronological study by U-Pb, Rb-Sr, and Sm-Nd methods, Proc. Lunar Sci. Conf. 7th, p. 2309-2333, 1976.

Neumann, E.-R., Compositional relations among pyroxenes, amphiboles and other mafic phases in the Oslo Region plutonic rocks, Lithos, 9, 85-109, 1976.

Neumann, E.-R., Petrology of the Larvikites and Associated Rocks in the Permian Oslo Rift, Studentsamskipnaden i Oslo, Oslo, 424 pp., 1979.

Neumann, E.-R., A. O. Brunfelt, and K. G. Finstad, Rare earth elements in some igneous rocks of the Oslo rift, Norway, Lithos, 10, 311-319, 1977.

Neumann, H., Apparent ages of Norwegian minerals and rocks, Norsk Geol. Tidsskr., 40, 173-191, 1960.

Notsu, K. and H. Mabuchi, The samarium-neodymium chronology of chondrites, Geochemical Journal, 9, 97-106, 1975.

Notsu, K., H. Mabuchi, O. Yoshioku, J. Matsuda, and M. Ozima, Evidence of the extinct nuclide ^{146}Sm in "Juvinas" achondrite, Earth Planet. Sci. Lett., 19, 29-36, 1973.

Nyquist, L. E., C.-Y. Shih, J. L. Wooden, B. M. Bansal, and H. Wiesmann, The Sr and Nd isotopic record of Apollo 12 basalts: Implications for lunar geochemical evolution, Proc. Lunar Sci. Conf. 10th (in press) 1979.

Oftedahl, C., and J. S. Petersen, Southern Part of the Oslo Rift, Norges Geologiske Undersøkelse, 337, 161-182, 1978.

O'Nions, R. K., and D. B. Clarke, Comparative trace element geochemistry of Tertiary basalts from Baffin Bay, Earth Planet. Sci. Lett., 15, 436-446, 1972.

O'Nions, R. K., and R. J. Pankhurst, Early Archaean rocks and geochemical evolution of the Earth's crust, Earth Planet. Sci. Lett., 38, 211-236, 1978.

O'Nions, R. K., S. R. Carter, R. S. Cohen, N. M. Evensen, and P. J. Hamilton, Pb, Nd, and Sr isotopes in oceanic ferromanganese deposits and ocean floor basalts, Nature, 273, 435-438, 1978.

O'Nions, R. K., N. M. Evensen, and P. J. Hamilton, Geochemical modeling of mantle differentiation and crustal growth, J. Geophys. Res., 84, 6091-6101, 1979.

O'Nions, R. K., N. M. Evensen, P. J. Hamilton, and S. R. Carter, Melting of the mantle past and present: isotope and trace element evidence, Phil. Trans. Roy. Soc. Lond., 258, 547-559, 1978.

O'Nions, R. K., P. J. Hamilton, and N. M. Evensen, Variations in $^{143}Nd/^{144}Nd$ and $^{87}Sr/^{86}Sr$ ratios in oceanic basalts, Earth Planet. Sci. Letts., 34, 13-22, 1977.

Ozima, M., Ar isotopes and earth-atmosphere evolution models, Geochim. Cosmochim. Acta, 39, 1127-1134, 1975.

Papanastassiou, D. A. and G. J. Wasserburg, Initial strontium isotopic abundances and the resolution of small time differences in the formation of planetary objects, Earth Planet. Sci. Lett., 5, 361-376, 1969.

Papanastassiou, D. A., D. J. DePaolo, and G. J. Wasserburg, Rb-Sr and Sm-Nd chronology and genealogy of basalts from the Sea of Tranquility, Proc. Lunar Sci. Conf. 8th, 1639-1672, 1977.

Patterson, C., Characteristics of lead isotope evolution on a continental scale in the earth, 244-268, in Craig, H. (ed.), Isotopic and Cosmic Chemistry, North Holland Pub. Co., Amsterdam, 553 p., 1964.

Patterson, C., and M. Tatsumoto, The significance of lead isotopes in detrital feldspar with respect to chemical differentiation within the earth's mantle, Geochim. Cosmochim. Acta, 28, 1-22, 1964.

Pidgeon, R. T., and A. A. Råheim, Geochronological investigation of the gneisses and minor intrusive rocks from Kristiansund, West Norway, Norsk Geologisk Tidsskrift, 52, 241-256, 1972.

Poldervaart, A., Chemistry of the Earth's crust, in Crust of the Earth, Geol. Soc. Am. Spec. Paper, 62, 119-144, 1955.

Powell, J. L., and K. Bell, Isotopic composition of strontium in alkalic rocks, 412-421, in Sørensen (ed.), The Alkaline Rocks, John Wiley and Sons, New York, 1974.

Ramberg, I. B., Gravity interpretation of the Oslo Graben and associated igneous rocks, Norges Geol. Unders., 325, 1-194, 1976.

Ramberg, I. B., and B. T. Larsen, Tectonomagmatic evolution, in Dons, J. A. and B. T. Larsen (eds.), The Oslo Paleorift, Norges Geol. Unders., 337, 56-73, 1978.

Richard, P., N. Shimizu, and C. J. Allègre, $^{143}Nd/^{146}Nd$, a natural tracer: an application to oceanic basalts, Earth Planet. Sci. Letts., 31, 269-278, 1976.

Richard, P., D. Rousseau, and C. J. Allègre, Nd and Sr systematics in ophiolites, U.S. Geol. Survey Open-File Report, 78-701, 350, 1978.

Richter, F. M., Focal mechanisms and seismic energy release of deep and intermediate earthquakes in the Tonga-Kermadec region and their bearing on the depth extent of mantle flow, J. Geophys. Res., 84, 6783-6795, 1979.

Ringwood, A. E., Composition and Petrology of the Earth's Mantle, 618 pp., McGraw-Hill, New York, 1975.

Ronov, A. B., and A. A. Yaroshevsky, A new model for the geochemical structure of the earth's crust, Geochem. Int., 13, 89-121, 1976.

Ross, J. E. and L. H. Aller, The chemical composition of the Sun, Science, 191, 1223-1229, 1976.

Russ, G. P., III, Neutron stratigraphy in the lunar regolith, Ph.D. Thesis, Calif. Inst. of Technol., Pasadena, 1974.

Russ, G. P., D. S. Burnett, R. E. Lingenfelter, and G. J. Wasserburg, Neutron capture on ^{147}Sm in lunar samples, Earth Planet. Sci. Lett., 13, 53-60, 1971.

Russell, R. D., Evolutionary model for lead isotopes in conformable ores and in ocean volcanics, Rev. Geophys. Space Phys., 10, 529-549, 1972.

Russell, R. D., and D. J. Birnie, A bi-directional mixing model for Pb-isotope evolution, Phys. Earth Plan. Interiors, 8, 158-166, 1974.

Saffman, L. and W. Whaling, Transition probabilities in Sm II and the solar abundance of samarium, J. Quant. Spectrosc. Radiat. Transfer, 21, 93-98, 1979.

Safranov, V. S., Evolution of the protoplanetary cloud and the formation of the earth and planets (in Russian), Nauka Moscow, English transl. as NASA TT F-677, NTIS, Springfield, VA, 1972.

Schilling, J. G., Sea-floor evolution: Rare earth evidence, Phil. Trans. Roy. Soc. London, Ser. A, 663-706, 1971.

Schilling, J. G., Iceland mantle plume: geochemical study of the Reykjanes Ridge, Nature, 242, 565-571, 1973.

Schmitt, R. A., R. H. Smith, J. E. Lasch, A. W. Mosen, P. A. Olehy, and J. Vasilevskis, Abundances of fourteen rare-earth elements, scandium and yttrium in meteoritic and terrestrial matter, Geochim. Cosmochim. Acta, 27, 577-622, 1963.

Schmitt, R. A., R. H. Smith, and D. A. Olehy, Rare earth, yttrium and scandium abundances in meteoritic and terrestrial matter - II, Geochim. Cosmochim. Acta, 28, 67-86, 1964.

Schnetzler, C. C. and M. L. Bottino, Some alkali, alkaline-earth and rare-earth element concentrations and the Rb-Sr age of the Lost City meteorite and separated phases, J. Geophys. Res., 76, 4061-4066, 1971.

Schramm, D. N., and G. J. Wasserburg, Nucleochronologies and the mean age of the elements, Astrophys. J., 162, 57-69, 1970.

Segalstad, T. V., Petrology of the Skien basaltic rocks, southwestern Oslo Region, Norway, Lithos, 12, 221-239, 1979.

Shaw, D. M., Trace element fractionation during anatexis, Geochim. Cosmochim. Acta, 34, 237-243, 1970.

Shaw, D. M., G. A. Reilly, J. R. Muysson, G. E. Pattenden, and F. E. Campbell, The chemical composition of the Canadian Precambrian shield, Can. J. Earth Sci., 4, 829-854, 1967.

Spooner, E. T. C., R. D. Beckinsale, W. S. Fyfe, and J. D. Smewing, O^{18}-enriched ophiolitic metabasic rocks from E. Liguria (Italy), Pindos (Greece), and Troodos (Cyprus), Contr. Mineral. Petrol., 47, 41-62, 1974.

Spooner, E. T. C., H. J. Chapman, and J. D. Smewing, Strontium isotopic contamination and oxidation during ocean floor hydrothermal metamorphism of the ophiolitic rocks of the Troodos Massif, Cyprus, Geochim. Cosmochim. Acta, 41, 873-890, 1977.

Stacey, J. S., and J. D. Kramers, Approximation of terrestrial lead isotope evolution by a two-stage model, Earth Planet. Sci. Lett., 26, 207-221, 1975.

Sun, S. S., and R. W. Nesbitt, Chemical heterogeneity of the Archaen mantle, composition of the earth and mantle evolution, Earth Planet. Sci. Lett., 35, 429-448, 1977.

Sun, S. S., M. Tatsumoto, and J. G. Schilling, Mantle plume mixing along the Reykjanes Ridge axis: lead isotopic evidence, Science, 190, 143-147, 1975.

Sundvoll, B., Rb-Sr-relationships in the Oslo igneous rocks, News from the Oslo region research group 6, 60, 1977.

Sundvoll, B., Rb/Sr-relationships in the Oslo igneous rocks, in E.-R. Neumann and I. B. Ramberg (eds.), Petrology and Geochemistry of Continental Rifts, 181-184, D. Reidel Publishing Company, Dordrecht, Holland, 1978.

Tanaka, T., and M. Masuda, Rare-earth elements in matrix, inclusions and chondrules of the Allende meteorite, Icarus, 19, 523-530, 1973.

Tatsumoto, M., Isotopic composition of lead in oceanic basalt and its implication to mantle evolution, Earth Planet. Sci. Lett., 38, 63-87, 1978.

Tatsumoto, M., R. J. Knight, and C. J. Allègre, Time differences in the formation of meteorites as determined from the ratio of lead-207 to lead-206, Science, 180, 1279-1283, 1973.

Taylor, P. N., An early Precambrian age for migmatitic gneisses from Vikan: Vesterålen, North Norway, Earth Planet. Sci. Lett., 27, 35-42, 1975.

Taylor, S. R., Island arc models and the composition of the continental crust, in M. Talwani and W. Pitman (eds.), Island Arcs Deep Sea Trenches and Back Arc Basins, Amer. Geophys. Union, Washington, D.C., 1977.

Taylor, S. R., and A. J. R. White, Geochemistry of andesites and the growth of continents, Nature, 205, 271-273, 1965.

Tera, F. and G. J. Wasserburg, U-Th-Pb systematics on lunar rocks and inferences about lunar evolution and the age of the moon, Proc. Lunar Sci. Conf. 5th, p. 1571-1599, 1974.

Turi, B., and H. P. Taylor, Oxygen isotope studies of potassic volcanic rocks of the Roman province, central Italy, Contrib. Mineral. Petrol., 55, 1-31, 1976.

Unruh, D. M., N. Nakamura, and M. Tatsumoto, History of the Pasamonte Achondrite: Relative susceptibility of the Sm-Nd, Rb-Sr, and U-Pb systems to metamorphic events, Earth Planet. Sci. Lett., 37, 1-12, 1977.

Veizer, J., and W. Compston, $^{87}Sr/^{86}Sr$ composition of seawater during the Phanerozoic, Geochim. Cosmochim. Acta, 38, 1461-1484, 1974.

Wasserburg, G. J., Geochronology and isotopic data bearing on the development of the continental crust, in Advances in Earth Sciences, M.I.T. Press, 1966.

Wasserburg, G. J., and D. J. DePaolo, Models of earth structure inferred from neodymium and strontium isotopic abundances, Proc. Natl. Acad. Sci., USA, 76, 8, 3594-3598, 1979.

Wasserburg, G. J. and D. A. Papanastassiou, Model ages, Nature, 259, 159-160, 1976.

Wasserburg, G. J., J. C. Huneke, and D. S. Burnett, Correlation between fission tracks and fission type Xenon in meteoritic whitlockite, J. Geophys. Res., 74, 4221-4232, 1969.

Wasserburg, G. J., D. A. Papanastassiou, and H. G. Sanz, Initial strontium for a chondrite and the determination of a metamorphism or formation interval, Earth Planet. Sci. Lett., 7, 33-43, 1969.

Wasserburg, G. J., F. Tera, D. A. Papanastassiou, and J. C. Huneke, Isotopic and chemical investigations on Angra dos Reis, Earth Planet. Sci. Lett., 35, 294-316, 1977.

Wasserburg, G. J., G. F. J. MacDonald, F. Hoyle, and W. A. Fowler, Relative contributions of uranium, thorium and potassium to heat production in the Earth, Science, 143, 465-467, 1964.

Weigand, P. W., Studies on the igneous rock complex of the Oslo region, XXIV. Geochemistry of the Oslo basaltic rocks, Skr. Norske Vidensk.-Akad. i Oslo, I. Mat.-naturo. Kl. Ny Serie, No. 34, 38 pp., 1975.

White, W. M., and J. G. Schilling, The nature and origin of geochemical variation in Mid-Atlantic Ridge basalts from the Central North Atlantic, Geochim. Cosmochim. Acta, 42, 1501-1516, 1978.

York, D., Least-squares fitting of a straight line, Can. J. Phys., 44, 1079-1086, 1966.

Zindler, A., C. Brooks, N. T. Arndt, and S. Hart, Nd and Sr isotope data from komatitic and tholeiitic rocks of Munro Township, Ontario, In Short Papers of the Fourth International Conference, Geochronology, Cosmochronology, Isotope Geology, U.S. Geol. Surv. Open-File Report, 78-701, 476 p., 1978.

APPENDIX 1.

Earth and Planetary Science Letters, 41 (1978) 245–253

[2]

INTERPRETATION OF Nd, Sr AND Pb ISOTOPE DATA FROM ARCHEAN MIGMATITES IN LOFOTEN-VESTERÅLEN, NORWAY

STEIN B. JACOBSEN and G.J. WASSERBURG

The Lunatic Asylum, Division of Geological and Planetary Sciences, California Institute of Technology, Pasadena, CA 91125 (U.S.A.)

Received May 16, 1978
Revised version received July 25, 1978

Sm-Nd data for the Archean granulite and amphibolite facies migmatites of Langøy and Hinnøy in Vesterålen are presented which indicate that their protoliths formed ~2.6 AE ago. Rubidium and U loss during a granulite facies metamorphism at ~1.8 AE caused serious disturbance of total-rock U-Pb and Rb-Sr systems. Therefore these systems do not provide any precise age information for the granulite facies migmatites. For the amphibolite facies migmatites of Vesterålen both Sm-Nd, Rb-Sr and Pb-Pb total-rock systems give model ages of ~2.6 AE. The results on both granulite and amphibolite facies rocks are thus in agreement. Previous interpretations based on Pb-Pb data, which indicated an age of 3.41 AE for the Archean terrane of Vesterålen, are not valid.

One Sm-Nd model age from the granulite facies migmatites at Moskenesøy in Lofoten indicates that the protoliths of these migmatites formed ~2.0 AE ago and are thus not related to the Vesterålen migmatites.

1. Introduction

In this report we discuss constraints on the time of crust formation in Lofoten-Vesterålen, Norway, and parent-daughter fractionation of Sm-Nd, Rb-Sr and U-Pb during the subsequent granulite facies metamorphism. This region exposes an unusually deep section through the continental crust. Taylor [1] proposed that some of the oldest terrestrial rocks occur in this area. The geologically oldest rocks in Lofoten-Vesterålen are migmatitic granulite and amphibolite facies gneisses of generally intermediate composition [8]. The migmatite complex occur over large areas of the islands of Langøy, Hinnøy and Moskenesøy. The migmatites are interpreted by Griffin et al. [8] as having formed by in-situ partial melting of volcanic rocks, accompanied by folding and boudinage, but without significant injection of any juvenile igneous component. Heier [2] and Heier and Adams [3] demonstrated for the first time that granulite facies rocks from this area are usually depleted in Rb and U.

A Rb-Sr whole-rock study by Heier and Compston [4] demonstrated a complex thermal history with events at ~2.8 AE and ~1.8 AE. Green et al. [5,6] showed that adjacent amphibolite facies gneisses have REE distribution patterns similar to the granulite facies gneisses, and Heier and Thoresen [7] in a more extensive study of both major and trace elements in these rocks demonstrated that the granulite facies rocks have been depleted in Rb, U and Th relative to the amphibolite facies rocks. Taylor [1] reported a Pb-Pb two-stage model whole-rock "isochron" age of 3.41 ± 0.07 AE and a Rb-Sr whole-rock "isochron" of 2.30 ± 0.15 AE with a high initial $^{87}Sr/^{86}Sr$ of 0.7126 for the migmatites at Vikan on the island of Langøy. He interpreted the inferred Pb-Pb age as the time of migmatite formation and the Rb-Sr age as the time of a granulite facies metamorphism resulting in Rb depletion and argued that the U-Pb system was not disturbed during granulite facies metamorphism. In an attempt to resolve this conflict, we analyzed these

Division of Geological and Planetary Sciences, Contribution No. 3094 (274).

rocks for Sm and Nd isotopes since the limited available data indicated that the REE did not fractionate during the granulite facies metamorphism. From previous studies [4,8] it seems firmly established that a period of granulite facies metamorphism took place ~1.8 AE ago and that the granulite facies assemblages were superimposed on rocks that had already been migmatized.

2. Approach

The notation with f and ϵ values (Table 2) and the approach follows that of DePaolo and Wasserburg [9,10]. We assume that the major REE fractionation for crustal rocks occurs during their derivation from a mantle reservoir. The mantle reservoir used as a reference for the Sm-Nd system (CHUR) has a nominal chondritic Sm/Nd ratio today with $(^{147}Sm/^{144}Nd)^0_{CHUR} = 0.1936$ and $^{143}Nd/^{144}Nd$ ratio today of $I^{Nd}_{CHUR}(0) = 0.511836$ [9]. $^{143}Nd/^{144}Nd$ in CHUR at any time T in the past is given by:

$$I^{Nd}_{CHUR}(T) = I^{Nd}_{CHUR}(0) - \left(\frac{^{147}Sm}{^{144}Nd}\right)^0_{CHUR} (e^{\lambda_{Sm}T} - 1)$$

where λ_{Sm} is the ^{147}Sm decay constant. The reference reservoir for Rb-Sr (UR) has $(^{87}Rb/^{86}Sr)^0_{UR} = 0.0839$ and the value of $^{87}Sr/^{86}Sr$ in UR at any time T in the past is given by:

$$I^{Sr}_{UR}(T) = I^{Sr}_{UR}(0) - \left(\frac{^{87}Rb}{^{86}Sr}\right)^0_{UR} (e^{\lambda_{Rb}T} - 1)$$

where $I^{Sr}_{UR}(0) = 0.7045$ is the value of $^{87}Sr/^{86}Sr$ in UR today [10] and λ_{Rb} is the ^{87}Rb decay constant. These reference reservoirs may be representative of the bulk earth.

Model ages T^{Nd}_{CHUR} and T^{Sr}_{UR} can be calculated relative to these reference reservoirs and date the time in the past at which $^{143}Nd/^{144}Nd$ and $^{87}Sr/^{86}Sr$ ratios in the samples were identical to those in the reference reservoirs CHUR and UR, respectively. The model ages are given by:

$$T^{Nd}_{CHUR} = \frac{1}{\lambda_{Sm}} \times \ln\left[1 + \frac{I^{Nd}_{CHUR}(0) - (^{143}Nd/^{144}Nd)_m}{(^{147}Sm/^{144}Nd)^0_{CHUR} - (^{147}Sm/^{144}Nd)_m}\right]$$

$$T^{Sr}_{UR} = \frac{1}{\lambda_{Rb}} \times \ln\left[1 + \frac{I^{Sr}_{UR}(0) - (^{87}Sr/^{86}Sr)_m}{(^{87}Rb/^{86}Sr)^0_{UR} - (^{87}Rb/^{86}Sr)_m}\right]$$

where the subscript m denotes the ratio measured in the rock today. All Archean rocks that have been measured so far have initial $^{143}Nd/^{144}Nd$ ratios very close to CHUR [9–11,19], strongly suggesting that T^{Nd}_{CHUR} model ages should be a reliable measure of the time of formation of continental crustal rocks. The approach outlined above have been used by McCulloch and Wasserburg [12] to ascertain the times at which new segments of continental crust were formed. They showed that for Canadian Shield composites $T^{Nd}_{CHUR} \simeq T^{Sr}_{UR}$ for samples ranging in age from ~1.0 to 2.7 AE.

Deviations of 1 to 2 parts in 10^4 from CHUR may well still exist for the Archean mantle sources. The lunar data [16] clearly shows that planetary differentiation processes exist that could have caused large deviations from CHUR in the sources of old terrestrial rocks. However, the terrestrial data suggest that the earth did not undergo an early differentiation event which caused large variations of the Sm/Nd ratio in the earth's early mantle. For small Sm/Nd fractionations relative to CHUR the T^{Nd}_{CHUR} model ages are very sensitive to uncertainties in the parameters used for the mantle sources. However, for the large Sm/Nd fractionations reported here an error of one part in 10^4 in $I^{Nd}_{CHUR}(0)$ will make an error of ~0.08 AE in the T^{Nd}_{CHUR} model age. Typically most quartzo-feldspathic continental crustal rocks show a marked LREE enrichment with respect to chondrites and a small range of Sm/Nd ratios [12]. This implies that this is a primary characteristic of continental crustal rocks and not due to later metamorphism or remelting of crustal materials. For T^{Nd}_{CHUR} ages to represent the time of formation of the protoliths of metamorphic rocks requires that the $^{147}Sm/^{144}Nd$ and $^{143}Nd/^{144}Nd$ ratios do not change during later metamorphic events. Since Sm and Nd will undoubtedly be redistributed between minerals during recrystallization sufficiently large samples representative of the mineralogic mode are needed.

As an alternative to the T^{Nd}_{CHUR} model age approach, Sm-Nd data can be considered in terms of the conventional isochron diagram with the usual assumptions

for such an approach. The initial ratio that may be obtained this way will place constraints upon the prehistory of the reservoir from which the crustal rocks were generated. However, due to the small range of Sm/Nd ratios in the rocks we analyzed this will be very critically dependent on the assumption that all the samples have a common age and initial $^{143}Nd/^{144}Nd$.

Rather than rely on the total-rock isochron approach we will emphasize comparison of T^{Sr}_{UR} and T^{Nd}_{CHUR} model ages for samples of various metamorphic grade. The major difference between the Rb-Sr system and Sm-Nd system is that for most continental crustal rocks $f_{Rb/Sr} \gg 0$ while $f_{Sm/Nd} < 0$. It is also well known that Rb and Sr may migrate on a whole-rock scale during metamorphism and commonly, metamorphic rocks do not therefore behave as simple closed systems. Thus disagreement between T^{Nd}_{CHUR} and T^{Sr}_{CHUR} model ages may be used to indicate redistribution of Rb and Sr on a whole-rock scale.

For the evolution of $^{206}Pb/^{204}Pb = \alpha$ and $^{207}Pb/^{204}Pb = \beta$ in the mantle we use [13,14]:

$$\alpha_I(T) = \alpha_I(T_E) + \mu(e^{\lambda T_E} - e^{\lambda T})$$

$$\beta_I(T) = \beta_I(T_E) + \frac{\mu}{137.8}(e^{\lambda' T_E} - e^{\lambda' T})$$

where $\lambda = 0.155125\ AE^{-1}$ and $\lambda' = 0.98485\ AE^{-1}$ are the decay constants for ^{238}U and ^{235}U, respectively, $T_E = 4.45$ AE, $\mu = 9.4$, $\alpha_I(T_E) = 9.307$ and $\beta_I(T_E) = 10.294$.

3. Samples

The Langøy and Hinnøy migmatites are extremely heterogeneous on the outcrop scale. The migmatites at Vakan, Langøy, are granodioritic to granitic in composition and markedly more silicic than the rest of the Langøy and Hinnøy migmatites which are tonalitic to granodioritic [8]. We have selected three samples from Vikan. The samples GS-5 and GS-23 are two of the samples analyzed by Taylor [1] for Pb isotopes. GS-23 is a granitic granulite that plots on Taylor's Pb-Pb "isochron". GS-5 is a dioritic granulite and is one of the three samples that plotted distinctly off the Pb-Pb "isochron". V-9 is a granodioritic granulite collected by us at Vikan in the same general locality as sampled by Taylor. GS-5 is a petrographically untypical sample from this locality while GS-23 and V-9 represent the major lithologies occurring at Vikan. V-34 is a tonalitic garnet granulite from Myhre, northwest Langøy and this is the most common rock type at this locality. AM-6 (tonalitic gneiss) is a typical sample of the heterogeneous amphibolite facies migmatites on Hinnøy. The Hinnøy migmatites grades into a large, heterogeneous body of granodioritic to granitic composition called the Gullesfjord granitic gneiss. GUG-2 is a representative sample from this body. The Moskenesøy migmatites are more basic in composition (dioritic to monzonitic) and more homogeneous than those of Langøy and Hinnøy [8]. TL-39 is a monzonitic granulite sample from Reine at Moskenesøy.

4. Experimental procedures and results

Samples GS-23, GS-5 and TL-39 were obtained in finely powdered form from the Mineralogical-Geological Museum in Oslo. The remaining samples were collected by us. Since the rocks have a metamorphic overprint we have used large (5–10 kg) samples believed to be representative of the mode. Typically large portions of these samples were split into ~5-g chips. Approximately 200–300 g of representative chips with fresh surfaces were then finely powdered in a stainless steel mortar. The homogeneity of the powders were checked by repeat dissolution of GS-5. The results for dissolution A (~80 mg) and B (~1.5 g) are in excellent agreement (Table 1).

Detailed descriptions of the chemical and mass spectrometric procedures are given by Papanastassiou and Wasserburg [15] for Rb and Sr, and by Papanastassiou et al. [16] for Sm and Nd. Errors given for the $^{143}Nd/^{144}Nd$ and $^{87}Sr/^{86}Sr$ are 2 σ mean of about 200–300 ratios for Nd and 100–200 ratios for Sr. Neodymium, Sm, Rb and Sr concentrations were obtained by isotope dilution techniques by total spiking of the samples. Small (<1%) aliquots of each sample were used for establishing the concentrations of Rb, Sr, Sm and Nd in a single mass spectrometer run. The remaining aliquot was then spiked optimally. The 2 σ mean errors given for the T^{Nd}_{CHUR} and T^{Sr}_{UR} ages only allow for analytical errors and do not include uncertainties in the parameters used for the mantle sources. Table 1 summarizes the data for the samples

TABLE 1

Analytical results

Sample	Sr (ppm)	Nd (ppm)	$^{87}Rb/^{86}Sr$ [a]	$^{87}Sr/^{86}Sr$	$^{147}Sm/^{144}Nd$ [b]	$^{143}Nd/^{144}Nd$ [c]
GS-5A	573	28.8	0.03681	0.70890 ± 8	0.10327	0.510410 ± 23
GS-5B [d]		28.7			0.10345	0.510418 ± 23
GS-23	142	37.0	2.015	0.79026 ± 6	0.08602	0.509961 ± 16
V-9	479	18.6	0.2800	0.72276 ± 3	0.09075	0.510042 ± 19
V-34	557	26.4	0.1997	0.70969 ± 6	0.07084	0.509731 ± 24
GUG-2	142	79.5	4.244	0.85847 ± 7	0.09146	0.510037 ± 14
AM-6	541	22.7	0.6621	0.72528 ± 3	0.07354	0.509719 ± 14
TL-39	1147	47.4	0.1361	0.70674 ± 4	0.10739	0.510679 ± 22

[a] Uncertainty ±0.4%.
[b] Uncertainty ±0.1%.
[c] Normalized to $^{146}Nd/^{142}Nd = 0.636151$.
[d] Repeat dissolution of finely powdered sample.

TABLE 2

Evolutionary parameters and model ages for Nd and Sr

Sample [a]	$f_{Rb/Sr}$ [c]	$\epsilon_{Sr}(0)$ [c]	$f_{Sm/Nd}$ [c]	$\epsilon_{Nd}(0)$ [c]	$T^{Sr}_{UR}(AE)$ [d]	$T^{Nd}_{CHUR}(AE)$ [d]
I. Langøy (granulite facies)						
GS-5A (dioritic granulite)	−0.5613	+62.5 ± 1.1	−0.4666	−27.9 ± 0.5	−7.06 ± 0.11	2.39 ± 0.04
GS-5B [b]			−0.4657	−27.7 ± 0.5		2.39 ± 0.04
GS-23 (granitic granulite)	+23.02	+1217.3 ± 0.8	−0.5557	−36.6 ± 0.3	3.13 ±0.02	2.64 ± 0.02
V-9 (granodioritic granulite)	+2.337	+259.2 ± 0.4	−0.5313	−35.1 ± 0.4	6.41 ± 0.05	2.64 ± 0.03
V-34 (tonalitic granulite)	+1.380	+73.7 ± 0.8	−0.6341	−41.1 ± 0.5	3.15 ± 0.06	2.60 ± 0.03
II. Hinnøy (amphibolite facies)						
GUG-2 (granitic gneiss)	+49.58	+2185.5 ± 0.8	−0.5276	−35.1 ± 0.3	2.61 ± 0.01	2.67 ± 0.02
AM-6 (tonalitic gneiss)	+6.892	+295.0 ± 0.4	−0.6201	−41.4 ± 0.3	2.54 ± 0.02	2.67 ± 0.02
III. Moskenesøy (granulite facies)						
TL-39 (monzonitic granulite)	+0.6222	+31.8 ± 0.6	−0.4453	−22.6 ± 0.4	3.02 ± 0.08	2.04 ± 0.04

[a] GS-23, GS-5 and V-9 are from Vikan [8, location 1], southwest Langøy; V-34 from Myhre, northwest Langøy; GUG-2 from the west side of Gullesfjord; AM-6 from Kringlen quarry northwest Hinnøy; and TL-39 from Reine [8, location 2].
[b] Repeat dissolution of finely powdered sample.
[c] Deviations from the reference reservoirs UR and CHUR given as $f_{Rb/Sr} = [(Rb/Sr)_m/(Rb/Sr)_{UR} - 1]$, $\epsilon_{Sr}(0) = [(^{87}Sr/^{86}Sr)_m/I^{Sr}_{UR}(0) - 1] \times 10^4$, $f_{Sm/Nd} = [(Sm/Nd)_m/(Sm/Nd)_{CHUR} - 1]$ and $\epsilon_{Nd}(0) = [(^{143}Nd/^{144}Nd)_m/I^{Nd}_{CHUR}(0) - 1] \times 10^4$.
[d] Decay constants $\lambda(^{147}Sm) = 0.00654\ AE^{-1}$; $\lambda(^{87}Rb) = 0.0139\ AE^{-1}$.

from Lofoten-Vesterålen used to calculate T^{Nd}_{CHUR} and T^{Sr}_{UR} model ages. Table 2 gives the f and ϵ values and the model ages.

5. Discussion

5.1. Present results

The Sm-Nd data are shown in Fig. 1. All the samples show strong LREE enrichment as the measured $f_{Sm/Nd}$ values are ~−0.45 to −0.63 (Table 2). This is consistent with previously published REE patterns for these rocks [5,6]. It is clear from Fig. 1 that all the data do not define an isochron. All the Langøy (granulite facies) and Hinnøy (amphibolite facies) data, excluding GS-5, define a good linear array in the Sm-Nd evolution diagram. These five samples represent major lithological units on Langøy and Hinnøy and have a rather small range of $^{147}Sm/$

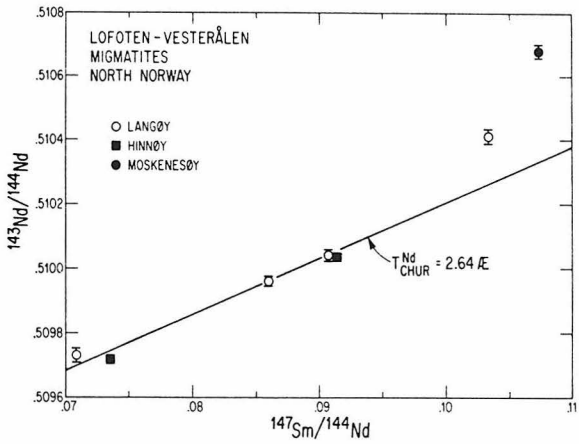

Fig. 1. Sm-Nd systematics of Lofoten-Vesterålen migmatites compared to a T^{Nd}_{CHUR} = 2.64 AE reference isochron. Samples that were fractionated from a chondritic reservoir at this time should be within error of this line. Deviations from the reference isochron are clearly significant. For the Hinnøy data the errors are of the same size as the symbol used. The five samples that plot close to the 2.64-AE reference isochron all represent major lithologies on Langøy and Hinnøy. The Langøy sample that plots distinctly off from this reference isochron indicates that younger lithic components also occur in these rocks. The Moskenesøy migmatites give T^{Nd}_{CHUR} = 2.04 ± 0.04 AE appear to be distinctly younger than the Langøy and Hinnøy migmatites.

^{144}Nd ratios from ~0.07 to 0.09. Therefore a best fit slope gives a rather imprecise age of 2.60 ± 0.36 AE and an initial ratio I_{Nd} = 0.50847 ± 20 that is within error of the CHUR evolution line.

As shown in Table 2 these five samples have very consistent T^{Nd}_{CHUR} model ages of 2.6–2.7 AE with a mean model age of 2.64 AE. Since this is true for both amphibolite and granulite facies samples that represent major lithologies in the area, it follows that Sm-Nd did not fractionate during the much later granulite facies metamorphism. If we look at the T^{Sr}_{UR} model ages in Table 2, it is clear that none of the T^{Sr}_{UR} model ages for the granulite facies samples agree with their T^{Nd}_{CHUR} model ages. Two granulite samples give geologically impossible ages. For the two amphibolite facies samples there is, however, a relatively good agreement between the T^{Nd}_{CHUR} and T^{Sr}_{UR} model ages. This demonstrates that the Rb-Sr total rock system was seriously disturbed during the much later granulite facies metamorphism. We consider the mean T^{Nd}_{CHUR} model age of 2.64 AE to provide the best estimate for the original time of formation of the protoliths of the Langøy and Hinnøy migmatites.

The dioritic granulite sample GS-5 from Vikan at Langøy plots distinctly off from the reference isochron in Fig. 1 and has a T^{Nd}_{CHUR} model age of 2.39 ± 0.04 AE. For samples strongly depleted in Rb, with Rb/Sr ratios lower than that of UR, it is possible to get negative T^{Sr}_{UR} model ages. An example is the dioritic sample which has T^{Sr}_{UR} = −7.06 ± 0.11 AE; so, with the presently low Rb/Sr ratio of this sample it would not develop the measured 87/86 ratio before ~7 AE in the future. This implies that for some time in the past this sample had a much higher Rb/Sr ratio. GS-5 is a petrographically untypical sample from Vikan (P.N. Taylor, personal communication). It is one of the samples that plotted distinctly off from Taylor's Pb-Pb two-stage model isochron for this locality. It is thus distinctly different in both Sm-Nd, Rb-Sr and U-Pb systematics from other samples at this locality. Therefore, there are lithic components in the migmatites at Vikan that are either somewhat younger than the typical migmatites or have been disturbed with respect to all three decay systems during the ~1.8 AE granulite facies metamorphism.

Sample TL-39 from Moskenesøy appears to be distinctly younger as it gives T^{Nd}_{CHUR} = 2.04 ± 0.04 AE. This sample has a T^{Sr}_{UR} model age of 3.02 ± 0.08 AE. However, the low measured $^{87}Sr/^{86}Sr$ ratio of 0.70674 makes this particularly sensitive to the assumptions involved in calculating the model age. The sample plots within error of a Rb-Sr total-rock isochron giving T = 1.78 ± 0.03 AE and I_{Sr} = 0.7037 ± 3 reported by Heier and Compston [4] for the Lofoten granulites. This isochron included samples of the Moskenesøy granulites. It has been suggested that the Moskenesøy granulites are as old as the Langøy and Hinnøy migmatites but that they have been updated during the 1.8-AE event by essentially complete removal of radiogenic Sr [4,8,20]. The distinctly younger T^{Nd}_{CHUR} model age indicates, however, that the protoliths of the Moskenesøy migmatites are distinctly younger and not related to the Langøy and Hinnøy migmatites.

The difficulty of identifying correlative lithologic units in such complex terranes is well known. There is always a danger that either the field observations or the isotopic data are interpreted erroneously. We believe that preceding arguments are sufficient to

demonstrate that the protoliths of the major portions of the migmatites on Langøy and Hinnøy formed ~2.6 AE ago and that distinctly younger ages are indicated for GS-5 and TL-39.

5.2. Comparison with and discussion of previous results

Taylor [1] obtained a fairly good linear array of data points in a Rb-Sr evolution diagram for the migmatites at Vikan; some scatter about the best-fit line, however, suggests a disturbed Rb-Sr system. We present three additional analyses from the same locality in Table 1. Two of these plot far from Taylor's Rb-Sr "isochron". Further, all the data from Vikan in Table 1 and Taylor's data plot to the left of a T_{UR}^{Sr} = 2.64 AE reference isochron which suggests Rb depletion significantly later than the time of formation of the protoliths of the migmatites. This is still true for reference isochrons with any other reasonable choice of $^{87}Sr/^{86}Sr$ in the mantle at this time. Therefore the high initial Sr values indicated are due to Rb loss rather than remelting of older crust. This means that for all samples which have higher Rb/Sr ratio than that of UR we get $T_{UR}^{Sr} > 2.64$ AE. Taylor excluded three data points from the Pb-Pb two-stage model "isochron" regression analysis and even then the analytical errors had to be expanded by a factor of seven for all the data to be within error of the best fit line. Thus the Pb-Pb and Rb-Sr data by Taylor [1] and our Rb-Sr data for the migmatites at Vikan display significant scatter and neither age nor initial Sr or Pb isotopic ratios can be precisely determined from these data.

Although there is no evidence for Rb or U depletion in the amphibolite-facies migmatites, previously published Rb-Sr data [4,8] imply that the Rb-Sr whole-rock systems have been significantly disturbed but still indicate an age of ~2.5 AE. The two amphibolite facies samples in Table 1 give T_{UR}^{Sr} model ages of 2.54 and 2.61 AE that are slightly lower than their T_{CHUR}^{Nd} ages of 2.67 AE. A Pb-Pb two-stage model total-rock isochron for the amphibolite facies migmatites also gives a similar result of 2.69 ± 0.07 AE [8].

The major Sm/Nd fractionation most likely occurs during the formation of the protoliths of the migmatites. However, large fractionations of Rb/Sr and U/Pb are expected both during the formation of the protoliths of the migmatites and during the subsequent migmatization. The fact that all three decay systems give similar ages for the amphibolite facies migmatites imply that the timespan between these two events must have been short, on the order of less than 0.1–0.2 AE. Therefore, this stage can for practical purposes be ignored in the following model calculations.

Taylor interpreted the linear Pb isotope array for the Vikan migmatites to give an age of 3.41 AE with a μ of 11.2 in the stage prior to this time and argued that the U-Pb system had essentially been left undisturbed from that time up to the present. For such a model his Pb-Pb data require μ's of 5–8 in the last stage for most of the samples and a total range of 3–12.

The average measured μ-values of the granulite facies rocks in this area calculated from the U-Pb data of Heier and Thoresen [7] is 2.0. Such low measured μ-values are also typical of other granulite facies terrains [17,18]. This shows that if Taylor's samples were at all representative of this rock complex it is not possible to explain the large range in measured α and β values in terms of his model. We therefore reject this interpretation. Instead we use the T_{CHUR}^{Nd} model age obtained from the Sm-Nd data and will show that the Pb and Sr isotope data can then be well explained in terms of a model, with the time of formation of these crustal rocks at T_x = 2.64 AE and the time of granulite facies metamorphism at T_M = 1.8 AE.

We can then calculate a μ_1 value for time interval from T_x to T_M (stage 1) and a μ_2 value for the time interval T_M to 0 (stage 2) from the following equations:

$$\alpha_m = \alpha_I(T_x) + \mu_1(e^{\lambda T_x} - e^{\lambda T_M}) + \mu_2(e^{\lambda T_M} - 1)$$

$$\beta_m = \beta_I(T_x) + \frac{\mu_1}{137.8}(e^{\lambda' T_x} - e^{\lambda' T_M}) + \frac{\mu_2}{137.8}(e^{\lambda' T_M} - 1)$$

where the subscript m denotes the ratio measured in the rock today. The μ_1 values calculated from Taylor's Pb data are in the range from 2 to 38 with an average of ~13. The highest values are found in the granitic rocks. Most of the calculated μ_2 values are in the range from 1 to 4, the total range is from 0.4 to 14 and the average is 3.0. The U/Pb fractionation factor at T_M is then given by $F_{U/Pb} = \mu_2/\mu_1$ and we calculate an aver-

age $F_{U/Pb}$ ~0.25, which compares well with the average μ_G/μ_A of ~0.33 (G = granulite facies, A = amphibolite facies) calculated from the U-Pb data of Heier and Thoresen [7] for these migmatites. The very low μ-values of the granulite facies gneisses today, indicated both by these calculations and the U-Pb data of Heier and Thoresen [7], imply that their Pb isotope composition has changed much less since 1.8 AE than in the time interval from 2.64 to 1.8 AE when the μ-values averaged ~13. Thus the isochron that was produced in the time interval from 2.64 to 1.8 AE has generally been preserved and has only been slightly shifted to the right in a α-β diagram. Our interpretation of the Pb data is shown in Fig. 2. The dashed line in this figure is the T = 3.41 AE two-stage model Pb-Pb isochron of Taylor.

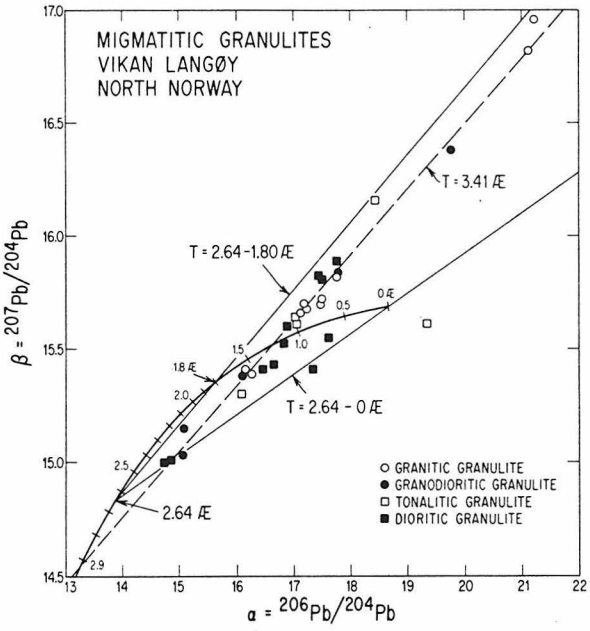

Fig. 2. Lead isotopic data on total rocks from Vikan [1]. The parameters for the growth curve shown are given in the text. The Sm-Nd data indicate that the protoliths of the Vikan migmatites formed 2.64 AE ago. We note that none of the total-rock leads are less radiogenic than expected for this age. Two reference isochrons are shown. If the protoliths formed at 2.64 AE with initial lead on the growth curve and lost all their U during the granulite facies metamorphism at T = 1.8 AE then all the total rocks should plot on the line labeled T = 2.64 – 1.80 AE. If they instead evolved from 2.64 to present without any disturbance of the U-Pb system they should all plot on the line labeled T = 2.64 – 0 AE. Most of the samples plot in the wedge between these two reference lines. This is expected if they were depleted in U relative to Pb at T = 1.8 AE. Only two points plot to the right of this line and this requires that U was enriched relative to Pb at T = 1.8 AE for these samples in terms of our episodic model. The three least radiogenic samples plot on the T = 2.64 – 0 reference line giving further evidence that 2.64 AE is the time of formation of the protoliths. The dashed line shows Taylor's [1] two-stage model Pb-Pb "isochron" that gives T = 3.41 AE and requires a very high μ-value of 11.2 in the stage from 4.45 AE to 3.41 AE.

Similarly, we can calculate an average Rb/Sr fractionation factor $F_{Rb/Sr} = (Rb/Sr)_2/(Rb/Sr)_1$ at T_M of ~0.46 from the equation:

$$(^{87}Sr/^{86}Sr)_m = I^{Sr}_{UR}(T_x) + (^{87}Rb/^{86}Sr)_1(e^{\lambda_{Rb}T_x} - e^{\lambda_{Rb}T_M}) + (^{87}Rb/^{86}Sr)_2(e^{\lambda_{Rb}T_M} - 1)$$

where $(^{87}Rb/^{86}Sr)_2$ is the ratio measured today. We may compare the Rb depletion indicated by the model calculations with that indicated by concentration data on the granulite facies relative to the amphibolite facies migmatites. From the concentration data of Heier and Thoresen, we obtain $(K/Rb)_A/(K/Rb)_G$ ~0.47. It thus appears that both concentration data and isotopic data are well explained by assuming a bulk loss of U and Rb from the granulite facies gneisses. If this model is approximately correct, then the isotopic data require this loss to have occurred at ~1.8 AE. This is one of the rather rare cases where granulite facies metamorphism postdates rock formation by as much as 0.8 AE.

We further note that the average $F_{U/Pb}$ and $F_{Rb/Sr}$ calculated from the isotopic data discussed above vary systematically with the mineralogy or major element composition of the gneisses at Vikan:

	$F_{U/Pb}$	$F_{Rb/Sr}$
granitic granulites	0.15	0.7
granodioritic-tonalitic granulites	0.4	0.25
dioritic granulites	0.5	0.15

This most likely reflects the difference in mineralogic changes with major element composition for the amphibolite-granulite transition.

6. Conclusions

Our results strongly suggest that total-rock Rb-Sr and Pb-Pb data have to be interpreted with great care for granulite facies gneisses. Complex Rb-Sr and U-Pb

systematics displayed by granulite facies gneisses may, however, be resolved by ages obtained with independent methods and can be used to trace U/Pb and Rb/Sr fractionation during high-grade metamorphism. For migmatite complexes T^{Nd}_{CHUR} model ages appear to provide the best time constraints for the formation of the protoliths as the dominating REE fractionation will be associated with this event rather than with subsequent metamorphic events. For the Vesterålen amphibolite facies migmatites both Sm-Nd, Rb-Sr and Pb-Pb give model ages of ~2.6 AE. However, for the granulite facies migmatites only the Sm-Nd system gives this age while the Rb-Sr and U-Pb total-rock systems do not provide any precise age information. If a granulite facies metamorphism occurred long after the time of crust formation, then in general we may expect $T^{Sr}_{UR} > T^{Nd}_{CHUR}$, except in more basic rocks where the measured Rb/Sr ratio may be lower than that of UR.

We conclude that the interpretation presented by Taylor [1] for a very ancient crustal component in the Archean terrane of Vesterålen is not valid. Instead this terrane appears to be part of the worldwide crustal forming event at 2.6 AE. The possibility that very ancient crustal segments may really be present in other areas of the Fennoscandian Shield must remain the subject of future investigations.

The approach used in this work suggests that Sm-Nd model ages as well as total-rock isochrons may be very valuable in identifying time equivalent lithic units in complex metamorphic terranes. The coordinated use of different isotopic systems which have different susceptibilities to metamorphism gives a much deeper insight into both the times and mechanisms of chemical fractionation.

Acknowledgements

Einar Tveten of the Norwegian Geological Survey (NGU) was most helpful in assisting us with the fieldwork and discussing the field relations in Vesterålen. We also appreciate the patience of his wife Laila and her younger assistant. We are grateful to K.S. Heier and W.L. Griffin for discussions and for making some of the arrangements for us to go there. Samples GS-5, GS-23 and TL-39 were supplied by I.K. Iden who also kindly made unpublished REE data available to us as a guidance for sample selection. Some of the Sm-Nd results and our interpretation of the U-Pb and Rb-Sr systematics were first presented in a seminar at the Mineralogical-Geological Museum in Oslo, August 1977, and we appreciate the discussion with W.L. Griffin and coworkers on that occasion. After this work was completed, we received from W.L. Griffin a revised preprint of [8] that reports the new Pb-Pb age by P.N. Taylor for the amphibolite facies migmatites and a revision of the Lofoten-Vesterålen chronology, which now agrees in outline with that suggested here.

One of us (S.B.J.) would like to thank K.S. Heier and P.N. Taylor for generating his interest in this and other problems concerning the nature of the lower crust.

S.B.J. also thanks D.J. DePaolo, D.A. Papanastassiou, and M.T. McCulloch for assistance and advice with the chemical and mass spectrometric procedures. F. Oberli and M.T. McCulloch provided constructive criticism of the manuscript. This paper has benefited from the reviews by P.N. Taylor, R.K. O'Nions and an anonymous reviewer. The first part of this work was done while the senior author held a Rotary Foundation Fellowship. This work has been supported by NSF grant EAR 76-22494.

References

1 P.N. Taylor, An early Precambrian age for migmatitic gneisses from Vikan: Vesterålen, North Norway, Earth Planet. Sci. Lett. 27 (1975) 35–42.
2 K.S. Heier, Rubidium/strontium and strontium-87/strontium 86 ratios in deep crustal material, Nature 202 (1964) 477–478.
3 K.S. Heier and J.A.S. Adams, Concentration of radioactive elements in deep crustal material, Geochim. Cosmochim. Acta, 29 (1965) 53–61.
4 K.S. Heier and W. Compston, Interpretation of Rb-Sr age patterns in high-grade metamorphic rocks, North Norway, Norsk Geol. Tidsskr., 49 (1969) 257–283.
5 T.H. Green, A.O. Brunfelt and K.S. Heier, Rare earth element distribution in anorthosites and associated high grade metamorphic rocks, Lofoten-Vesterålen, Norway, Earth Planet. Sci. Lett., 7 (1969) 93–98.
6 T.H. Green, A.O. Brunfelt and K.S. Heier, Rare-earth element distribution and K/Rb ratios in granulites, mangerites and anorthosites, Lofoten-Vesterålen, Norway, Geochim. Cosmochim. Acta, 36 (1972) 241–257.
7 K.S. Heier and K. Thoresen, Geochemistry of high grade metamorphic rocks, Lofoten-Vesterålen, North Norway, Geochim. Cosmochim. Acta, 35 (1971) 89–99.

8 W.L. Griffin, P.N. Taylor, J.W. Hakkinen, K.S. Heier, I.K. Iden, E.J. Krogh, O. Malm, K.I. Olsen, D.E. Ormaasen and E. Tveten, Archean and Proterozoic crustal evolution in Lofoten-Vesterålen, Norway, J. Geol. Soc. London, (in press).
9 D.J. DePaolo and G.J. Wasserburg, Nd isotopic variations and petrogenetic models, Geophys. Res. Lett., 3 (1976) 249–252.
10 D.J. DePaolo and G.J. Wasserburg, Inferences about magma sources and mantle structure from variations of $^{143}Nd/^{144}Nd$, Geophys. Res. Lett., 3 (1976) 743–746.
11 P.J. Hamilton, R.K. O'Nions and N.M. Evensen, Sm-Nd dating of Archean basic and ultrabasic volcanics, Earth Planet. Sci. Lett., 36 (1977) 263–268.
12 M.T. McCulloch and G.J. Wasserburg, Sm-Nd and Rb-Sr chronology of continental crust formation, Science 200 (1978) 1003–1011.
13 A.J. Gancarz and G.J. Wasserburg, Initial Pb of the Amitsoq Gneiss, West Greenland, and implications for the age of the earth, Geochim. Cosmochim. Acta, 41 (1977) 1283–1301.
14 B.R. Doe and J.S. Stacey, The application of lead isotopes to the problem of ore genesis and ore prospect evaluation: a review, Econ. Geol. 69 (1974) 757–776.
15 D.A. Papanastassiou and G.J. Wasserburg, Rb-Sr ages and initial strontium in basalts from Apollo 15, Earth Planet. Sci. Lett. 17 (1973) 324–337.
16 D.A. Papanastassiou, D.J. DePaolo and G.J. Wasserburg, Rb-Sr and Sm-Nd chronology and genealogy of mare basalts from the Sea of Tranquility, Proc. 8th Lunar Sci. Conf. (1977) 1639–1672.
17 C.M. Gray and V.M. Oversby, The behaviour of lead isotopes during granulite facies metamorphism, Geochim. Cosmochim. Acta, 36 (1972) 939–952.
18 S. Moorbath, H. Welke and N.H. Gale, The significance of lead isotope studies in ancient, high-grade metamorphic basement complexes, as examplified by the Lewisian rocks of Northwest Scotland, Earth Planet. Sci. Lett., 6 (1969) 245–256.
19 P.J. Hamilton, R.K. O'Nions, N.M. Evensen, D. Bridgwater and J.H. Allaart, Sm-Nd isotopic investigations of Isua supracrustals and implications for mantle evolution, Nature 272 (1978) 41–43.
20 W.L. Griffin and K.S. Heier, Parageneses of garnet in granulite-facies rocks, Lofoten-Vesterålen, Norway, Contrib. Mineral. Petrol., 23 (1969) 89–116.

APPENDIX 2.

VOL. 84, NO. B13 JOURNAL OF GEOPHYSICAL RESEARCH DECEMBER 10, 1979

Nd and Sr Isotopic Study of the Bay of Islands Ophiolite Complex and the Evolution of the Source of Midocean Ridge Basalts

STEIN B. JACOBSEN AND G. J. WASSERBURG

The Lunatic Asylum of the Charles Arms Laboratory, Division of Geological and Planetary Sciences California Institute of Technology, Pasadena, California 91125

Two Sm-Nd internal isochrons for pyroxene gabbros of the Bay of Islands Ophiolite Complex give well-defined ages of 508 ± 6 m.y. and 501 ± 13 m.y. with initial $^{143}Nd/^{144}Nd$ of $\varepsilon_{Nd} = +7.7 \mp 0.1$ and $\varepsilon_{Nd} = +7.5 \mp 0.2$, respectively. Total rock samples from pillow basalts, sheeted dikes, trondhjemites, hornblende gabbros, pyroxene gabbros, and an orthopyroxenite layer from the harzburgite give initial ε_{Nd} in the range from +6.5 to +8.1 with an average value of +7.6. The initial $^{87}Sr/^{86}Sr$ obtained on a pyroxene-gabbro is $\varepsilon_{Sr} = -19.3 \pm 0.3$, which is typical of oceanic samples. However, the initial $^{87}Sr/^{86}Sr$ within the different phases of the complex is found to be highly variable (~52 ε units) and shows the effect of sea water alteration. The ε_{Nd} values demonstrate a clear oceanic affinity for the Bay of Islands complex and support earlier interpretations made on the basis of structure and geochemistry. The magnitudes of the initial ε_{Nd} values (+7.6) are somewhat smaller than for typical present-day midocean ridge basalts (MORB) (+10). This is most likely due to differential evolution over the past 0.5 aeon of the oceanic mantle relative to the bulk earth. The observed shift is quantitatively what should be expected for a simple single-stage evolution. For a model with a single differentiation event at time T_D to produce the depleted mantle, both Sm-Nd and Rb-Sr data for MORB and the Bay of Islands Complex give $T_D \approx 1.8$ aeons. This age is, however, interpreted as the mean age of the MORB source and does not refer to a unique event. The total time for producing this source by a uniform process would be of the order of 3.6 aeons. The Nd isotopic signature of oceanic crust is clearly present in this Paleozoic ophiolite and suggests that typical high-ε_{Nd} reservoirs are sources of oceanic crust through the Phanerozoic. This implies relatively rapid turnover between oceanic crust and mantle sources and a good mixing of oceanic mantle for the past 1.0 aeon, including contributions from recycled continental materials. These data indicate that the major distinction between oceanic basalts and continental basalts observed in recent rocks is also preserved through the Phanerozoic. These isotopic differences clearly imply a long time distinction between the magma sources of these basalt types. It should be possible to apply the distinctive ε_{Nd} values of oceanic crust and mantle to identify old obducted oceanic segments on continental blocks.

INTRODUCTION

There is a considerable amount of Nd, Sr, and Pb isotopic data available on both old and young continental crustal rocks. These data have contributed significantly to our understanding of the evolution of the continental crust. For the oceanic crust, only very young samples have been measured because the present-day oceanic crust is geologically very young (≤ 0.18 aeon) (1 aeon = 1 AE = 10^9 years) in comparison with the continental crust (0–3.8 aeon). Remnants of oceanic type crust appear to be present within the continental crust back through the Phanerozoic, although they are in places difficult to recognize. Very little is known, however, about oceanic magma genesis in the Precambrian, and clear evidence for preserved Precambrian oceanic crust is at present lacking.

Constraints on the evolution of oceanic crust and mantle are provided by available Rb-Sr, U-Th-Pb, and Sm-Nd data on young oceanic basalts. It is well known that Rb/Sr ratios in many midocean ridge basalts (MORB) are too low to support their $^{87}Sr/^{86}Sr$ ratios [*Tatsumoto et al.*, 1965]. Assuming that Rb/Sr ratios of MORB are not less than those for their source regions, it follows that the mantle source for MORB has been depleted in Rb in relation to Sr [*Tatsumoto et al.*, 1965; *Gast*, 1968]. *Gast* [1968] proposed that MORB are derivatives of a mantle which has been left as a residue from previous partial melting in the mantle.

DePaolo and Wasserburg [1976*a*, *b*, 1979*c*] showed that continental flood basalts (CFB) are derived from reservoirs which have condritic Sm/Nd ratios and that MORB were derived from ancient reservoirs which are distinct from those of the continental basalts and characterized by higher Sm/Nd. *DePaolo and Wasserburg* [1976*b*] and *O'Nions et al.* [1977] also showed that for young volcanic rocks with $^{87}Sr/^{86}Sr$ ratios less than ~0.705 there is a strong correlation between initial $^{143}Nd/^{144}Nd$ and initial $^{87}Sr/^{86}Sr$. The correlation is broadly consistent with known solid/liquid distribution coefficients which indicate that a residue after partial melting would be expected to have had its Sm/Nd ratio increased and its Rb/Sr ratio decreased. However, such a strong correlation was not expected.

The timing of the fractionation events in the MORB sources is of considerable current interest. The data have been interpreted in terms of a single mantle fractionation event. Pb-Pb two-stage model isochrons [*Church and Tatsumoto*, 1975; *Sun and Jahn*, 1975] and Rb-Sr 'mantle isochrons' [*Brooks et al.*, 1976 *a*, *b*] have been used to infer differentiation ages of the order of 1.5–1.8 aeons, while Sm-Nd model ages for primitive oceanic tholeiites suggest a differentiation age of ~1.1 aeons for the MORB source [*Carlson et al.*, 1978]. However, the data do not exactly fit a two-stage model, so multistage models or continuous fractionation models have also been favored [*O'Nions et al.*, 1978*b*].

All the above cited data were obtained on young oceanic basalts. There is at present no isotopic study available on ancient oceanic crust. Most geologists now agree upon an oceanic origin for the ophiolites found in many mountain belts. Ophiolites are believed to be pieces of oceanic crust and

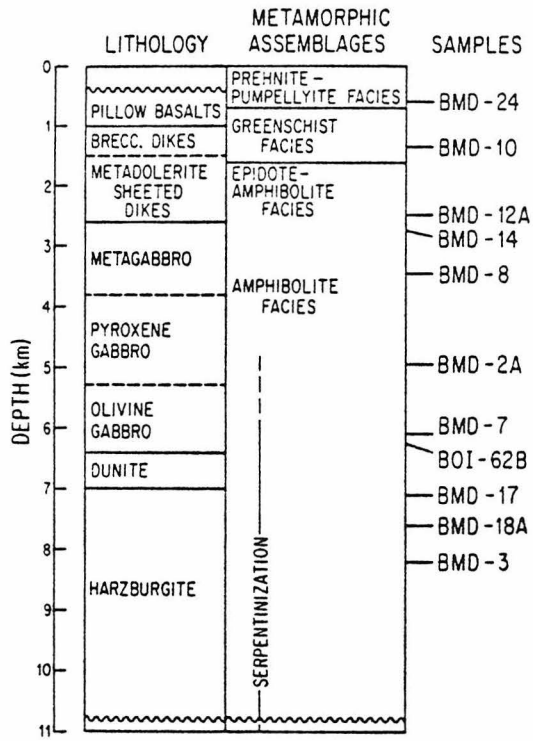

Fig. 1. Idealized stratigraphy of the Blow-Me-Down massif after *Salisbury and Christensen* [1978]. The sample numbers show the location of samples in the stratigraphy.

mantle emplaced on the continent during the early stages of orogenesis resulting from plate collision. Studies of thickness, structure, seismic wave velocities, and geochemistry of ophiolite suites indicate a close analogy between ophiolites and oceanic crust and mantle formed at midocean ridges (for a review, see *Coleman* [1977]). Spreading plate margins occur also in small ocean basins, and these are of considerable importance as proposed origins of ophiolite complexes [*Dewey and Bird*, 1971; *Karson and Dewey*, 1978]. We have therefore carried out a Nd and Sr isotopic study of an early Paleozoic ophiolite, the Bay of Islands Complex, in order to (1) characterize the source of the magmas which formed this ophiolite, (2) determine if these magmas were derived from a mantle reservoir similar to that of MORB, (3) determine the age by the internal Sm-Nd mineral isochron method and establish whether or not a Sm-Nd whole rock isochron exists for the complex, and (4) discuss the evolution of the oceanic mantle through time and attempt to understand the significance of proposed differentiation ages of the MORB source.

The Blow-Me-Down Massif of the Bay of Islands Complex

Geology

The Bay of Islands Complex (~750 km^2) is the best preserved of the early Paleozoic ophiolites in the Appalachians. It is located on the western coastline of Newfoundland and consists of four isolated massifs. The Blow-Me-Down massif is structurally the least complicated and is stratigraphically nearly complete (Figure 1). The geology of the Blow-Me-Down massif has been described by *Smith* [1958], *Williams and Malpas* [1972], *Williams* [1973], and *Salisbury and Christensen* [1978]. *Salisbury and Christensen* [1978] showed that the seismic velocity structure of the massif is indistinguishable from that of normal oceanic crust. The Bay of Islands Ophiolite Complex is widely believed to represent a section of normal oceanic crust and upper mantle. However, some other 'ophiolitic' complexes in Newfoundland are thought to represent the foundation of island arc complexes, seamounts, and oceanic fracture zones [*Williams and Talkington*, 1977; *Williams and Stevens*, 1974; *Karson and Dewey*, 1978].

In the Blow-Me-Down massif the ultramafic rocks are dominantly harzburgitic; however, a considerable thickness of spinel lherzolite occurs at the base of the northernmost massif (Table Mountain). Both types clearly display tectonite fabrics thought to have developed by solid state deformation in the mantle. The tectonite fabric both cuts and is cut by numerous orthopyroxenite and dunite veins that probably crystallized from liquids trapped in the harzburgite during its ascent as a plastic mass from below a spreading center. The harzburgite is thought to represent depleted upper mantle peridotite produced by partial melting of lherzolite and subsequent removal of the basaltic liquid [*Irvine and Findlay*, 1972; *Malpas*, 1978]. The spinel lherzolite may represent this source lherzolite or may be partially melted mantle material with incomplete liquid extraction. Overlying the harzburgites are dunites and feldspathic dunites with cumulate textures. Cumulate gabbros lie above the ultramafic rocks, and an interbanded zone of anorthosites, troctolites, and feldspathic dunites separates these two rock types. The gabbros are clearly enriched in cumulate plagioclase. The crystallization sequence of the gabbros is olivine followed by olivine + plagioclase and olivine + plagioclase + clinopyroxene. In the upper parts of the gabbro, late differentiates of trondhjemite occur. Dolerite dikes increase in quantity at the top of the gabbro, and higher up they become 'sheeted' (100% dikes) and feed the overlying pillow lavas. The sheeted dike complex and the pillow lavas reach a total thickness of about 2.5 km where they are overlain by sediments. There is a rapid downward increase in metamorphic grade from zeolite through prehnite-pumpellyite to greenschist facies, suggesting ocean floor metamorphism under a high geothermal gradient [*Einarson*, 1975; *Salisbury and Christensen*, 1978].

Samples

Samples were collected by one of us (S.B.J.) during the summer of 1978 along the same general profile used by *Salisbury and Christensen* [1978]. Sample BOI-62B was obtained from N. Christensen. The Blow-Me-Down massif shows little evidence for postemplacement metamorphism, and good exposures with minimal weathering occur at all structural levels. Care was taken to obtain large samples free of weathering, but the alteration features characteristic of ophiolites could not be avoided. Above the pyroxene gabbro, all rocks are strongly altered to zeolite, greenschist, or amphibolite facies owing to preemplacement metamorphism, although relict igneous textures are common. Rocks with only minor alteration were found within the pyroxene and olivine gabbro units. The ultramafic rocks are serpentinized throughout the section, but care was taken to obtain samples with minimal serpentinization.

The stratigraphic position of the samples is shown in Figure 1. BMD-18A and BMD-3 are harzburgites where the primary assemblage appears to have been 77% olivine, 20% orthopyroxene, and 3% chrome spinel. About 50% of the olivine is

altered to serpentine, and ~50% of the orthopyroxene is altered to bastite. BMD-17 is a sample from a 10-cm-thick layer of 1- to 3-cm-sized orthopyroxene crystals which occurs between ~10-cm-thick layers of dunite within the harzburgite. The cumulate gabbro samples BMD-2A, BOI-62B, and BMD-7 were selected for their freshness and preservation of primary magmatic minerals. They all have ~50% plagioclase, 20–30% clinopyroxene, and variable amounts of olivine, brown and green primary hornblende, and rare orthopyroxene. BOI-62B is the only gabbro sample where orthopyroxene is a major phase (~20%). BMD-2A shows only very minor saussuritization of plagioclase and rare alteration of olivine to serpentine. BOI-62B and BMD-7 show minor saussuritization of plagioclase, some secondary amphibole, and minor alteration of olivine to serpentine. BMD-8 is a metagabbro with green hornblende, epidote, and plagioclase, and BMD-14 is a trondhjemite from the upper part of the metagabbro. Both samples have strongly saussuritized plagioclase. BMD-12A is from the sheeted dike complex and has ~45% secondary green amphibole, 50% plagioclase, and <1% of relict clinopyroxene. The plagioclase is brownish, cloudy, and saussuritized. Chlorite and blue-green amphibole also occur, but the relict subophitic texture shows the original dike rock was a dolerite. BMD-10 is a fine-grained greenschist facies metadolerite from the upper brecciated part of the sheeted dike complex. BMD-24 is a fine-grained pillowed metabasalt with a highly altered brownish groundmass with relict clinopyroxene and highly altered clinopyroxene and plagioclase phenocrysts. Zeolites and calcite occur in separate clusters in the groundmass and within amygdules.

Experimental Procedures and Data Representation

Mineral separates were obtained magnetically and purified by handpicking. The plagioclase separates are better than 99% pure. The clinopyroxene separate for BMD-2A contains ~20% plagioclase and ~80% clinopyroxene due to the fine-scale intergrowth of plagioclase and pyroxene. For BMD-7 the clinopyroxene separate was free of plagioclase; however, it contains some primary green amphibole. Whole rock samples of ~20 g were crushed, and 1- to 3-g splits were dissolved in HF and $HClO_4$. Sample BMD-18A had an insoluble residue of chrome spinel. Detailed descriptions of procedures are given by *Papanastassiou and Wasserburg* [1973] and by *Papanastassiou et al.* [1977]. Errors given for $^{143}Nd/^{144}Nd$ and $^{87}Sr/^{86}Sr$ are 2σ mean of 200–300 ratios for Nd and 100–200 ratios for Sr. K, Ba, Rb, Sr, Sm, and Nd concentrations were obtained by isotope dilution techniques. Small (<1%) aliquots of each sample were used to establish the approximate concentrations of these elements and the remaining solution was then spiked optimally to determine precise concentrations and isotopic compositions. Typically, an aliquot containing ~100- to 200-mg sample was processed through the ion exchange columns a single time with a blank of 25 pg for Nd and 100 pg for Sr. For sample BMD-18A an aliquot containing 500 mg of sample was split into two aliquots, which were separately passed through the first ion exchange column. The rare earth element (REE) fractions from these two aliquots were then together passed through the second column for separation of Nd and Sm. The estimated blank for this procedure is 50 pg for Nd. For this sample a blank correction was made corresponding to 0.4 ϵ units for $^{143}Nd/^{144}Nd$ and 1.0% to the $^{147}Sm/^{144}Nd$ ratio.

Tables 1 and 3 summarize the analytical data. Excellent reproducibility is shown by repeat runs for BOI-62B and BMD-7 in Table 3. The nonradiogenic isotopes were measured in every experiment and found to be in excellent agreement with those of *DePaolo and Wasserburg* [1976*a*].

The initial $^{143}Nd/^{144}Nd$ and $^{87}Sr/^{86}Sr$ ratios of a rock of age T are expressed as fractional deviations in parts in 10^4 (called ϵ units) from the values in a uniform mantle reference reservoir at time T and denoted by ϵ_{Nd} and ϵ_{Sr}, respectively. The notation with f and ϵ values follows that of *DePaolo and Wasserburg* [1976*a*, *b*, 1977]. The mantle reservoir used as a reference for the Sm-Nd system (CHUR) has a nominal chondritic Sm/Nd ratio with $(^{147}Sm/^{144}Nd)_{CHUR}^0 = 0.1936$ and $^{143}Nd/^{144}Nd$ ratio today of $I_{CHUR}^{Nd}(0) = 0.511836$ [*DePaolo and Wasserburg*, 1976*a*]. The ratio $^{143}Nd/^{144}Nd$ in CHUR at any time T in the past is given by

$$I_{CHUR}^{Nd}(T) = I_{CHUR}^{Nd}(0) - \left(\frac{^{147}Sm}{^{144}Nd}\right)_{CHUR}^{0} (e^{\lambda_{Sm}T} - 1) \quad (1)$$

where $\lambda_{Sm} = 0.00654$ aeon^{-1}. The reference reservoir for Rb-Sr (UR) is taken to have $(^{87}Rb/^{86}Sr)_{UR}^0 = 0.0827$, and the value of $^{87}Sr/^{86}Sr$ in UR at any time T in the past is given by

$$I_{UR}^{Sr}(T) = I_{UR}^{Sr}(0) - \left(\frac{^{87}Rb}{^{86}Sr}\right)_{UR}^{0} (e^{\lambda_{Rb}T} - 1) \quad (2)$$

where $I_{UR}^{Sr}(0) = 0.7045$ is the value in UR today [*DePaolo and Wasserburg*, 1976*b*] and $\lambda_{Rb} = 0.0142$ aeon^{-1}. These reference reservoirs may be representative of the bulk earth.

The $^{147}Sm/^{144}Nd$ and $^{87}Rb/^{86}Sr$ ratios are expressed as enrichment factors in relation to CHUR and UR and are denoted $f^{Sm/Nd}$ and $f^{Rb/Sr}$, respectively, where

$$f^{Sm/Nd} = \left[\frac{(Sm/Nd)_M}{(Sm/Nd)_{CHUR}} - 1\right]$$
$$f^{Rb/Sr} = \left[\frac{(Rb/Sr)_M}{(Rb/Sr)_{UR}} - 1\right] \quad (3)$$

and M denotes the measured value. We emphasize the fact that the precise values for the bulk earth are not well known, although the estimates given above are widely used. However, it seems unlikely that the value of $I_{CHUR}^{Nd}(0)$ which we are using is more than 2–3 ϵ units different from the true value [*DePaolo and Wasserburg*, 1976*a*, *b*]. This will not significantly alter the following discussion, although it might change substantial details of interpretation.

Discussion of Results for the Bay of Islands Complex

LIL Element Patterns

From the major element chemistry it is clear that the Bay of Islands Ophiolite Complex is tholeiitic [*Malpas*, 1978]. It is therefore of interest to compare the trace element data for the Bay of Islands Ophiolite (Table 1) with those of a variety of oceanic and continental tholeiitic basalts (Table 2) to see whether these data indicate an oceanic affinity independent of inferences based on geologic structure or isotopic ratios. It has been known for over a decade that midocean ridge tholeiites have very distinctive large ion lithophile (LIL) element depleted patterns [*Tatsumoto et al.*, 1965; *Engel et al.*, 1965]. However, a recent study of incompatible element variations along the Mid-Atlantic ridge [*White and Schilling*, 1978] has shown that tholeiites from certain ridge segments are anoma-

TABLE 1. Trace Element Concentrations

Sample		K	Rb	Sr	Ba	Nd	Sm	Rb/Sr	Sm/Nd	K/Rb	K/Ba	Sr/Nd	Ba/Nd
BMD-24	pillow basalt	1328	1.06	156	21	8.63	2.76	0.0068	0.320	1253	63	18.1	2.4
BMD-10	dolerite	5505	2.61	274	32	9.75	3.27	0.0095	0.335	2109	172	28.1	3.3
BMD-12A	dolerite	3819	1.93	333	31	9.17	3.06	0.0058	0.334	1979	123	36.3	3.4
BMD-14	trondhjemite	3172	2.00	137	94	24.6	7.20	0.0146	0.293	1586	34	5.6	3.8
BMD-8	hornblende gabbro	2930	1.75	407	...	5.74	2.00	0.0043	0.348	1674	...	70.9	...
BMD-2A	pyroxene gabbro	132	0.073	140	...	0.990	0.437	0.00052	0.442	1808	10	141	...
BMD-2A	clinopyroxene	100	0.076	83	...	0.793	0.367	0.00092	0.463	1316	...	105	...
BMD-2A	plagioclase	147	0.050	218	...	0.570	0.172	0.00023	0.301	2940	...	382	...
BOI-62B	pyroxene gabbro	178	0.135	125	5.4	1.49	0.674	0.0011	0.452	1319	33	83.9	3.6
BMD-7	clinopyroxene	75	0.131	22	...	2.09	1.06	0.0060	0.509	573	...	10.7	...
BMD-7	plagioclase	...	0.394	283	...	0.659	0.108	0.0014	0.164	...	...	429	...
BMD-17	orthopyroxenite	18	0.120	0.598	...	0.0148	0.00455	0.201	0.308	150	...	40.4	...
BMD-18A	harzburgite	25	0.124	0.065	0.63	0.00223	0.000626	1.90	0.281	202	40	28.1	272
BMD-3	harzburgite	14	0.061	0.034	...	0.00087	...	1.79	...	230	...	39.1	...

Values are in parts per million.

TABLE 2. Trace Element Concentrations in Tholeiitic Basalts From Various Tectonic Environments and in Chondrites

	K	Rb	Sr	Ba	Nd	Sm	Rb/Sr	Sm/Nd	K/Rb	K/Ba	Sr/Nd	Ba/Nd	References*
Normal midocean ridges	732	0.75	92	6.2	6.2	2.4	0.008	0.387	976	118	14.8	1.0	1
Anomalous midocean ridges	5960	13.2	265	183	19.3	4.8	0.050	0.249	452	32.6	13.7	9.5	1
Back arc basins	3040	4.4	182	55	8.9	3.0	0.024	0.337	691	55.2	20.4	6.2	2, 3, 4, 5
Island arcs	2100	4.8	190	90	5.8	1.9	0.025	0.328	438	23.3	32.8	15.5	3, 6
Ocean islands	3160	5.3	231	110	17.0	4.65	0.023	0.274	596	28.7	13.6	6.5	7, 8, 9
Continental flood basalts	6400	17	320	336	28	7.0	0.053	0.250	376	19.0	11.4	12.0	2, 10, 11, 12, 13
Chondrites	805	2.3	11.0	3.8	0.630	0.203	0.209	0.322	350	212	17.5	6.03	14, 15

Values are in parts per million.

*References are 1, *White and Schilling* [1978]; 2, *Carlson et al.* [1978]; 3, *Hawkesworth et al.* [1977]; 4, *Hart et al.* [1972]; 5, *Hawkins* [1976]; 6, *Hart et al.* [1970]; 7, *O'Nions et al.* [1976]; 8, *O'Nions et al.* [1977]; 9, *Hart* [1973]; 10, *Herrmann* [1969–1974]; 11, *Leeman* [1976]; 12, *McDougall* [1976]; 13, *Frey et al.* [1978]; 14, *Hubbard and Gast* [1971]; and 15, *Nakamura* [1974].

TABLE 3. Rb–Sr and Sm–Nd Isotopic Results

Sample*	$^{87}Rb/^{86}Sr$†	$^{87}Sr/^{86}Sr$‡	$^{147}Sm/^{144}Nd$§	$^{143}Nd/^{144}Nd$‖
BMD-24-TR	0.01964	0.70448 ± 2	0.19329	0.512222 ± 16
BMD-10-TR	0.02754	0.70519 ± 3	0.20301	0.512283 ± 25
BMD-12A-TR	0.01678	0.70523 ± 2	0.20212	0.512277 ± 25
BMD-14-TR	0.04224	0.70649 ± 4	0.17763	0.512142 ± 26
BMD-8-TR	0.01243	0.70561 ± 3	0.21014	0.512284 ± 25
	...	...	0.21014	0.512258 ± 13
BMD-2A-TR	0.001511	0.70254 ± 5	0.26722	0.512472 ± 28
BMD-2A-CPX	0.002670	0.70258 ± 4	0.27995	0.512516 ± 15
BMD-2A-PLAG	0.000666	0.70255 ± 2	0.18236	0.512191 ± 34
BOI-62B-TR-A	0.003029	0.70317 ± 4	0.27363	0.512435 ± 20
	...	...	0.27363	0.512433 ± 14
BOI-62B-TR-B	...	...	0.27340	0.512445 ± 24
BMD-7-CPX	0.01720	0.70285 ± 3	0.30765	0.512588 ± 23
	...	...	0.30765	0.512594 ± 33
BMD-7-PLAG	0.004035	0.70275 ± 2	0.09914	0.511906 ± 25
	...	...	0.09914	0.511908 ± 20
BMD-17-TR	0.5856	0.70804 ± 4	0.18653	0.512190 ± 40
BMD-18A-TR	5.485	0.7313 ± 2	0.16973	0.51192 ± 60

*TR is total rock, CPX is clinopyroxene, PLAG is plagioclase, and OPX is orthopyroxene.
†Uncertainty, ±1.0%.
‡Normalized to $^{86}Sr/^{88}Sr = 0.1194$; errors are 2σ mean.
§Maximum uncertainty, ±0.1%.
‖Normalized to $^{146}Nd/^{142}Nd = 0.636151$; errors are 2σ mean.

lous in that they show strong LIL element enrichment and resemble tholeiites from oceanic islands or continents. These occurrences are presumably rare, and it is reasonable to assume that the LIL-depleted patterns are characteristic of the predominant oceanic tholeiites. The extent to which this trace element chemistry is characteristic throughout geologic time remains a fundamental question. The pillow basalt BMD-24 has concentration levels and a K/Rb ratio that compare well with normal midocean ridge tholeiites; however, its K/Ba ratio is lower than that of typical MORB. The dolerite samples BMD-10 and BMD-12A have somewhat higher concentrations and high K/Ba ratios typical of MORB. Alteration of ocean floor basalts generally leads to an increase in the concentration of K, Rb, and Ba and the K/Ba ratio [*Hart et al.*, 1974]. Therefore even considering the altered nature of these samples, we conclude that they show an affinity with normal midocean ridge tholeiites. The LIL element patterns also are distinctly different from those of oceanic island, island arc, and continental tholeiites but similar to those of tholeiites from marginal basins.

Rare earth patterns from the Bay of Islands Complex have been reported by *Malpas* [1978], and our Sm and Nd concentrations and the implied fractionation patterns are compatible with these. There is a clear similarity of the REE pattern of the pillow lavas with the light rare earth element (LREE)-depleted patterns of normal midocean ridge basalts. The dolerites have a somewhat lower REE abundance and stronger LREE depletion than the pillow lavas. The gabbros have very low Rb and REE concentrations and show strong LREE depletion and positive Eu anomalies. This is consistent with the interpretation that they are plagioclase-enriched cumulates.

Analyses of other ophiolites show the same pattern of REE, K, Rb, Sr, and Ba contents [*Allègre et al.*, 1973; *Montigny et al.*, 1973; *Kay and Senechal*, 1976] for basalts, dolerites, and gabbros as those of the Bay of Islands Complex. *Allègre et al.* [1973] have shown that these typical REE patterns for the pillow lavas, dolerites, and cumulate gabbros of ophiolites can be modeled by closed system fractional crystallization using the observed cumulate assemblages in the gabbros.

The harzburgites show extremely low contents of incompatible elements (Table 1). The concentrations of Nd and Sm are a factor of ~500 lower than chondritic abundances and a factor of $\sim 10^4$ lower than in the dolerites and basalts. These low concentrations support the hypothesis that the harzburgite is the residual mantle remaining after extraction of midocean ridge basalt magmas, although owing to the serpentinized nature of these samples, details of the interpretation are not clear. Available data on harzburgites from other ophiolites show that they also have very low REE concentrations [*Allègre et al.*, 1973; *Montigny et al.*, 1973; *Kay and Senechal*, 1976]. However, their Sm and Nd concentrations are lower by only a factor of ~300 in relation to overlying basalts and dolerites. In all cases, however, very efficient extraction of LIL elements from the source of midocean ridge basalts is indicated.

For the interpretation of Nd and Sr isotopic data on midocean ridge (MOR) basalts and ophiolites it is of importance to have good estimates of $f^{Rb/Sr}$ and $f^{Sm/Nd}$ in their sources. The average values for the oceanic crust may presumably be taken as the average value for the present-day MORB source. The average of individual ophiolites may be taken as estimates for their sources. This should be a good approximation, since the harzburgite residue left in the mantle after production of MOR tholeiite magmas contains insignificant amounts of LIL elements as discussed above. Oceanic gabbros and ophiolitic gabbros give an average $f^{Rb/Sr} = -0.95 \pm 0.05$ [*Kay et al.*, 1970; *Spooner et al.*, 1977] (see Table 4). The average value for unaltered normal MORB is $f^{Rb/Sr} = -0.8 \pm 0.1$. The average Sr concentration is about 100 ppm in both the upper (basalt and dolerite) and the lower (gabbro) oceanic crust, which as a final result gives an average value for oceanic crust of $f^{Rb/Sr} = -0.9^{+0.1}_{-0.05}$. From the data in Table 4 this f value also seems to apply to the Bay of Islands Complex. The average of 30 normal MORB gives $f^{Sm/Nd} = +0.12$ and Nd = 6.5 ppm [*Kay et al.*, 1970; *O'Nions et al.*, 1977; *Carlson et al.*, 1978], and the average of 6 oceanic gabbros [*Masuda and Jibiki*, 1973; *Kay et al.*, 1970] gives $f^{Sm/Nd} = +0.42$ and Nd = 3.3 ppm. Similar estimates are indicated from data on ophiolites [*Montigny et al.*, 1973; *Kay and Senechal*, 1976]. The average for the Bay of Islands Complex appears to be $f^{Sm/Nd} \approx +0.2$

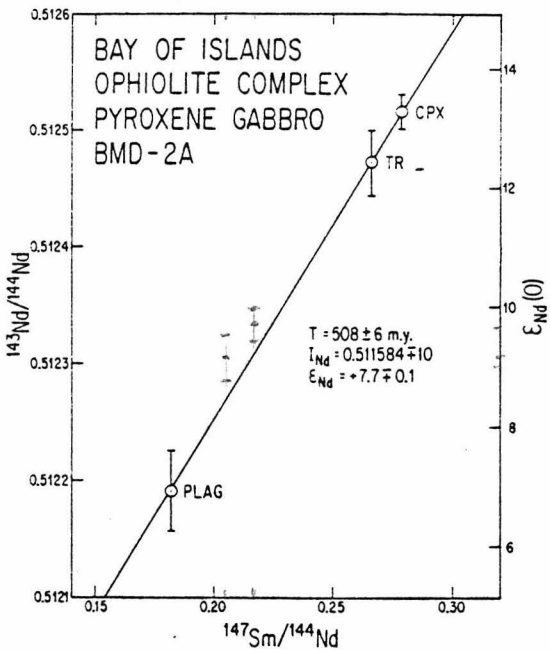

Fig. 2. Sm-Nd evolution diagram showing the mineral isochron determined for the pyroxene gabbro sample BMD-2A.

from the data in Table 4 and the REE patterns of *Malpas* [1978]. Assuming that the lower half of the oceanic crust is made of gabbro, this gives $f^{Sm/Nd} = +0.22$ and (Sr/Nd) ≈ 22 for the average oceanic crust.

Age and Initial Nd and Sr

We have attempted to determine the crystallization age using the ^{147}Sm-^{143}Nd method on two unaltered gabbro samples BMD-2A and BMD-7. The difficulty of obtaining precise dates on old terrestrial mafic and ultramafic rocks is well known. Other methods (K-Ar, Rb-Sr, U-Th-Pb) are much more susceptible to element redistribution subsequent to the time of crystallization and in many cases give a metamorphic age or intermediate ages of doubtful meaning rather than the time of crystallization. Using these methods, it is often necessary to use minor phases and/or associated differentiated rocks whose relationship to the mafic/ultramafic rocks is difficult to establish unequivocally. However, with the Sm-Nd method it is possible to determine directly the crystallization age of major mafic/ultramafic igneous rocks. Sufficiently large differences in Sm/Nd ratios exist between plagioclase and pyroxene, which are the most common phases in gabbroic rocks, such that the Sm-Nd system can be used to obtain precise ages for most gabbroic rocks. The success of this approach has been shown for anhydrous systems in meteoritic and lunar basic rocks [*Lugmair*, 1974; *Lugmair et al.*, 1976; *Papanastassiou et al.*, 1977] and in a hydrous environment in a terrestrial gabbro [*DePaolo and Wasserburg*, 1979*b*]. A successful total rock approach has been reported by *Hamilton et al.* [1977].

The Sm-Nd data for BMD-2A are given in Table 3 and Figure 2. The plagioclase separate shows $^{147}Sm/^{144}Nd \simeq 0.18$, much lower than that of the total rock (0.27). The pyroxene separate contained 20% plagioclase and therefore has an Sm/Nd ratio only slightly higher than the total rock. The data define an age of 508 ± 6 m.y. and initial $^{143}Nd/^{144}Nd$ of $\epsilon_{Nd} = +7.7 \mp 0.1$ but only show a relatively small range in $^{143}Nd/^{144}Nd$ of ~6 ϵ units. The small uncertainty given by a *York* [1966] fit is due to the fact that the three data points are centered on the isochron to within 0.1 ϵ units. The total rock points have higher concentration of Nd than both the pyroxene and plagioclase, so it seems unlikely that the line is a two-component mixing line. To confirm this age, we analyzed a second pyroxene gabbro. The Sm-Nd data on BMD-7 are shown in Table 3 and Figure 3. The plagioclase and the pyroxene show a much larger spread in $^{147}Sm/^{144}Nd$ (0.099–0.31) than that of BMD-2A. BMD-7 yields an age of 501 ± 13 m.y. and an initial $\epsilon_{Nd} = 7.5 \mp 0.2$. The uncertainties represent our best estimates and correspond to the maximum change in the slope of the isochron allowed by the 1σ uncertainties of the duplicate analyses of both data points. The large range of ~14 ϵ units permits this precise age determination. The concordant Sm/Nd ages for the two pyroxene gabbros strongly indicate that this is the time of crystallization. Insofar as the mobility of Sm and Nd during metamorphism and weathering is negligible, and since the data were obtained on primary magmatic phases, these ages are interpreted to be the crystallization age of the gabbro at the time of its emplacement in the oceanic crust. A nominal age of 505 m.y. is assigned to both samples. We have relied on an internal isochron, since ages obtained by total rock isochrons depend on the assumption that all the rocks had the same initial isotopic composition and age. This would not be expected to be a problem for minerals from a single total rock sample. The internal isochron has the disadvantage that later metamorphism is more likely to cause isotopic equilibration on the scale of minerals than on the scale of total rocks. We therefore also compare data from several other total rock samples with the internal isochron (Table 3 and Figure 4). One two-pyroxene gabbro plots off the isochron by ~1.1 ϵ units and must represent a distinctly different age or initial value. The other samples plot on the mineral isochron. The harzburgite BMD-18A is compatible with the mineral isochron, but the $^{143}Nd/^{144}Nd$ ratio is much less precise, since it was measured on 1 ng of Nd and no firm conclusion can be drawn other than that it is not grossly aberrant.

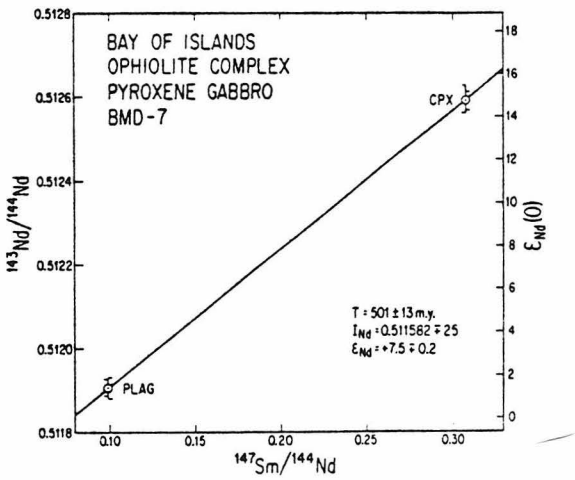

Fig. 3. Sm-Nd evolution diagram showing the mineral isochron determined for the pyroxene gabbro sample BMD-7.

TABLE 4. Evolutionary Parameters for Nd and Sr

Sample*	$f^{Rb/Sr}$	ϵ_{Sr}	$f^{Sm/Nd}$	ϵ_{Nd}
		Pillow Lavas		
BMD-24-TR	−0.7625	+6.2 ± 0.3	−0.0016	+7.6 ± 0.3
		Sheeted Dikes		
BMD-10-TR	−0.6670	+15.4 ± 0.4	+0.0486	+8.1 ± 0.5
BMD-12A-TR	−0.7971	+17.1 ± 0.3	+0.0440	+8.1 ± 0.5
		Trondhjemite		
BMD-14	−0.4892	+32.5 ± 0.6	−0.0825	+7.0 ± 0.5
		Gabbros		
BMD-8	−0.8497	+23.0 ± 0.4	+0.0854	+7.7 ± 0.5
	...	...	...	+7.2 ± 0.3
BMD-2A-TR	−0.9817	−19.6 ± 0.7	+0.3803	+7.7 ± 0.6
BMD-2A-CPX	−0.9677	−19.1 ± 0.6	+0.4460	+7.7 ± 0.3
BMD-2A-PLAG	−0.9919	−19.3 ± 0.3	−0.0581	+7.7 ± 0.7
BOI-62B-TR-A	−0.9634	−10.7 ± 0.6	+0.4134	+6.5 ± 0.4
	...	...	...	+6.5 ± 0.3
BOI-62B-TR-B	...	...	+0.4122	+6.7 ± 0.5
BMD-7-CPX	−0.7920	−16.7 ± 0.4	+0.5891	+7.3 ± 0.4
	...	...	...	+7.4 ± 0.6
BMD-7-PLAG	−0.9512	−16.8 ± 0.3	−0.4879	+7.5 ± 0.5
	...	...	...	+7.5 ± 0.4
		Harzburgite		
BMD-17-TR	+6.057	−0.9 ± 0.6	−0.0365	+7.4 ± 0.8
BMD-18A-TR	+65.32	−171.6 ± 16.0	−0.1333	+3.2 ± 11.7

ϵ values calculated for an age of 505 m.y.
*See Table 3 footnotes.

The ϵ_{Nd} values for all samples are given for a nominal age of 505 m.y. in Table 4. We obtain initial ϵ_{Nd} in the range from +7.0 to +8.1 for metagabbro, trondhjemite, and metadolerite samples. The pillow basalt sample has a $^{147}Sm/^{144}Nd$ ratio which is very near to chondritic, so the initial value for this sample relative to the CHUR evolution line can be established as $\epsilon_{Nd} = +7.6 \pm 0.3$, essentially independent of its age. The orthopyroxenite layer (BMD-17) from the harzburgite has a similar value of $\epsilon_{Nd} = +7.4 \pm 0.8$. This indicates that the harzburgite is cogenetic with the remaining part of the ophiolite and supports the hypothesis that the harzburgite represents residual mantle remaining from the partial melting which produced the rest of the ophiolite. If we assume the same age for BOI-62B, we obtain a distinctly lower initial value of $\epsilon_{Nd} = +6.5 \pm 0.4$. The observed inhomogeneity in initial Nd in this complex obviously makes precise age determinations by whole rock measurements difficult. Although field and petrologic evidence may suggest that all the samples appear to be differentiation products of the same magma, the data require that the parent magma was isotopically inhomogeneous owing to contamination or that the complex is the result of multiple injection from mantle sources with variable Nd isotopic composition. The total rock Sm-Nd method has been used to obtain ages often over a broad geologic scale and including distinctive lithic units [*Hamilton et al.*, 1977, 1978, 1979; *Zindler et al.*, 1978], although it is evident that the assumption of uniform initial isotopic composition does not apply even within a single profile through a well-defined complex as the Bay of Islands. Some caution using this approach may be necessary.

The Rb-Sr data are also shown in Table 3, and the ϵ_{Sr} values are given for a nominal age of 505 m.y. in Table 4. The data for the gabbros, dolerites, and pillow basalts are shown in Figure 5. They all have very low $^{87}Rb/^{86}Sr$ ratios (<0.02) and would not have changed their $^{87}Sr/^{86}Sr$ due to in situ decay of ^{87}Rb by any substantial amount. It is clear that the different total rock samples show a wide scatter on the Rb-Sr evolution diagram. Samples of minerals and total rock from the fresh gabbro BMD-2A give measured $^{87}Sr/^{86}Sr$ ratios which are all the same within error. The clinopyroxene has the highest $^{87}Rb/^{86}Sr$ ratio of 0.0027. The total evolution in $^{87}Sr/^{86}Sr$ for this phase in 505 m.y. is 0.3 ϵ units, so an estimate

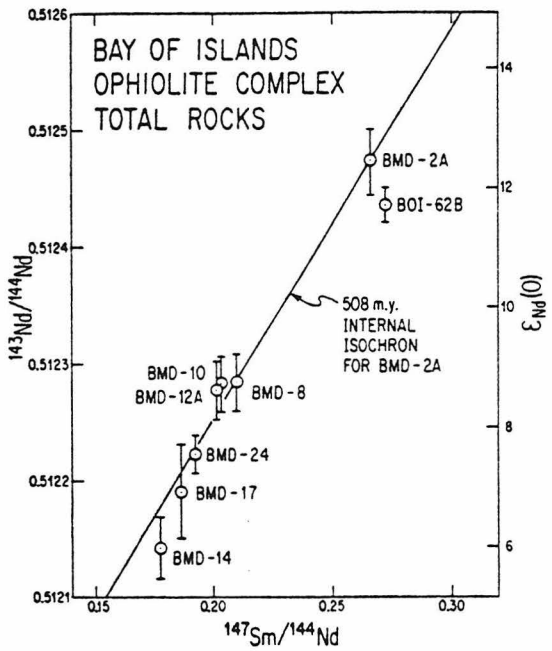

Fig. 4. Sm-Nd evolution diagram showing the data for whole rock samples of pillow basalt, sheeted dikes, trondhjemite, gabbros, and an orthopyroxenite layer in the harzburgite. The 508-m.y. mineral isochron for BMD-2A is shown for reference. All the data do not fit the isochron. Note that BOI-62B does not lie on the mineral isochron and indicates a distinctive initial value. The data point for the orthopyroxenite BMD-17 indicates that the harzburgite is cogenetic with the upper mafic part of the ophiolite.

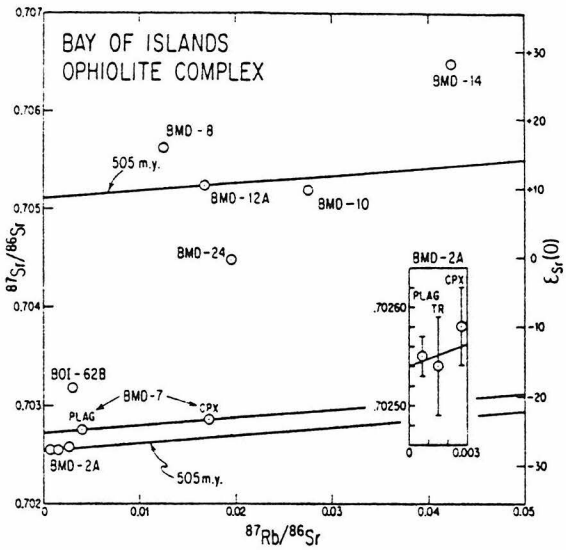

Fig. 5. Rb-Sr evolution diagram showing the mineral and total rock data for samples from the Blow-Me-Down massif. Reference lines with slopes corresponding to the Sm/Nd age are shown. Note the wide range in initial $^{87}Sr/^{86}Sr$ for different samples and the implied range in initial strontium.

of the age cannot be obtained from these data. The initial $^{87}Sr/^{86}Sr$ value is 0.70254 ± 2, or $\epsilon_{Sr} = -19.3 \pm 0.3$. For BMD-7 both clinopyroxene and plagioclase give the same initial $^{87}Sr/^{86}Sr$ ratios of 0.70272 ± 2, or $\epsilon_{Sr} = -16.8 \pm 0.3$. Since the minerals would have different susceptibilities to Sr migration and have the same ϵ_{Sr}, this is good evidence that we are measuring the Sr isotope composition of these rocks at the time of crystallization. The two-pyroxene gabbro BOI-62B also has a very low $^{87}Rb/^{86}Sr$ ratio of ~0.003 and gives an initial $^{87}Sr/^{86}Sr$ of 0.70315 ± 4. This is higher than that of BMD-2A and BMD-7, and since the sample shows only minor signs of alteration, we take this to indicate a significantly different initial Sr value from the two other samples. The difference in $^{87}Sr/^{86}Sr$ cannot be due to an age difference. It appears that the three pyroxene gabbros show significant differences in initial Sr. BOI-62B also shows a significantly different initial Nd from those of BMD-7 and BMD-2A.

Sr analyses were carried out also on samples of metagabbro, trondhjemite, metadolerite, and pillow basalt which had obviously been subject to hydrothermal metamorphism. These samples give a wide spread in ϵ_{Sr} from +6.2 to +32.5, which is very different from the tightly clustered ϵ_{Nd} data. We note that the ϵ_{Sr} values in general show an increase with the degree of metamorphism and alteration. This further demonstrates the much larger mobility of Rb-Sr compared to Sm and Nd during hydrothermal and metamorphic processes, as has been evident from previous studies. This is most likely due to the lower solubility of REE in aqueous solutions and the difference in diffusivity in the solid phases, as compared to Rb-Sr.

The harzburgite BMD-18A has both a high $^{87}Rb/^{86}Sr$ ratio and $^{87}Sr/^{86}Sr$ ratio for an ultramafic rock (Table 3). The $^{87}Sr/^{86}Sr$ ratio for this sample is less precise than for other samples, since it was measured on only 20 ng of Sr. It yields a T_{BABI} model age of 414 ± 6 m.y., and, following the discussion of T_{BABI} model ages by *Wasserburg and Papanastassiou* [1975], this demonstrates that this sample has been disturbed subsequent to this time. Rb-Sr data for harzburgites from alpine peridotites and ophiolites by other workers show that primary minerals have much lower Rb/Sr ratios [*Menzies and Murthy*, [1978] and that secondary phases often have high Rb/Sr ratios [*Brueckner*, 1975]. The high Rb/Sr ratio measured in BMD-18A may thus be related to serpentinization of the sample. The serpentinization of harzburgites in ophiolites is known to occur after their emplacement on the continents [*Wenner and Taylor*, 1973], so the younger age is plausible. The relatively fresh orthopyroxenite BMD-17 also has a relatively high Rb/Sr ratio, but it is only one tenth of that in the harzburgite.

Strontium Isotope Contamination

Isotopic studies of ocean floor basalts and of the Troodos ophiolite have clearly demonstrated that $^{87}Sr/^{86}Sr$ in altered samples generally has been increased owing to interaction with seawater [*Dasch et al.*, 1973; *Hart et al.*, 1974; *Spooner et al.*, 1977]. Changes in $^{87}Sr/^{86}Sr$ by seawater interaction have, however, not been observed to be accompanied by significant changes in $^{143}Nd/^{144}Nd$ ratios [*O'Nions et al.*, 1977, 1978*a*]. Present-day oceans appear to be large, well-mixed reservoirs of Sr with $^{87}Sr/^{86}Sr = 0.7091 \pm 1$, or $\epsilon_{Sr}(0) = +65.3 \pm 1.4$ [*Papanastassiou et al.*, 1970; *Hildreth and Henderson*, 1971], and a Sr concentration of 7.9 ppm [*Holland*, 1978] and are thus isotopically distinct from oceanic basalts. The $^{143}Nd/^{144}Nd$ ratio in seawater show a large range from $\epsilon_{Nd}(0) = -1$ to −14 [*DePaolo and Wasserburg*, 1977; *O'Nions et al.*, 1978*a*; *Piepgras et al.*, 1979], which is also distinct from oceanic basalt values. The concentration of Nd in seawater is only 3×10^{-6} ppm [*Högdahl et al.*, 1968] and is the reason why changes in $^{143}Nd/^{144}Nd$ ratios have not been observed in altered ocean floor basalts.

Rocks from the Bay of Islands ophiolite have a range of 1.6 ϵ units in initial Nd, while the initial ϵ_{Sr} values show a range of 52 ϵ units. The initial magmatic $^{87}Sr/^{86}Sr$ is in the range $\epsilon_{Sr} = -19.3$ to −10.7 on fresh gabbro samples. Higher ϵ_{Sr} values are associated with hydrothermally metamorphosed samples. Since there is a general increase in the ϵ_{Sr} value with the degree of alteration, we attribute these higher values to contamination by seawater. The magnitude of the ϵ_{Sr} shifts is similar to that observed in the much younger Troodos ophiolite [*Spooner et al.*, 1977].

The amount of seawater needed for the observed ϵ_{Sr} shift may be calculated. The volumetric water/rock ratio (= W/R) is given by

$$\frac{W}{R} = \frac{\epsilon_{Sr} - \epsilon_{Sr}^{B}}{\epsilon_{Sr}^{SW} - \epsilon_{Sr}} \frac{Sr_B}{Sr_{SW}} \rho \qquad (4)$$

where B denotes the unaltered sample and SW denotes seawater. We use $\epsilon_{Sr}^{B} = -19.3$ and $\epsilon_{Sr}^{SW} = +72$ (estimated for Cambrian seawater; [*Veizer and Compston*, 1974]) and $\rho \simeq 3$ g/cm^3. This model assumes 100% efficiency in Sr exchange and therefore gives a minimum water/rock ratio. The bulk seawater rock ratio for the metagabbro is thus at least ~130:1 and for the pillow basalt at least ~23:1.

Using the above mentioned parameters for Sr and assuming that Cambrian seawater has $\epsilon_{Nd} = -5$, we can calculate the mixing curve between an uncontaminated rock (Nd = 8 ppm and Sr = 120 ppm) and seawater. The shape of the mixing curve depends on the parameter $K_{Sr/Nd}^{R-W} = (Sr/Nd)_{rock}/(Sr/Nd)_{seawater} = 5.7 \times 10^{-6}$. The mixing line in the ϵ_{Nd}-ϵ_{Sr} diagram is horizontal almost until it reaches the seawater value for ϵ_{Sr}

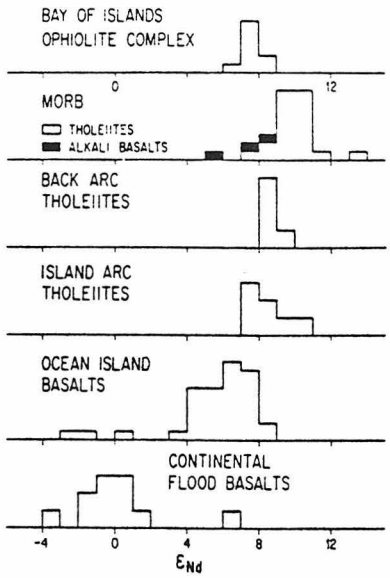

Fig. 6. Histogram comparing initial ϵ_{Nd} values from the Bay of Islands Complex with values for young basalts. Data are from *DePaolo and Wasserburg* [1976*a*, *b*, 1977], *Richard et al.* [1976], *O'Nions et al.* [1977], *Hawkesworth et al.* [1977], and *Carlson et al.* [1978]. The Bay of Islands Complex clearly has an oceanic affinity. The average value (+7.6) is, however, somewhat smaller than the average value of MORB (+10). This is most likely due to differential evolution of the oceanic mantle relative to the bulk earth over the past 0.5 aeon.

(Figure 7). The water/rock ratios shown on the mixing line in Figure 7 assume 100% efficiency of exchange for Nd and Sr. In this case the ϵ_{Nd} value cannot change significantly before the water/rock ratio is $\sim 10^5$.

Oxygen and Sr isotope data and Fe_2O_3/FeO^* ratios together with other geological evidence strongly suggest that the pervasive hydrothermal metamorphism observed in the pillow lavas and sheeted dikes of ophiolites occurred in a sub-seafloor geothermal system at a spreading center [*Spooner et al.*, 1974, 1977]. The Bay of Islands data indicate that similar geothermal systems may have been active in Cambrian ocean ridges. The upper oceanic crust (pillow lavas and sheeted dikes) seems to have been a sink for Sr from seawater throughout the Phanerozoic. This can result in recycling of continental Sr into the mantle in subducted oceanic slabs. Nd and Sr isotopic studies of some young island arc tholeiites and dacites [*DePaolo and Wasserburg*, 1977; *Hawkesworth et al.*, 1977] suggest that they may be derived from altered oceanic crust, since they plot to the right of the MORB field in an ϵ_{Nd}-ϵ_{Sr} diagram, as do altered oceanic basalts. The data presented here suggest that this may be a characteristic of island arc rocks back to Cambrian times if they were derived by melting subducted oceanic slabs.

Observed $\epsilon_{Nd} - \epsilon_{Sr}$ and Their Correlation

We show a histogram of ϵ_{Nd} for young oceanic and continental basalts and for the Bay of Islands Complex in Figure 6. The initial ϵ_{Nd} values for the Bay of Islands samples are in the range from +6.5 to +8.1, lie slightly lower than those for typical present-day midocean ridge tholeiites, and are thus clearly distinct from CFB. The Nd isotopic affinity with oceanic basalts can be easily seen. *Richard et al.* [1978] have reported ϵ_{Nd} (0) and ϵ_{Sr} (0) values for some young ophiolitic gabbros that also indicate their oceanic nature.

We now examine how the Bay of Islands ophiolite data plot on the $\epsilon_{Nd} - \epsilon_{Sr}$ correlation diagram to determine whether the regularities observed for young oceanic samples also apply to old samples. Previous studies have shown that ϵ_{Nd} and ϵ_{Sr} correlate well, especially for ocean ridge and oceanic island basalts. This regularity does not appear to be valid for island arcs owing to Sr contamination by seawater [*DePaolo and Wasserburg*, 1976*b*, 1977; *Hawkesworth et al.*, 1977]. Mid-ocean ridge basalts have the highest ϵ_{Nd} and lowest ϵ_{Sr} and a restricted range of values. Ocean islands have somewhat lower ϵ_{Nd} and higher ϵ_{Sr}. The correlation is also valid for selected

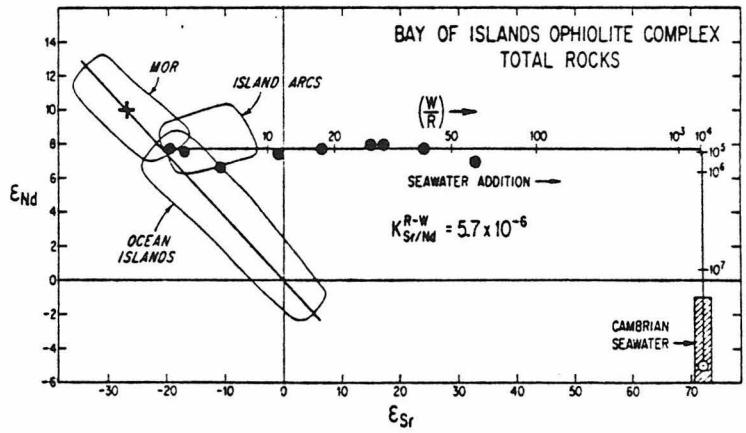

Fig. 7. An $\epsilon_{Nd} - \epsilon_{Sr}$ diagram showing the data for the Bay of Islands samples. The cross represents average modern MOR tholeiites. The line through this cross and $\epsilon_{Nd} = \epsilon_{Sr} = 0$ represents the main correlation in young basaltic rocks ($\epsilon_{Nd} = -0.37\epsilon_{Sr}$), which is called the Mantle Array. The fields of young MOR tholeiites, island are tholeiites, and ocean island basalts are shown. The ϵ_{Nd} and ϵ_{Sr} values of the unaltered pyroxene gabbros plot on the Mantle Array and show that mantle sources of the early Paleozoic follow a pattern similar to that found in present-day mantle sources. The large dispersion in ϵ_{Sr} and an almost constant ϵ_{Nd} is due to interaction with Cambrian seawater. A mixing curve between seawater and the inferred composition of uncontaminated samples is given with the tick marks giving the volumetric water (W/R) to rock ratio and show that $W/R > 10^5$ before ϵ_{Nd} values are affected.

continental basalts. The CFB have ϵ_{Nd} in the neighborhood of zero but tend to spread out to very high ϵ_{Sr} values and negative ϵ_{Nd} resulting from crustal contamination [*DePaolo and Wasserburg*, 1976*b*, 1979*a*]. Figure 7 shows the fields of various types of young basaltic rocks. The data for the pyroxene gabbros plot in the upper part of the oceanic island field and near the lower end of the MORB field. The field of island arc tholeiites also includes these data points. However, the structure and geochemistry of the Bay of Islands Complex strongly suggest that it formed at a chemically normal midocean ridge. Total rock samples of pillow basalts, dolerites, hornblende gabbros, and trondhjemites have high ϵ_{Sr} values and plot to the right of the island arc field owing to submarine hydrothermal metamorphism. This behavior of Bay of Islands samples with shifts to the right is similar to that found for altered ocean floor basalts [*O'Nions et al.*, 1977, 1978*a*]. We conclude from the data presented here that the primary magmatic ϵ_{Nd} and ϵ_{Sr} for the Bay of Islands Complex lie on the correlation line for young volcanic rocks and exhibit clear oceanic affinity. It follows that the mantle sources of early Paleozoic oceanic rocks follow a pattern similar to that found in young oceanic rocks. However, typical ϵ_{Nd} and ϵ_{Sr} values for young normal ridge segments are +10 and −27, respectively (Figures 6 and 7). Therefore ϵ_{Nd} values for the Bay of Islands Complex are displaced down along the correlation line by ~2–3 ϵ units from typical present-day MORB. We conclude from the data that the average initial Nd value for the Bay of Islands is $\epsilon_{Nd} = +7.6$, and for average initial Sr we assume that $\epsilon_{Sr} = -19.3$ as for BMD-2A, since this value makes it plot on the correlation line. A shift toward lower ϵ_{Nd} values and higher ϵ_{Sr} values is expected for old oceanic samples, since $f^{Sm/Nd} > 0$ and $f^{Rb/Sr} < 0$ for the MORB source. However, in order to predict where the MORB field in Figure 7 should be for old samples, it is necessary to utilize specific models of mantle evolution.

This 0.5-aeon-old ophiolite has characteristic oceanic ϵ_{ND} values which have been preserved both for altered and unaltered samples. This shows that the Nd isotopic signature may be used as a method to trace remnants of obducted oceanic crust in the Appalachian-Caledonian mountain chain in places where later tectonism and metamorphism have destroyed other geologic evidence.

Comparison With Previous Age Data

Late Precambrian flood basalt and associated feeder dikes that intrude Precambrian basement gneisses in northwest Newfoundland are overlain by arkosic sandstones and Lower Cambrian shales [*Williams and Stevens*, 1969]. They are believed to have formed during the initial continental rifting which produced the Proto-Atlantic (Iapetus) Ocean [*Bird and Dewey*, 1970]. *Stukas and Reynolds* [1974*a*] obtained a $^{40}Ar/^{39}Ar$ age for these dikes of 615 ± 10 m.y., which they interpreted as the age of emplacement. All K/Ar ages have been recalculated with the decay constants $\lambda_\beta = 0.4962$ aeon^{-1}, $\lambda_\epsilon = 0.0581$ aeon^{-1}, and $^{40}K = 0.01167$ atomic %. The ophiolites in Newfoundland occur in allochthonous thrust slices, so a stratigraphic lower limit to their age is not well defined, but if the above arguments are correct, they should be younger than 615 m.y. Stratigraphic evidence further indicates that the main closure of Iapetus was completed by Middle Ordovician [*Williams and Talkington*, 1977]. Tremadocian sediments, associated with ophiolitic rocks of the Little Port Complex [*Williams*, 1973], indicate a minimum age of ~490 m.y. The Little Port Complex is a polyphase deformed ophiolitic assemblage which lies to the west and is in steep structural and igneous contact with the Bay of Islands Complex [*Karson and Dewey*, 1978].

The Bay of Islands Complex was apparently emplaced on the continent while still at elevated temperatures, since a metamorphic aureole occurs along the surface of obduction. Amphiboles from the aureole give a $^{40}Ar/^{39}Ar$ age of 469 ± 5 m.y. [*Dallmeyer and Williams*, 1975] and a $^{40}K/^{40}Ar$ age of 463 ± 9 m.y. [*Archibald and Farrar*, 1976]. Amphiboles from sheeted dikes and gabbros give a $^{40}K-^{40}Ar$ age of 461 ± 12 m.y. and an $^{40}Ar/^{39}Ar$ age of 467 ± 7 m.y. [*Archibald and Farrar*, 1976]. These ages (~470 m.y.) were interpreted as the time of tectonic emplacement (obduction) of the ophiolite. Dated amphiboles within sheeted dikes and gabbros give argon ages indistinguishable from those of the metamorphic aureole. The time of final emplacement is bracketed by the middle Llanvirnian age of the youngest autochthonous rocks beneath the Humber Arm Allochthon and the late Llandeilian age of the oldest unit of the neoautochthonous Long Point Group which unconformably overlies the allochton [*Bergström et al.*, 1974]. Using the revised Ordovician time scale of *Churkin et al.* [1977], this corresponds to 455–465 m.y. It appears that the Bay of Islands ophiolite was providing clastic detritus to greywackes of the Humber Arm Supergroup by the late Arenegian [*Stevens*, 1970], which indicates that the initial obduction of the ophiolite occurred at or before this stratigraphic time. The 470-m.y. age of the metamorphic aureole is currently used as an important reference point in the calibration of the absolute Ordovician time scale [*Dallmeyer and Williams*, 1975; *Churkin et al.*, 1977].

U-Pb data for zircons from a trondhjemite from within the Blow-Me-Down gabbro have been interpreted to give a time of crystallization of the complex of 504 ± 10 m.y., assuming that 460 m.y. represents a time of isotopic disturbance [*Mattinson*, 1976]. The three data points plot on a discordia line between these two times, but they are all within error of the concordia curve at significantly different times. This is because the concordia curve is nearly a straight line for this time interval, and it is thus difficult to interpret the U-Pb data. *Mattinson* [1975] reports U-Pb data on zircons from a trondhjemite of the adjacent Little Port Complex which give an age of 508 ± 5 m.y. This was also interpreted as the time of crystallization of this complex. The data from this complex define a discordia between $T \sim 0$ and $T = 510$ m.y., with all the data close to the upper intercept. There is no indication of a 470-m.y. event in the U-Pb data, although amphiboles from this complex give K-Ar ages of ~470 m.y. [*Archibald and Farrar*, 1976]. The U-Pb ages strictly provide only minimum age limits for these complexes. The Sm-Nd internal isochrons on gabbros BMD-2A and BMD-7 reported in this work give ages of 508 ± 6 m.y. and 501 ± 13 m.y. The similarity of the Sm-Nd and U-Pb ages gives further evidence for interpretation of this as the original time of crystallization of the oceanic crust now occurring in the Bay of Islands Complex.

Age data exist for two other ophiolites in Newfoundland. U-Pb data on zircons from a trondhjemite dike cutting the Nippers Harbor (Betts Cove) ophiolite define a discordia between $T \sim 0$ and $T = 463 \pm 6$ m.y., with all the data close to the upper intercept [*Mattinson*, 1975]. Mattinson interpreted this as the time of formation of the ophiolite. The Betts Cove ophiolite is overlain by Early Ordovician (Arenigian) sediments, so unless the Ordovician time scale is drastically revised, this suggests that the rock dated by Mattinson does not

belong to the ophilite or that the U-Pb system in the zircons was reset during a later thermal event. A $^{40}Ar/^{39}Ar$ age of 504 ± 5 m.y. was determined by *Stukas and Reynolds* [1974b] on large crystals of primary hornblende from the Brighton gabbro, which intrudes the Lushs Bight sheeted dikes and pillow lavas in central Newfoundland. The age was interpreted with some caution as the time of primary crystallization.

The precise times of formation of these ophiolites and their time of emplacement are important in plate tectonic models for the Appalachian-Caledonian mountain chain and for establishing the absolute time scale of the lower Paleozoic. From the data outlined above, the times of formation of the Bay of Islands Complex, both as a segment of oceanic crust at 505 m.y. and of obduction at 470 m.y., seem now to be well established.

Models for the Evolution of the Source of Midocean Ridge Basalts

From the ϵ_{Nd} and ϵ_{Sr} values of midocean ridge basalts it is clear that the MORB have been derived from a mantle reservoir that has suffered depletion of LIL elements and this reservoir must have existed for long times. The only plausible long-lived LIL element enriched reservoir that could be the complement to the MORB source is the continental crust. The MORB source is thus likely to have formed as a residue after previous partial melting events in the mantle that formed part or all of the continental crust.

Discrete Differentiation Event

For simplicity, let us first consider a model in which a LIL-depleted and a LIL-enriched reservoir is formed by partial melting from an undifferentiated reservoir (CHUR, UR) in a single differentiation event at time T_D. Then as shown by *DePaolo and Wasserburg* [1976a], at a time T subsequent to the time of differentiation T_D we have to a good approximation

$$\epsilon_{Nd}(T) = Q_{Nd} f^{Sm/Nd}(T_D - T) \tag{5a}$$

$$\epsilon_{Sr}(T) = Q_{Sr} f^{Rb/Sr}(T_D - T) \tag{5b}$$

where

$$Q_{Nd} \equiv \frac{\lambda_{Sm}(^{147}Sm/^{144}Nd)_{CHUR}{}^{0} \cdot 10^{4}}{I_{CHUR}{}^{Nd}(0)} = 24.74 \text{ aeon}^{-1} \tag{5c}$$

$$Q_{Sr} \equiv \frac{\lambda_{Rb}(^{87}Rb/^{86}Sr)_{UR}{}^{0} \cdot 10^{4}}{I_{UR}{}^{Sr}(0)} = 16.70 \text{ aeon}^{-1} \tag{5d}$$

and f is the enrichment factor for either the LIL-depleted residue after melting (f_s) or the LIL-enriched partial melt (f_m). Using f_m as measured for the sample, the time T_D calculated for $\epsilon_{Nd}(0)$ and $\epsilon_{Sr}(0)$ (at $T = 0$) corresponds to $T_{CHUR}{}^{Nd}$ and $T_{UR}{}^{Sr}$ for Sm/Nd and Rb/Sr, respectively, as defined by *McCulloch and Wasserburg* [1978]. The f values for the parent reservoirs are not measured directly; in particular, for the depleted residue it is necessary to make some estimates of the f_s values to find T_D for the MORB source from (5). In the section on the LIL element patterns we estimated $f_s^{Rb/Sr} = -0.9$ and $f_s^{Sm/Nd} = +0.22$. For a simple model with a single differentiation event these f_s values should be the same for all time in the LIL-depleted residue. Normal modern MORB have average $\epsilon_{Sr} = -27$ and $\epsilon_{Nd} = +10$, so by using the above f_s values and (5) we get T_D of 1.8 aeons for both Sm/Nd and Rb/Sr. As $f_s^{Rb/Sr}$ is close to its limit of -1, it is therefore not subject to substantial error. Since $f_s^{Rb/Sr} > -1$, it also follows that $T_D >$ 1.6 aeons. Note that we use average values estimated for the MORB source reservoir for these calculations. *Carlson et al.* [1978] used $f^{Sm/Nd}$ and ϵ_{Nd} values for individual MORB samples and obtained a diversity of $T_{CHUR}{}^{Nd}$ model ages (1.0–1.3 aeons). Whether this dispersion reflects real variation in source ages or changes in $f^{Sm/Nd}$ during magmatic differentiation is not yet understood. Typical values for the Bay of Islands source from the data in this paper were inferred to be $\epsilon_{Nd} = +7.6$ and $\epsilon_{Sr} = -19.3$. Using these values, the age of 0.5 aeon and the above f_s values give T_D of 1.9 and 1.8 aeon for Sm/Nd and Rb/Sr, respectively. The fact that we get nearly the same value for T_D for two different points in time could be taken as evidence that this time represents a unique differentiation event. Note, however, that the depleted mantle could also be produced over a time of the order of 3.6 aeons and have a mean age of 1.8 aeons, and the value of T_D calculated does thus not necessarily define a single event. In discussing whether the MORB source was in fact produced in a single event, it is necessary to address the problem of whether a single-event model can explain the dispersion in the data for young MORB samples and also the mantle array (Figure 9). We will therefore discuss how ϵ_{Nd} and ϵ_{Sr} depend on the times of differentiation and Rb/Sr and Sm/Nd fractionations in the mantle by assuming equilibrium melting.

Modeling of Fractionation Patterns in the MORB Source and the Timing of Fractionation Events

It has been shown previously that modeling the relationship between $f^{Rb/Sr}$ and $f^{Sm/Nd}$ for melts and residual solid can aid in the interpretation of Sm-Nd and Rb-Sr isotopic data [*O'Nions et al.*, 1977; *Carter et al.*, 1978; *O'Nions et al.*, 1978b; *Hawkesworth et al.*, 1978; *DePaolo*, 1979].

In the following we discuss the systematics of ϵ_{Nd} and ϵ_{Sr} values and the $f^{Rb/Sr}$ and $f^{Sm/Nd}$ in the residual solid which is the parent reservoir of the basalts. The residual solid is assumed to be produced after partial melting of an undepleted mantle reservoir. We assume equilibrium partial melting. The relationship between ϵ_{Nd} and ϵ_{Sr} in the depleted reservoir depends on the function G:

$$f_s^{Sm/Nd} = G(f_s^{Rb/Sr}) \tag{6}$$

From (5) and (6) we get

$$\epsilon_{Nd}(T) = Q_{Nd}(T_D - T) G\left(\frac{\epsilon_{Sr}(T)}{Q_{Sr}(T_D - T)}\right) \tag{7}$$

For melting where complete chemical equilibrium is maintained between bulk liquid and all phases present in the solid, the previous melting history is not relevant if the system remains closed. The bulk distribution coefficient is defined by

$$D = \frac{C_s}{C_m} = \sum_i X_i K_i \tag{8}$$

where C_s is the concentration in the solid, C_m the concentration in the liquid, X_i the mass fraction of mineral i in residual solid, and K_i the mineral/melt partition coefficient for mineral i. The concentration in the melt relative to that in the initial total system C_0 is given by

$$\frac{C_m}{C_0} = \frac{1}{F + D(1 - F)} \tag{9}$$

where F is the mass fraction of the system that is present as

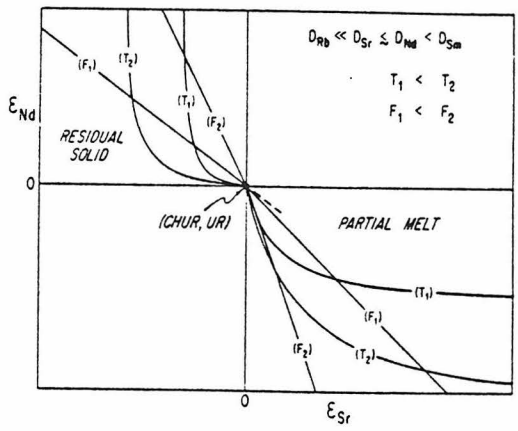

Fig. 8. Cartoon showing the expected relationships between residual solid and partial melts in an $\epsilon_{Nd} - \epsilon_{Sr}$ diagram at T_1 and T_2 years subsequent to the melting event and for various degrees of melting F. The line segments of constant F cover a range of times. The intersection of a constant T curve with a constant F curve determines the values of F and T at that point.

melt [*Shaw*, 1970; *Consolmango and Drake*, 1976]. The concentration in the residual solid is given by

$$\frac{C_s}{C_0} = \frac{D}{F + D(1 - F)} \tag{10}$$

where D is a function of the degree of melting. Assuming that the phases always melt in constant proportions, then D is related to the initial bulk distribution coefficient $D_0 = \sum_i X_i^0 K_i$, where X_i^0 is the mass fraction of mineral i in the original solid. Let p_i be the mass fraction of mineral i in the melt and $P = \sum_i p_i K_i$. Then

$$D = \sum_i \frac{X_i^0 - Fp_i}{1 - F} K_i = \frac{D_0 - FP}{1 - F}$$
$$\frac{C_m}{C_0} = \frac{1}{D_0 + F(1 - P)} \tag{11}$$

which are equations (12) and (15) of *Shaw* [1970]. For the residual solid, (8) and (11) give

$$\frac{C_s}{C_0} = \frac{D_0 - PF}{1 - F}\left(\frac{C_m}{C_0}\right) = \frac{D_0 - PF}{(1 - F)[D_0 - F(1 - P)]} \tag{12}$$

Enrichment factors for liquid and residual solid as a function of F are then given by

$$f_m^{Sm/Nd} = \frac{D_{0,Nd} + F(1 - P_{Nd})}{D_{0,Sm} + F(1 - P_{Sm})} - 1 \tag{13}$$

$$f_s^{Sm/Nd} = \frac{(D_{0,Sm} - P_{Sm}F)[D_{0,Nd} + F(1 - P_{Nd})]}{(D_{0,Nd} - P_{Nd}F)[D_{0,Sm} + F(1 - P_{Sm})]} - 1 \tag{14}$$

Equivalent formulas hold for $f_m^{Rb/Sr}$ and $f_s^{Rb/Sr}$. The function G is thus determined by formulas for $f_s^{Rb/Sr}$ and $f_s^{Sm/Nd}$ through the fraction of melt F. Equations analogous to (14) have been given by *DePaolo* [1979] for equilibrium melting and fractional melting in the special case when $D_0 = P$.

The limiting slope for the residual solid as $F \to 0$ is

$$\lim_{F \to 0}\left(\frac{df_s^{Sm/Nd}}{df_s^{Rb/Sr}}\right) = \frac{D_{0,Sm}^{-1} - D_{0,Nd}^{-1}}{D_{0,Rb}^{-1} - D_{0,Sr}^{-1}} = \left(\frac{f_s^{Sm/Nd}}{f_s^{Rb/Sr}}\right)_{F=0} \tag{15}$$

DePaolo [1979] has shown that (15) also holds for modal equilibrium melting and modal fractional melting. It can in fact be shown from (10) that (15) holds for any kind of equilibrium melting.

The relationships between ϵ_{Nd} and ϵ_{Sr} in the residual solid subsequent to a partial melting event at time T_D may be calculated from (5) and (14). Basalts generated by subsequent melting of the residue will have ϵ_{Nd} and ϵ_{Sr} values of the residue at the time of later melting as given by (5) for $f_s^{Rb/Sr}$ and $f_s^{Sm/Nd}$ calculated from (14). A cartoon illustrating various constant $(T_D - T)$ curves and constant F curves is shown in Figure 8 for the case where $D_{Rb} \ll D_{Sr} \lesssim D_{Nd} < D_{Sm}$. For a constant gree of melting or for asymptotically small amounts of melting, $f_s^{Sm/Nd} = \alpha f_s^{Rb/Sr}$, where α is a constant which may be calculated from (14). It follows that

$$\epsilon_{Nd}(T) = \frac{\alpha Q_{Nd}}{Q_{Sr}} \epsilon_{Sr}(T) \tag{16}$$

All reservoirs with the same degree of melting will thus lie on a line for all times. The position of the melt on the line will depend on $(T_D - T)$ as given by (5). The area in Figure 8 labeled partial melt corresponds to the evolution in time of the melt removed from the residual solid at T_D. This complementary material presumably represents crustal material formed at that time. For a constant degree of melting the relationship between the slopes for residual solid and partial melt is given by

$$\frac{(d\epsilon_{Nd}/d\epsilon_{Sr})_m}{(d\epsilon_{Nd}/d\epsilon_{Sr})_s} = \frac{D_{Nd}}{D_{Sr}} = \frac{(Sr/Nd)_m}{(Sr/Nd)_s} \tag{17}$$

The break in slope at the origin for constant F curves may be calculated from (17). For various degrees of melting, all reservoirs with the same value of $(T_D - T)$ will lie on a curve whose shape depends on the function G in (6). Figure 8 shows schematically the relationship between lines and curves expected for different values of F and $(T_D - T)$. If we derive magmas today from residual mantle reservoirs formed in a partial melting event T_1 years ago with a range in degree of melting between F_1 and F_2, then they should have initial ϵ_{Nd} and ϵ_{Sr} which plot on the curve for $(T_D - T) = T_1$ and be bounded by the intersections with the lines labeled F_1 and F_2. We note that since depleted mantle reservoirs have Sr/Nd ratios close to chondritic, mixing curves between depleted and undepleted reservoirs would be essentially straight lines between the end-members. If mixing occurred between these reservoirs and an undepleted mantle reservoir at the origin, then magmas derived today may have values anywhere in the field bounded by the curve T_1 and the lines F_1 and F_2.

We will now apply the above relations to a specific example. For the original unfractionated reference reservoir we assume a fertile garnet peridotite mineralogy with the initial mass fractions of the various phases: olivine = 0.55, orthopyroxene = 0.15, clinopyroxene = 0.15, and garnet = 0.15. Various mineralogies have been suggested on the basis of modeling of geophysical data [*Ahrens*, 1973], the modal abundances in mantle xenoliths [*Harris et al.*, 1967; *Jackson and Wright*, 1970; *Carter*, 1970; *Maaløe and Aoki*, 1977], and geochemical models [*Ringwood*, 1975]. Our choice is fairly similar to the pyrolite model of *Ringwood* [1975]. The melting proportions of the above phases are assumed to be 0.03, 0.07, 0.45, and 0.45, respectively, and will leave a residue of harzburgite after 33% melting. The LIL element distribution are not sen-

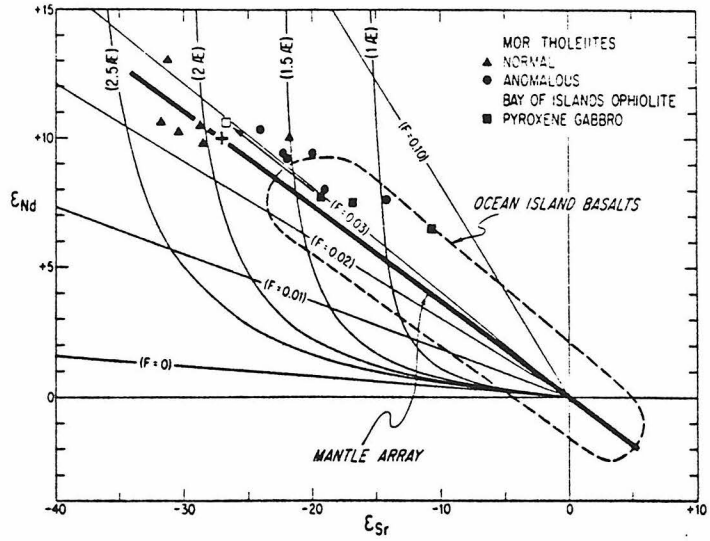

Fig. 9. An $\epsilon_{Nd} = \epsilon_{Sr}$ diagram showing data for young MOR tholeiites and the 505-m.y.-old Bay of Islands pyroxene gabbros. Constant T_D curves are shown for a range of ages from 1 to 2.5 aeons (AE) and were calculated using the partial melting model discussed in the text. Constant degree of melting curves are also shown. Typical values for the Bay of Islands source are inferred to be $\epsilon_{Nd} = +7.6$ and $\epsilon_{Sr} = -19.3$, identical to the values for one of the pyroxene gabbros (BMD-2A). This corresponds to $F = 0.03$ and a time $(T_D - T)$ of 1.35 aeons, which corresponds to an isolation of the source 1.85 aeons ago. The expected value for the Bay of Islands source, if sampled today, is shown by the open square and is close to the average value for modern MOR tholeiites (cross).

sitive to the choice of eutectic proportions. The distributions coefficients used (Table 5) were selected, if possible, for basaltic systems at temperatures of 1200°–1300°C. The mineralogy used in the present model gives the following bulk distribution coefficients: $D_{0.Rb} = 0.0025$, $D_{0.Sr} = 0.033$, $D_{0.Nd} = 0.044$, and $D_{0.Sm} = 0.080$. The melting proportions used give $P_{Rb} = 0.006$, $P_{Sr} = 0.091$, $P_{Nd} = 0.12$, and $P_{Sm} = 0.21$.

The resulting constant F and constant $(T_D - T)$ curves are shown in an ϵ_{Nd}–ϵ_{Sr} diagram together with the data for MOR tholeiites and the Bay of Islands ophiolite (Figure 9). The calculated constant $(T_D - T)$ curves all have an initital slope given by the line labeled $F = 0$. This initial slope is much less than that of the Mantle Array, so it cannot be explained by asymptotic behavior of the constant $(T_D - T)$ curves. With increasing degree of melting the constant $(T_D - T)$ curves get steeper and intersect the Mantle Array. The shape of these curves is a result of the fact that the bulk distribution coefficients $D_{Rb} \ll D_{Sr} \leq D_{Nd} < D_{Sm}$ for our choice of source mineralogy. From the distribution coefficients given in Table 5, it seems likely that the constant $(T_D - T)$ curves would have this shape for the most reasonable choices of source mineralogy if the major phases are controlling the LIL element fractionation during partial melting. If minor phases like amphibole, phlogopite, or apatite are important residual phases, then this is not necessarily true (Table 5), and the Mantle Array could possibly be due to asymptotic behavior of the constant $(T_D - T)$ curves. However, then this would require that the initial mineralogy melted always should have constant proportions of these minor phases to satisfy (15). We feel that at present there is insufficient evidence for this and conclude that the shape of the constant $(T_D - T)$ curves in Figure 9 is correct. We also note that the degree of melting assigned to each point on a constant $(T_D - T)$ curve will be much more model dependent than the shape of the curve, since the steep part is due to the fact that as $f^{Rb/Sr}$ approaches its lower limit of -1, the position of the curve is not model dependent.

The data points for pyroxene gabbros from the Bay of Islands Complex are shown in Figure 9. As discussed previously, the gabbro with the lowest ϵ_{Sr} value is thought to have the typical value of ϵ_{Nd} and ϵ_{Sr} for the Bay of Islands source. Using the time grid on Figure 9, this corresponds to an intersection of a curve with $(T_D - T) = 1.35$ aeons and a line with $F = 0.03$. The source may thus have been derived from a layer segregated 1.35 aeons prior to the formation of the 0.5-aeon-old Bay of Islands Complex, which corresponds to an isolation of the source 1.85 aeons ago. This is again consistent with the T_D value obtained previously for young MORB. This single-stage model allows us to evaluate the position of the Bay of Islands source if it had evolved up to the present instead of being partially melted ~500 m.y. ago. This displacement is shown by the arrow in Figure 9 and indicates that the Bay of Islands source would have had $\epsilon_{Nd} \sim 10.5$ and $\epsilon_{Sr} \sim -27$ if it had evolved up to today in this single-stage model.

TABLE 5. Mineral/Melt Partition Coefficients

	Rb	Sr	Nd	Sm
Clinopyroxene	0.003	0.12	0.17	0.26
Garnet	0.01	0.08	0.087	0.217
Orthopyroxene	0.003	0.02	0.013	0.022
Olivine	0.0002	0.0002	0.007	0.010
Amphibole	0.045	0.188	0.19	0.34
Phlogopite	3.0	0.081	0.03	0.03
Apatite	...	...	26	20

Sources are *Griffin and Murthy* [1969], *Philpotts and Schnetzler* [1970], *Schnetzler and Philpotts* [1970], *Hart and Brooks* [1974], *Shimizu* [1974], *Grutzeck et al.* [1975], *Shimizu and Kushiro* [1975], *Weill and McKay* [1975], *McKay and Weill* [1976], and *Beswick and Carmichael* [1978].

It is of special interest here to look in detail at the data base for present day MORB. Figure 9 shows existing data for normal and chemically anomalous MOR tholeiites. The data for anomalous MORB [*O'Nions et al.*, 1977; *Richard et al.*, 1976] are mainly from the geochemical transition zone south of the Azores and have trace element and isotopic characteristics intermediate between the Azores platform and normal ridge tholeiites [*White and Schilling*, 1978]. One sample [*O'Nions et al.*, 1977] is from the geochemical gradient observed along the Reykjanes Ridge south of Iceland [*Schilling*, 1973; *Sun et al.*, 1975]. The data for normal MORB spread out along the Mantle Array as shown in Figure 9, and the data cannot be explained as samples of different reservoirs with different f, values formed at one time, since they do not follow the steep part of any constant $(T_D - T)$ curve. The diagram rather indicates that the source of the normal MORB formed as residue after melting over a time interval from ~2.3 to 1.5 aeons ago with a relatively constant degree of melting of $F = 0.025$–0.40 to form the continents. The MORB may, of course, represent an arbitrary degree of melting which is not directly related to the values of F given here. The average MORB represented by the cross in Figure 9, indicates that the mean value of T_D is 1.9 aeons for the MORB source today. The anomalous MORB are displaced toward somewhat lower ϵ values along the Mantle Array. Younger differentiation ages are thus indicated for the source of anomalous MORB in the range from 1.7 to 1.0 aeons ago. The oceanic island magmas mainly cluster around $\epsilon_{Nd} = +6$ but spread out along the correlation line to $\epsilon_{Nd} \sim 0$, and this may indicate even younger differentiation ages for their sources. We conclude that while it is possible to explain the MORB data alone by partial melting of a reservoir formed in a unique event, it is not possible to explain the anomalous MORB or the Mantle Array by such a one-stage model. It is possible that one may have a variety of depleted mantle reservoirs formed at different times owing to partial melting events with relatively constant degree of melting. The set of all such reservoirs would, if sampled today, plot on a line. One may thus get the Mantle Array by having layers of different T_D and with F in the range from ~ 0.02 to 0.04 as indicated in Figure 9. Today this would give the isotopic characteristics of basalts which lie on the correlation line. Mixtures of such reservoirs formed at different times would then also always lie on the correlation line. The simplest choice is to have only two reservoirs, the samples with isotopic characteristics intermediate between these two reservoirs being blends of these two sources. The simplest choice of end-members is the endpoints of the Mantle Array. We thus choose the source of normal MORB for the LIL-depleted end-member and the origin (CHUR, UR) as the undepleted end-member. This model must still explain the scatter around the Mantle Array which is not addressed here. The age of the undepleted reservoir is 4.55 aeons, while the age of the depleted reservoir is probably of the order of 3.6 aeons, as discussed previously, and its mean age is ~1.8 aeons. Interpretation of the Mantle Array as a mixing line is basically in agreement with the interpretations by *Schilling* [1973], *Sun et al.* [1975], and *White and Schilling* [1978] that anomalous MORB magmas are derived by mantle plume mixing with a LIL-depleted asthenosphere. We conclude that the Mantle Array may be most simply explained as a result of mixing of the MORB source and an undifferentiated mantle source [*DePaolo and Wasserburg*, 1976*b*; *Hawkesworth et al.*, 1978; *DePaolo and Wasserburg*, 1979*a*; *DePaolo*, 1979].

Significance of Differentiation Ages for the MORB Source

Single-stage Rb-Sr and Sm-Nd differentiation ages for the MORB source give ~1.8 aeons. This is similar to differentiation ages derived from mantle isochrons [*Sun and Hanson*, 1975; *Sun and Jahn*, 1975; *Brooks et al.*, 1976*a*, *b*; *Church and Tatsumoto*, 1975; *Tatsumoto*, 1978] for both MORB and ocean island basalts. This would suggest that the widespread formation of continental crust ~1.8 aeons ago is coincident with the formation of the MORB source reservoir. We believe that a single differentiation event cannot explain the ϵ_{Nd} and ϵ_{Sr} data for MORB and the Mantle Array and that the range in observed values is most likely due to mixing of depleted mantle with undepleted mantle. The continental crust is also known to have formed in many events, with the most important occurring at ~0, 0.5, 1.0, 1.8, 2.6, and 3.6 aeons ago. Each crust-forming event must also have produced a complementary depleted mantle reservoir. The average $f_{s}^{Sm/Nd}$ value for the depleted mantle is +0.22, so we should see a range of ϵ_{Nd} values from 0 to +20 for depleted mantle formed over a time span of 3.6 aeons if no mixing occurred in the depleted mantle. Instead, the normal oceanic mantle shows a rather limited range from +8 to +12, implying relatively rapid mixing in the depleted mantle. The average $f^{Sm/Nd}$ is +0.12 for the upper oceanic crust and is +0.42 for the lower oceanic crust. If large blocks of the oceanic crust made up of these different materials were preserved, then heterogeneities of ~4 ϵ_{Nd} units should develop on a time scale of 0.5 aeon unless these units get well mixed after being subducted back to the oceanic mantle. As the total range in ϵ_{Nd} today is ~4 ϵ units and the Bay of Islands Complex gives an ϵ_{Nd} value consistent with the mean $f_{s}^{Sm/Nd}$ value for the MORB source, we therefore infer that rapid mixing must have occurred in the oceanic mantle for at least the last 1.0 aeon. The reason that we get consistent differentiation ages for the MORB source from two decay systems using its average ϵ and f values is thus likely to be due to the oceanic mantle having been relatively well mixed through time rather than having it formed in a discrete event. The mantle isochrons referred to above are thus interpreted as mixing lines between undepleted mantle and depleted mantle of mean age ~1.8 aeons. This times does not refer to any differentiation event, and the time scale of formation of this reservoir must be of the order of 3.6 aeons, which is compatible with the evidence from ages of continental crustal rocks. In a companion paper on mean ages of mantle and crustal reservoirs [*Jacobsen and Wasserburg*, 1979] we will discuss models where the continental crust and a complementary depleted mantle reservoir are built gradually throughout the history of the earth.

Conclusions

The time of crystallization of the Bay of Islands Complex has been determined as 508 ± 6 m.y. and 501 ± 13 m.y. by two Sm-Nd mineral isochrons on the pyroxene gabbros from the Blow-Me-Down massif. This time refers to the time of crystallization as a part of the Iapetus oceanic crust. This age agrees with a previously determined age by U-Pb on zircons from a trondhjemite and demonstrates the usefulness of the Sm/Nd technique for dating gabbroic rocks in ophiolites. The time of obduction of the Bay of Islands Complex is determined by previously published K-Ar ages as 470 m.y.

The oceanic nature of the complex was previously demonstrated by its structure and petrology. The LIL element pat-

terns and isotopic data presented here are clearly in agreement with this interpretation. The origin of many early Paleozoic greenstone sequences, gabbros, and ultramafics is uncertain owing to the fact that later metamorphism and tectonism have obliterated evidence for their oceanic or continental nature. It appears that the distinctive ϵ_{Nd} values of oceanic crust may now be used to identify ancient obducted oceanic lithosphere.

A small range of initial Nd of $\epsilon_{Nd} = +6.5$ to $+8.1$ is observed for different rocks within the complex including an orthopyroxenite layer from the harzburgite, whereas the initial Sr on the same samples show a large range of ϵ_{Sr} from -19 to $+33$. The observed change in ϵ_{Nd} from $+7.6$ to $+10$ for the oceanic mantle over the last 0.5 aeon is quantitatively expectable for a simple single-stage model of mantle evolution. The large range observed in ϵ_{Sr} values cannot be explained by mantle evolution. The wide range in ϵ_{Sr} with an almost constant ϵ_{Nd} is due to major interaction with seawater and thus show that the early Paleozoic ocean floors were also important sinks for radiogenic crustal Sr.

Modeling of the Rb-Sr and Sm-Nd fractionation patterns in the source of MORB strongly suggests that the data array cannot be explained by a single differentiation event to form the depleted mantle but instead most likely requires mixing of depleted and undepleted mantle sources. Single-stage differentiation ages for the source of MORB are identical for modern MORB and the Bay of Islands Complex and give ~1.8 aeons. This is similar to previously proposed differentiation ages derived from mantle isochrons. This age is, however, interpreted as the mean age of the MORB source and does not refer to a unique event. The total time for producing this source by a uniform process would be of the order of 3.6 aeons.

Normal MORB today show a limited range of ϵ_{Nd} from +8 to +12. This limited range and the consistent results for the 0.5-aeon-old Bay of Islands Complex must imply relatively rapid mixing in the source of the MORB for at least the last 1 aeon.

Acknowledgments. We wish to thank N. Christensen and H. Williams for their advice during the planning of the field work in Newfoundland and H. Williams for his hospitality. We particularly appreciate H. Williams's cleansing of the ophiolite samples from possible tuber malignancies and his help with importing the specimens. N. Christensen also provided one of the samples so that some data could be gathered prior to the field work during the summer of 1978. D. Papanastassiou, M. McCulloch, and the reviewers H. Williams and W. M. White provided numerous helpful comments and suggestions on the manuscript. We also want to thank A. M. Ziegler for stimulating discussions of the ophiolite problem. This work has been supported by NSF grant EAR 76-22494. Division of Geological and Planetary Sciences contribution 3210 (291).

References

Ahrens, T. J., Petrologic properties of the upper 670 km of the earth's mantle: Geophysical implications, *Phys. Earth Planet. Interiors, 7*, 167–186, 1973.

Allègre, C. J., R. Montigny, and Y. Bottinga, Cortège ophiolitique et cortège oceanique, géochimie comparée et mode de genèse, *Bull. Soc. Geol. Fr., 15*, 461–477, 1973.

Archibald, D. A., and E. Farrar, K-Ar ages of amphiboles from the Bay of Islands ophiolite and the Little Port Complex, Western Newfoundland, and their geological implications, *Can. J. Earth Sci., 13*, 520–529, 1976.

Bergström, S., J. Riva, and M. Kay, Significance of conodonts, graptolites and shelly faunas from the Ordovician of western and north-central Newfoundland, *Can. J. Earth Sci., 11*, 1025–1160, 1974.

Beswick, A. E., and I. S. E. Carmichael, Constraints on mantle source compositions imposed by phosphorus and rare-earth elements, *Contrib. Mineral. Petrol., 67*, 317–330, 1978.

Bird, J. M., and J. F. Dewey, Lithosphere plate–continental margin tectonics and the evolution of the Appalachian orogen, *Geol. Soc. Amer. Bull., 81*, 1031–1060, 1970.

Brooks, C., S. R. Hart, A. Hoffman, and D. E. James, Rb-Sr mantle isochrons from oceanic regions, *Earth Planet. Sci. Lett., 32*, 51–61, 1976*a*.

Brooks, C., D. E. James, and S. R. Hart, Ancient lithosphere: Its role in young continental volcanism, *Science, 193*, 1086–1094, 1976*b*.

Brueckner, H. K., Contact and fracture ultramafic assemblages from Norway: Rb-Sr evidence for crustal contamination, *Contrib. Mineral. Petrol., 49*, 39–48, 1975

Carlson, R. W., J. D. MacDougall, and G. W. Lugmair, Differential Sm/Nd evolution in oceanic basalts, *Geophys. Res. Lett., 5*, 229–232, 1978.

Carter, J. L., Mineralogy and chemistry of the Earth's upper mantle based on partial-fusion, partial-crystallization model, *Geol. Soc. Amer. Bull., 81*, 2021–2034, 1970.

Carter, S. R., N. M. Evenson, P. J. Hamilton, and R. K. O'Nions, Continental volcanics derived from enriched and depleted source regions: Nd- and Sr-isotope evidence, *Earth Planet. Sci Lett., 37*, 401–408, 1978.

Church, S. E., and M. Tatsumoto, Lead isotope relations in oceanic ridge basalts from the Juan de Fuca-Gorda Ridge area, N. E. Pacific Ocean, *Contrib. Mineral. Petrol., 53*, 253–279, 1975

Churkin, M., Jr., C. Carter, and B. Johnson, Subdivision of the Ordovician and Silurian time scale using accumulation rates of graptolitic shale, *Geology, 5*, 452–456, 1977

Coleman, R. G., *Ophiolites*, Springer, New York, 1977.

Consolmagno, G. J., and M. J. Drake, Equivalence of equations describing trace element distribution during equilibrium partial melting, *Geochim. Cosmochim. Acta, 40*, 1421–1422, 1976.

Dallmeyer, R. D., and H. Williams, $^{40}Ar/^{39}Ar$ ages from the Bay of Islands metamorphic aureole: Their bearing on the timing of Ordovician ophiolite obduction, *Can. J. Earth Sci., 12*, 1685–1690, 1975.

Dasch, E. J., C. E. Hedge, and J. Dymond, Effect of sea water interaction on strontium isotope composition of deep-sea basalts, *Earth Planet. Sci. Lett., 19*, 177–183, 1973.

DePaolo, D. J., Implications of correlated Nd and Sr isotopic variations for the chemical evolution of the crust and mantle, *Earth Planet. Sci. Lett., 43*, 201–211, 1979.

DePaolo, D. J., and G. J. Wasserburg, Nd isotopic variations and petrogenetic models, *Geophys. Res Lett., 3*, 249–252, 1976*a*.

DePaolo, D. J., and G. J. Wasserburg, Inferences about magma sources and mantle structure from variations of $^{143}Nd/^{144}Nd$, *Geophys. Res. Lett., 3*, 743–746, 1976*b*.

DePaolo, D. J., and G. J. Wasserburg, The sources of island arcs as indicated by Nd and Sr isotopic studies, *Geophys. Res. Lett., 4*, 465–468, 1977.

DePaolo, D. J., and G. J. Wasserburg, Petrogenetic mixing models and Nd-Sr isotopic patterns, *Geochim. Cosmochim. Acta, 43*, 615–627, 1979*a*.

DePaolo, D. J., and G. J. Wasserburg, Sm-Nd age of the Stillwater Complex and the mantle evolution curve for neodymium, *Geochim. Cosmochim. Acta, 43*, 999–1008, 1979*b*.

DePaolo, D. J., and G. J. Wasserburg, Nd isotopes in flood basalts from the Siberian Platform and inferences about their mantle sources, *Proc. Nat. Acad. Sci. U.S.*, in press, 1979*c*.

Dewey, J. F., and J. M. Bird, Origin and emplacement of the ophiolite suite: Appalachian ophiolites in Newfoundland, *J. Geophys. Res., 76*, 3179–3206, 1971.

Einarson, G. W., Low rank metamorphism in the Bay of Islands ophiolite complex, western Newfoundland, *Geol. Ass. Can. Program Abstr., 752*, 1975.

Engel, A. E. J., C. G. Engel, and R. G. Havens, Chemical characteristics of oceanic basalts and the upper mantle, *Geol. Soc. Amer. Bull., 76*, 719–734, 1965.

Frey, F. A., D. H. Green, and S. D. Roy, Integrated models of basalt petrogenesis: A study of olivine tholeiites to olivine melilitites from south eastern Australia utilizing geochemical and experimental petrologic data, *J. Petrology, 19*, 463–513, 1978.

Gast, P. W., Trace element fractionation and the origin of tholeiitic and alkaline magma types, *Geochim. Cosmochim. Acta, 32*, 1057–1086, 1968.

Griffin, W. L., and V. R. Murthy, Distribution of K, Rb, Sr, and Ba in some minerals relevant to basalt genesis, *Geochim. Cosmochim. Acta, 33*, 1389–1414, 1969.

Grutzeck, M., S. Kridelbaugh, and D. Weill, The distribution of Sr

and REE between diopside and silicate liquid, *Geophys. Res. Lett.*, *1*, 273–275, 1974.

Hamilton, P. J., R. K. O'Nions, and N. M. Evensen, Sm-Nd dating of Archean basic and ultrabasic volcanics, *Earth Planet. Sci Lett.*, *36*, 263–268, 1977.

Hamilton, P. J., R. K. O'Nions, N. M. Evensen, D. Bridgwater, and J. Allart, Sm-Nd isotopic investigations of the Isua supracrustals, West Greenland: Implications for mantle evolution, *Nature*, *272*, 41–43, 1978.

Hamilton, P. J., N. M. Evensen, R. K. O'Nions, and J. Tarney, Sm-Nd systematics of Lewisian gneisses: Implications for the origin of granulites, *Nature*, *277*, 25–28, 1979.

Harris, P. G., A. Reay, and I. G. White, Chemical composition of the upper mantle, *J. Geophys. Res.*, *72*, 6359–6369, 1967.

Hart, S. R., Submarine basalts from Kilauea rift, Hawaii: Non-dependence of trace element composition on extrusion depth, *Earth Planet. Sci. Lett.*, *20*, 201–203, 1973.

Hart, S. R., and C. Brooks, Clinopyroxene matrix partitioning of K, Rb, Cs, Sr, and Ba, *Geochim. Cosmochim. Acta*, *38*, 1799–1803, 1974.

Hart, S. R., C. Brooks, T. E. Krogh, G. L. Davis, and D. Nava, Ancient and modern volcanic rocks: A trace element model, *Earth Planet. Sci. Lett.*, *10*, 17–28, 1970.

Hart, S. R., W. E. Glassley, and D. E. Karig, Basalts and sea floor spreading behind the Mariana Island arc, *Earth Planet. Sci. Lett.*, *15*, 12–18, 1972.

Hart, S. R., A. J. Erlank, and E. J. D. Kable, Sea floor basalt alteration: Some chemical and Sr isotopic effects, *Contrib. Mineral. Petrol.*, *44*, 219–230, 1974.

Hawkesworth, C. J., R. K. O'Nions, R. J. Pankhurst, P. J. Hamilton, and N. M. Evensen, A geochemical study of island-arc and back-arc tholeiites from the Scotia Sea, *Earth Planet. Sci. Lett.*, *36*, 253–262, 1977.

Hawkesworth, C. J., M. J. Norry, J. C. Roddick, and R. Vollmer, The significance of trace element modeling calculations for the evolution of Sr and Nd isotopes in the mantle, *Open File Rep. 78-701*, pp 162–164, U.S. Geol. Surv., Reston, Va., 1978.

Hawkins, J. W., Petrology and geochemistry of basaltic rocks of the Lau Basin, *Earth Planet. Sci. Lett.*, *28*, 283–297, 1976.

Herrmann, A. G., Yttrium and lanthanides, 39, 57–71, in *Handbook of Geochemistry*, vol. II, part 5, edited by K. H. Wedepohl, Springer, New York, 1969–1974.

Hildreth, R. A., and W. T. Henderson, Comparison of $^{87}Sr/^{86}Sr$ for seawater strontium and the Eimer and Amend $SrCO_3$, *Geochim. Cosmochim. Acta*, *35*, 235–238, 1971.

Høgdahl, O. T., B. T. Bowen, and S. Melson, Neutron activation analysis of lanthanide elements in sea water, *Advan. Chem. Ser.*, *73*, 308–325, 1968.

Holland, H., *The Chemistry of the Atmosphere and Oceans*, John Wiley, New York, 1978.

Hubbard, N. J., and P. W. Gast, Chemical composition and origin of nonmare lunar basalts, *Proc. Lunar Sci. Conf. 2nd*, *2*, 999–1020, 1971.

Irvine, T. N., and T. C. Findlay, Alpine-type peridotite with particular reference to the Bay of Islands complex, *Publ. 42*, pp. 97–128, Earth Phys. Br., Dep. of Energ., Mines, and Resour., Ottawa, Ont., Canada, 1972.

Jackson, E. D., and T. L. Wright, Xenoliths in the Honolulu volcanic series, *J. Petrology*, *11*, 405–430, 1970.

Jacobsen, S. B., and G. J. Wasserburg, The mean age of mantle and crustal reservoirs, *J. Geophys. Res.*, *84*, this issue, 1979.

Karson, J., and J. F. Dewey, Coastal Complex, western Newfoundland: An early Ordovician oceanic fracture zone, *Geol. Soc. Amer. Bull.*, *89*, 1037–1049, 1978.

Kay, R. W., and R. G. Senechal, The rare earth chemistry of the Troodos ophiolite complex, *J. Geophys. Res.*, *81*, 964–970, 1976.

Kay, R., N. J. Hubbard, and P. W. Gast, Chemical characteristics and origin of oceanic ridge volcanic rocks, *J. Geophys. Res.*, *75*, 1585–1613, 1970

Leeman, W. P., Petrogenesis of McKinney (Snake River) olivine tholeiite in light of rare-earth element and Cr/Ni distributions, *Geol. Soc. Amer. Bull.*, *87*, 1582–1586, 1976.

Lugmair, G. W., Sm-Nd ages: A new dating method (abstract), *Meteoritics*, *9*, 369, 1974.

Lugmair, G. W., K. Marti, J. P. Kurtz, and N. B. Scheinin, History and genesis of lunar troctolite 76535 or: How old is old?, *Proc. Lunar Sci. Conf. 7th*, 2009–2033, 1976.

Maaløe, S., and K. Aoki, The major element composition of the upper mantle estimated from the composition of lherzolites, *Contrib. Mineral. Petrol.*, *63*, 161–173, 1977.

Malpas, J., Magma generation in the upper mantle, field evidence from ophiolite suites, and application to the generation of oceanic lithosphere, *Phil. Trans. Roy. Soc. London, Ser. A*, *288*, 527–546, 1978.

Masuda, A., and H. Jibiki, Rare-earth patterns of Mid-Atlantic Ridge gabbros: Continental nature?, *Geochem. J.*, *7*, 55–65, 1973.

Mattinson, J. M., Early Paleozoic ophiolite complexes of Newfoundland: Isotopic ages of zircons, *Geology*, *3*, 181–183, 1975.

Mattinson, J. M., Ages of zircons from the Bay of Islands Ophiolite Complex, western Newfoundland, *Geology*, *4*, 393–394, 1976.

McCulloch, M. T., and G. J. Wasserburg, Sm-Nd and Rb-Sr chronology of continental crust formation, *Science*, *200*, 1003–1011, 1978.

McDougall, I., Geochemistry and origin of basalt of the Columbia River Group, Oregon and Washington, *Geol. Soc. Amer. Bull.*, *87*, 777–792, 1976.

McKay, G. A., and D. F. Weill, Petrogenesis of KREEP, *Proc. Lunar Sci. Conf. 7th*, 2427–2447, 1976.

Menzies, M. M., and V. R. Murthy, Strontium isotope geochemistry of alpine tectonite lherzolites: Data compatible with a mantle origin, *Earth Planet. Sci. Lett.*, *38*, 346–354, 1978.

Montigny, R., H. Bougault, Y. Bottinga, and C. J. Allègre, Trace element geochemistry and genesis of the Pindos ophiolite suite, *Geochim. Cosmochim. Acta*, *37*, 2135–2147, 1973.

Nakamura, N., Determination of REE, Ba, Fe, Mg, Na and K in carbonaceous and ordinary chondrites, *Geochim. Cosmochim. Acta*, *38*, 757–775, 1974.

O'Nions, R. K., R. J. Pankhurst, and K. Grønvold, Nature and development of basalt magma sources beneath Iceland and the Reykjanes Ridge, *J. Petrology*, *17*, 315–338, 1976.

O'Nions, R. K., P. J. Hamilton, and N. M. Evensen, Variations in $^{143}Nd/^{144}Nd$ and $^{87}Sr/^{86}Sr$ ratios in oceanic basalts, *Earth Planet. Sci. Lett.*, *34*, 13–22, 1977.

O'Nions, R. K., S. R. Carter, R. S. Cohen, N. M. Evensen, and P. J. Hamilton, Pb, Nd and Sr isotopes in oceanic ferromanganese deposits and ocean floor basalts, *Nature*, *273*, 435–438, 1978*a*.

O'Nions, R. K., N. M. Evensen, P. J. Hamilton, and S. R. Carter, Melting of the mantle past and present: Isotope and trace element evidence, *Phil Trans. Roy. Soc. London, Ser. A*, *288*, 547–559, 1978*b*.

Papanastassiou, D. A., and G. J. Wasserburg, Rb-Sr ages and initial strontium in basalts from Apollo 15, *Earth Planet. Sci. Lett.*, *17*, 324–337, 1973.

Papanastassiou, D. A., G. J. Wasserburg, and D. S. Burnett, Rb-Sr ages of lunar rocks from the Sea of Tranquility, *Earth Planet. Sci. Lett.*, *8*, 1–9, 1970.

Papanastassiou, D. A., D. J. DePaolo, and G. J. Wasserburg, Rb-Sr and Sm-Nd chronology and genealogy of basalts from the Sea of Tranquility, *Proc. Lunar Sci. Conf. 8th*, 1639–1672, 1977.

Philpotts, J. A., and C. C. Schnetzler, Phenocryst-matrix partition coefficients for K, Rb, Sr and Ba, with applications to anorthosite and basalt genesis, *Geochim. Cosmochim. Acta*, *34*, 307–322, 1970.

Piepgras, D. J., G. J. Wasserburg, and E. J. Dasch, The isotopic composition of Nd in different ocean masses, *Earth Planet. Sci. Lett.*, in press, 1979.

Richard, P., N. Shimizu, and C. J. Allègre, $^{143}Nd/^{146}Nd$, a natural tracer, an application to oceanic basalts, *Earth Planet. Sci. Lett.*, *31*, 269–278, 1976.

Richard, P., D. Rousseau, and C. J. Allègre, Nd and Sr systematics in ophiolites, *Open File Rep. 78-701*, p. 350, U.S. Geol. Surv., Reston, Va., 1978.

Ringwood, A. E., *Composition and Petrology of the Earth's Mantle*, 618 pp., McGraw-Hill, New York, 1975.

Salisbury, M. H., and N. I. Christensen, The seismic velocity structure of a traverse through the Bay of Islands Ophiolite Complex, Newfoundland, an exposure of oceanic crust and upper mantle, *J. Geophys. Res.*, *83*, 805–817, 1978.

Schilling, J. G., Iceland mantle plume: Geochemical study of the Reykjanes Ridge, *Nature*, *242*, 565–571, 1973.

Schnetzler, C. C., and J. A. Philpotts, Partition coefficients of rare-earth elements between igneous matrix material and rock-forming phenocrysts, II, *Geochim. Cosmochim. Acta*, *34*, 331–340, 1970.

Shaw, D. M., Trace element fractionation during anatexis, *Geochim. Cosmochim. Acta*, *34*, 237–243, 1970.

Shimizu, N., An experimental study of the partitioning of K, Rb, Cs,

Sr and Ba between clinopyroxene and liquid at high pressures, *Geochim. Cosmochim. Acta, 38*, 1789–1798, 1974.

Shimizu, N., and I. Kushiro, The partition of rare earth elements between garnet and liquid at high pressures: Preliminary experiments, *Geophys. Res. Lett., 2*, 413–416, 1975.

Smith, C. H., Bay of Islands igneous complex, western Newfoundland, *Geol. Surv. Can. Mem., 290*, 132 pp., 1958.

Spooner, E. T. C., R. D. Beckinsale, W. S. Fyfe, and J. D. Smewing, O^{18}-enriched ophiolitic metabasic rocks from E. Liguria (Italy), Pindos (Greece), and Troodos (Cyprus), *Contrib. Mineral. Petrol., 47*, 41–62, 1974.

Spooner, E. T. C., H. J. Chapman, and J. D. Smewing, Strontium isotopic contamination and oxidation during ocean floor hydrothermal metamorphism of the ophiolitic rocks of the Troodos Massif, Cyprus, *Geochim. Cosmochim. Acta, 41*, 873–890, 1977.

Stevens, R. K., Cambro-Ordovician flysch sedimentation and tectonics in west Newfoundland and their possible bearing on a proto-Atlantic ocean, Flysch Sedimentology in North America, *Geol. Ass. Can. Spec. Pap. 7*, 165–177, 1970.

Stukas, V., and P. H. Reynolds, $^{40}Ar/^{39}Ar$ dating of the Long Range dikes, Newfoundland, *Earth Planet. Sci. Lett., 22*, 256–266, 1974*a*.

Stukas, V., and P. H. Reynolds, $^{40}Ar/^{39}Ar$ dating of the Brighton gabbro complex, Lushs Bight terrane, Newfoundland, *Can. J. Earth Sci., 11*, 1485–1488, 1974*b*.

Sun, S. S., and G. N. Hanson, Evolution of the mantle: Geochemical evidence from alkali basalts, *Geology, 3*, 297–302, 1975.

Sun, S. S., and B. Jahn, Lead and strontium isotopes in post-glacial basalts from Iceland, *Nature, 255*, 527–530, 1975.

Sun, S. S., M. Tatsumoto, and J. G. Schilling, Mantle plume mixing along the Reykjanes Ridge axis: Lead isotopic evidence, *Science, 190*, 143–147, 1975.

Tatsumoto, M., Isotopic composition of lead in oceanic basalt and its implication to mantle evolution, *Earth Planet. Sci. Lett., 38*, 63–87, 1978.

Tatsumoto, M., C. E. Hedge, and A. E. J. Engel, K, Rb, Sr, Th, U and $^{87}Sr/^{86}Sr$ in oceanic tholeiitic basalt, *Science, 150*, 886–888, 1965.

Veizer, J., and W. Compston, $^{87}Sr/^{86}Sr$ composition of seawater during the Phanerozoic, *Geochim. Cosmochim. Acta, 38*, 1461–1484, 1974.

Wasserburg, G. J., and D. A. Papanastassiou, Model ages, *Nature, 259*, 159–160, 1976.

Weill, D. F., and G. A. McKay, The partitioning of Mg, Fe, Sr, Ce, Sm, Eu and Yb in lunar igneous systems and a possible origin of KREEP by equilibrium partial melting, *Proc. Lunar Sci. Conf. 6th*, 1143–1158, 1975.

Wenner, D. B., and H. P. Taylor, Jr., Oxygen and hydrogen isotope studies of serpentinization of ultramafic rocks in oceanic environments and continental ophiolite complexes, *Amer. J. Sci., 273*, 207–239, 1973.

White, W. M., and J. G. Schilling, The nature and origin of geochemical variation in Mid-Atlantic Ridge basalts from the central north Atlantic, *Geochim. Cosmochim. Acta, 42*, 1501–1516, 1978.

Williams, H., The Bay of Islands map area, Newfoundland, *Geol. Surv. Can. Pap., 72-34*, 1–7, 1973.

Williams, H., and J. Malpas, Sheeted dikes and brecciated dike rocks within transported igneous complexes, Bay of Islands, western Newfoundland, *Can. J. Earth Sci., 9*, 1216–1229, 1972.

Williams, H., and R. K. Stevens, Geology of Belle Isle—Northern extremity of the deformed Appalachian miogeosynclinal belt, *Can. J. Earth Sci., 6*, 1145–1157, 1969.

Williams, H., and R. K. Stevens, The ancient continental margin of eastern North America, in *The Geology of Continental Margins*, edited by C. Burke and C. Drake, pp. 781–796, Springer, New York, 1974.

Williams, H., and R. W. Talkington, Distribution and tectonic setting of ophiolites and ophiolitic melanges in the Appalachian orogen, North American Ophiolites, *Oreg. Dep. Geol. Min. Ind. Bull., 95*, 1–11, 1977.

York, D., Least-squares fitting of a straight line, *Can. J. Phys., 44*, 1079–1086, 1966.

Zindler, A., C. Brooks, N. T. Arndt, and S. Hart, Nd and Sr isotope data from komatiitic and tholeiitic rocks of Munro Township, Ontario, Short Papers of the Fourth International Conference, Geochronology, Cosmochronology, Isotope Geology, *Open File Rep. 78-701*, 476 pp., U.S. Geol. Surv., Reston, Va., 1978.

(Received May 10, 1979;
revised July 27, 1979;
accepted July 31, 1979.)

APPENDIX 3.

VOL. 84, NO. B13 JOURNAL OF GEOPHYSICAL RESEARCH DECEMBER 10, 1979

The Mean Age of Mantle and Crustal Reservoirs

STEIN B. JACOBSEN AND G. J. WASSERBURG

The Lunatic Asylum of the Charles Arms Laboratory, Division of Geological and Planetary Sciences California Institute of Technology, Pasadena, California 91125

Mantle and crust evolution is discussed in terms of two simple transport models. In model I, continents ($j = 3$) are derived by melt extraction over the history of the earth from undepleted mantle ($j = 1$), and the residue forms a depleted mantle ($j = 2$), which today is the source of mid-ocean ridge basalts. In model II, new additions to continents are derived from a mantle reservoir 2, which becomes more depleted through time by repeated extraction of melts. Transport equations were solved for stable s, radioactive r, and daughter d isotopes for arbitrary mass growth curves $M_j(\tau)$. For both models the isotopic composition and concentrations of trace elements are shown to reduce to simple mathematical expressions which readily permit calculations of basic evolutionary parameters from the data. For long-lived isotopes ($\lambda^{-1} \gg 4.5$ aeons) for model I the deviations in parts in 10^4 of the ratio of a daughter isotope to a stable reference isotope of the same element in reservoirs $j = 2, 3$ from that of 1 is given by $\epsilon_{dj}^* = Q_d^* \tilde{t}_{M,j} f_j'^{/s}$. Here $\tilde{t}_{M,j}$ is the mean age of the mass of j, $f_j'^{/s}$ is the enrichment factor of the ratio of a radioactive isotope to a stable isotope relative to that in 1, and $Q_d^* \simeq$ const. Thus for long-lived isotopes such as ^{147}Sm and ^{87}Rb the only time information that can be obtained from model I from measurement of the relative chemical enrichment factors and isotopic ratios at a single time is the mean age of the mass of the continental crust and the complementary depleted mantle reservoir. This mean age is independent of the long-lived parent-daughter system. An analogous result is obtained for model II, where $\epsilon_{d,2}^* = Q_d^* \langle f_2'^{/s} \rangle \tau$. Here $\langle f_2'^{/s} \rangle$ is the weighted time average of the enrichment factor, and τ is the time measured from the origin of the earth. The mean age of the mass of the crust ($\tilde{t}_{M,3}$) and the time parameter $\tilde{t}_{r/s} = \tau(f_2'^{/s})/f_2'^{/s}$ for the crust in model II will for long-lived parent-daughter systems be different depending on the element fractionation during partial melting. Decay systems with small parent-daughter fractionations during partial melting may, however, be used to estimate the mean age of the continental crust. Sm-Nd and Rb-Sr isotopic data for continental crust, depleted and undepleted mantle, have been used to evaluate both models and yield young mean ages for the mass of the continental crust of 1.8 and 1.5 aeons for model I and model II, respectively. Both models also suggest that the rate of growth of the continents for the last 0.5 aeon is much less than the average growth rate. The young mean age of the continents implies either rapid refluxing of crustal materials to the mantle in the period from 4.5 to 3.6 aeons or that very little early crust ever formed. Mass balance calculations for both models show that the continents were only formed from ~30% of the total mantle, leaving 70% of the mantle as undepleted. The major difference in the two models lies in the difference in the compositions of newly derived crust. For model I the trace element concentrations in new additions to the crust is constant, and the isotopic values are those of the undepleted mantle reservoir, in agreement with recent Nd isotopic studies. The correlation line between ϵ_{Nd} and ϵ_{Sr} for young basalts can be explained with model I by mixing depleted and undepleted mantle, but it cannot in any simple way be explained by model II. Model II implies that new additions to the continents have the isotopic characteristics of depleted mantle and that the concentration of Rb, U, Ba, and other highly incompatible trace elements in newly added material have changed by a factor of ~10 through time, for which there is no evidence. For both models the simple analytical expressions derived herein permit calculations of earth models with great facility without requiring a computer calculation.

INTRODUCTION

Over the past few years a substantial amount of new data has become available on the Sm-Nd and Rb-Sr isotope characteristics of mantle and crustal reservoirs. These data have been used to determine the times of additions of new continental crustal materials [*McCulloch and Wasserburg*, 1978] and in discussions of the evolution of the mantle sources of modern continental and oceanic basalts. These studies have demonstrated that the mid-ocean ridge basalts (MORB) have been derived from a depleted mantle source [*DePaolo and Wasserburg*, 1976*a*, *b*; *Richard et al.*, 1976] and that young continental flood basalts and new additions to the continents throughout most of the earth's history appear mainly to have been derived from undepleted mantle reservoirs [*DePaolo and Wasserburg*, 1976*b*, 1979*b*]. Recently, data on the initial isotopic composition of 0.5-aeon-old (1 aeon = 1 AE = 10^9 years) oceanic crust have become available which permit an estimate of the composition of the oceanic mantle in the early paleozoic [*Jacobsen and Wasserburg*, 1979]. The simplest model for explaining the observed isotopic heterogeneities in the mantle would be to assume that they formed in a single event [*Brooks et al.*, 1976*a*, *b*; *Brooks and Hart*, 1978]. However, as was discussed by *O'Nions et al.* [1978], *Tatsumoto* [1978], and *Jacobsen and Wasserburg* [1979], available Pb, Nd, and Sr isotopic data on young basalts do not appear to fit such a single-stage model, and it is not compatible with our knowledge that the continental crust has evolved in many stages over geologic time [see, for example, *Moorbath*, 1978; *O'Nions and Pankhurst*, 1978; *McCulloch and Wasserburg*, 1978]. Because of these considerations it is necessary to analyze the data in terms of continuous or multiepisodic mantle-crust transport models.

In this study we present an analysis of two simple transport models for trace elements and relate them to the isotopic abundance patterns that can be observed. The general transport equations for transfer of stable, radioactive, and daughter isotopes between n reservoirs were given by *Wasserburg* [1964]. The models presented here assume that the transport is solely from mantle to continental crust and do not treat the flux back to the mantle of continental crustal material for simplicity, but the treatment may be simply extended to include this. In the first model (model I) the mechanism for crustal

growth is by deriving melts over the age of the earth by equilibrium partial melting from undepleted mantle. In the second model (model II), melts that form new continental crust are being derived from a mantle reservoir that is continuously depleted through time. We will show that although the models involve rather heavy algebra, they lead to exceedingly simple expressions for the isotopic ratios and trace element abundances in terms of the mass of continental crust and depleted mantle which are evolved. The models apply to arbitrary crustal growth rates in contrast to previous transport models [*Patterson*, 1964; *Patterson and Tatsumoto*, 1964; *Wasserburg*, 1966; *Armstrong*, 1968; *Hart and Brooks*, 1970; *Russell*, 1972; *Russell and Birnie*, 1974; *DePaolo*, 1978; *O'Nions et al.*, 1979]. This approach is a generalization of the treatment of nucleosynthetic time scales given by *Schramm and Wasserburg* [1970]. The results may be used directly to discuss earth models using available isotopic data and concentration data for mantle and crustal rocks. This treatment appears to give a deep and direct insight into the problems of mantle evolution.

Mantle-Crust Transport Models

Model I

We first consider a model of crustal growth from an undifferentiated mantle reservoir (reservoir 1) with a given segment of the mantle being differentiated to form two reservoirs: a depleted mantle (reservoir 2) and a continental crust (reservoir 3). The model is shown schematically in Figure 1. We define M_j, $N_{i,j}$, and $C_{i,j}$ to be the total mass of reservoir j, number of atoms of species i in reservoir j, and the concentration of species i in reservoir j, respectively. Differential masses added to or subtracted from the total reservoir j are denoted by δM_j. The number of species i and the concentration of i in the differential mass δM_j are denoted by $\delta N_{i,j}$ and $c_{i,j}$, respectively. Let us assume that a mass δM_1 is removed from reservoir 1 and a partially melted fraction F is extracted from this differential mass to form new crust with added mass δM_3 and a new residual mass δM_2 is added to the depleted mantle. This gives $\delta M_3/\delta M_1 = F$ and $\delta M_2/\delta M_1 = 1 - F$. We imagine that the crust is thus increased by the amount δM_3 and the undifferentiated mantle reservoir is diminished in amount by mass δM_1. The mass δM_2 is added to the depleted mantle, which we assume to be otherwise isolated from the remaining undifferentiated reservoir 1.

The number of atoms of species i in each differential mass j in this unit process is $\delta N_{i,j}$, which gives

$$\delta N_{i,1} = \delta N_{i,2} + \delta N_{i,3} \tag{1}$$

The number of species i in the differential mass δM_j may be written $\delta N_{i,j} = c_{i,j}\delta M_j$. Conservation of species and mass gives

$$c_{i,1} = c_{i,2}(1 - F) + c_{i,3}F \tag{2}$$

Trace elements are fractionated between melts and residue with an effective partition coefficient. The effective partition coefficient D_i for element i between the residue (δM_2) and the partial melt (δM_3) is defined by $D_i = c_{i,2}/c_{i,3}$. The concentration in δM_3 is

$$c_{i,3} = \frac{c_{i,1}}{F + D_i(1 - F)} = \frac{c_{i,2}}{D_i} \tag{3}$$

We may thus express the number of species i in the differential masses j in terms of their masses δM_j and the concentration in reservoir 1, since $c_{i,1} = C_{i,1}$:

$$\delta N_{i,j} = \frac{D_{i,j}C_{i,1}}{F + D_i(1 - F)}\,\delta M_j \tag{4}$$

$$D_{i,j} = D_i \qquad j = 2$$

$$D_{i,j} = 1 \qquad j = 3$$

We consider the following species: (1) a stable index isotope s of an element which is not affected by radioactive decay, (2) a radioactive isotope r with decay constant λ, and (3) a daughter isotope d which is the decay product of r and of the same chemical element as s.

The transport equations for the total reservoir j containing the number $N_{i,j}$ of each isotope $i = s, r, d$ are

$$\frac{dN_{i,j}(\tau)}{d\tau} = \frac{\delta N_{i,j}}{\delta\tau} - \lambda_i N_{r,j}(\tau) \tag{5}$$

$$\lambda_i = 0 \quad i = s$$

$$\lambda_i = \lambda \quad i = r$$

$$\lambda_i = -\lambda \quad i = d$$

where $dN_{i,j}/d\tau$ is the time derivative and $\delta N_{i,j}/\delta\tau$ is the flux of species i into reservoir j. In this treatment, $\delta\tau$ is the time over which mass δM_1 is differentiated at time τ. For simplicity we have chosen to ignore transport between 2 and 3. Using the expressions for $\delta N_{i,j}$ in terms of $C_{i,1}$ and δM_j and calling $\delta M_j/\delta\tau \equiv M_j'(\tau)$, which is the rate of mass growth of reservoir j, we obtain the basic transport equation for model I,

$$\frac{dN_{i,j}}{d\tau} = \frac{D_{i,j}C_{i,1}(\tau)}{F + D_i(1 - F)}\,M_j'(\tau) - \lambda_i N_{r,j}(\tau) \tag{6}$$

where $D_{i,j}$ and λ_i are defined as in (4) and (5). The first term on the right-hand side of (6) is the transport term, and the second term is due to either radioactive decay or production.

The general solution of (6) for a stable index isotope is

$$N_{s,j}(\tau) = \frac{D_{s,j}}{F + D_s(1 - F)} \int_0^\tau C_{s,1}(\xi)M_j'(\xi)\,d\xi \tag{7}$$

The equation was integrated with the assumption that the time $\tau = 0$ at the time of initial chemical differentiation of the earth and $N_{s,j}(0) = 0$. The earth is taken to be initially homogeneous.

The undifferentiated reservoir is characterized by a closed system behavior for intensive quantities, so that the concentration for species s, r, and d are

$$C_{s,1}(\tau) = C_{s,1}(0) \tag{8}$$

$$C_{r,1}(\tau) = C_{r,1}(0)e^{-\lambda\tau} \tag{9}$$

$$C_{d,1}(\tau) = C_{d,1}(0) + C_{r,1}(0)[1 - e^{-\lambda\tau}] \tag{10}$$

The relationship between the masses of reservoirs 2 and 3 is given by $M_3(\tau) = [F/(1 - F)]M_2(\tau)$. Substituting (8) into (7) gives the following general solutions for stable isotopes in reservoirs 2 and 3:

$$N_{s,2}(\tau) = \frac{D_sC_{s,1}(0)}{F + D_s(1 - F)}\,M_2(\tau) \tag{11}$$

$$N_{s,3}(\tau) = \frac{C_{s,1}(0)}{F + D_s(1 - F)}\,M_3(\tau) \tag{12}$$

The above equation for a stable isotope in the crust may also be written as $C_{s,3}(\tau) = C_{s,1}(0)/[F + D_s(1 - F)]$, which is equivalent to the equation for equilibrium partial melting derived by *Consolmagno and Drake* [1976] which showed that previous equations given by *Shaw* [1970], *Schilling* [1971], and *O'Nions and Clarke* [1972] all reduce to this general form.

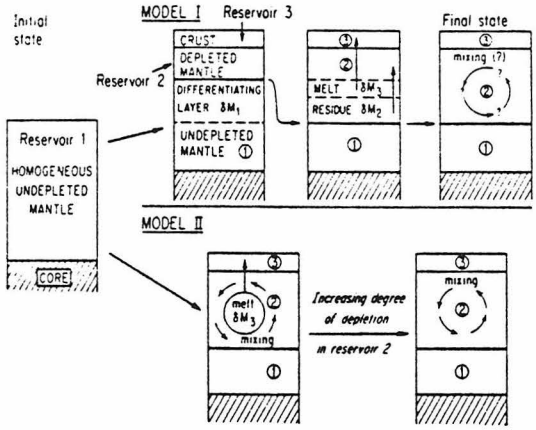

Fig. 1. Cartoon showing the processes in model I and model II. Model I is a three-layer model consisting of undepleted mantle (1), depleted mantle (2), and continental crust (1), as indicated under the final state. In model I a given segment (the differentiating layer δM_1) of undepleted mantle (1) is being differentiated by equilibrium partial melting and added to two reservoirs: a depleted mantle (2) and a continental crust (3). We assume that a differential mass δM_1 is removed from reservoir 1 and a partially melted fraction F is extracted from this differential mass to form new crust with added mass δM_3 and that a new residual mass δM_2 is added to the depleted mantle. In this differentiation process the masses of reservoirs 1, 2, and 3 are conserved. The masses of the depleted mantle and the crust increase with time, and the undepleted mantle decreases with time. The upper boundary of the undepleted mantle is thus lowered, and the volumes of both depleted mantle and crust increased. These stages are shown in the second and third columns. In model II the crust grows from an initially undifferentiated mantle reservoir (2), which is depleted at all times subsequent to the initial chemical differentiation as a result of continuing crustal growth. This reservoir may make up all or part of the mantle. Layers 2 and 3 are thus the only active regions in this model. The remaining undifferentiated mantle is passive and is still indicated as layer 1. In this model we assume that a differential mass δM^* of reservoir 2 is being differentiated into a melt δM_3, which is added to the continental crust and a residue $\delta M_R{}^*$. The degree of melting F is taken as finite. The residue after removal of a melt fraction from reservoir 2 is assumed to be homogenized instantaneously with the remaining part of the depleted mantle. The total mass of reservoirs 2 and 3 is conserved; the continental crust increases in mass with time, and the depleted mantle decreases in mass with time. In both models the depleted mantle is taken to include the basaltic part of the oceanic crust, since it is derived from the depleted mantle and is subducted back to the depleted mantle at a short time scale (<0.2 aeon).

Solutions of (6) analogous to (7) may also be obtained for radioactive isotopes. Substituting (9) into these gives the following result for reservoirs 2 and 3:

$$N_{r,2}(\tau) = \frac{D_r e^{-\lambda\tau} C_{r,1}(0)}{F + D_r(1-F)} M_2(\tau) \tag{13}$$

$$N_{r,3}(\tau) = \frac{e^{-\lambda\tau} C_{r,1}(0)}{F + D_r(1-F)} M_3(\tau) \tag{14}$$

Similarly, by substituting (10), (13), and (14) into (6) we obtain the following equations for daughter isotopes in reservoirs 2 and 3:

$$N_{d,2}(\tau) = \left\{ D_d \left[C_{d,1}(\tau) M_2(\tau) + \lambda C_{r,1}(0) \left[\frac{F + D_d(1-F)}{F + D_r(1-F)} \left(\frac{D_r}{D_d} \right) - 1 \right] \right. \right.$$
$$\left. \left. \int_0^\tau M_2(\xi) \exp[-\lambda\xi]\, d\xi \right] \right\} [F + D_d(1-F)]^{-1} \tag{15}$$

$$N_{d,3}(\tau) = \left\{ C_{d,1}(\tau) M_3(\tau) + \lambda C_{r,1}(0) \left[\frac{F + D_d(1-F)}{F + D_r(1-F)} - 1 \right] \right.$$
$$\left. \int_0^\tau M_3(\xi) \exp[-\lambda\xi]\, d\xi \right\} [F + D_d(1-F)]^{-1} \tag{16}$$

where $D_s = D_{s^*}$ since d and s are isotopes of the same element, and $C_{d,1}(\tau)$ is given by (10).

The enrichment factor of the ratio of a radioactive isotope to a stable isotope in a reservoir j relative to that in reservoir 1 is called $f_j^{r/s}$. This enrichment factor is the same both for new additions to j and for the total reservoir j, and it is defined by

$$f_j^{r/s} \equiv \frac{N_{r,j}(\tau)/N_{s,j}(\tau)}{N_{r,1}(\tau)/N_{s,1}(\tau)} - 1 \tag{17}$$

For this model the enrichment factor is independent of time and is given by

$$f_2^{r/s} + 1 = \left(\frac{D_r}{D_s} \right) \frac{F + D_s(1-F)}{F + D_r(1-F)} = \left(\frac{D_r}{D_s} \right) (f_3^{r/s} + 1) \tag{18}$$

As $D_s = D_{s^*}$ the ratio of a daughter isotope to a stable reference isotope of the same element (with no parent) in each reservoir is given by

$$\frac{N_{d,j}(\tau)}{N_{s,j}(\tau)} = \frac{N_{d,1}(\tau)}{N_{s,1}(\tau)} + \frac{N_{r,1}(\tau)}{N_{s,1}(\tau)} \frac{f_j^{r/s}\lambda}{M_j(\tau)} \cdot \int_0^\tau M_j(\xi) \exp[\lambda(\tau - \xi)]\, d\xi \tag{19}$$

In terms of deviations $\epsilon_{d,j}{}^*(\tau)$ in parts in 10^4 from the ratios in the undifferentiated reference reservoir we obtain the final equations to be used in calculations for this model for arbitrary rates of growth of the crust and mantle:

$$\epsilon_{d,j}{}^*(\tau) = \frac{Q_d{}^*(\tau) f_j^{r/s}}{M_j(\tau)} \int_0^\tau M_j(\xi) \exp[\lambda(\tau - \xi)]\, d\xi \tag{20a}$$

and

$$\frac{\epsilon_{d,3}{}^*(\tau)}{\epsilon_{d,2}{}^*(\tau)} = \frac{f_3^{r/s}}{f_2^{r/s}} \tag{20b}$$

where

$$Q_d{}^*(\tau) = \left[10^4 \lambda \left(\frac{N_{r,1}(\tau)}{N_{s,1}(\tau)} \right) \right] \Big/ \left(\frac{N_{d,1}(\tau)}{N_{s,1}(\tau)} \right) \tag{20c}$$

The time parameter τ is the time running forward from the initial state (cf. equation (7)), and the time measured backward from the present will as usual be called T (see Figure 2). Here $\epsilon_{d,j}{}^*(\tau) = \epsilon_{d,j}{}^*(T_0 - T) \equiv \epsilon_{d,j}(T)$, where $T = T_0 - \tau$, T_0 is the age of the earth today, and $\epsilon_{d,j}(T)$ corresponds to ϵ_{Nd} and ϵ_{Sr} as defined by *DePaolo and Wasserburg* [1976*a*, 1977]. The asterisks denote the functional form of the deviations 'ϵ' relative to a time variable with an origin at the time of formation of the earth. Similarly, we define $Q_d{}^*(\tau) = Q_d{}^*(T_0 - T) \equiv Q_d(T)$ and note that $Q_d(0)$ is equal to the constants Q_{Nd} and Q_{Sr} used by *DePaolo and Wasserburg* [1976*a*, 1979*a*] for the Sm/Nd and Rb/Sr systems, respectively. If $\lambda\tau \ll 1$, then we have a good approximation that $Q_d{}^*(\tau) = Q_d(0)$. We note that the

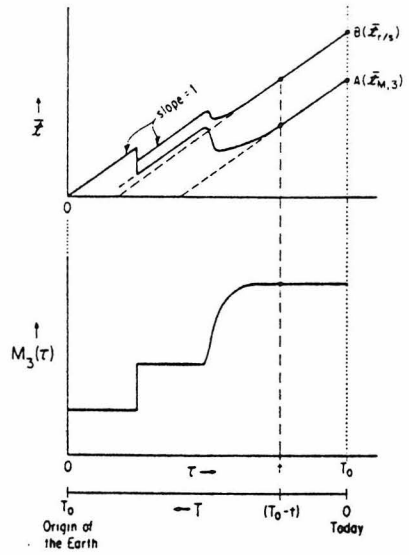

Fig. 2. Cartoon showing the relationship between a mean age $\bar{t}$ and the corresponding mass growth curve $M_3(\tau)$ for the crust. Two time variables are shown, where τ is the time measured from the origin of the earth and T is the time measured backward from today. The vertical dashed line is shown for a time $\tau = t$ years after the origin of the earth, which corresponds to a time $T_0 - t$ years ago. Curve A shows the mean age of the mass of the crust $\bar{t}_{M,3}$ versus time τ. The breaks in curve A correspond to the breaks in $M_3(\tau)$. Rapid addition of new material implies a rapid decrease in $\bar{t}_{M,3}$ of the continental crust. For periods where no significant new mass is added, $(d\bar{t}/d\tau) = 1$. This is valid for any model. For models such as model I, where the concentration of stable isotopes does not vary with time, $\bar{t}_{M,3}$ is also the mean age of any stable isotope $\bar{t}_{s,3}$ in the crust. For parent-daughter systems with $\lambda\tau \ll 1$, $\bar{t}_{M,3}$ is also the mean age of the parent and daughter isotopes in the crust (i.e., $\bar{t}_{M,3} = \bar{t}_{d,3} = \bar{t}_{r,3}$). Curve B shows the case where a stable isotope is strongly enriched in the crust earlier in time and the concentration in the bulk crust decreases monotonically with time. This weights the older material more strongly and raises the value of $\bar{t}_{s,3}$ above $\bar{t}_{M,3}$ (curve A). The curve $\bar{t}_{s,3}$ for model II has a more subdued behavior compared with model I for more recent additions. Similarly, if a long-lived parent is much more strongly enriched than the daughter in the crust, then the factor $\bar{t}_{r/s}$ shows a behavior like that of curve B. Subsequent to $\tau = t$ no mass is added, so $(d\bar{t}/d\tau) = 1$ for both curves for the time interval $\tau = t$ to $\tau = T_0$. The difference between the two curves is given by (66).

values of $\epsilon_{d,j}^*$ are the average values in each reservoir. Insofar as each new added segment was isolated, the added segment would follow its own evolutionary path governed by its initial state. This model has the property that new crustal and new mantle material would at the time of addition have the isotopic values of the undifferentiated reservoir 1. Magmas derived from subsequent melting of the crust or the depleted mantle would have distinctive characteristics at a given time. For a constant rate of crustal growth, (20*a*) takes the following form:

$$\epsilon_{d,j}^*(\tau) = \frac{Q_d^*(\tau) f_j^{r/s}}{\lambda}\left[\frac{e^{\lambda\tau} - 1}{\lambda\tau} - 1\right] \tag{21a}$$

and if $\lambda\tau \ll 1$, this equation reduces to

$$\epsilon_{d,j}^*(\tau) = Q_d^* f_j^{r/s}(\tau/2) \tag{21b}$$

The average time of residence $(\bar{t})$ of a stable atom s, which is not produced by radioactive decay, in reservoir j ($j = 2$ or 3) at a time τ is, using (11) and (12),

$$\bar{t}_{s,j} \equiv \langle(\tau - \xi)\delta N_{s,j}(\xi)/N_{s,j}(\tau)\rangle = \frac{1}{N_{s,j}(\tau)}\int_0^\tau (\tau - \xi)\left(\frac{\delta N_{s,j}}{\delta\xi}\right) d\xi$$

$$= \frac{1}{M_j(\tau)}\int_0^\tau (\tau - \xi) M_j'(\xi)\, d\xi = \frac{1}{M_j(\tau)}\int_0^\tau M_j(\xi)\, d\xi \tag{22}$$

We have here assumed that there was initially no crust or depleted mantle, so that $N_{s,j}(0) = M_j(0) = 0$. Expression (22) is equivalent to the average age as measured today of continental crustal material if $\tau = T_0$, the age of the earth, otherwise it is the average age as measured $T = T_0 - \tau$ years ago. Note that for this model, $\bar{t}_{s,j}$ is the same as the average age of the crust or depleted mantle and is independent of the species or of the reservoir. We may therefore drop the subscripts on $\bar{t}$ for this model.

Defining

$$\langle t^n\rangle \equiv \frac{1}{M_j(\tau)}\int_0^\tau (\tau - \xi)^n\left(\frac{dM_j}{d\xi}\right) d\xi$$

$$= \frac{n}{M_j(\tau)}\int_0^\tau (\tau - \xi)^{n-1} M_j(\xi)\, d\xi \tag{23}$$

where n is an integer, then the integral in (20) can be written in the following form:

$$I_j(\tau) \equiv \frac{1}{M_j(\tau)}\int_0^\tau M_j(\xi)\exp[\lambda(\tau - \xi)]\, d\xi$$

$$= \frac{1}{M_j(\tau)}\int_0^\tau \sum_{n=0}^{\infty}\frac{\lambda^n}{n!}(\tau - \xi)^n M_j(\xi)\, d\xi = \sum_{n=1}^{\infty}\frac{\lambda^{n-1}}{n!}\langle t^n\rangle \tag{24}$$

Then we have from (20)

$$\epsilon_{d,j}^*(\tau) = Q_d^*(\tau) f_j^{r/s}\sum_{n=1}^{\infty}\frac{\lambda^{n-1}}{n!}\langle t^n\rangle$$

$$= Q_d^*(\tau) f_j^{r/s}\langle t^1\rangle\left[1 + \frac{\lambda\langle t^2\rangle}{2\langle t^1\rangle} + \frac{\lambda^2\langle t^3\rangle}{6\langle t^1\rangle} + \cdots\right] \tag{25}$$

We note that for long-lived isotopes with $\lambda\tau \ll 1$ we get, to a good approximation,

$$\epsilon_{d,j}^*(\tau) = Q_d^*(\tau) f_j^{r/s}\bar{t} \tag{26}$$

or

$$\epsilon_{d,j}(T) = Q_d(T) f_j^{r/s}\bar{t}$$

as $\bar{t} = \langle t^1\rangle$.

If we can measure $\epsilon_{d,j}^*(\tau)$ and $f_j^{r/s}$ for a very long lived isotope at $T = T_0 - \tau$ years ago, then the only information we can obtain is the mean age of reservoir j as measured $T = T_0 - \tau$ years ago. The resulting mean age is independent of which very long lived species is used. This is independent of the rate of growth of the mass of reservoir j or the rate of transport of species i. This general treatment gives an integral which resembles a Laplace transform of $M_j(\tau)$ with a transform variable λ. This would permit a unique inversion for $M_j(\tau)$ if the transform was known for all values of λ. Insofar as

TABLE 1. Values of $I_j(\tau)$ at $\tau = 4.55$ Aeons for Various Parent-Daughter Systems for a Constant Rate of Crustal Growth With a Mean Age of $\bar{i} = 2.275$ Aeons

Radioactive Parent	Decay Constant, aeons^{-1}	$I_j(\tau)$, aeons
...	0	2.275
^{147}Sm	0.00654	2.30
^{87}Rb	0.0142	2.32
^{187}Re	0.0161	2.33
^{176}Lu	0.0198	2.34
^{232}Th	0.049475	2.45
^{238}U	0.155125	2.92
^{40}K	0.5543	6.39
^{235}U	0.98485	18.77
^{244}Pu	8.48	1.44×10^{15}

there is only a limited number of decay schemes a unique inversion is not possible, although a substantial amount of information may be deduced. We have calculated $I_j(\tau)$ for a constant rate of crustal growth for various parent-daughter systems (Table 1) for $\tau = 4.55$ aeons and thus a mean age of the mass of j of 2.275 aeons. The isotopes ^{147}Sm, ^{87}Rb, ^{187}Re, ^{176}Lu, and ^{232}Th all have mean lives that are sufficiently long so that $I_j(\tau) \simeq \bar{i}$ as shown in Table 1. The concordant results obtained by *Jacobsen and Wasserburg* [1979] for Rb-Sr and Sm-Nd single-stage ages for the oceanic mantle clearly do not represent a unique time event but an average age and the concordance for model I is a consequence of the long mean lives of both ^{147}Sm and ^{87}Rb. Inspection of Table 1 shows that ^{238}U has a significant deviation from the case with $\lambda = 0$, and ^{40}K and ^{235}U are greatly different from this case. These species have sufficiently short mean lives that the higher-order terms become important, and the equations are no longer redundant. From this result it is clear that the detailed history of the early earth must be derived from the latter two decay schemes. These different decay schemes when taken together yield information on the detailed time evolution by measurement at a single point in time.

The mean age $\bar{i}$ shows the relationship

$$\frac{d\bar{i}}{d\tau} = 1 - \frac{\bar{i}}{M}\left(\frac{dM}{d\tau}\right) = 1 - \bar{i}\left(\frac{d \ln M}{d\tau}\right) \tag{27}$$

so that for $(dM/d\tau) > 0$, $(d\bar{i}/d\tau) < 1$. When $(dM/d\tau) = 0$, it follows that $(d\bar{i}/d\tau) = 1$. We also note that $(d \ln \bar{i}/d\tau) \geq -(d \ln M/d\tau)$ and that $(d\bar{i}/d\tau) \leq 0$ if $(d \ln M/d\tau) \geq (1/\bar{i})$. This is shown schematically in Figure 2. It follows from (27) that a similar relationship must hold for the ϵ value for all systems involving very long lived isotopes. If we know $\bar{i}$ as a function of time and the mass of the crust today, then we may calculate the mass of the continents as a function of time from the following equation:

$$M_3(\tau) = M_3(T_0)\,\frac{\bar{i}(T_0)}{\bar{i}(\tau)} \exp\left[-\int_\tau^{T_0} \frac{d\xi}{\bar{i}(\xi)}\right] \tag{28}$$

where T_0 is the age of the earth as measured today.

Geometrical Constraints for Model I

The mechanism for crustal growth in this model is by deriving melts from undepleted mantle. The mass transfer from a deep-seated undepleted reservoir may occur through rising blobs. At shallow levels in the mantle the blobs may intersect the solidus and be partially melted. However, only a fraction β of the blobs may rise underneath the continental crust and contribute to crustal growth. The remaining fraction of the blobs $(1 - \beta)$ rise underneath the oceanic crust and may contribute to oceanic volcanism. However, these may be mixed back into the mantle with a short time scale (<0.2 eon) owing to the rapid turnover in the oceanic mantle implied by sea floor spreading and not become attached to the continents. This would correspond to adding undifferentiated mantle to the depleted mantle. The possiblity that undifferentiated mantle in this way gets mixed with depleted mantle may easily be incorporated in the equations for model I. We assume that a differential mass δM_1 is derived from reservoir 1 and adds a differential mass δM_0^* to blobs underneath the oceans and δM_C^* to blobs rising underneath the continental crust. Then we have that $\delta M_C^*/\delta M_1 = \beta$ and $\delta M_0^*/\delta M_1 = 1 - \beta$, where β is the probability that a mass taken from reservoir 1 is directed toward a continental segment. The blobs underneath the continental crust are partially melted to a degree F and thus the differential mass added to the crust is $\delta M_3 = F\delta M_C^*$, and the corresponding residue R of $\delta M_R^* = (1 - F)\delta M_C^*$ is left in the mantle and remixed. The blobs δM_0^* which rise in the oceanic regions will also differentiate but are not isolated and are taken to be remixed consistent with the general scheme of model I. The contributions of δM_0^* to reservoir 2 are thus not depleted. In this process a mass $\delta M_2 = \delta M_0^* + \delta M_R^*$ is added to reservoir 2. Conservation of mass and species implies that the concentration of i in the crust $c_{i,3}$ is given by $C_{i,1} = c_{i,3}[F + D_i(1 - F)]$ as before (equation (3)). However, the relationship between the rates of growth of the crust and depleted mantle and the composition of the depleted mantle will be changed. The relationship between the masses of reservoirs 2 and 3 is given by

$$M_3(\tau) = M_2(\tau)\left[\frac{\beta F}{1 - \beta F}\right] \tag{29}$$

In this case we have from mass and species conservation that $C_{i,1} = c_{i,3}\beta F + \bar{c}_{i,2}(1 - \beta F)$, where $\bar{c}_{i,2}$ is the effective concentration in the total material added to layer 2 in masses δM_0^* and δM_R^*. The concentration of species i in reservoir 2 is given by

$$\frac{\bar{c}_{i,2}}{C_{i,1}} = \frac{F(1 - \beta) + D_i(1 - F)}{(1 - F\beta)[F + D_i(1 - F)]} \tag{30}$$

where $(\bar{c}_{i,2}/C_{i,1}) > D_i/[F + D_i(1 - F)]$. This version of model I changes (3), (4), and (6) for reservoir 2 and gives $(\delta N_{i,2}/\delta\tau) = \bar{c}_{i,2}(\delta M_2/\delta\tau)$ in (5). All the equations for the continental crust will be the same as those derived previously. For reservoir 2 the transport equation corresponding to (6) is

$$\frac{dN_{i,2}}{d\tau} = \frac{F(1 - \beta) + D_i(1 - F)}{(1 - F\beta)[F + D_i(1 - F)]}\, C_{i,1}(\tau) M_2'(\tau) - \lambda_i N_{i,2}(\tau) \tag{31}$$

The solution of (31) for a stable isotope is

$$N_{i,2}(\tau) = \frac{F(1 - \beta) + D_i(1 - F)}{(1 - \beta F)[\mu + D_i(1 - F)]}\, C_{i,1}(0) M_2(\tau) \tag{32}$$

and corresponding changes for radioactive and daughter isotopes have to be made in (13) and (15) given previously. The

enrichment factor as defined in (17) is then given for reservoir 2 by

$$f_2'^{/s} = \left[\frac{F(1-\beta)+D_r(1-F)}{F(1-\beta)+D_s(1-F)}\right]\left[\frac{F+D_s(1-F)}{F+D_r(1-F)}\right]-1 \quad (33)$$

and this value should be used in (19) and (20). From the mass and species conservation equations given previously for this case written for radioactive and stable species it may be shown that

$$D_s = \left\{\frac{(\beta-1)f_2'^{/s}+\beta\,[1-(C_{r,3}/C_{r,1})F]}{(C_{r,3}/C_{r,1})F\beta+f_2'^{/s}}\right\}\frac{F}{1-F} > 0 \quad (34)$$

Since $0 < F(C_{r,3}/C_{r,1}) < 1$, it follows from (34) that for $f_2'^{/s} < 0$ and $0 < D_r < D_s < 1$ that

$$\beta > (C_{r,3}/C_{r,1})F\beta > -f_2'^{/s} \quad (35)$$

and for $f_2'^{/s} > 0$ and $0 < D_s < D_r < 1$ we have that

$$\beta > \frac{f_2'^{/s}}{f_2'^{/s}+1} \quad (36)$$

Thus given a value for $f_2'^{/s}$, this may put serious constraints on the value of β. If, for example, the continents always occupied 1/3 of the surface area and if the continents only grew from rising material by this geometrical consideration, then β would be 1/3. Were it possible to show that β is very different from this, then this would indicate that the geometrical considerations were not controlling the rate of continental growth and some sweeping or disaggregation process was required. We note that the case with $\beta < 1$ has many similarities with models involving refluxing of material from the crust to the depleted mantle. If a fraction $1-\beta$ of new additions to the crust is always immediately subducted back to the depleted mantle, then the exact solution of this problem is also given by (29)–(36) above. Similarly, these equations also describe the case where a fraction $1-\beta$ of the melt is always trapped in the residual solid. The conceptual pictures in Figure 1 and the descriptions of model I in the text do not fully describe the variety of physical circumstances which are represented by the equations derived for model I.

Model II

We now consider a model where the continental crust 3 grows from an initially undifferentiated mantle reservoir 2 which is depleted at all times subsequent to $\tau = 0$ as a result of crustal growth. This reservoir 2 may make up all or part of the mantle. We define a reference reservoir 1 which corresponds to the total of reservoirs 2 and 3. Initially, the whole mantle is supposed to be homogeneous and undifferentiated. A remaining portion of the mantle which is not involved in crust formation may remain isolated and undifferentiated. This reservoir will follow the isotopic evolution of the reference reservoir 1 but otherwise has nothing to do with the model. The model is shown in Figure 1. Let us assume that a differential mass is removed from reservoir 2 as a partial melt to form new crust and increases the mass of the crust by δM_3 and decreases the mass of reservoir 2 by $\delta M_2 = -\delta M_3$. The concentration of an element i in the partial melt at time τ is $c_{i,3}(\tau)$.

There are two different cases of this model that merit discussion. For case A, assume that the differential melt δM_3 equilibrates with all of reservoir 2. Then the mass of the residue is all of reservoir 2, and the degree of melting $F = \delta M_3/M_2$ must be a differential. This means that for an element i with bulk distribution coefficient $D_i = 0$ all of the element would be transported into the crust as soon as any differential melt formed from reservoir 2. This does not seem physically realistic. For case B, assume that a differential mass δM^* of reservoir 2 is differentiated into a melt δM_3 and a residue δM_R^* with the degree of melting F being finite. Case B seems physically more realistic than case A. For case B we have that $\delta M_3/\delta M^* = F$ and $\delta M_R^*/\delta M^* = 1-F$. The residue after removal of a melt fraction from reservoir 2 is assumed to be homogenized instantaneously with the remaining part of the depleted mantle. Conservation of species and mass gives $C_{i,2}(\tau)\delta M^* = c_{i,3}(\tau)\delta M_3 + c_{i,R}(\tau)\delta M_R^*$, and since $c_{i,R}(\tau)/c_{i,3}(\tau) = D_i$, it follows that $c_{i,3}(\tau) = d_i C_{i,2}(\tau)$, where

$$d_i = 1/[F + D_i(1-F)] \quad (37)$$

This case thus corresponds to the melting law in model I. The difference is that in model II the residue always has to be homogenized with the remaining part of the mantle reservoir it is derived from, and this reservoir is continuously depleted. Case B will be used in the following discussion.

The number of species i in the differential melt (δM_3) that is added to the crust is given by

$$\delta N_{i,3}(\tau) = c_{i,3}(\tau)\delta M_3 = d_i\frac{\delta M_3}{M_2(\tau)}N_{i,2}(\tau) \quad (38)$$

If $\delta\tau$ is the time over which the mass δM_3 is added to the continental crust, then the transport equations for reservoirs $j = 2, 3$ are

$$\frac{dN_{i,j}(\tau)}{d\tau} = (-1)^{j+1}\left(\frac{\delta N_{i,3}}{\delta\tau}\right)-\lambda_i N_{r,j}(\tau) \quad (39)$$

$$\lambda_i = 0 \quad i = s$$
$$\lambda_i = \lambda_r \quad i = r$$
$$\lambda_i = -\lambda_r \quad i = d$$

For simplicity we again ignore mass transport from 3 to 2. Using the expression for $\delta N_{i,3}$ and calling $\delta M_3/\delta\tau \equiv M_3'(\tau)$, we obtain the following basic transport equations for model II:

$$\frac{dN_{i,j}(\tau)}{d\tau} = (-1)^{j+1}d_i\frac{M_3'(\tau)}{M_2(\tau)}N_{i,2}(\tau)-\lambda_i N_{r,j}(\tau) \quad (40)$$

The masses of the total reservoirs 2 and 3 must satisfy

$$M_2(\tau)+M_3(\tau) = M_2(0) \qquad M_2'(\tau) = -M_3'(\tau) \quad (41)$$

The integrals of the transport equations for a stable species s in reservoirs 2 and 3 are

$$N_{s,2}(\tau) = N_{s,2}(0)\left[\frac{M_2(\tau)}{M_2(0)}\right]^{d_s} \quad (42)$$

$$N_{s,3}(\tau) = N_{s,2}(0)-N_{s,2}(\tau) \quad (43)$$

Equation (42) for a stable isotope in reservoir 2 may be written in the following form:

$$C_{s,2}(\tau) = C_{s,2}(0)\left[1-\frac{M_3(\tau)}{M_2(0)}\right]^{(d_s-1)}$$

This expression has the same general form as the equation of *Shaw* [1970] for the solid residue after modal fractional (Rayleigh) melting, however, d_s takes the place of the inverse bulk distribution coefficient and the degree of crust formation $M_3(\tau)/M_2(0)$ takes the place of the degree of melting.

The solutions of (40) for radioactive and daughter isotopes are

$$N_{r,2}(\tau) = N_{r,2}(0)e^{-\lambda\tau}\left[\frac{M_2(\tau)}{M_2(0)}\right]^{d_r} \tag{44}$$

$$N_{r,3}(\tau) = N_{r,2}(0)e^{-\lambda\tau} - N_{r,2}(\tau) \tag{45}$$

$$N_{d,2}(\tau) = \left\{N_{d,2}(0) + N_{r,2}(0)\lambda \int_0^\tau \left[\frac{M_2(\xi)}{M_2(0)}\right]^{(d_r-d_s)} \cdot \exp\left[-\lambda\xi\right] d\xi\right\}\left[\frac{M_2(\tau)}{M_2(0)}\right]^{d_s} \tag{46}$$

$$N_{d,3}(\tau) = N_{d,2}(0) + N_{r,2}(0)[1 - e^{-\lambda\tau}] - N_{d,2}(\tau) \tag{47}$$

where $d_r = d_p$ since d and s are isotopes of the same element. The ratios of a radiogenic isotope to a stable isotope for the two reservoirs are

$$\frac{N_{d,2}(\tau)}{N_{s,2}(\tau)} = \frac{N_{d,1}(\tau)}{N_{s,1}(\tau)} - \lambda\,\frac{N_{r,1}(\tau)}{N_{s,1}(\tau)} \int_0^\tau \left\{1 - \left[\frac{M_2(\xi)}{M_2(0)}\right]^{(d_r-d_s)}\right\} \cdot \exp\left[\lambda(\tau - \xi)\right] d\xi \tag{48}$$

$$\frac{N_{d,3}(\tau)}{N_{s,3}(\tau)} = \frac{N_{d,1}(\tau)}{N_{s,1}(\tau)} - \lambda\,\frac{N_{r,1}(\tau)}{N_{s,1}(\tau)} \left\{\int_0^\tau \left[1 - \left(\frac{M_2(\xi)}{M_2(0)}\right)^{(d_r-d_s)}\right] \exp\left[\lambda(\tau - \xi)\right] d\xi\right\}\left[1 - \left(\frac{M_2(\xi)}{M_2(0)}\right)^{(-d_s)}\right]^{-1} \tag{49}$$

From (17) and (42)–(45) the enrichment factors of the ratio of a radioactive isotope to a stable isotope in the total reservoirs 2 and 3 to that in reservoir 1 are given by

$$f_2^{r/s}(\tau) = \left[\frac{M_2(\tau)}{M_2(0)}\right]^{(d_r-d_s)} - 1 \approx \exp\left[-(d_r - d_s)\frac{M_3(\tau)}{M_2(0)}\right] - 1 \tag{50}$$

$$\frac{f_2^{r/s}(\tau)}{f_3^{r/s}(\tau)} = 1 - \left[\frac{M_2(\tau)}{M_2(0)}\right]^{(-d_s)} \approx 1 - \exp\left[d_s\frac{M_3(\tau)}{M_2(0)}\right] \tag{51}$$

where the approximations hold for the mass of the crust much smaller than that of the depleted mantle $[(M_3(\tau)/M_2(0)) \ll 1]$. Equations (48) and (49) may be written in terms of deviations in parts in 10^4 from the reference reservoir 1:

$$\epsilon_{d,2}^*(\tau) = Q_d^*(\tau) \int_0^\tau f_2^{r/s}(\xi) \exp\left[\lambda(\tau - \xi)\right] d\xi \tag{52}$$

$$\epsilon_{d,3}^*(\tau) = \epsilon_{d,2}^*(\tau)\,\frac{f_3^{r/s}(\tau)}{f_2^{r/s}(\tau)} \tag{53}$$

where $Q_d^*(\tau)$ is defined by (20). Equations (50)–(53) in conjunction with (37) are the basic equations for calculations with this model for arbitrary rates of crustal growth. In this class of models the average enrichment factors are a function of the time and correspond to a time dependent chemical evolution. For $\lambda\tau \ll 1$ the deviation $\epsilon_{d,i}^*$ are then proportional to the weighted time average of the enrichment factors $\langle f_j^{r/s}\rangle$ and given by

$$\epsilon_{d,2}^*(\tau) = Q_d^*(\tau)\langle f_2^{r/s}(\tau)\rangle\tau \tag{54}$$

$$\epsilon_{d,3}^*(\tau) = Q_d^*(\tau)\,\frac{f_3^{r/s}(\tau)}{f_2^{r/s}(\tau)}\langle f_2^{r/s}(\tau)\rangle\tau \tag{55}$$

This means that the simple species independent time averages which govern the ϵ function for models of type I no longer apply, and an average age is not directly applicable to reservoir 2.

In this model the depleted mantle is assumed to always be homogeneous. For the crust the equations give the average values. If each new addition to the crust is isolated, then the new individual segments follow their own evolutionary path. The initial states of new additions to 3 at time τ' are given by

$$f_{\text{new}}{}^{r/s}(\tau') = \frac{d_r}{d_s}\left[f_2^{r/s}(\tau') + 1\right] - 1 \tag{56}$$

$$\epsilon_{d,\text{new}}{}^*(\tau') = \epsilon_{d,2}{}^*(\tau') \tag{57}$$

and subsequent evolution will follow:

$$\epsilon_{d,\text{new}}{}^*(\tau) = \epsilon_{d,3}{}^*(\tau') + \frac{Q_d^*(\tau)}{\lambda} f_{\text{new}}{}^{r/s}(\tau')\,\{\exp\left[\lambda(\tau - \tau')\right] - 1\} \tag{58}$$

This model has the property that new crust would at the time of addition have the isotopic values of depleted mantle 2, and the interpretation of $T_{\text{CHUR}}{}^{\text{Nd}}$ model ages [*McCulloch and Wasserburg*, 1978] of new crust would depend on the detailed history of reservoir 2.

For this model we may again define the mean age of species s in the crust 3 by

$$\bar{t}_{s,3} = \frac{1}{N_{s,3}(\tau)}\int_0^\tau (\tau - \xi)\,\frac{dN_{s,3}}{d\xi}\,d\xi = \frac{1}{N_{s,3}(\tau)}\int_0^\tau N_{s,3}(\xi)\,d\xi \tag{59}$$

and the mean age of the mass M_3 by

$$\bar{t}_{M,3} = \frac{1}{M_3(\tau)}\int_0^\tau (\tau - \xi)M_3'(\xi)\,d\xi = \frac{1}{M_3(\tau)}\int_0^\tau M_3(\xi)\,d\xi \tag{60}$$

The mean age of the depleted mantle reservoir 2 may not be defined in the same manner. Note that for model II, $N_{s,3}(\tau)/M_3(\tau)$ is not a constant independent of τ, so that $\bar{t}_{s,3} \neq \bar{t}_{M,3}$. The result of this is distinct from model I and is shown schematically in Figure 2. Using (43) and (59), we may write

$$\bar{t}_{s,3} = \left\{1\Big/\left[1 - \left(1 - \frac{M_3(\tau)}{M_2(0)}\right)^{d_r}\right]\right\}\int_0^\tau \left\{1 - \left[1 - \frac{M_3(\xi)}{M_2(0)}\right]^{d_s}\right\} d\xi$$

$$\approx \left\{1\Big/\left[1 - \exp\left(-\frac{d_r M_3(\tau)}{M_2(0)}\right)\right]\right\}\int_0^\tau \left\{1 - \exp\left[-d_s\frac{M_3(\xi)}{M_2(0)}\right]\right\} d\xi \tag{61}$$

assuming that $(M_3(\tau)/M_2(0)) \ll 1$ in the second expression. In the case that $[d_r M_3(\tau)/M_2(0)] \ll 1$, then $\bar{t}_{s,3} \approx \bar{t}_{M,3}$. If $[d_r M_3(\tau)/M_2(0)] \gg 1$ for $\tau \geq \tau^*$, then $\bar{t}_{s,3} \approx \text{const} + (\tau - \tau^*)$ for $\tau \geq \tau^*$, and $(d\bar{t}_{s,3}/d\tau) = 1$. This corresponds to the bulk of the species s being transported into the crust by time τ^* after the formation of the earth. The mass transfer is then subsequently decoupled from addition of the trace element s, and the average age of the mass $\bar{t}_{M,3}$ may be substantially younger than $\bar{t}_{s,3}$ as the different trace element abundances of the crust change with time. The difference between $\bar{t}_{s,3}$ and $\bar{t}_{M,3}$ is of interest and may be evaluated quantitatively. We have

$$\bar{t}_{s,3} - \bar{t}_{M,3} = \left\{\int_0^\tau \left[M_3(\tau) - M_3(\xi) + M_3(\xi)\exp\left(-d_r\frac{M_3(\tau)}{M_2(0)}\right) - M_3(\tau)\exp\left(-d_s\frac{M_3(\xi)}{M_2(0)}\right)\right] d\xi\right\}\left\{\left[1 - \exp\left(-d_s\frac{M_3(\tau)}{M_2(0)}\right)\right] M_3(\tau)\right\}^{-1}$$

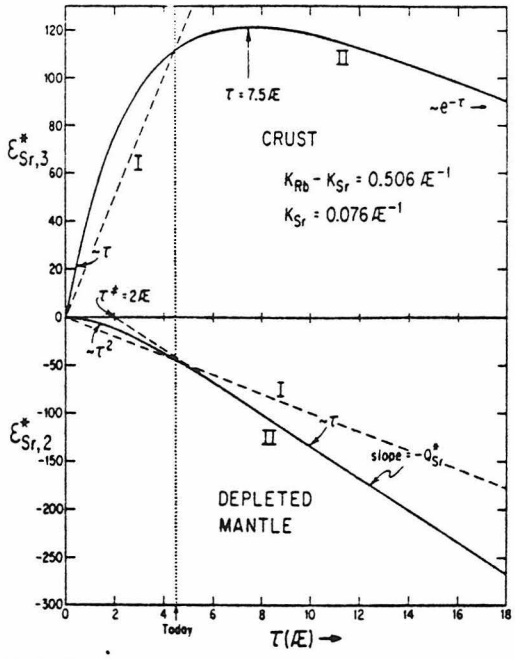

Fig. 3. Shown are $\epsilon_{Sr,j}{}^*$ curves for the bulk depleted mantle (2) and the bulk crust (3) as a function of time τ for a constant rate of growth of the crust. Curves that give the same present day $\epsilon_{Sr}{}^*$ values are shown for both model I and model II and are identified by the symbols I and II, respectively. Note the marked difference in behavior for $\epsilon_{Sr}{}^*$ as a function of time τ for the two models. Model I is a straight line for both reservoirs, and model II starts out as nearly a straight line for the crust but with a significantly different slope. The curves for model II are constrained to give $f_2^{Rb/Sr} = -0.9$ and $f_3^{Rb/Sr} = +2.18$ today. The implied values of $K_{Rb} - K_{Sr}$ and K_{Sr} are given. The systematics shown is valid for decay systems with $\lambda\tau \ll 1$ and $(d_r - d_s) > 0$.

$$= \left\{\left(\frac{d_r}{M_2(0)}\right)^2 \int_0^\tau M_3(\xi)\left[\sum_{n=2}^{\infty} \frac{(-1)^n}{n!}\left(M_3(\tau)\left(\frac{d_r M_3(\tau)}{M_2(0)}\right)^{n-2}\right.\right.$$

$$\left.\left. - M_3(\xi)\left(\frac{d_r M_3(\xi)}{M_2(0)}\right)^{n-2}\right]\right] d\xi\Bigg\} \left\{\left[1 - \exp\left(-d_r \frac{M_3(\tau)}{M_2(0)}\right)\right]\right\}^{-1} \quad (62a)$$

If $d_r < 0$, it may be seen that $\tilde{t}_{r,3} - \tilde{t}_{M,3} < 0$. This expression converges rather well even for large values of $d_r[M_3(\tau)/M_2(0)]$ ($\lesssim 2$). In the limit for small $d_r/M_2(0)$ we have rather precisely

$$\frac{\tilde{t}_{r,3} - \tilde{t}_{M,3}}{(d_r/M_2(0))} \approx \frac{1}{2M_3(\tau)} \int_0^\tau M_3(\xi)[M_3(\tau) - M_3(\xi)]\, d\xi \quad (62b)$$

so in this approximation, $\tilde{t}_{r,3} - \tilde{t}_{M,3} > 0$ for $d_r > 0$. For a model of a constant rate of crustal growth we obtain

$$\tilde{t}_{r,3} - \tilde{t}_{M,3} \approx \frac{d_r M_3(\tau)}{12M_2(0)}\tau \quad (62c)$$

which gives a difference of 0.65 eon for $d_r = 100$ with $M_3(\tau)/M_2(0) = 0.0174$. It follows that for $d_r \leq 10$ there are only small differences in the mean ages.

We note that the expressions for ϵ^* ((52) and (53)) may be written in a form analogous to that for model I. Inspection of (61) and (52) shows that $\epsilon_{d,2}{}^*$ may be written as

$$\epsilon_{d,2}{}^*(\tau) = Q_d{}^*(\tau) f_2^{r/s}(\tau)\tilde{t}_{r/s} \quad (63)$$

where

$$\tilde{t}_{r/s} \equiv \frac{1}{f_2^{r/s}(\tau)} \int_0^\tau f_2^{r/s}(\xi)\, d\xi = \frac{\tau\,\langle f_2^{r/s}(\tau)\rangle}{f_2^{r/s}(\tau)} \quad (64)$$

The factor $\tilde{t}_{r/s}$ is the time weighted average of $f_2^{r/s}$ for reservoir 2. If $d_r - d_s > 0$, this is equivalent to the mean age of an element r/s with a distribution coefficient $d_{r/s} = d_r - d_s$ and an enrichment factor $f_2^{r/s}$. Note that $\tilde{t}_{r/s}$ is explicitly dependent on the particular parent-daughter system as distinct from the case for model I. If the differentiation took place in only a single event, then $t_{r/s} = t_{M,3}$. More generally, there will be a difference between $\tilde{t}_{r/s}$ and $\tilde{t}_{M,3}$, which may be calculated from

$$\tilde{t}_{r/s} - \tilde{t}_{M,3} \approx \frac{d_r - d_s}{2M_3(\tau)M_2(0)} \int_0^\tau M_3(\xi)[M_3(\tau) - M_3(\xi)]\, d\xi \quad (65)$$

The derivation of expression (65) follows that given previously for $\tilde{t}_{s,3} - \tilde{t}_{M,3}$. For a model of constant rate of crustal growth we have

$$\tilde{t}_{r/s} - \tilde{t}_{M,3} = \frac{(d_r - d_s)M_3(\tau)}{12M_2(0)}\tau \quad (66)$$

If $|(d_r - d_s)M_3(\tau)/M_2(0)| \ll 1$, then (50) and (52) may for very long lived isotopes be approximated by

$$\epsilon_{d,2}{}^*(\tau) \approx -(d_r - d_s)\frac{Q_d{}^*(\tau)M_3(\tau)}{M_2(0)}\tilde{t}_{M,3} \quad (67)$$

and

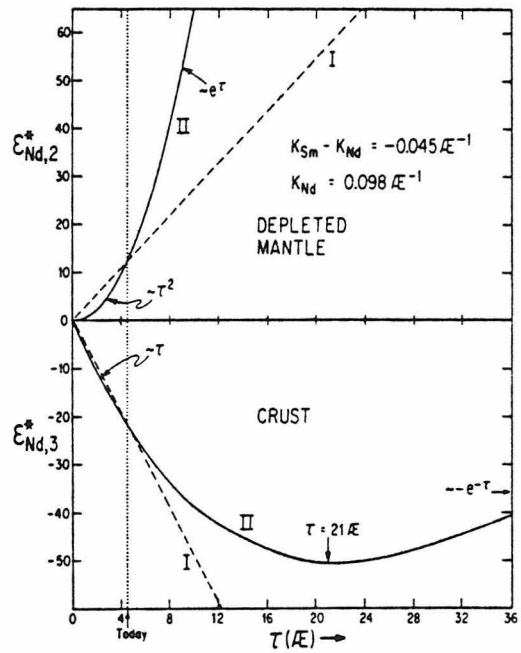

Fig. 4. Shown are $\epsilon_{Nd,j}{}^*$ curves for bulk depleted mantle (2) and bulk crust (3) as a function of time τ for a constant rate of growth of the crust. The notation is the same as in Figure 3. The curves for model II are constrained to give $f_2^{Sm/Nd} = +0.225$ and $f_3^{Sm/Nd} = -0.4$ today. The implied values of $K_{Sm} - K_{Nd}$ and K_{Nd} are shown. Note that the curves are reversed from those in Figure 3 owing to the change in sign of $K_r - K_s$. The systematics shown is valid for decay systems with $\lambda\tau \ll 1$ and $(d_r - d_s) < 0$.

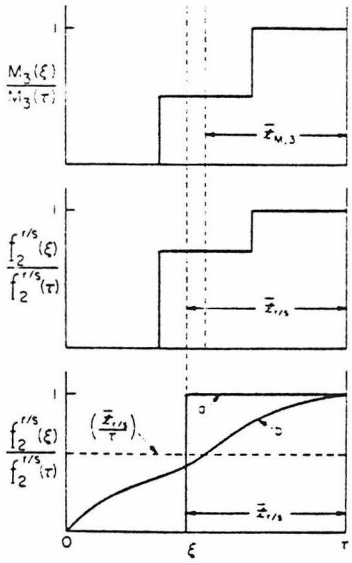

Fig. 5. Cartoon showing the relationship between the mean age of the mass of the crust $\bar{t}_{M,3}$, the mass growth curve of the crust M_3, the enrichment factor of the depleted mantle $f_2^{r/s}$, and the factor $\bar{t}_{r/s}$. The upper diagram shows a mass growth curve where the crust is formed in two stages with a mean age $\bar{t}_{M,3}$ at time τ. The middle diagram shows the corresponding change in $f_2^{r/s}$ with time if $(d_r - d_s) = 100$ and $[M_3(\tau)/M_2(0)] = 0.0174$. The difference between $\bar{t}_{r/s}$ and $\bar{t}_{M,3}$ is also indicated. If we know $\bar{t}_{r/s}$, $f_2^{r/s}$, and M_3 today, there is insufficient information to determine a unique solution for $M_3(\xi)$ and $f_2^{r/s}(\xi)$. In the lower part of the diagram some other possible $f_2^{r/s}$ curves that give the same value for $\bar{t}_{r/s}$ are shown. For a given curve, $f_2^{r/s}$ with knowledge of $(d_r - d_s)$ determines a corresponding M_3 curve from (50). The area underneath the $[f_2^{r/s}(\xi)/f_2^{r/s}(\tau)]$ curve must be the same for all M_3 curves with the same value for $\bar{t}_{r/s}$; $\bar{t}_{r/s}$ is the shortest time in which differentiation could have occurred as a single-stage process, and curve a shows such an evolution. Curve b shows a possible continuous curve. The dashed horizontal curve gives $[\langle f_2^{r/s}\rangle/f_2^{r/s}(\tau)] = [\bar{t}_{r/s}/\tau]$. All of these curves in the lower figure are compatible with the $\bar{t}_{r/s}$ fixed by the assumed model with $M_3(\xi)$ as given in the top and the $f_2^{r/s}(\tau)$ value.

$$f_2^{r/s}(\tau) \approx -(d_r - d_s)\frac{M_3(\tau)}{M_2(0)} \tag{68}$$

If it also holds that $[d_r M_3(\tau)/M_2(0)] \ll 1$, then

$$f_3^{r/s}(\tau) \approx (d_r/d_s) - 1 \tag{69}$$

and

$$\epsilon_{d,3}^*(\tau) \approx Q_d^*(\tau)[(d_r/d_s) - 1]\bar{t}_{M,3} \tag{70}$$

An important special case is when $(dM_3/d\tau)$ is a constant. In this case, $M_3(\tau) = [M_3(T_0)/T_0]\tau$, and defining $K_i = [(d_i M_3(T_0))/(T_0 M_2(0))]$ then for very long lived isotopes,

$$\epsilon_{d,2}^*(\tau) = -Q_d^*(\tau)\left\{\tau - \frac{1 - \exp[-(K_r - K_s)\tau]}{(K_r - K_s)}\right\} \tag{71}$$

$$f_2^{r/s}(\tau) = \exp[-(K_r - K_s)\tau] - 1 \tag{72}$$

$$\frac{f_2^{r/s}(\tau)}{f_3^{r/s}(\tau)} = 1 - \exp(K_s\tau) \tag{73}$$

$$\epsilon_{d,3}^*(\tau) = \frac{\epsilon_{d,2}^*(\tau)}{1 - \exp(K_s\tau)} \tag{74}$$

There are two different classes of solutions depending on whether $(d_r - d_s)$ is negative (as for Sm-Nd) or positive (as for Rb-Sr). Examples are shown for Rb-Sr and Sm-Nd in Figures 3 and 4, respectively. For short times we have in both cases that $\epsilon_{d,2}^* \propto \tau^2$ and $\epsilon_{d,3}^* \propto \tau$. For long times we get $\epsilon_{Sr,2}^* \approx -Q_{Sr}^*(\tau - \tau^\dagger)$, where $\tau^\dagger = 1/(K_{Rb} - K_{Sr}) = 2$ aeons and $\epsilon_{Nd,2}^* \propto \exp[-(K_{Sm} - K_{Nd})\tau]$ for the depleted mantle. The curves for the crust go to an extremum and then asymptotically approach zero. The inclusion of the term $\exp[\lambda(\tau - \xi)]$ for shorter-lived isotopes in the exact integral of (52) will, of course, quantitatively alter the nature of these results. The curve for $\epsilon_{Sr,3}^*$ has a maximum at $\tau = 7.5$ aeons, and for much longer times $\epsilon_{Sr,3}^* \propto \exp[-K_{Sr}\tau]$. Similarly, the $\epsilon_{Nd,3}^*$ curve for the crust has a minimum at $\tau = 21$ aeons, and $\epsilon_{Nd,3}^* \propto -\exp[-K_{Nd}\tau]$ for much longer times. These solutions enable us to qualitatively understand the nature of the results for more general cases of crustal growth with time. From these results we may infer that for any continuous or multiepisodic mass growth of the crust the basic isotopic systematics for long-lived isotopes must follow those outlined in Figures 3 and 4. We note that for the case of episodic mass growth, $\epsilon_{d,3}^*$ will be discontinuous owing to the factor $f_3^{r/s}/f_2^{r/s}$ outside of the integral in (53). The value of $\epsilon_{d,2}^*$ for the depleted mantle will still be continuous but will show changes in slope corresponding to the discontinuities in the mass growth curve. The general case for arbitrary mass transport is of course included in the exact basic equations (50)–(53).

Calculations with model II are more complex than with model I, where the average age $\bar{t}$ is independent of species. For the mantle we have previously obtained the exact results:

$$\epsilon_{d,2}^* = Q_d^*(\tau)\langle f_2^{r/s}\rangle\tau = Q_d^*(\tau) f_2^{r/s}(\tau)\bar{t}_{r/s} \tag{75}$$

It follows that if $\epsilon_{d,2}^*(\tau)$ is known at τ, then $\langle f_2^{r/s}\rangle$ is determined. If $\epsilon_{d,2}^*$ and $f_2^{r/s}$ are known, then $(d_r - d_s)$ is known from (50), and $\bar{t}_{r/s}$ is determined; $\bar{t}_{r/s}$ is the time required to generate $\epsilon_{d,2}^*$ with the present value of $f_2^{r/s}$. As $f_2^{r/s}$ is monotonic in this model, $\bar{t}_{r/s}$ is the shortest time in which differentiation could have occurred (as a single-stage process). All possible crustal mass growth laws $M_3(\tau)$ must satisfy the relationship between $f_2^{r/s}$ and M_3. The relationships are shown schematically in Figure 5. If decay schemes with very long lived parents have $|(d_r - d_s)M_3/M_2(0)| \ll 1$, then they will all yield the same values of $\bar{t}_{r/s}$ and no further information may be derived about the change of M_3 with time from the different systems at one time τ. If two systems have distinctive parameters (such as Rb-Sr and Sm-Nd), then they will have different values of $\bar{t}_{r/s}$ which will give more information about $M_3(\tau)$. For N independent values of $\bar{t}_{r/s}$ from N different decay schemes with $\lambda\tau \ll 1$, it is, in principle, possible to calculate models of multiple-stage mass evolution with time. For example, for an n stage evolution we write

$$\bar{t}_{r/s} = \sum_{i=1}^{n} \frac{\exp[-\alpha_{r/s}X_{i-1}] - 1}{\exp[-\alpha_{r/s}] - 1}(\tau_i - \tau_{i-1}) \tag{76}$$

where $\tau_0 = 0$, $\tau_n = \tau$, $X_{n-1} = 1$, and $X_0 = 0$. The solutions for X_i may in general not be a unique description of earth evolution. Here $X_i - X_{i-1}$ is the fraction of $M_3(\tau)$ made at time τ_i, and $\alpha_{r/s} = (d_r - d_s)M_3(\tau)/M_2(0)$. Such equations may be solved numerically for the X_i and τ_i which must provide simultaneous solutions for different $\bar{t}_{r/s}$ values. In the degenerate case when $\alpha_{r/s} \ll 1$,

$$\bar{t}_{r/s} = \sum_{i=1}^{n} X_{i-1}(\tau_i - \tau_{i-1}) \tag{77}$$

which is independent of r/s.

TABLE 2. Masses of Various Reservoirs in the Earth

Reservoir	Mass, 10^{25} grams	Fraction of Total Earth Mass
Continental crust	1.807	0.003023
Subcontinental crust	0.430	0.000719
Oceanic sediment (layer 1)*	0.019	0.000032
Total continental crust plus subcontinental crust plus oceanic sediment	2.256	0.003774
Oceanic crust (layers 2 and 3)†	0.590	0.000987
Mantle	400.5	0.6701
Mantle plus crust	403.4	0.6749
Core	194.3	0.3251
Total earth	597.7	1

Masses of core and mantle are from *Smith* [1971], and masses of the crustal reservoirs are from *Renov and Yaroshevsky* [1976].

*Considered to be mainly derived by werathering of continental crust.

†Basaltic part of the oceanic crust.

Boundary Conditions for the Models

The parameters involved for both models described above are the initial and final concentrations and isotopic compositions for each reservoir j, the solid/melt distribution coefficients, and the mass of reservoir j as a function of time. All these parameters need not be specified, and in the following we will choose the parameters we believe are the best known and use them to make estimates of others. We will limit the discussion to the Rb-Sr and Sm-Nd decay systems, but their relation to the concentrations of K, Ba, and U will also be discussed. The masses of the various reservoirs in the earth are given in Table 2. In both models the depleted mantle is taken to include the basaltic part of the oceanic crust, since it is derived from the depleted mantle and is subducted back to the depleted mantle at a short time scale (<0.2 aeon). The total mass of the continental crust (2.256×10^{25} grams) is taken as the total amount of continental materials including layer 1 of the oceanic crust, which is considered to be mainly sediments derived from weathering of continental crust. The bulk earth values (reservoir 1) used for Rb-Sr and Sm-Nd are given in the appendix. By definition, $\epsilon_{d,1} = f_1^{r/s} = 0$ for reservoir 1 (undepleted mantle). Estimates of ϵ and f values for the depleted mantle and the continental crust are given in Table 3, and partition coefficients for garnet peridotite minerals in Table 4. The values for the depleted mantle in Table 3 are the estimates for the MORB source given by *Jacobsen and Wasserburg* [1979], where the estimates for 0.5 aeon ago are based on data from the Bay of Islands complex.

The silicate portion of the earth is assumed to be initially chemically homogeneous, and the core is assumed to have insignificant amounts of the lithophile elements considered here. The concentrations of these elements in the silicate portion of the earth are thus 1.48 times their concentrations in the total earth. It is known that the earth is depleted in volatile elements relative to chondrites [*Gast*, 1960]. However, the ratios of refractory elements in the earth appear to be equal to those in chondrites from both isotopic studies [*DePaolo and Wasserburg*, 1976*a*] and chemical studies [*Sun and Nesbitt*, 1977]. This gives a minimum of 1.48 times chondritic abundances for these elements in the silicate portion of the earth. If a steady state relationship between heat production from radioactive sources and heat flow exist, then the U content of the crust plus mantle is 35 ppb [*Wasserburg et al.*, 1964; *Tera et al.*, 1974] or 46 ppb if the new global heat flow estimate of *Williams and Von Herzen* [1975] is used [*O'Nions and Pankhurst*, 1977]. Ordinary chondrites have 13 ppb U, so the heat flow data give an upper limit of 2.7 or 3.5 times chondrites for the concentration of U and other refractory elements for the silicate portion of the earth. It has been concluded elsewhere that the concentrations of Ca, Al, U, Th, Ba, Sr, and REE in the mantle are about 2.0 ± 0.5 those in ordinary chondrites [*Frey and Green*, 1974; *Loubet et al.*, 1975; *Sun and Nesbitt*, 1977]. We have thus used a value 2 times ordinary chondrites for the refractory elements in the crust plus mantle. Estimates for the Rb and K concentrations in the silicate portion of the earth can then be estimated from the bulk earth Rb/Sr ratio of 0.029 [*DePaolo and Wasserburg*, 1976*b*] and the bulk earth K/U ratio. Previous estimates of the K/U ratio of the earth [*Heier and Rogers*, 1963; *Wasserburg et al.*, 1964] were based mainly on upper crustal rocks and are very close to 10^4. This is most likely a lower limit, since lower crustal granulites have (K/U) > 10^4 [*Lambert and Heier*, 1968*b*] and since it seems plausible that U is more enriched in the crust than K. Our estimates of the concentrations of K, U, Ba, Rb, Sr, Sm, and Nd in the crust plus mantle are compared with other recent estimates in Table 5. Most estimates agree to within a factor of 2. The largest disagreement for element ratios is with the Sm/Nd ratio of *Smith* [1977] and the Sr/Nd ratio of *O'Nions et al.* [1978].

Extensive work has established that the upper crustal composition is close to that of granodiorite [*Poldervaart*, 1955; *Shaw et al.*, 1967; *Eade and Fahrig*, 1971]. The most recent estimates for the elements of interest here [*Shaw et al.*, 1976] are given in Table 6. It is well known from the heatflow data that the upper crustal concentrations of K, U, and Th cannot extend to a depth of more than 10–15 km, so that the lower crust must be depleted in these elements [*Heier*, 1965, 1973]. This had led to the hypothesis that the lower crust is made up of dry granulite facies rocks and related igneous rocks, since they show the necessary depletions in U and Th [*Heier*, 1965], and they also show Rb depletions and generally low Rb/Sr ratios [*Heier*, 1964]. Extensive geochemical studies of granulite facies rocks with particular emphasis on the distribution of heat-producing elements have been carried out in Australia and Norway [*Heier and Adams*, 1965; *Lambert and Heier*, 1967, 1968*a*, *b*; *Heier and Thoresen*, 1971]. The estimates of

TABLE 3. Ranges of Parameters Based on Directly Observed Average Values

	T, aeons	$f^{Rb/Sr}$	ϵ_{Sr}	$f^{Sm/Nd}$	ϵ_{Nd}
Depleted mantle	0	$-0.9\ ^{+0.1}_{-0.05}$	−27 ± 5	$+0.22\ ^{+0.08}_{-0.07}$	+10 ± 2
	0.5	−0.9	−19.3	−+0.2	+7.6
Continental crust	0	+1 to +10	+60 to +250	−0.4 ± 0.1	−10 to −25

Sources are *McCulloch and Wasserburg* [1978], *DePaolo and Wasserburg* [1979*a*], and *Jacobsen and Wasserburg* [1979].

TABLE 4. Mineral/Melt and Bulk Partition Coefficients

	K	Rb	Sr	Ba	Nd	Sm	U
Clinopyroxene	0.003	0.003	0.12	0.002	0.17	0.26	0.003
Garnet	0.006	0.01	0.08	0.003	0.087	0.217	0.003
Orthopyroxene	0.003	0.003	0.02	0.002	0.013	0.022	0.0001
Olivine	0.0002	0.0002	0.0002	0.0001	0.007	0.010	0.0001
Initial bulk distribution coefficient*							
$D_{0,K}$	0.002						
$D_{0,Rb}$		0.0025					
$D_{0,Sr}$			0.033				
$D_{0,Ba}$				0.0014			
$D_{0,Nd}$					0.044		
$D_{0,Sm}$						0.080	
$D_{0,U}$							0.001

Sources: *Griffin and Murthy* [1969], *Philpotts and Schnetzler* [1970], *Schnetzler and Philpotts* [1970], *Hart and Brooks* [1974], *Shimizu* [1974], *Grutzeck et al.* [1975], *Shimizu and Kushiro* [1975], *Weill and McKay* [1975], *McKay and Weill* [1976], *Benjamin et al.* [1978].

$D_U^{cpx/ol} \approx D_U^{cpx/opx} \approx 30$, *Tatsumoto* [1978].

$D_U^{cpx/ga} \approx 1$, *Morgan and Lovering* [1971].

*Calculated for a garnet peridotite mineralogy with the following initial mass fractions of the various phases: olivine = 0.55, orthopyroxene = 0.15, clinopyroxene = 0.15, garnet = 0.15.

the concentrations in the lower crust from *Heier and Thoresen* [1971] are given in Table 6. *Lambert and Heier* [1968*b*] used estimates of the heat-producing elements in upper and lower crustal materials together with constraints from heatflow to calculate concentration profiles of K, U, and Th through the continental crust. They estimated total crust concentrations of K = 1.5 wt % and U = 0.7 ppm for Precambrian shields. Similar reasoning gives K/Rb ≈ 450 for the total crust on the basis of upper and lower crustal K and Rb concentrations. To arrive at the estimates we give for the total crust in Table 6, we have used the estimates of *Lambert and Heier* [1968*b*] for K and U together with K/Rb ≈ 450 and K/Ba ≈ 30 [*Philpotts and Schnetzler*, 1970]. Most estimates of the average Sr concentration in crustal materials lie in the range 320–400 ppm [*Taylor*, 1964; *Hurley*, 1968*a*, *b*; *Larimer*, 1971; *Taylor*, 1977] typically with an average value of ~370 ppm which we have used.

Average Sm and Nd concentrations seem to be approximately the same in both upper and lower crustal rocks. We have thus used Nd = 26 ppm from *Shaw et al.* [1976]. Average continental crustal materials typically have $f_{Sm/Nd} \approx -0.4$ [*McCulloch and Wasserburg*, 1978], and this gives Sm = 5 ppm in the total crust.

Results for Model I

We now will attempt to evaluate the parameters of this model for both Rb-Sr and Sm-Nd by first only considering estimates from observed ϵ values and f values (Table 3) using (26). These parameters are more directly known than the concentrations in the various reservoirs. The enrichment factor for Rb-Sr in the MORB source is estimated to be $sf_2^{Rb/Sr} = -0.9$. As $f_2^{Rb/Sr}$ is close to the limit of -1, it is therefore not subject to substantial error. The mean ϵ_{Sr} value of MORB is -27. These values give a reliable estimate of the mean age of the MORB source today ($\bar{t} = 1.8$ aeons). If the rate of production of crust were constant over 4.5 aeons, then $\bar{t} = T_0/2 = 2.3$ aeons. As $\bar{t}$ is much less than 2.3 aeons, this shows that if model I is valid, the rate of crustal and mantle formation was much greater in the time subsequent to 1.8 aeons in comparison with the rate between 1.8 and 4.55 aeons. It is of interest to note that for a uniform rate of crustal formation, we calculate $T_0 = 3.6$ aeons the age of the oldest known terrestrial rocks. This model suggests a low initial rate of crustal formation. The MORB show a range of $f_2^{Sm/Nd}$ from ~0 to +0.4, but their average $\epsilon_{Nd,2} = +10$ is well defined. As the model has the same value of $\bar{t}$ for different species, we therefore use the mean age of 1.8 aeons from the Rb-Sr data to arrive at a self-consistent estimate of $f_2^{Sm/Nd} = +0.225$. This compares well with the estimate given in Table 3 of $f_2^{Sm/Nd} = +0.22$. For the continental crust the only parameter for which we have a reliable estimate is $f_3^{Sm/Nd} = -0.4$. With our estimate of the mean age $\bar{t} = 1.8$ aeons this gives $\epsilon_{Nd,3}(0) = -17.8$, which is in the middle of the range of values reported for Canadian shield composite samples and sedimentary rocks by *McCulloch and Wasserburg* [1978]. Reliable estimates of $\epsilon_{Sr,3}$ and $f_3^{Rb/Sr}$ for the continental crust are much harder to obtain directly, owing to the strong upward concentration of Rb in the crust as discussed previously. Estimates of $f^{Rb/Sr}$ for the upper crust give $f^{Rb/Sr} \sim +10$ [*McCulloch and Wasserburg*, 1978]. However, average continental runoff shows $\epsilon_{Sr}(0) = +163$ [*Veizer and Compston*, 1974], which would yield $f_3^{Rb/Sr} = +5.4$ if $\bar{t} = 1.8$ aeons. Strontium has a short residence time in sea water (4×10^6 yr), and if we assume that the sea water ($\epsilon_{Sr}(0) = +65$) [*Papanastassiou et al.*, 1970; *Hildreth and Henderson*, 1971] represents average crust, then we get $f_3^{Rb/Sr} = +2.16$. This is identical to our estimate in Table 6 based on a crustal model with a granulite facies lower crust. However, the similarity may be fortuitous, as Sr in seawater may be affected by isotope exchange with oceanic crust during hydrothermal convection within oceanic ridges [*Spooner*, 1976]. The self-consistent values of the model parameters discussed above are given in Table 7.

Assuming that the Bay of Islands data are a proper representation of the MORB source of 0.5 aeon ago (Table 3), we may calculate the various model parameters at that time. For Rb-Sr using $f_2^{Rb/Sr} = -0.9$ from Table 7 and the observed $\epsilon_{Sr,2} = -19.3$, we obtain $\bar{t} = 1.3$ aeons at 0.5 aeon ago. Similarly, for Sm-Nd using the observed $\epsilon_{Nd,2} = +7.6$ and the parameters in Table 7, we get $\bar{t} = 1.4$ aeons. Equation (27) gives the variation of the mean age with time. Since $d\bar{t}/d\tau = 1 - \bar{t}(d \ln M/d\tau) \leq 1$, it follows that $\bar{t}$ (today) $- \bar{t}$ (0.5 aeon ago) ≤ 0.5. For Rb/Sr this difference is 0.5, implying that $dM/d\tau \cong 0$ for the last 500 m.y. For Sm/Nd this difference is 0.4, implying that $(d \ln M/d\tau) = 0.11$ aeon^{-1} for the last 500 m.y., which is half of the

TABLE 5. Recent Estimates of Average Lithophile Element Concentrations, in Parts per Million, in the Silicate Portion of the Earth (Crust Plus Mantle)

Author	K	Rb	Sr	Ba	Sm	Nd	U	$f^{Rb/Sr}$	$f^{Sm/Nd}$	Sr/Nd	Sr/U	K/Rb	K/U
Hurley [1968*a*, *b*]	207	0.59	17.8	...	...	...	0.0148	+0.16	...	...	1187	331	1.4×10^4
Larimer [1971]	192	0.62	17.8	7.8	...	...	0.0178	+0.22	...	...	1000	310	1.1×10^4
Shaw [1972]	160	0.59	27	5.5	...	...	0.027	−0.24	...	...	1000	271	0.6×10^4
Ganapathy and Anders [1974]	252	0.86	26.9	7.5	0.38	1.27	0.0266	+0.12	−0.07	21.2	1011	293	0.944×10^4
Tera et al. [1974]	350	1.2	31	...	...	...	0.035	+0.35	...	...	886	292	10^4
Ringwood and Kesson [1977]*	286	0.85	24.2	8.4	0.42	1.39	0.0286	+0.23	=0	17.5	846	341	10^4
Smith [1977]	192	0.73	29.6	7.3	0.33	1.78	0.0385	−0.14	−0.42	16.6	769	263	0.5×10^4
Sun and Nesbitt [1977]†	237	0.67	22	7.6	0.406	1.26	0.026	+0.06	=0	17.5	846	353	0.9×10^4
O'Nions et al. [1978]	462	1.31	41	...	0.30	0.95	0.046	+0.12	=0	43.2	891	350	10^4
This work	≥260	0.63	22	7.6	0.406	1.26	0.026	=0	=0	17.5	846	≥413	$\geq 10^4$
Chondrites‡	805	2.3	11	3.8	0.203	0.63	0.013	+6.2	=0	17.5	846	350	6.2×10^4

We assume that these elements are totally excluded from the core, and all bulk earth concentrations from the literature have therefore been recalculated to the average value for the crust-mantle system (total earth mass = 1.48 × (crust + mantle)).

*Refractory elements = 2.2 × ordinary chondrites, (K/U) = 10^4 and Rb/U = 29.2.

†Refractory elements = 2.0 × chondrites.

‡*Hubbard and Gast* [1971], *Nakamura* [1974], and *Mason* [1971].

TABLE 6. Estimates of Lithophile Element Concentrations in the Continental Crust

	K	Rb	Sr	Ba	Sm	Nd	U	$f^{Rb/Sr}$	$f^{Sm/Nd}$	Sr/Nd	Sr/U	K/Rb	K/U
Upper crust, *Shaw et al.* [1976]	2.57	110	316	1070	4.5	26	2.45	+11	−0.46	12.2	129	234	10^4
Lower crust, *Heier and Thoresen* [1971]	2.49	56	572	1162	(4.8)*	(28)*	0.5	+2.4	(−0.47)*	20.4	1144	629	5×10^4
Total crust, *Lambert and Heier* [1968]	1.50	...	...	...	...	...	0.7	...	...	...	...	...	2×10^4
This work	1.50	33	370	500	5	26	0.7	+2.1	−0.40	14.2	528	450	2×10^4

*Estimated from REE patterns of *Green et al.* [1972] on some of the samples used by *Heier and Thoresen* [1971].

average growth rate of the crust [$(1/T_0) = 0.22$ aeon^{-1}]. However, if the mean age measured 0.5 aeon ago was 1.5 aeons instead of 1.3 or 1.4 aeons, then $(dM/d\tau)$ for the last 0.5 aeon would be equal to the average growth rate of the crust. Thus the value for $(dM/d\tau)$ during the last 0.5 aeon is very sensitive to small differences in the mean ages. No firm conclusion can be drawn, but the data suggest that the average growth rate of the continents and the rate of differentiation of the mantle for the last 0.5 aeon is less than half of the average value over the history of the earth.

We now turn to the problem of evaluating the concentrations of Rb, Sr, Nd, and Sm and the masses of the various reservoirs. The concentrations used for the undepleted mantle and the crust are those from Tables 5 and 6, respectively, except for the Rb concentration in the crust, which will be calculated in the following. These parameters are given in Table 7. From conservation of mass and species we have as before that $C_{i,1} = C_{i,2}(1 - x) + C_{i,3}x$, where $x = M_2/(M_2 + M_3)$ for both stable and radioactive isotopes. This together with the definition of $f_j^{r/s}$ (equation (17)) leads to the following equation that relates the masses of reservoirs 2 and 3 to the f values of 2 and 3 and the concentrations of the stable isotope in 1 and 3:

$$\frac{M_3(\tau)}{M_2(\tau) + M_3(\tau)} = \frac{f_2^{r/s}(\tau)C_{s,1}(\tau)}{[f_2^{r/s}(\tau) - f_3^{r/s}(\tau)]C_{s,3}(\tau)} \tag{78}$$

This equation holds for any model as long as reservoirs 2 and 3 are derived from the reference reservoir 1. For model I the left-hand side of (78) must be equal to the degree of melting $F = M_3(\tau)/[M_2(\tau) + M_3(\tau)]$. The degree of melting must be the same for all species, so (78) gives us a relation between the f values for the Rb/Sr and the Sm/Nd system. From the values of $f_2^{Sm/Nd}$, $f_3^{Sm/Nd}$, $C_{Nd,1}$, and $C_{Nd,3}$ in Table 7, it follows that $F = 0.0174$. Using this value and the mass of the total continental crust given in Table 2, we get that the mass of the depleted mantle today is 127×10^{25} grams. This corresponds to approximately the upper 650 km of the mantle or $\sim 1/3$ of the mass of the mantle. As was noted previously, the values of $f_3^{Rb/Sr}$ and $C_{Rb,3}$ are not well known. We therefore use (78), the values of $f_2^{Rb/Sr}$, $C_{Sr,1}$, and $C_{Sr,2}$ from Table 7, and $F = 0.0174$ as estimated above to calculate $f_3^{Rb/Sr} = 2.18$ and $C_{Rb,3} = 33.7$. This is identical to estimates made previously of these parameters, and it gives $\epsilon_{Sr,3}(0) = +65.5$ if $\bar{t} = 1.8$ aeons. From this information we can calculate the concentrations of all the elements in reservoir 2 and the bulk distribution coefficients using (11) and (12). The complete set of self-consistent parameters for Rb, Sr, Sm, and Nd are given in Table 7 for model I. The calculated bulk distribution coefficients agree to better than a factor of 2 with garnet peridotite bulk distribution coefficients estimated from the mineral melt distribution coefficients from Table 4 ($D_{Rb} \approx 0.0025$, $D_{Sr} \approx 0.033$, $D_{Nd} \approx 0.044$, and $D_{Sm} \approx 0.080$ for small degrees of melting of garnet peridotite).

This approach can also be extended to include other elements by using (11) and (12). We briefly investigate the consequences of this model for K, U, and Ba, since these are strongly incompatible elements with $D_i \approx 0$. If $D_i = 0$, then $C_{i,3}/C_{i,1} = 57$ for $F = 0.0174$, which is the maximum enrichment we may have for this model. Bulk distribution coefficients estimated in Table 4 for these elements are $D_K = 0.002$, $D_{Ba} = 0.0014$, and $D_U = 0.001$, and these values will be used for the calculations. The concentrations for reservoirs 1 and 3 are obtained from Tables 5 and 6. The concentration of K in the total crust (1.5 wt.%) is used with the above mentioned parameters to get $C_{K,1} = 290$ ppm and $C_{K,2} = 30$ ppm. It follows then that the bulk earth K/Rb ratio is 460 and that this ratio is 680 in the depleted mantle. This ratio for the depleted mantle still seems somewhat low, as K/Rb $\sim$ 1000 for MORB, but this difference may be accounted for by only increasing D_K from 0.002 to 0.003. For Ba and U the concentrations in the undepleted mantle are considered to be better established than for K (Table 5). Using (11), we get $C_{Ba,3} = 405$ ppm and $C_{U,3} = 1.4$ ppm, which compare reasonably well with the estimates given for the average total crust in Table 6. The calculated concentrations in the depleted reservoir are $C_{Ba,2} = 0.57$ ppm and $C_{U,2} = 1.4$ ppb. Existing data for K, Rb, and Ba are thus reasonably consistent with model I.

We will now consider the possibility that undifferentiated material is being mixed with the depleted mantle by the mechanism described by (29)–(33). In this case, $\beta F = M_3(\tau)/(M_2(\tau) + M_3(\tau))$. From the value of $f_2^{Rb/Sr} = -0.9$ from Table 7 we get from (35) that $\beta > 0.9$. This means that the amount of undifferentiated material that may be mixed with the depleted mantle is less than 10%. Considering only the surface area covered by continents and oceans today, we would expect that $\beta = 0.42$ using the surface areas given by *Ronov and Yaroshevsky* [1976]. This suggests that if model I is valid, there must be some mechanism for efficient addition to continents of melt fractions from undifferentiated material that differentiates beneath oceans. As was discussed previously, we may also consider the case $\beta < 1$ to be analogous to refluxing of crust to depleted mantle in a generalized version of model I. This shows that only 10% of the total amount of material added to the crust may have been subducted back to the depleted mantle.

Results for Model II

We now evaluate the present day parameters for this model. As for model I, we again start out with the most reliable values given in Table 3. Substituting $\epsilon_{Sr,2} = -27$ and $f_2^{Rb/Sr} = -0.9$ into (63) gives $\bar{t}_{Rb/Sr} = 1.8$ aeons. It follows for this model that the mean mass age of the continents is substantially less than $(T_0/2) = 2.3$ aeons. This clearly implies that the rate of growth of the continental crust yields a mass growth curve which accelerates with time; i.e., the crustal growth rate for the past 2 aeons being much higher than for the period from 4.5 to 3.6 aeons. This result can be modified only if the bulk earth parameters for Rb-Sr given in the Appendix were substantially altered. To obtain self-consistent values for the Sm-Nd system, we note that the possible fractional range of $f^{Sm/Nd}$ values for the depleted mantle is substantially larger than the corresponding fractional range of $f^{Rb/Sr}$ and the range in possible crustal ϵ_{Nd} values is also large, thus placing only rather broad bounds on the value of $\bar{t}_{Sm/Nd}$. Stricter bounds of $f^{Sm/Nd}$ are placed by using $\bar{t}_{Rb/Sr}$, since $\bar{t}_{M,3} \approx \bar{t}_{Sm/Nd} \leq \bar{t}_{Rb/Sr} = 1.8$ aeons. So from (63) we get $f_2^{Sm/Nd} \geq 0.225$, and the direct observational upper bound from the Appendix is $f_2^{Sm/Nd} \leq 0.3$. Note that for model II, knowledge of the present day f_2 values explicitly determines the quantity $\alpha_{r/s}(T_0) = [(d_r - d_s)M_3(T_0)/M_2(0)]$ using (50). Using $f_2^{Rb/Sr}(T_0) = -0.9$ for the present value, we obtain $\alpha_{Rb/Sr}(T_0) = +2.30$. This shows that $f_2^{Rb/Sr} = \exp[-\alpha_{Rb/Sr}(\tau)] - 1$ is in the strongly nonlinear range. In contrast, $0.225 \leq f_2^{Sm/Nd} \leq 0.3$, which implies that $-0.264 \leq \alpha_{Sm/Nd}(T_0) \leq -0.203$, so that $f_2^{Sm/Nd}$ is determined to within 10% by the first-order expansion over the history of the earth. This contrast between Rb-Sr and Sm-Nd is different from that of model I and reflects the fundamental

TABLE 7. A Self-Consistent Set of Parameters for Model I

Reservoir j	$C_{Rb,j}$	$C_{Sr,j}$	$f_j^{Rb/Sr}$	$\epsilon_{Sr,j}(0)$	$C_{Sm,j}$	$C_{Nd,j}$	$f_j^{Sm/Nd}$	$\epsilon_{Nd,j}(0)$	$M_j^{(today)}$, g
Continental crust $j = 3$	33.7	370	2.18	65.5	5.0	26	−0.4	−17.8	2.256×10^{25}
Depleted mantle $j = 2$	0.044	15.8	−0.9	−27	0.32	0.82	0.225	10	127.4×10^{25}
Undepleted mantle $j = 1$	0.63	22	≡0	≡0	0.406	1.26	≡0	≡0	273.7×10^{25}

$\bar{t} = 1.8$ aeons; $F = 0.0174$; $\beta = 1$; $D_{Rb} = 0.0013$; $D_{Sr} = 0.043$; $D_{Nd} = 0.032$; $D_{Sm} = 0.065$.
Concentrations are given in parts per million.

differences between the two models. The values of $\alpha_{Rb/Sr}$ and $\alpha_{Sm/Nd}$ may be used to find $M_2(0)$ and $(d_r - d_s)$ using the value of $M_3(T_0)$ from Table 2. If we assume that the whole mantle is involved in crust formation, then $[M_3(T_0)/M_2(0)] = 0.00448$, which implies that $d_{Rb} - d_{Sr} = 513$ and $d_{Sm} - d_{Nd} = -46$. We now assume that reasonable values for the degree of melting F would be in the range from 0.5 to 5% by mass. Using the bulk distribution coefficients from Table 3, we find a range of $(d_{Rb} - d_{Sr})$ from 7 to 108 for Rb-Sr (equation (50)). This implies that $[M_3(T_0)/M_2(0)]$ should be in the range from 0.021 to 0.33 using $\alpha_{Rb/Sr} = 2.3$. Similarly, we get that $(d_{Sm} - d_{Nd})$ must be in the range from −8.7 to −3, and using the range of $\alpha_{Sm/Nd}$ given previously implies that $0.023 \leq [M_3(T_0)/M_2(0)] \leq 0.081$. We may also estimate $M_3(T_0)/M_2(0)$ from (78) using $C_{Nd,1} = 1.26$ ppm and $C_{Nd,3} = 26$ ppm. Since $f_3^{Sm/Nd} = -0.4$ and $0.225 \leq f_2^{Sm/Nd} \leq 0.3$ as discussed previously, it follows from (78) that $0.0174 \leq [M_3(T_0)/M_2(0)] \leq 0.0208$. From these estimates the most reasonable choice seems to be $M_3(T_0)/M_2(0) = 0.020 \pm 0.003$, and this gives $M_2(T_0) = 110.5 \times 10^{25}$ grams, which is 28% of the mantle. Using this value for $M_3(T_0)/M_2(0)$ in (78) gives $f_2^{Sm/Nd} = +0.281$ and thus $\alpha_{Sm/Nd} = -0.248$. From (63) it now follows that $\bar{t}_{Sm/Nd} = 1.44$ aeons, which together with $f_3^{Sm/Nd} = -0.4$ gives $\epsilon_{Nd,3} = 14.3$. Similarly, using (78) for Rb-Sr with $f_2^{Rb/Sr} = -0.9$, $[M_3(T_0)/M_2(0)] = 0.02$, $C_{Sr,1} = 22$ ppm, and $C_{Sr,3} = 370$ ppm, we get $f_3^{Rb/Sr} = +1.78$, $C_{Rb,3} = 29.4$ ppm, and since $\bar{t}_{Rb/Sr} = 1.8$ aeons it also follows that $\epsilon_{Sr,3} = +53.4$.

We have now determined a self-consistent set of f and ϵ values for model II, which are given in Table 8. From the values $f_2'^{/s}$ and $f_3'^{/s}$ for Sm/Nd and Rb/Sr together with $[M_3(T_0)/M_2(0)] = 0.020$ we can, by using (50) and (51), determine all the d values which are given in Table 8. Since $D_{Rb} > 0$, it follows from the value we calculated for $d_{Rb} = 135.5$ that $F < 0.0076$. Choosing $D_{Rb} = 0.0025$ from Table 4 gives $F = 0.005$. Using this value of F, we may calculate D_{Sr}, D_{Nd}, and D_{Sm} (Table 8). From the d values listed in Table 8 and the concentrations of the undepleted reservoir we may now calculate the concentrations of these elements in the depleted reservoir. A complete set of self-consistent parameters for Rb, Sr, Sm, and Nd are given in Table 8 for model II. The parameters for Rb imply that the concentration of Rb in new additions to the crust has changed from 86 ppm initially to 6 ppm today giving an average concentration today of ~30 ppm. This large change of Rb concentration in the crust over geologic time does not appear supportable from the existing data. The magnitude of this time dependence is not changed by any choice of parameters so long as $f_2^{Rb/Sr}$ is close to its lower limit of −1.

We now turn our attention to see what the data can tell us about the time evolution of the continental crust. The simplest growth model would be $(dM_3/d\tau) = \text{const}$ over the history of the earth. Using this assumption, we get $\bar{t}_{Sm/Nd} - \bar{t}_{M,3} = -0.09$ aeon from (66) with $\tau = 4.5$ aeons and $\alpha_{Sm/Nd} = -0.248$, so since $\bar{t}_{Sm/Nd} = 1.44$ aeons, it follows that $\bar{t}_{M,3} \approx 1.5$ aeons. However, since $\bar{t}_{M,3} \leq \bar{t}_{Rb/Sr} = 1.8$ aeons $< (T_0/2)$, this would require that the crust started to form late. The longest time compatible with a uniform growth may be determined from (71) and (72). For Rb-Sr we get 2.7 aeons and for Sm-Nd we get 3.0 aeons for the longest time compatible with a constant growth rate of the crust using the f and ϵ values for reservoir 2 given in Table 3. These are both unrealistically low values, so we must conclude that a uniform growth rate can hardly explain the data. It is, however, clear that this model also requires the dominant parts of the continents to have formed late in the earth's history.

From the Bay of Islands data [*Jacobsen and Wasserburg*, 1979], similar estimates can be made for the depleted mantle 0.5 aeon ago using the values given in Table 3. Our estimates of the enrichment factors for the Bay of Islands source are $f_2^{Rb/Sr} = -0.9$ and $f_2^{Sm/Nd} \approx +0.2$ (Table 3). For Rb-Sr using $\epsilon_{Sr,2} = -19.3$, we obtain $\bar{t}_{Rb/Sr} = 1.3$ aeons at 0.5 aeon ago, which indicates that $(dM_3/d\tau) \approx 0$ for the last 500 m.y. as in model I. For Sm-Nd using $\epsilon_{Nd,2} = +7.6$, we obtain by using the estimate of the present day $f_2^{Sm/Nd}$ of +0.28 (Table 8) that $\bar{t}_{Sm/Nd} \approx 1.1$ aeons. From (66) we get $\bar{t}_{Sm/Nd} - \bar{t}_{M,3} = -0.08$ at 0.5 aeon ago, so it follows that $\bar{t}_{M,3} \approx 1.2$ aeons at that time for this model. This is only slightly lower than the value obtained for model I.

Discussion of the Models and Conclusions

The basic transport equations for the earth differentiation models shown in Figure 1 give simple results when solved for arbitrary mass growth curves $M_j(\tau)$ for the continental crust ($j = 3$) and the depleted mantle ($j = 2$). The solution for model I is

$$\epsilon_{d,j}^*(\tau) = \frac{Q_d^*(\tau) f_j'^{/s}}{M_j(\tau)} \int_0^\tau M_j(\xi) \exp[\lambda(\tau - \xi)]\, d\xi$$

where

$$Q_d^*(\tau) = 10^4 \lambda \left[\frac{N_{r,1}(\tau)}{N_{d,1}(\tau)}\right]$$

and $f_j'^{/s}$ is the enrichment factor, which is constant for all time. The mean age $\bar{t}_{s,j}$ of stable isotopes is equal to the mean age of the mass of j; $\bar{t}_{M,j} = \int_0^\tau [M_j(\xi)/M_j(\tau)]\, d\xi$. For long-lived isotopes ($\lambda^{-1} \gg 4.5$ aeons), $\epsilon_{d,j}^* = Q_d^* f_j'^{/s} \bar{t}_{M,j}$, and $Q_d^* \approx$ const. Knowledge of $\epsilon_{d,j}^*$ and $f_j'^{/s}$ at a single time fixes $\bar{t}_{M,j}$. The mean age shows the relationship $(d\bar{t}/d\tau) = 1 - \bar{t}(d \ln M_j/d\tau)$, so if $M_j(\tau)$ and $f_j'^{/s}$ are known, then $\bar{t}_{M,j}$ and $\epsilon_{d,j}^*(\tau)$ are known.

For model II which has continuous fractionation in the source reservoir the concentrations are functions of time, and we get

$$\epsilon_{d,2}^*(\tau) = Q_d^*(\tau) \int_0^\tau f_2'^{/s}(\xi) \exp[\lambda(\tau - \xi)]\, d\xi$$

$$\epsilon_{d,3}^*(\tau) = \epsilon_{d,2}^*(\tau) \frac{f_3'^{/s}(\tau)}{f_2'^{/s}(\tau)}$$

TABLE 8. A Self-Consistent Set of Parameters for Model II at $\tau = T_0$ (Today)

Reservoir j	$C_{Rb,j}$	$C_{Sr,j}$	$f_j^{Rb/Sr}$	$\epsilon_{Sr,j}^*$	$C_{Sm,j}$	$C_{Nd,j}$	$f_j^{Sm/Nd}$	$\epsilon_{Nd,j}^*$	M_j, g
Continental crust $j = 3$	29.4	370	1.78	53.4	5.0	26	−0.4	−14.3	2.256×10^{25}
Depleted mantle $j = 2$	0.041	14.5	−0.9	−27	0.29	0.74	0.281	10	110.5×10^{25}
Undepleted mantle $j = 1$	0.63	22	≡0	≡0	0.406	1.26	≡0	≡0	290.6×10^{25}

$T_{Rb/Sr} = 1.8$ aeons; $T_{Sm/Nd} = 1.44$ aeons; $T_{M,3} = 1.5$ aeons; $M_3(T_0)/M_2(0) = 0.020$; $d_{Rb} = 135.5$; $d_{Sr} = 20.5$; $d_{Nd} = 26.6$; $s_{Sm} = 16.2$; $\alpha_{Rb/Sr}(T_0) = +2.30$; $\alpha_{Sm/Nd}(T_0) = -0.248$; $F = 0.005$; $D_{Rb} = 0.0025$; $D_{Sr} = 0.044$; $D_{Nd} = 0.033$; $D_{Sm} = 0.057$.

Concentrations are given in parts per million.

$$f_2^{\prime/s}(\tau) = \left[\frac{M_2(\tau)}{M_2(0)}\right]^{(d_r - d_s)}$$

$$\frac{f_2^{\prime/s}(\tau)}{f_3^{\prime/s}(\tau)} = 1 - \left[\frac{M_2(\tau)}{M_2(0)}\right]^{(-d_s)}$$

Define $\bar{t}_{r/s} \equiv \int_0^\tau [f_2^{\prime/s}(\xi)/f_2^{\prime/s}(\tau)]\, d\xi$. Then for long-lived isotopes we have $\epsilon_{d,j}^*(\tau) = Q_d^* f_j^{\prime/s}(\tau) \bar{t}_{r/s}$ where $\bar{t}_{r/s}$ is the time required to generate $\epsilon_{d,j}^*$ with the present value of $f_j^{\prime/s}$. Note that $\bar{t}_{r/s}$ depends on the parent-daughter system and is in general different from $\bar{t}_{M,3}$. The difference is given by

$$\bar{t}_{r/s} - \bar{t}_{M,3} \approx \frac{(d_r - d_s)}{2M_3(\tau)M_2(0)} \int_0^\tau M_3(\xi)[M_3(\tau) - M_3(\xi)]\, d\xi$$

for small $[(d_r - d_s)/M_2(0)]$. Decay systems with small $(d_r - d_s)$ may be used to estimate $\bar{t}_{M,3}$. These simple expressions may be used to calculate earth models with great facility without requiring a computer calculation.

We first compare the results from models I and II (Tables 7 and 8). The mean age of the crust is 1.8 aeons for model I and 1.5 aeons for model II, so a young mean age of the crust is confirmed by both models. Similarly, both models indicate that the rate of growth over the last 0.5 aeon is much less than the average rate of growth. Therefore most of the crust probably formed in the time interval from ~0.5 to ~3 aeons ago. Both models also require the depleted mantle complementary to the continental crust to make up about 1/3 of the mantle, which corresponds approximately to the upper 650 km of the mantle. This does not seem to be compatible with whole mantle convection as discussed by *Hager and O'Connell* [1979]. In future studies it is of importance to arrive at mantle structure models which satisfy both the boundary conditions on mantle convection and isotope geochemistry. The present day ϵ and f values and the concentration in each reservoir are fairly similar for both models as shown in Tables 7 and 8. Insofar as the mantle consists of an undepleted reservoir and a depleted reservoir that is complementary to the crust, the above conclusions are basically model independent. Model I indicates a larger degree of melting (1.7%) than model II (0.5%). At the present time both of these values seem to be plausible estimates of the average degree of melting through time. The major difference in the results for the two models is in the composition of new additions to continental crust. Model I predicts that $\epsilon_{Nd} = \epsilon_{Sr} = 0$ for new additions to the continental crust, and model II predicts that the ϵ_{Sr} and ϵ_{Nd} of new additions are those of the source of MORB. The fact that island arcs have bulk composition and REE abundances similar to average continental crust and that they usually are found at or near continental margins has led to the hypothesis that the continents grow by accreting island arcs along their margins [*Taylor and White*, 1965; *Ringwood*, 1975]. If this is the case, then the Nd isotopic studies reported by *DePaolo and Wasserburg* [1977] and *Hawkesworth et al.* [1977] show that new continental material should have ϵ_{Nd} values similar to MORB and are thus derived from depleted mantle. This mechanism for continental growth is thus described by model II. However, this model cannot explain why typically most continental crustal materials have $\epsilon_{Nd} \approx 0$ [*DePaolo and Wasserburg*, 1976*a*, *b*; *McCulloch and Wasserburg*, 1978; *Hamilton et al.*, 1977, 1978, 1979] throughout the earth's history. While values of $\epsilon \approx 0$ may be obtained at early times for both models, it is not possible to continue production of such materials in more recent geologic time for model II.

In model I the concentrations of stable isotopes in new additions to the crust are the same for all time, however, in model II the concentrations may decrease by over a factor of 10 for highly incompatible elements as K, Rb, Ba, and U. There is no evidence for such drastic changes with time. We therefore conclude that model I best describes crust and mantle evolution. Some additions to the continents during the last 1.5 aeons have $\epsilon_{Nd} > 0$ [*DePaolo and Wasserburg*, 1976*a*, *b*], so some new additions to the crust may follow model II. A modified version of model I where it is allowed for mixing of undepleted mantle with depleted mantle shows that this contribution must be less than 10%. This model also shows that less than 10% of the total continental crust has been refluxed back to the depleted mantle.

Recent isotopic studies of young volcanic rocks have shown that ϵ_{Nd} and ϵ_{Sr} are strongly correlated in ocean floor and ocean island basalts and selected continental basalts [*DePaolo and Wasserburg*, 1976*b*; *O'Nions et al.*, 1977]. This correlation line is assumed to be due to mantle characteristics and has been called the 'mantle array' by *DePaolo and Wasserburg* [1979*a*]. Magmas in model I may be mixtures derived from depleted and undepleted mantle and may thus explain the mantle array. Model II does not explain the mantle array unless a range of source reservoirs individually following this model are involved. This would, however, require that some of them be close to undepleted mantle material, but it is not clear that this would satisfy a strict correlation between initial Nd and initial Sr.

Considering the young mean ages derived for the continents, we are left with very little evidence of crust forming very early in the earth's history. Search for old crustal rocks by direct dating has established a low abundance of ~3.6-aeon-old crustal rocks and the apparent absence of much older rocks at the surface of the earth. An alternative way of looking for old crust is to look at the residue in the mantle after crust formation. If the pre-3.6-aeon-old crust were buried in the lower crust, then we would still expect to see it in the isotopic systematics of the depleted mantle. The depleted mantle gives a young mean age of ~1.8 aeons, and this implies either that very little early crust ever formed or that the early crust was destroyed by rapid refluxing into the mantle in the period from 4.5 to 3.6 aeons ago. If the latter is the case, then this would have caused early degassing of the earth's Ar as suggested by $^{40}Ar/^{36}Ar$ ratios in the mantle [*Ozima*, 1975]. The detailed history of this time period must be derived from

data for ^{40}K and ^{235}U and perhaps also ^{244}Pu and the extinct ^{129}I.

Appendix: Present Day Bulk Earth Values

The following values are from *DePaolo and Wasserburg* [1976*a*, *b*] and *O'Nions et al.* [1977]:

$$\frac{^{87}Sr(T_0)_I}{^{86}Sr(T_0)_I} = 0.7045 \qquad \frac{^{87}Rb(T_0)_I}{^{86}Sr(T_0)_I} = 0.0827$$

$$\frac{^{143}Nd(T_0)_I}{^{144}Nd(T_0)_I} = 0.511836 \qquad \frac{^{147}Sm(T_0)_I}{^{144}Nd(T_0)_I} = 0.1936$$

$$Q_{Nd}^*(T_0) = 24.74 \text{ aeons}^{-1} \qquad Q_{Sr}^*(T_0) = 16.70 \text{ aeons}^{-1}$$

The decay constants used are $\lambda(^{87}Rb) = 0.0142$ aeons^{-1} and $\lambda(^{147}Sm) = 0.00654$ aeons^{-1}. $T_0 = 4.55$ aeons.

Acknowledgments. This work has been supported by NSF grant EAR 76-22494 and NASA grant NGL 05-002-188. We wish to thank R. J. O'Connell for his thorough and scholarly analysis of the manuscript, which resulted in several substantial improvements. Supporting and critical discussions with our colleagues M. McCulloch and R. Jeanloz were of great value. We thank the editor, T. J. Ahrens, and the associate editor, J. Hayes, for careful attention to the manuscript and the reviewers, M. J. Drake and G. Wetherill, for their attention to what might be viewed as a difficult manuscript. G. Wetherill pointed out to us that the earth probably looks more like a $10 ice cream sundae than an oil refinery with discrete storage tanks. We hope some day to share the $10 ice cream sundae with him. Contribution #3251 (306).

References

Armstrong, R. L., A model for the evolution of strontium and lead isotopes in a dynamic earth, *Rev. Geophys. Space Phys., 6*, 175–199, 1968.

Benjamin, T. M., R. Heuser, and D. S. Burnett, Solar system actinide abundances, I, Laboratory partitioning between whitlockite, diopsidic clinopyroxene and anhydrous melt (abstract), in *Lunar and Planetary Science*, vol. 9, pp. 70–77, The Lunar and Planetary Institute, Houston, 1978.

Brooks, C., and S. R. Hart, Rb-Sr mantle isochrons and variations in the chemistry of Gondwanaland's lithosphere, *Nature, 271*, 220–223, 1978.

Brooks, C., S. R. Hart, A. Hoffman, and D. E. James, Rb-Sr mantle isochrons from oceanic regions, *Earth Planet. Sci. Lett., 32*, 51–61, 1976*a*.

Brooks, C., D. E. James, and S. R. Hart, Ancient lithosphere: Its role in young continental volcanism, *Science, 193*, 1086–1094, 1976*b*.

Consolmagno, G. J., and M. J. Drake, Equivalence of equations describing trace element distribution during equilibrium partial melting, *Geochim. Cosmochim. Acta, 40*, 1421–1422, 1976.

DePaolo, D. J., Study of magma sources, mantle structure and the differentiation of the earth using variations of $^{143}Nd/^{144}Nd$ in igneous rocks, Ph.D. thesis, Calif. Inst. of Technol., Pasadena, 1978.

DePaolo, D. J., and G. J. Wasserburg, Nd isotopic variations and petrogenetic models, *Geophys. Res. Lett., 3*, 249–252, 1976*a*.

DePaolo, D. J., and G. J. Wasserburg, Inferences about magma sources and mantle structure from variations of $^{143}Nd/^{144}Nd$, *Geophys. Res. Lett., 3*, 743–746, 1976*b*.

DePaolo, D. J., and G. J. Wasserburg, The sources of island arcs as indicated by Nd and Sr isotopic studies, *Geophys. Res. Lett., 4*, 465–468, 1977.

DePaolo, D. J., and G. J. Wasserburg, Petrogenetic mixing models and Nd-Sr isotopic patterns, *Geochim. Cosmochim. Acta, 43*, 615–627, 1979*a*.

DePaolo, D. J., and G. J. Wasserburg, Nd isotopes in flood basalts from the Siberian Platform and inferences about their mantle sources, *Proc. Nat. Acad. Sci. U.S., 76*, 3056–3060, 1979*b*.

Eade, K. E., and W. F. Fahrig, Chemical evolutionary trends of continental plates—A preliminary study of the Canadian shield, *Bull. Geol. Surv. Can., 179*, 1971.

Frey, F. A., and D. H. Green, The mineralogy, geochemistry, and origin of lherzolite inclusions in Victorian basanites, *Geochim. Cosmochim. Acta, 38*, 1023–1059, 1974.

Ganapathy, R. M., and E. Anders, Bulk compositions of the moon and earth estimated from meteorites, *Proc. Lunar Sci. Conf. 5th*, 1181–1206, 1974.

Gast, P. W., Limitations on the composition of the upper mantle, *J. Geophys. Res., 65*, 1287–1297, 1960.

Green, T. H., A. O. Brunfelt, and K. S. Heier, Rare-earth element distribution and K/Rb ratios in granulites, mangerites and anorthosites, Lofoten-Vesteraalen, Norway, *Geochim. Cosmochim. Acta, 36*, 241–257, 1972.

Griffin, W. L., and V. R. Murthy, Distribution of K, Rb, Sr, and Ba in some minerals relevant to basalt genesis, *Geochim. Cosmochim. Acta, 33*, 1389–1414, 1969.

Grutzeck, M., S. Kridelbaugh, and D. Weill, The distribution of Sr and REE between diopside and silicate liquid, *Geophys. Res. Lett., 1*, 273–275, 1974.

Hager, B. H., and R. J. O'Connell, Kinematic models of large-scale flow in the earth's mantle, *J. Geophys. Res., 84*, 1031–1048, 1979.

Hamilton, P. J., R. K. O'Nions, and N. M. Evensen, Sm-Nd dating of Archean basic and ultrabasic volcanics, *Earth Planet. Sci. Lett., 36*, 263–268, 1977.

Hamilton, P. J., R. K. O'Nions, N. M. Evensen, D. Bridgwater, and J. Allart, Sm-Nd isotopic investigations of the Isua supracrustals, West Greenland: Implications for mantle evolution, *Nature, 272*, 41–43, 1978.

Hamilton, P. J., N. M. Evensen, R. K. O'Nions, and J. Tarney, Sm-Nd systematics of Lewisian gneisses: Implications for the origin of granulites, *Nature, 277*, 25–28, 1979.

Hart, S. R., and C. Brooks, Rb-Sr mantle evolution models, *Carnegie Inst. Wash. Yearb., 69*, 426–429, 1970.

Hart, S. R., and C. Brooks, Clinopyroxene matrix partitioning of K, Rb, Cs, Sr, and Ba, *Geomchim. Cosmochim. Acta, 38*, 1799–1803, 1974.

Hawkesworth, C. J., R. K. O'Nions, R. J. Pankhurst, P. J. Hamilton, and N. M. Evensen, A geochemical study of island-arc and back-arc tholeiites from the Scotia Sea, *Earth Planet. Sci. Lett., 36*, 253–262, 1977.

Heier, K. S., Rubidium/strontium and strontium-87/strontium-86 ratios in deep crustal material, *Nature, 202*, 477–478, 1964.

Heier, K. S., Radioactive elements in the continental crust, *Nature, 208*, 479–480, 1965.

Heier, K. S., A model for the composition of the deep continental crust, *Fortschr. Mineral., 50*, 174–187, 1973.

Heier, K. S., and J. A. S. Adams, Concentration of radioactive elements in deep crustal material, *Geochim. Cosmochim. Acta, 29*, 53–61, 1965.

Heier, K. S., and J. J. Rogers, Radiometric determination of thorium, uranium, and potassium in basalts and in two magmatic differentiation series, *Geochim. Cosmochim. Acta, 27*, 137–154, 1963.

Heier, K. S., and K. Thoresen, Geochemistry of high grade metamorphic rocks, Lofoten-Vesterålen, North Norway, *Geochim. Cosmochim. Acta, 35*, 89–99, 1971.

Hildreth, R. A., and W. T. Henderson, Comparison of $^{87}Sr/^{86}Sr$ for seawater strontium and the Eimer and Amend $SrCO_3$, *Geochim. Cosmochim. Acta, 35*, 235–238, 1971.

Hubbard, N. J., and P. W. Gast, Chemical composition and origin of nonmare lunar basalts, in *Proceedings of the Second Lunar Science Conference*, vol. 2, pp. 999–1020, MIT Press, Cambridge, Mass., 1971.

Hurley, P. M., Absolute abundance and distribution of Rb, K and Sr in the earth, *Geochim. Cosmochim. Acta, 32*, 273–283, 1968*a*.

Hurley, P. M., Correction to: Absolute abundance and distribution of Rb, K, and Sr in the earth, *Geochim. Cosmochim. Acta, 32*, 1025–1030, 1968*b*.

Jacobsen, S. B., and G. J. Wasserburg, Nd and Sr isotopic study of the Bay of Islands Ophiolite Complex and the evolution of the source of mid-ocean ridge basalts, *J. Geophys. Res., 84*, this issue, 1979.

Lambert, I. B., and K. S. Heier, The vertical distribution of uranium, thorium, and potassium in the continental crust, *Geochim. Cosmochim. Acta, 31*, 377–390, 1967.

Lambert, I. B., and K. S. Heier, Geochemical investigations of deep-seated rocks in the Australian shield, *Lithos, 1*, 30–53, 1968*a*.

Lambert, I. B., and K. S. Heier, Estimates of the crustal abundance of thorium, uranium and potassium, *Chem. Geol., 3*, 233–238, 1968*b*.

Larimer, J. W., Composition of the earth: Chondritic or Achondritic? *Geochim. Cosmochim. Acta, 35*, 769–786, 1971.

Loubet, M., N. Shimizu, and C. J. Allègre, Rare earth elements in alpine peridotites, *Contrib. Mineral. Petrol., 53*, 1–12, 1975.

Mason, B., *Handbook of Elemental Abundances in Meteorites*, 131 pp., Gordon and Breach, New York, 1971.

McCulloch, M. T., and G. J. Wasserburg, Sm-Nd, and Rb-Sr chronology of continental crust formation, *Science, 200*, 1003–1011, 1978.

McKay, G. A., and D. F. Weill, Petrogenesis of Kreep, *Proc. Lunar Sci. Conf. 7th*, 2427–2447, 1976.

Moorbath, S., Age and isotope evidence for the evolution of continental crust, *Phil. Trans. Roy. Soc. London, Ser. A, 288*, 401–413, 1978.

Morgan, J. W., and J. F. Lovering, Uranium and thorium in some basic and ultrabasic rocks of possible deep-seated origin, in *Activation Analysis in Geochemistry and Cosmochemistry*, edited by A. O. Brunfelt and E. Steinnes, pp. 445–454, Universitetsforlaget, Oslo, Norway, 1971.

Nakamura, N., Determination of REE, Ba, Fe, Mg, Na and K in carbonaceous and ordinary chondrites, *Geochim. Cosmochim. Acta, 38*, 757–775, 1974.

O'Nions, R. K., and D. B. Clarke, Comparative trace element geochemistry of Tertiary basalts from Baffin Bay, *Earth Planet. Sci. Lett., 15*, 436–446, 1972.

O'Nions, R. K., and R. J. Pankhurst, Early Archaean rocks and geochemical evolution of the earth's crust, *Earth Planet. Sci. Lett., 38*, 211–236, 1978.

O'Nions, R. K., P. J. Hamilton, and N. M. Evensen, Variations in $^{143}Nd/^{144}Nd$ and $^{87}Sr/^{86}Sr$ ratios in oceanic basalts, *Earth Planet. Sci. Lett., 34*, 13–22, 1977.

O'Nions, R. K., N. M. Evensen, P. J. Hamilton, and S. R. Carter, Melting of the mantle past and present: Isotope and trace element evidence, *Phil. Trans. Roy. Soc. London, 258*, 547–559, 1978.

O'Nions, R. K., N. M. Evensen, and P. J. Hamilton, Chemical constraints on the evolution of the earth's crust and mantle (abstract), in *Lunar and Planetary Science*, vol. 10, pp. 937–949, The Lunar and Planetary Institute, Houston, 1979.

Ozima, M., Ar isotopes and earth-atmosphere evolution models, *Geochim. Cosmochim. Acta, 39*, 1127–1134, 1975.

Papanastassiou, D. A., G. J. Wasserburg, and D. S. Burnett, Rb-Sr ages of lunar rocks from the Sea of Tranquility, *Earth Planet. Sci. Lett., 8*, 1–9, 1970.

Patterson, C., Characteristics of lead isotope evolution on a continental scale of the earth, in *Isotopic and Cosmic Chemistry*, edited by H. Craig, pp. 248–268, North-Holland, Amsterdam, 1964.

Patterson, C., and M. Tatsumoto, The significance of lead isotopes in detrital feldspar with respect to chemical differentiation within the earth's mantle, *Geochim. Cosmochim. Acta, 28*, 1–22, 1964.

Philpotts, J. A., and C. C. Schnetzler, Phenocryst-matrix partition coefficients for K, Rb, Sr and Ba, with applications to anorthosite and basalt genesis, *Geochim. Cosmochim. Acta, 34*, 307–322, 1970.

Poldervaart, A., Chemistry of the earth's crust, Crust of the Earth, *Geol. Soc. Amer. Spec. Pap., 62*, 119–144, 1955.

Richard, P., N. Shimizu, and C. J. Allègre, $^{143}Nd/^{146}Nd$, a natural tracer, an application to oceanic basalts, *Earth Planet. Sci. Lett., 31*, 269–278, 1976.

Ringwood, A. E., *Composition and Petrology of the Earth's Mantle*, 618 pp., McGraw-Hill, New York, 1975.

Ringwood, A. E., and S. E. Kesson, Basaltic magmatism and the bulk composition of the moon, II, Siderophile and volatile elements in moon, earth and chondrites: Implications for lunar origin, *Moon, 16*, 425–464, 1977.

Ronov, A. B., and A. A. Yaroshevsky, A new model for the geochemical structure of the earth's crust, *Geochem. Int., 13*, 89–121, 1976.

Russell, R. D., Evolutionary model for lead isotopes in conformable ores and in ocean volcanics, *Rev. Geophys. Space Phys., 10*, 529–549, 1972.

Russell, R. D., and D. J. Birnie, A bi-directional mixing model for Pb-isotope evolution, *Phys. Earth Planet. Interiors, 8*, 158–166, 1974.

Schilling, J. G., Sea-floor evolution: Rare earth evidence, *Phil. Trans. Roy. Soc. London, Ser. A, 268*, 663–706, 1971.

Schnetzler, C. C., and J. A. Philpotts, Partition coefficients of rare-earth elements between igneous matrix material and rock-forming phenocrysts, II, *Geochim. Cosmochim. Acta, 34*, 331–340, 1970.

Schramm, D. N., and G. J. Wasserburg, Nucleochronologies and the mean age of the elements, *Astrophys. J., 162*, 57–69, 1970.

Shaw, D. M., Trace element fractionation during anatexis, *Geochim. Cosmochim. Acta, 34*, 237–243, 1970.

Shaw, D. M., Development of the early continental crust, I, Use of trace element distribution coefficient models for the protoarchaean crust, *Can. J. Earth Sci., 9*, 1577–1595, 1972.

Shaw, D. M., G. A. Reilly, J. R. Muysson, G. E. Pattenden, and F. E. Campbell, The chemical composition of the Canadian Precambrian shield, *Can. J. Earth Sci., 4*, 829–854, 1967.

Shaw, D. M., J. Dostal, R. R. Keays, Additional estimates of continental surface Precambrian shield composition in Canada, *Geochim. Cosmochim. Acta, 40*, 73–83, 1976.

Shimizu, N., An experimental study of the partitioning of K, Rb, Cs, Sr and Ba between clinopyroxene and liquid at high pressures, *Geochim. Cosmochim. Acta, 38*, 1789–1798, 1974.

Shimizu, N., and I. Kushiro, The partition of rare earth elements between garnet and liquid at high pressures: Preliminary experiments, *Geophys. Res. Lett., 2*, 413–416, 1975.

Smith, J. V., Possible controls on the bulk composition of the earth: Implications for the origin of the earth and moon, *Proc. Lunar Sci. Conf. 8th*, 333–369, 1977.

Spooner, E. T. C., The strontium isotopic composition of seawater, and seawater-oceanic crust interaction, *Earth Planet. Sci. Lett., 31*, 167–174, 1976.

Sun, S. S., and R. W. Nesbitt, Chemical heterogeneity of the Archaen mantle, composition of the earth and mantle evolution, *Earth Planet. Sci. Lett., 35*, 429–448, 1977.

Tatsumoto, M., Isotopic composition of lead in oceanic basalt and its implication to mantle evolution, *Earth Planet. Sci. Lett., 38*, 63–87, 1978.

Taylor, S. R., Trace element abundances and the chondritic earth model, *Geochim. Cosmochim. Acta, 28*, 1989–1998, 1964.

Taylor, S. R., Island arc models and the composition of the continental crust, in *Island Arcs, Deep Sea Trenches, and Back Arc Basins*, edited by M. Talwani and W. Pitman, AGU, Washington, D. C., 1977.

Taylor, S. R., and A. J. R. White, Geochemistry of andesites and the growth of continents, *Nature, 205*, 271–273, 1965.

Tera, F., D. A. Papanastassiou, and G. J. Wasserburg, Isotopic evidence for a terminal lunar cataclysm, *Earth Planet. Sci. Lett., 22*, 1–21, 1974.

Wasserburg, G. J., Pb-U-Th evolution models for homogenous systems with transport (abstract), *Eos Trans. AGU, 45*, 111, 1964.

Wasserburg, G. J., Geochronology and isotopic data bearing on the development of the continental crust, in *Advances in Earth Sciences*, MIT Press, Cambridge, Mass., 1966.

Wasserburg, G. J., G. F. J. MacDonald, F. Hoyle, and W. A. Fowler, Relative contributions of uranium, thorium and potassium to heat production in the earth, *Science, 143*, 465–467, 1964.

Weill, D. F., and G. A. McKay, The partitioning of Mg, Fe, Sr, Ce, Sm, Eu and Yb in lunar igneous systems and a possible origin of Kreep by equilibrium partial melting, *Proc. Lunar Sci. Conf. 6th*, 1143–1158, 1975.

Veizer, J., and W. Compston, $^{87}Sr/^{86}Sr$ composition of seawater during the Phanerozoic, *Geochim. Cosmochim. Acta, 38*, 1461–1484, 1974.

Williams, D. L., and R. P. von Herzen, Heat loss from the earth; New estimate, *Geology, 2*, 327–328, 1975.

(Received May 22, 1979;
accepted August 14, 1979.)

APPENDIX 4.

Sm-Nd ISOTOPIC EVOLUTION OF CHONDRITES

Stein B. Jacobsen and G. J. Wasserburg

The Lunatic Asylum of the Charles Arms Laboratory
Division of Geological and Planetary Sciences
California Institute of Technology
Pasadena, California 91125

Division Contribution Number 3371 (336)

Abstract

The $^{143}Nd/^{144}Nd$ and $^{147}Sm/^{144}Nd$ ratios have been measured in chondrites. In addition an analysis of the Juvinas achondrite was carried out. The range in $^{143}Nd/^{144}Nd$ is 3.4 ε-units (0.511767 to 0.511845) normalized to $^{150}Nd/^{142}Nd = 0.2096$. This is correlated with the variation of 2.6% in $^{147}Sm/^{144}Nd$ (0.1920 to 0.1969). Assuming a 4.6 AE reference isochron, it is shown that none of the samples deviate more than 0.5 ε-units from this. Insofar as there is a range of values of $^{147}Sm/^{144}Nd$ there is no unique way of picking solar or average chondritic values. From these data we have selected a new set of reference values for CHUR ("chondritic uniform reservoir"). The evolution of $^{143}Nd/^{144}Nd$ in CHUR is defined by a self-consistent set of present-day values of $(^{143}Nd/^{144}Nd)^{o}_{CHUR} = 0.511836$ and $(^{147}Sm/^{144}Nd)^{o}_{CHUR} = 0.1967$. The new $^{147}Sm/^{144}Nd$ value is 1.6% higher than the previous value assigned to CHUR using the Juvinas data of Lugmair. The data presented here appear to be self-consistent and may be used as reference values for CHUR. This will cause a small but significant change in the CHUR evolution curve that is used for reference. Some terrestrial samples of Archean age show clear deviations from the new CHUR curve. If the CHUR curve is representative of undifferentiated mantle then it demonstrates that depleted sources were also tapped early in the Archean. Such a depleted layer may represent the early evolution of the source of present-day MORB. There exist a variety of discrepancies with earlier data which require clarification in order to permit reliable inter-laboratory comparisons.

Introduction

In this paper we present Sm-Nd results for two carbonaceous chondrites (Murchison and Allende), three ordinary chondrites (Peace River, Guareña, and St. Severin), and one achondrite (Juvinas). Murchison is classified as a CM2 chondrite which comprises the most abundant type of carbonaceous chondrites. Allende is a CV3 chondrite and is considered the petrologically most primitive class of carbonaceous chondrites. It contains inclusions of high-temperature condensates, some of which have the most primitive $^{87}Sr/^{86}Sr$ ratio so far found (Gray, Papanastassiou, and Wasserburg, 1973), and inclusions which are isotopically anomalous for Sm and Nd (McCulloch and Wasserburg, 1978a,b) as well as for other elements. Peace River is an L6 chondrite which is a class that constitutes the most abundant of ordinary chondrites. Guareña and St. Severin are H6 and LL6 chondrites, respectively, which have been extensively studied for Rb-Sr, U-Th-Pb, and I-Pu-Xe systematics because of their high content of whitlockite (Wasserburg, Papanastassiou, and Sanz, 1969; Wasserburg, Huneke, and Burnett, 1969; Manhes, Minster and Allègre, 1978). Finally, Juvinas is a basaltic achondrite which has a Sm/Nd ratio close to the average chondritic value and apparently crystallized early in the history of a basaltic achondrite parent body (Lugmair, 1974).

The long-lived isotope ^{147}Sm which decays to ^{143}Nd is an important tracer for chemical differentiation processes affecting the REE and other large ion lithophile (LIL) elements during planetary evolution. The purpose of this paper is to obtain an estimate of the average solar system values for $^{147}Sm/^{144}Nd$ and $^{143}Nd/^{144}Nd$ using chondrite samples. Our ability to determine the solar values depends

on whether the solar nebula was initially isotopically homogeneous for the elements of interest and whether we have samples of material which is chemically unfractionated in Sm relative to Nd. Direct measurements of the abundances of Nd and Sm in the sun have recently been made by Maier and Whaling (1977) and Saffman and Whaling (1979) respectively. These studies give log $(A_{Sm}/A_{Nd})_{\odot} = -0.46\pm0.25$ from which we calculate $(^{147}Sm/^{144}Nd)_{\odot} = 0.22$. From the summary of solar abundances by Ross and Aller (1976), we get log $(A_{Sm}/A_{Nd})_{\odot} = -0.51\pm0.6$ from which we calculate $(^{147}Sm/^{144}Nd)_{\odot} = 0.19$. These values can serve as a guide in the subsequent discussion.

The first survey of REE in chondrites (Schmitt, Smith, Lasch, Mosen, Olehy, and Vasilevskis, 1963; Schmitt, Smith, and Olehy, 1964) demonstrated a reasonable degree of consistency in relative abundances of REE with an accuracy of about 10%. Later the isotope dilution technique was applied to REE in chondrites (Gast, Hubbard, and Weismann, 1970; Schnetzler and Bottino, 1971; Masuda, Nakamura, and Tanaka, 1973; Nakamura and Masuda, 1973; Nakamura, 1974; Evensen, Hamilton, and O'Nions, 1978) with the precision for individual REE considered to be 1 to 2%. The concentration levels of REE in chondrites are fairly low (~0.6 ppm Nd) and no measurements exist on chondrites for both $^{143}Nd/^{144}Nd$ and $^{147}Sm/^{144}Nd$ except for the very approximate data of Notsu and Mabuchi (1975). A 1% error in the Sm/Nd ratio adds an error of 1.1 parts in 10^4 to the $^{143}Nd/^{144}Nd$ ratio over 4.5 AE. Therefore, it is necessary to measure both the $^{147}Sm/^{144}Nd$ and $^{143}Nd/^{144}Nd$ ratios with high precision to establish a $^{143}Nd/^{144}Nd$ evolution curve. We are currently able to routinely measure the $^{147}Sm/^{144}Nd$ ratio with an accuracy of 0.5‰ and the error added to a $^{143}Nd/^{144}Nd$ evolution curve from the measurement of the Sm/Nd ratio is therefore insignificant

(i.e., it is 6 parts in 10^6). The first serious meteorite measurements were made by Lugmair, Scheinin, and Marti (1975a), who chose a basaltic achondrite (Juvinas) which had a $^{147}Sm/^{144}Nd$ isotope ratio close to the average chondritic value. Therefore, if the source of Juvinas on the basaltic achondrite parent body (BACH) did not have a long pre-history as suggested by Rb-Sr and Sm-Nd internal isochrons for Juvinas (Allègre, Birck, Fourcade, and Semet, 1975; Lugmair, 1974), this should give close to the correct values. Lugmair et al. (1975b) used the Juvinas values as an approximation to chondritic Sm-Nd evolution.

Sm-Nd systematics of chondrites

The refractory lithophile elements Si, Mg, and Cr show a factor of two fractionation relative to Al between individual chondrite classes. This is most likely due to fractional condensation (Larimer, 1979). The isotope dilution measurements of REE patterns in chondrites referred to above also indicate a large range of $^{147}Sm/^{144}Nd$ from 0.183 to 0.236; however, the averages of each class of chondrites show a smaller range in $^{147}Sm/^{144}Nd$. The averages of C, E, H, L, and LL chondrites are 0.196, 0.196, 0.195, 0.194, and 0.197, respectively. These values are all within error of each other and identical to the less precisely known solar value of $(^{147}Sm/^{144}Nd)_{\odot} = 0.2$. The extent to which fractional condensation processes have fractionated Sm relative to Nd of individual chondrite classes relative to each other and the average solar system is not known. Clearly variation of a few percent in the Sm/Nd ratio can be allowed for from the data. Much of the variation between individual total rock samples must be due to sample heterogeneity rather than differences between the parent bodies as different total rock samples of a single meteorite may show a variation comparable to

the range in chondrites.

The chemical abundances in CI1 carbonaceous chondrites have a special significance since they compare very closely with the abundances of the condensable elements which can be reliably measured from studies of the photospheric spectrum of the Sun. However, they are not pristine samples of solar system condensate as they show the highest degree of low-temperature alteration among the carbonaceous chondrites (McSween, 1979). The average $^{147}Sm/^{144}Nd$ of CI1 chondrites is 0.197 (Nakamura, 1974; Evensen et al., 1978) and is close to that of other chondrite classes. They, however, do show a 6% range in $^{147}Sm/^{144}Nd$ (0.192 to 0.204) so it appears that a unique value cannot be obtained from these objects. Other classes of chondrites also show variable degrees of alteration and metamorphism. Thus only the consistency of results from a variety of meteorite classes can tell us how well we can estimate the average solar system values.

Some simple evolutionary histories of planetary objects that condensed and accreted from the solar nebula are shown schematically in Fig. 1. At T_C (about 4.6 AE ago) solid objects began condensing from the solar nebula (SN), from which the planets and meteorites are ultimately derived. The rate of growth of $^{143}Nd/^{144}Nd$ in these planetary objects may be different from the solar value due to variations in the relative chemical abundances of Sm and Nd during condensation and accretion. If a reservoir j is a closed system, then the evolution of $^{143}Nd/^{144}Nd$ as a function of time T is defined as $I_j^{Nd}(T)$ with $I_j^{Nd}(0)$ being the present-day value. The value of $^{143}Nd/^{144}Nd$ at any time in the past in reservoir j is

$$I_j^{Nd}(T) = I_j^{Nd}(0) - \left(\frac{^{147}Sm}{^{144}Nd}\right)_j^{o} (\exp(\lambda T) - 1) \qquad (1)$$

where $(^{147}Sm/^{144}Nd)_j^{o}$ is the value in j today. Most meteorites come from small planetary objects and have ages within ~0.1 AE of the time of condensation from the solar nebula and provide important clues to the Sm/Nd isotopic evolution of the solar system. The objects of interest include meteorites which formed by melting processes on parent planets such as achondrites and the more primitive chondrites which appear to be aggregates of high- and low-temperature condensates from the solar nebula. DePaolo and Wasserburg (1976a) introduced the acronym CHUR ("chondritic uniform reservoir") for a bulk planet with $^{147}Sm/^{144}Nd$ and $^{143}Nd/^{144}Nd$ isotopic ratios the same as in average chondrites.

The evolution of chondritic meteorite parent bodies is shown schematically in Fig. 1; Planet A accretes at time T_{A1} with an Sm/Nd ratio lower than the solar value and Planet B accretes at time T_{A2} with Sm/Nd higher than the solar value.

In contrast to chondrites, achondrites are fragments of planetary crusts that began to form by partial melting at the time of early chemical differentiation of a parent body (T_D) subsequent to the time of condensation and will show an evolution as is illustrated schematically in Fig. 1. Magmatic rocks formed subsequent to T_D at T_X may be derived from depleted mantle. There could be a 0.1 AE time difference between planet formation and melting, which for a source region having an enrichment factor $f^{Sm/Nd} = +0.2$ would give 1.0 ε-units difference from the solar value of the $^{143}Nd/^{144}Nd$ growth curve at the time of melting.

If there were reservoirs that were isolated with negligible

amounts of the radioactive parent ^{147}Sm near T_C (Sm/Nd ≈ 0), samples of such materials would record today the $^{143}Nd/^{144}Nd$ value at or near the time of condensation. Because of the limited range in Sm/Nd for minerals in meteorites, it has so far proven difficult to measure $I_{\odot}^{Nd}(T_C)$ precisely. The evolution of $^{143}Nd/^{144}Nd$ in the solar nebula is therefore a rather insensitive chronometer for the relative times of condensation of solid objects from the solar nebula. It is instructive to compare the Sm-Nd system with the solar evolution of the Rb-Sr and U-Th-Pb systems. There is such major chemical fractionation in the U-Th-Pb and Rb-Sr systems that ancient materials exist today which contain Pb and Sr that are very close to the initial solar system values. For example, troilite inclusions in iron meteorites give $^{238}U/^{204}Pb = 0.01$ and have measured $^{206}Pb/^{204}Pb$ isotope ratios within error of the primordial values (Patterson, Brown, Tilton, and Inghram, 1953; Tatsumoto, Knight, and Allegre, 1973). For the U-Pb system the radiogenic daughter Pb is a volatile element and has a low solar value of $(^{238}U/^{204}Pb)_{\odot} \approx 0.2$ (Ross and Aller, 1976), hence the $(^{206}Pb/^{204}Pb)_{\odot}$ today is only slightly evolved relative to primordial lead. In contrast high-temperature condensates, earth, moon, and eucrites have bulk $^{238}U/^{204}Pb$ in the range from ~10 to 250 and thus have highly radiogenic leads. Initial Pb values for meteorites are therefore insensitive to the times of condensation from the solar nebula, while the highly radiogenic leads in volatile poor objects are good chronometers for early solar system processes. For Rb-Sr, achondrites, some ancient lunar samples and high-temperature condensates in Allende have $^{87}Rb/^{86}Sr$ in the range 0.001-0.003 (Papanastassiou and Wasserburg, 1969; Wasserburg, Tera, Papanastassiou, and Huneke, 1977), so their initial $^{87}Sr/^{86}Sr$ can

be almost directly obtained essentially independent of their precise age. The radioactive parent ^{87}Rb is a volatile element and the Sun has a high $(^{87}Rb/^{86}Sr) = 1.4$ (Hauge, 1972) and consequently a highly radiogenic $^{87}Sr/^{86}Sr$ ratio. The Rb-Sr system is, therefore, a very sensitive chronometer for the relative times of condensation of solid objects from the solar nebula.

Samples

The Allende sample (A6) is a split from a 30 gram total meteorite sample prepared by Gray et al. (1973). For Guareña a 193 gram total meteorite sample was powdered from which the metallic phase was removed. The total meteorite concentrations of Sm and Nd in Table 1 have been corrected for the removed metal. St. Severin is known to consist of light and dark colored areas (Wasserburg et al., 1969). A 3 gram piece from a light area of sample H2402b was used for this work. The Peace River sample is a split from a 200 gram total meteorite sample prepared by Gray et al. (1973). The Juvinas sample (#40, Piece A) is a 1.2 gram piece of the total meteorite. For Murchison sample Me2642, two different pieces (#1 and #2) weighing several grams were powdered. The amount of material dissolved in each experiment is given in Table 1.

Analytical procedures

Separation of Sm and Nd follows the procedure described for Gd by Eugster, Tera, Burnett, and Wasserburg (1970) with the slight modifications reported by DePaolo and Wasserburg (1976a). The total procedural blank for Nd is 25 pg or less and $^{147}Sm/^{144}Nd = 0.14$ for the blank. Individual separations from meteorites yielded 60 ng of Nd or more so the blanks are insignificant. Nd and Sm isotopic compositions were

measured on the Lunatic I and III mass spectrometers (Wasserburg, Papanastassiou, Nenow, and Bauman, 1969) as NdO^+ and Sm^+, respectively, following the procedures described in detail by DePaolo and Wasserburg (1976a) and Papanastassiou, DePaolo, and Wasserburg (1977). Concentrations were determined using ^{150}Nd and ^{147}Sm tracers. Extensive calibrations of tracers with normal solutions made up from ultrapure Nd and Sm metals from Ames Laboratory, Iowa, demonstrate that we can routinely measure the $^{147}Sm/^{144}Nd$ ratio to 0.5‰. Details of these calibrations will be discussed elsewhere. The grand mean values of terrestrial normals for nonradiogenic Nd isotopes (Table 1) used are those by McCulloch and Wasserburg (1978a) which are updated values compared to those of DePaolo and Wasserburg (1976b) and Papanastassiou et al. (1977). The grand mean values of terrestrial normals for Sm isotopes (Table 1) used is that of Russ (1974) which are updated values compared to those of Russ, Burnett, Lingenfelter, and Wasserburg (1971). These updated abundances for both Nd and Sm show no change with time and the acquisition of new data and are essentially indistinguishable from the original values of DePaolo and Wasserburg (1976b) and Russ et al. (1971).

Results

The Sm-Nd results are given in Tables 1 and 2 and Fig. 2. We first note that all non-radiogenic isotope ratios are within error of the grand mean of our terrestrial normals and lunar samples measured in this laboratory (Papanastassiou et al., 1977). There are thus no widespread isotopic anomalies in Nd for bulk chondrite samples to within ±0.5 ε-units. For Sm we routinely measured all isotopes except ^{150}Sm and ^{144}Sm and confirmed that $^{149}Sm/^{154}Sm$ and $^{152}Sm/^{154}Sm$ are within error

(±1.0 ε-units) the same as the terrestrial values. The absence of any neutron capture effects on ^{149}Sm is consistent with the short exposure ages of these meteorites (Eugster et al., 1970; Russ et al., 1971). This justifies the use of $^{143}Nd/^{144}Nd$ and $^{147}Sm/^{144}Nd$ isotope ratios calculated from spiked runs using the grand mean values of terrestrial normals for Sm and Nd isotopic compositions.

The data in Table 1 are shown on a Sm-Nd evolution diagram relative to a reference line with a slope corresponding to an age of ~4.6 AE. A variety of chondrites and the achondrite Juvinas lie within ±0.5 ε-units of the reference line shown. This conclusion is insensitive to the particular choice of age in a plausible neighborhood of 4.6 AE. The present-day range in these chondrites is, however, only 3.4 ε-units in $^{143}Nd/^{144}Nd$ and 2.6% in $^{147}Sm/^{144}Nd$ and there is no evidence of large variations. If all chondrites are isochronous and from an isotopically uniform source, they should today lie on a line with a slope of 4.6 AE in a Sm-Nd evolution diagram. Insofar as there is variation in the Sm/Nd ratio between chondrite samples, there is no unique way of picking a set of values for $^{143}Nd/^{144}Nd$ and $^{147}Sm/^{144}Nd$ as representing the true solar ratio. The best we can do from the data is to pick a single set of reference values for $^{143}Nd/^{144}Nd$ and $^{147}Sm/^{144}Nd$ today that are consistent with the data array in Fig. 2. The approach used here will be to define the best present-day "solar" reference values rather than initial value $I_j^{Nd}(T_C)$ since the initial state is not well constrained. This follows the view adopted by DePaolo and Wasserburg (1976a) who referred evolution curves to determinations of the modern values rather than the derived initial values. For

simplicity the approach we have chosen is the modern value for $^{143}Nd/^{144}Nd = 0.511836$, which is the currently used value for CHUR, as this will cause the least shift in the data representations and is fully consistent with the chondritic values. The corresponding $^{147}Sm/^{144}Nd$ ratio on the reference isochron is 0.1967 and lies between the data for Allende and one of the Murchison samples. This is also very close to the average $^{147}Sm/^{144}Nd$ of chondrites discussed earlier. Including the new data in Table 1 there are now 61 determinations of $^{147}Sm/^{144}Nd$ in bulk chondrite samples by isotope dilution. All these data are shown in a histogram in Fig. 3. As shown the value we have chosen lies close to the peak of the histogram. The previously published data are not accurate to better than about ±2% and most of the data actually are within 2% of the average value chosen for chondrites. However, clear exceptions occur especially for the E-chondrites which show a variation in $^{147}Sm/^{144}Nd$ from 0.183 to 0.236. In general, the $^{143}Nd/^{144}Nd$ chosen here is close to that of Lugmair, Marti, Kurtz, and Scheinin (1976) for Juvinas, however the Sm/Nd ratio is 1.6% higher.

Comparison with previously published data

Previously published data on basaltic achondrites that fall in the neighborhood of our chondrite data are shown (Fig. 4) together with our new data on chondrites and Juvinas. The isochrons of ADOR and Moama are also shown, although all the data for these meteorites plot far outside the diagram. Let us first compare the Juvinas total rock data from various laboratories. The first report was by Notsu, Mabuchi, Yoshioku, Matsuda, and Ozima (1973) who presented some rather approximate data. The first high-precision data were published by Lugmair (1974) and

Lugmair, Scheinin, and Marti (1975a). The total rock value used by Lugmair, Scheinin, and Marti (1975b) (L1) is about 3.8 ε-units above our 4.6 AE reference line. A revised value (L2) with the same Sm/Nd ratio was reported by Lugmair et al. (1976) and is still 1.9 ε-units above our reference line. Lugmair and Carlson (1978) reported a 1.4 ε-unit reduction in the measured $^{143}Nd/^{144}Nd$ ratio for their laboratory standard. They chose, however, to correct their new data such that they were compatible with their previously published data. Their currently measured Juvinas value (L3) should thus be 1.4 ε-unit lower and as shown in Fig. 4 this value is within error of our 4.6 AE reference line. The values obtained by Nakamura, Tatsumoto, Nunes, Unruh, Schwab, and Wildeman (1976) for Juvinas plot distinctly higher. Their value is the same as L3 for $^{143}Nd/^{144}Nd$ but has a lower Sm/Nd ratio. Recently Nyquist, Shih, Wooden, Bansal, and Wiesman (1979) published data on Juvinas which agree with the measured (not corrected) $^{143}Nd/^{144}Nd$ L3 ratio by Lugmair and the value by Nakamura et al. (1976) but with a significantly higher $^{147}Sm/^{144}Nd$ ratio. Data on Juvinas by Nyquist et al. (1979) and the data obtained independently by us agree to within 1‰ for $^{147}Sm/^{144}Nd$ and 0.3 ε-units for $^{143}Nd/^{144}Nd$. It would appear that the data of Nakamura et al. (1976) and the revised data (L3) of Lugmair and Carlson (1978) are consistent with the $^{143}Nd/^{144}Nd$ obtained by Nyquist et al. (1979) and ourselves, but their $^{147}Sm/^{144}Nd$ ratios are significantly lower and suggest an error in tracer calibrations by these workers. The data for Pasamonte (Unruh, Nakamura, and Tatsumoto, 1977), Moama (Hamet, Nakamura, Unruh, and Tatsumoto, 1978), and ADOR (Lugmair and Marti, 1977) also lie significantly above our

reference line (Fig. 4). Comparison between the results of Nyquist et al. (1979) and our data on achondrites seems to be confirmatory. We note, however, that Nyquist et al. (1979) obtained metals for tracer calibration from the same source that we have been using (Ames Laboratory, Iowa), so both laboratories could have the same systematic errors in tracer calibrations. The normal values measured for $^{142}Nd/^{144}Nd$, $^{150}Nd/^{144}Nd$ reported by Nyquist et al. (1979) differ significantly from our values while the remaining isotope ratios show good agreement. Thus the results from these two laboratories are not as consistent as might be believed. It is apparent that the actual cause of all the above discrepancies must be resolved before any progress can be made in interlaboratory comparisons. Using two different mass spectrometers in this laboratory for hundreds of Nd analyses, we observe no shift in the values of the nonradiogenic Nd isotopes over the past five years. In the same period, three different Nd and three different Sm tracer calibrations show no discrepancies exceeding 1‰. We measure Nd as NdO^+ so if the oxygen isotope composition used to reduce the data is incorrect then our data will be systematically biased (Papanastassiou et al., 1977). Unless this procedure is subject to serious problems, we consider the measurements presented here to be reliable and provide reasonable and consistent values for the chondritic $^{143}Nd/^{144}Nd$ and $^{147}Sm/^{144}Nd$ today and may be used as the basis for calculating the CHUR curve.

Initial values

The $^{143}Nd/^{144}Nd$ in CHUR as a function of time in the neighborhood of 4.5 AE is shown in Fig. 5. Assuming that a meteorite formed from this reservoir at T = 4.6 AE, it should have an initial $^{143}Nd/^{144}Nd$

value of 0.505829. We note that $^{143}Nd/^{144}Nd$ changes by 1 ε-unit in 39 m.y. The timescale for condensation and chemical fractionation from the solar nebula is probably on the order of only a few million years as suggested by the presence of ^{26}Al (Lee, Papanastassiou, and Wasserburg, 1976,1977). If the ^{26}Al is the cause of widespread heating and differentiation of small parent bodies, then these planets must have accreted within ~2 m.y. of the time of condensation from the solar nebula (Wasserburg et al., 1977). Chondrites (e.g., Allende) exist that appear to preserve direct early condensates from the solar nebula which are only partly affected by later metamorphism. A reliable value for the solar system initial Nd value may be gotten if it is possible to obtain precise ages (±10 m.y.) and initial values to ±0.3 ε-units on such samples with an internal mineral isochron. If large planetary objects took 10^8 years to form as suggested by Safronov (1969), Tera and Wasserburg (1974), and Gancarz and Wasserburg (1977), then the initial $^{143}Nd/^{144}Nd$ could be 2.5 ε-units higher than that from the early condensates from the solar nebula. Although the initial state is not well known, we may in principle pick any set of self-consistent initial $^{143}Nd/^{144}Nd$, age and Sm/Nd ratio that plot on the CHUR curve as reference values to describe the CHUR evolution curve instead of the present-day values we are using. In absence of directly measured initial solar values [i.e., $T_C, I_{\odot}^{Nd}(T_C)$], it is important to pick a set of reference values which the solar system is believed to have passed through and that is prior to planetary differentiation processes. Model ages (cf. Wasserburg and Papanastassiou, 1975) may be calculated relative to such a chosen initial Nd value ($I_{\odot}^{Nd}(T_C)$) for the solar system

$$T_M^{Nd} = \frac{1}{\lambda} \ln \left[1 + \frac{(^{143}Nd/^{144}Nd)_{MEAS} - I_{\odot}^{Nd}(T_C)}{(^{147}Sm/^{144}Nd)_{MEAS}} \right] \quad (2)$$

and should be compared to the corresponding initial time T_C on the CHUR curve. We may pick the values shown in Fig. 5 as T_C = 4.6 AE and $I(T_C)$ = 0.505829. Samples which have T_M^{Nd} close to T_C may represent ancient materials with a simple history. If $T_M^{Nd} \gg T_C$ or $T_M^{Nd} \ll T_C$, then this demonstrates open system behavior at times less than 4.6 AE. The model age T_M^{Nd} is a strict upper limit to the last time of disturbance of the system. As chemical fractionation for Sm relative to Nd is often small for total rocks, the T_M^{Nd} model ages are currently of far less utility than corresponding model ages for the Rb-Sr system where large chemical fractionations are common.

Hamilton, O'Nions, Evensen, Bridgwater, and Allaart (1978) have chosen an initial state using the initial Nd from ADOR and the age of ADOR together with average Sm/Nd determined from REE-studies of chondrites by Evensen et al. (1978) as a reference value for the CHUR curve. This selection is inconsistent with the new CHUR curve presented here due to the fact that the ADOR initial value does not plot on it.

Data representation

Following DePaolo and Wasserburg (1976a) the $^{143}Nd/^{144}Nd$ ratio in a reservoir j at time T is expressed as the fractional deviation in parts in 10^4 from that in CHUR at time T and denoted by $\varepsilon_{Nd}^{j}(T)$. Let $I_j^{Nd}(T)$ be the $^{143}Nd/^{144}Nd$ ratio in a reservoir j at time T, then we have

$$\varepsilon_{Nd}^{j}(T) = 10^4 \left[\frac{I_j^{Nd}(T)}{I_{CHUR}^{Nd}(T)} - 1 \right] \quad (3)$$

Here $I^{Nd}_{CHUR}(T)$ is given by equation (1) with j = CHUR. Initial $^{143}Nd/^{144}Nd$ ratios for a rock may be expressed in ε-units relative to the CHUR curve using equation (3). Then $I^{Nd}_{j}(T)$ is the initial value determined by an internal isochron as calculated from the present-day values of $^{143}Nd/^{144}Nd$ and $^{147}Sm/^{144}Nd$ of the rock and an independently determined age through equation (1). The measured present-day values of $^{143}Nd/^{144}Nd$ in rock samples relative to $I^{Nd}_{CHUR}(0)$ are also often given in ε-units and are denoted $\varepsilon_{Nd}(0)$. We have chosen $I^{Nd}_{CHUR}(0)$ = 0.511836 as before and a new value $(^{147}Sm/^{144}Nd)^{o}_{CHUR}$ = 0.1967 which is 1.6% higher than the previous value of 0.1936. Values of $\varepsilon_{Nd}(0)$ will be unchanged if they are referred to the above $I^{Nd}_{CHUR}(0)$ value. However, the $I^{Nd}_{CHUR}(T)$ values calculated from (1) will be changed and consequently $\varepsilon_{Nd}(T)$ will also be changed due to the new value for $(^{147}Sm/^{144}Nd)^{o}_{CHUR}$. The $^{147}Sm/^{144}Nd$ ratio in a reservoir j is expressed as the enrichment factor relative to CHUR

$$f_j^{Sm/Nd} = \frac{(^{147}Sm/^{144}Nd)_j}{(^{147}Sm/^{144}Nd)^{o}_{CHUR}} - 1 \qquad (4)$$

and this value will also be changed. Model calculations for crust and mantle evolution can be made with linearized equations due to the long halflife of ^{147}Sm. Consider a reservoir j which is derived from CHUR in a single differentiation event at time T_D. As shown by DePaolo and Wasserburg (1976a), at a time T subsequent to the time of differentiation we have to a good approximation that

$$\varepsilon^{j}_{Nd}(T) = Q_{Nd}\, f_j^{Sm/Nd}(T_D - T) \qquad (5)$$

where

$$Q_{Nd} = 10^4\lambda \left(\frac{^{147}Sm}{^{143}Nd}\right)^{o}_{CHUR} \qquad (6)$$

Similar equations have been shown by Jacobsen and Wasserburg (1979) to be valid for models of continuous or multiepisodic evolution of crust and mantle, the only difference being the interpretation of the time parameter. The new values for CHUR give $Q_{Nd} = 25.13\ AE^{-1}$ for $\lambda = 0.00654\ AE^{-1}$ as compared to the previous value of $24.73\ AE^{-1}$. These small changes will not cause any major revisions in previous model calculations.

The Nd evolution curve for the earth

The old CHUR curve was shown to be a good representation of the terrestrial values, although there are clear discrepancies. We now want to address what the correlation looks like back through time using the new parameters. We therefore consider the data on Archean rocks where the claim has been made that most of the data fit the CHUR curve. All available Archean data are shown in Fig. 6. The small shifts in the CHUR evolution curve reported here do not alter the basic conclusions by other workers that the isotopic composition of Nd in a variety of crustal rocks follows the evolution of a reservoir with chondritic Sm/Nd. However, the more refined results reported here make it evident that more stringent tests are needed. The data on the Lewisian rocks (2.9 AE) and the Isua volcanics (3.8 AE) now plot ~2.5 ε-units above the curve. These positive ε_{Nd} values indicate the presence of a depleted layer in the mantle throughout the Archean. Such a layer may represent the early evolution of the source of the present-day mid-ocean ridge basalts which have $\varepsilon_{Nd} \approx +10$. This implies that the source of the Isua volcanics was residual mantle

material that was involved in crust-forming events at least 4.2 AE ago. Most of the other data are still within error of the CHUR curve; however, they are subject to rather large uncertainties. The only precise data point is for the Stillwater (DePaolo and Wasserburg, 1979) which plots distinctly below the curve. The apparent deviations from the CHUR curve in this time region are rather large and comparable with the modern variations considering the shortened time scale. For a detailed understanding of the evolution of the Archean mantle, it will be necessary to obtain much more precise initial values and ages for Archean samples than are currently available.

We note that we are not able to define the present-day $^{143}Nd/^{144}Nd$ in chondrites uniquely due to variability of their Sm/Nd ratio. It is possible that this is a sampling problem and that all planets formed with exactly the same values. Alternatively, bulk planets could be fractionated by 1 to 2% from the solar Sm/Nd ratio. It is well established that $\varepsilon_{Nd}(0) \approx +10$ for mid-ocean ridge basalts which clearly must sample a depleted mantle (DM). The only major enriched reservoir in the earth is the continental crust (CC) which has $\varepsilon_{Nd} \approx -18$ and is complementary to the depleted mantle (see for example, DePaolo and Wasserburg, 1976a; Jacobsen and Wasserburg, 1979). The bulk earth value has to be somewhere in between these two values. A logical choice is $\varepsilon_{Nd}(0) \approx 0$ for the bulk earth. Currently we would assign some special significance to young rocks that cluster in the range between A and B on Fig. 7, namely that they are derived from a chondritic undifferentiated reservoir. However, if $\varepsilon_{Nd}^{\oplus}(0) = +2$ as shown schematically in Fig. 7, then undifferentiated mantle materials would have this value and basalts with a value of $\varepsilon_{Nd}(0) \approx 0$ would then be assumed to represent mixtures of magmas derived from depleted mantle

and old continental crust. If many terrestrial samples plotted precisely on a curve close or identical to the CHUR curve back through time, then this would be strong evidence that these rocks were derived through time from undifferentiated mantle materials. As discussed previously at present the terrestrial data do not precisely define a curve back through time. This makes it difficult to decide whether the data are sufficient evidence for an undifferentiated reservoir in the earth or whether the terrestrial data that roughly follow the CHUR curve represent mixtures of depleted mantle and old continental crust back through time. In the absence of a very well-defined curve based on terrestrial samples, we will use the CHUR curve as an approximation to the bulk earth. Model ages T^{Nd}_{CHUR} may be calculated relative to the CHUR curve (DePaolo and Wasserburg, 1976b)

$$T^{Nd}_{CHUR} = \frac{1}{\lambda} \ell n \left[1 + \frac{(^{143}Nd/^{144}Nd)_{MEAS} - I^{Nd}_{CHUR}(0)}{(^{147}Sm/^{144}Nd)_{MEAS} - (^{147}Sm/^{144}Nd)^{o}_{CHUR}} \right] \quad (7)$$

For typical continental crustal rocks with $f^{Sm/Nd} \approx -0.4$, the new model parameters will only cause small changes in the previously published T^{Nd}_{CHUR} model ages. For small fractionations like those observed in the lunar highland samples of $f^{Sm/Nd} \approx -0.14$, the T^{Nd}_{CHUR} model ages have large uncertainties and are very sensitive to small changes in the model parameters (Oberli, McCulloch, Tera, Papanastassiou, and Wasserburg). The new CHUR values change the T^{Nd}_{CHUR} model ages of Oberli *et al.* (1978) to values $\sim$0.5 AE younger and thus are more in agreement with Rb-Sr and U-Pb data on the same samples.

Conclusions

From the data presented we conclude that a self-consistent set of average present-day values for chondritic meteorites are $^{143}Nd/^{144}Nd = 0.511836$ and $^{147}Sm/^{144}Nd = 0.1967$. $^{143}Nd/^{144}Nd$ changes by 1 ε-unit in 39 m.y. in CHUR so the uncertainty in the initial time makes it difficult at present to know the initial solar value for $^{143}Nd/^{144}Nd$ precisely. These values are not consistent with most previously published achondrite data, but are consistent with our achondrite data and that reported by Nyquist et al. (1979). The presence of inter-laboratory discrepancies in meteorite data is evident and may be due to errors in Sm and Nd spike calibrations or to measurement of isotopic abundances. Some terrestrial Archean samples now show clear positive deviations from the CHUR evolution curve, which were not evident using the old model parameters for CHUR. The new parameters only make small changes in published T^{Nd}_{CHUR} model ages for highly fractionated samples.

Acknowledgments

This work has been supported by NSF grant EAR 76-22494 and NASA grant NGL 05-002-188. We thank D. A. Papanastassiou for his comments on the manuscript and his generous aid in matters spectrometric. The sources of the meteorite samples are as follows: Murchison, Field Museum of Natural History, Chicago. St. Severin, Museum of Natural History, Paris. Juvinas, Arizona State University. Peace River, University of Alberta. Guareña, Museo Nacional de Ciencias Naturales de Madrid.

References

Allègre, C. J., J. L. Birck, S. Fourcade, and M. Semet, $^{87}Rb/^{87}Sr$ age of the Juvinas achondrite and early igneous activity of the solar system, Science, 187, 436-438, 1975.

DePaolo, D. J. and G. J. Wasserburg, Nd isotopic variations and petrogenetic models, Geophys. Res. Letts., 3, 249-252, 1976a.

DePaolo, D. J. and G. J. Wasserburg, Inferences about magma sources and mantle structure from variations of $^{143}Nd/^{144}Nd$, Geophys. Res. Letts., 3, 743-746, 1976b.

DePaolo, D. J. and G. J. Wasserburg, Sm-Nd age of the Stillwater Complex and the mantle evolution curve for Neodymium, Geochim. Cosmochim Acta, 43, 999-1008, 1979.

Eugster, O., F. Tera, D. S. Burnett, and G. J. Wasserburg, The isotopic composition of Gadolinium and neutron capture effects in some meteorites, J. Geophys. Res., 75, 2753-2768, 1970.

Evensen, N. M., P. J. Hamilton, and R. K. O'Nions, Rare-earth abundances in chondritic meteorites, Geochim. Cosmochim. Acta, 42, 1199-1212, 1978.

Gancarz, A. J. and G. J. Wasserburg, Initial Pb of the Amitsoq gneiss, west Greenland, and implications for the age of the earth, Geochim. Cosmochim. Acta, 41, 1283-1301, 1977.

Gast, P. W., N. J. Hubbard, and H. Weismann, Chemical composition and petrogenesis of basalts of Tranquility Base, In Proc. Apollo 11 Lunar Sci. Conf., pp. 1143-1163, Pergamon Press, 1970.

Gray, C. M., D. A. Papanastassiou, and G. J. Wasserburg, The identification of early condensates from the solar nebula, Icarus, 20, 213-239, 1973.

Hamet, J., N. Nakamura, D. M. Unruh, and M. Tatsumoto, Origin and history of the adcumulate eucrite, Moama as inferred from REE abundances, Sm-Nd and U-Pb systematics, Proc. Lunar Planet. Sci. Conf. 9th, p. 1115-1136, 1978.

Hamilton, P. J., R. K. O'Nions, and N. M. Evensen, Sm-Nd dating of Archean basic and ultrabasic volcanics, Earth Planet. Sci. Lett., 36, 263-268, 1977.

Hamilton, P. J., R. K. O'Nions, N. M. Evensen, D. Bridgwater, and J. Allaart, Sm-Nd isotopic investigations of the Isua supracrustals, West Greenland: implications for mantle evolution, Nature, 272, 41-43, 1978.

Hamilton, P. J., N. M. Evensen, R. K. O'Nions, and J. Tarney, Sm-Nd systematics of Lewisian gneisses: implications for the origin of granulites, Nature, 277, 25-28, 1979.

Hamilton, P. J., N. M. Evensen, R. K. O'Nions, H. S. Smith, and A. J. Erlank, Sm-Nd dating of Onverwacht Group Volcanics, southern Africa, Nature, 279, 298-300, 1979.

Hauge, O., A search for the solar ^{87}Sr content and the solar Rb/Sr ratio, Solar Phys., 26, 276-282, 1972.

Jacobsen, S. B. and G. J. Wasserburg, The mean age of mantle and crustal reservoirs, J. Geophys. Res., 84, 7411-7427, 1979.

Larimer, J. W., The condensation and fractionation of refractory lithophile elements, Icarus, 40, 446-454, 1979.

Lee, T., D. A. Papanastassiou, and G. J. Wasserburg, Demonstration of ^{26}Mg excess in Allende and evidence for ^{26}Al, Geophys. Res. Lett., 3, 109-112, 1976.

Lee, T., D. A. Papanastassiou, and G. J. Wasserburg, ^{26}Al in the early solar system: Fossil or fuel?, The Astrophysical J. Lett., 211, 107-110, 1977.

Lugmair, G. W., Sm-Nd ages: a new dating method (abs.) Meteoritics, 9, 369, 1974.

Lugmair, G. W., N. B. Scheinin, and K. Marti, Search for extinct ^{146}Sm, 1. The isotopic abundance of ^{142}Nd in the Juvinas meteorite, Earth Planet. Sci. Lett., 27, 79-84, 1975a.

Lugmair, G. W., N. B. Scheinin, and K. Marti, Sm-Nd age and history of Apollo 17 basalt 75075: Evidence for early differentiation of the Lunar exterior, Proc. Lunar Sci. Conf. 6th, 1419-1429, 1975b.

Lugmair, G. W., K. Marti, J. P. Kurtz, and N. B. Scheinin, History and genesis of lunar troctolite 76535 or: How old is old? Proc. Lunar Sci. Conf. 7th, 2009-2033, 1976.

Lugmair, G. W. and K. Marti, Sm-Nd-Pu timepieces in the Angra dos Reis meteorite, Earth Planet. Sci. Lett., 35, 273-284, 1977.

Lugmair, G. W. and R. W. Carlson, The Sm-Nd history of KREEP, Proc. Lunar Sci. Conf. 9th, 689-704, 1978.

Maier, R. S. and W. Whaling, Transition probabilities in Nd (II) and the solar neodymium abundance, J. Quant. Spectrosc. Radiat. Transfer, 18, 501-507, 1977.

Manhes, G., J. F. Minster, and C. J. Allègre, Comparative uranium-thorium-lead and rubidium-strontium study of the Saint Sèverin amphoterite: consequences for early solar system chronology, Earth. Planet. Sci. Lett., 39, 14-24, 1978.

Masuda, A., N. Nakamura, and T. Tanaka, Fine structures of mutually normalized rare-earth patterns of chondrites, Geochim. Cosmochim. Acta, 37, 239-248, 1973.

McCulloch, M. T. and G. J. Wasserburg, Barium and Neodymium isotopic anomalies in the Allende meteorite, The Astrophysical J., 220, L15-L19, 1978a.

McCulloch, M. T. and G. J. Wasserburg, More anomalies from the Allende meteorite: Samarium, Geophys. Res. Lett., 5, 599-602, 1978b.

McCulloch, M. T. and G. J. Wasserburg, Sm-Nd and Rb-Sr chronology of continental crust formation, Science, 200, 1003-1011, 1978c.

McCulloch, M. T., Part I. Sm-Nd and Rb-Sr chronology of crustal formation. Part II. Ba, Nd, and Sm isotopic anomalies in the Allende meteorite, Ph.D. thesis, California Institute of Technology, Pasadena, 1979.

McSween, H. Y., Are carbonaceous chondrites primitive or processed? Rev. Geophys. Space Phys., 17, 1059-1078, 1979.

Nakamura, N., Determination of REE, Ba, Fe, Mg, Na, and K in carbonaceous and ordinary chondrites, Geochim. Cosmochim. Acta, 38, 757-775, 1974.

Nakamura, N. and A. Masuda, Chondrites with peculiar rare-earth element patterns, Earth Planet. Sci. Lett., 9, 359-364, 1973.

Nakamura, N., M. Tatsumoto, P. D. Nunes, D. M. Unruh, A. P. Schwab, and T. R. Wildeman, 4.4 b.y.-old clast in Boulder 7, Apollo 17: A comprehensive chronological study by U-Pb, Rb-Sr, and Sm-Nd methods, Proc. Lunar Sci. Conf. 7th, p. 2309-2333, 1976.

Notsu, K. and H. Mabuchi, The samarium-neodymium chronology of chondrites, Geochemical Journal, 9, 97-106, 1975.

Notsu, K., H. Mabuchi, O. Yoshioku, J. Matsuda, and M. Ozima, Evidence of the extinct nuclide ^{146}Sm in "Juvinas" achondrite, Earth Planet. Sci. Lett., 19, 29-36, 1973.

Nyquist, L. E., C.-Y. Shih, J. L. Wooden, B. M. Bansal, and H. Wiesmann, The Sr and Nd isotopic record of Apollo 12 basalts: Implications for lunar geochemical evolution, Proc. Lunar Sci. Conf. 10th (in press) 1979.

Oberli, F., M. T. McCulloch, F. Tera, D. A. Papanastassiou, and G. J. Wasserburg, Early lunar differentiation constraints from U-Th-Pb, Sm-Nd, and Rb-Sr model ages (abs.), In Lunar and Planetary Science IX, p. 832-834, Lunar and Planetary Institute, Houston, 1978.

Papanastassiou, D. A. and G. J. Wasserburg, Initial strontium isotopic abundances and the resolution of small time differences in the formation of planetary objects, Earth Planet. Sci. Lett., 5, 361-376, 1969.

Papanastassiou, D. A., D. J. DePaolo, and G. J. Wasserburg, Rb-Sr and Sm-Nd chronology and genealogy of basalts from the Sea of Tranquility, Proc. Lunar Sci. Conf. 8th, 1639-1672, 1977.

Patterson, C. C., H. Brown, G. R. Tilton, and M. Inghram, Concentration of uranium and lead and the isotopic composition of lead in meteoritic material, Phys. Rev., 92, 1234-1235, 1953.

Ross, J. E. and L. H. Aller, The chemical composition of the Sun, Science, 191, 1223-1229, 1976.

Russ, G. P., III, Neutron stratigraphy in the lunar regolith, Ph.D. thesis, California Institute of Technology, Pasadena, 1974.

Russ, G. P., D. S. Burnett, R. E. Lingenfelter, and G. J. Wasserburg, Neutron capture on ^{147}Sm in lunar samples, Earth Planet. Sci. Lett., 13, 53-60, 1971.

Saffman, L. and W. Whaling, Transition probabilities in Sm II and the solar abundance of samarium, J. Quant. Spectrosc. Radiat. Transfer, 21, 93-98, 1979.

Safranov, V. S., Evolution of the protoplanetary cloud and the formation of the earth and planets (in Russian), Nauka Moscow, English transl. as NASA TT F-677, NTIS, Springfield, VA, 1972.

Schmitt, R. A., R. H. Smith, J. E. Lasch, A. W. Mosen, P. A. Olehy, and J. Vasilevskis, Abundances of fourteen rare-earth elements, scandium and yttrium in meteoritic and terrestrial matter, Geochim. Cosmochim. Acta, 27, 577-622, 1963.

Schmitt, R. A., R. H. Smith, and D. A. Olehy, Rare earth, yttrium and scandium abundances in meteoritic and terrestrial matter - II, Geochim. Cosmochim. Acta, 28, 67-86, 1964.

Schnetzler, C. C. and M. L. Bottino, Some alkali, alkaline-earth and rare-earth element concentrations and the Rb-Sr age of the Lost City meteorite and separated phases, J. Geophys. Res., 76, 4061-4066, 1971.

Tanaka, T. and M. Masuda, Rare-earth elements in matrix, inclusions and chondrules of the Allende meteorite, Icarus, 19, 523-530, 1973.

Tatsumoto, M., R. J. Knight, and C. J. Allègre, Time differences in the formation of meteorites as determined from the ratio of lead-207 to lead-206, Science, 180, 1279-1283, 1973.

Tera, F. and G. J. Wasserburg, U-Th-Pb systematics on lunar rocks and inferences about lunar evolution and the age of the moon, Proc. Lunar Sci. Conf. 5th, p. 1571-1599, 1974.

Unruh, D. M., N. Nakamura, and M. Tatsumoto, History of the Pasamonte Achondrite: Relative susceptibility of the Sm-Nd, Rb-Sr, and U-Pb systems to metamorphic events, Earth Planet. Sci. Lett., 37, 1-12, 1977.

Wasserburg, G. J., J. C. Huneke, and D. S. Burnett, Correlation between fission tracks and fission type Xenon in meteoritic whitlockite, J. Geophys. Res., 74, 4221-4232, 1969.

Wasserburg, G. J. and D. A. Papanastassiou, Model ages, Nature, 259, 159-160, 1976.

Wasserburg, G. J., D. A. Papanastassiou, E. V. Nenow, and C. A. Bauman, A programmable magnetic field mass spectrometer with on-line data processing, Rev. Sci. Inst., 40, 288-295, 1969.

Wasserburg, G. J., D. A. Papanastassiou, and H. G. Sanz, Initial strontium for a chondrite and the determination of a metamorphism or formation interval, Earth Planet. Sci. Lett., 7, 33-43, 1969.

Wasserburg, G. J., F. Tera, D. A. Papanastassiou, and J. C. Huneke, Isotopic and chemical investigations on Angra dos Reis, Earth Planet. Sci. Lett., 35, 294-316, 1977.

Zindler, A., C. Brooks, N. T. Arndt, and S. Hart, Nd and Sr isotope data from komatitic and tholeiitic rocks of Munro Township, Ontario, In Short Papers of the Fourth International Conference, Geochronology, Cosmochronology, Isotope Geology, U.S. Geol. Surv. Open-File Report, 78-701, 476 p., 1978.

Table 1. Sm-Nd isotopic results.[c]

Sample	Weight[d] (grams)	Nd(ppm)	Sm(ppm)	$\frac{^{147}Sm}{^{144}Nd}$	$\frac{^{143}Nd}{^{144}Nd}$	
I. Murchison (CM2)						
#1-ALIQ-1	0.51	0.63495	0.20671	0.19693	-	a
ALIQ-2		-	-	-	0.511845±29	b
ALIQ-3		0.63506	0.20672	0.19691	0.511816±25	a
#2	0.44	0.67034	0.21409	0.19320	0.511738±34	a
II. Allende (CV3)						
ALIQ-1	2.61	0.86957	0.28230	0.19639	-	a
ALIQ-2		-	-	-	0.511809±26	b
ALIQ-2		-	-	-	0.511839±25	b
III. Guareña (H6)						
	2.52	0.90208	0.29031	0.19468	0.511769±24	a
IV. Peace River (L6)						
ALIQ-1	2.97	0.69854	0.22615	0.19584	-	a
ALIQ-2		-	-	-	0.511831±32	b
V. St. Severin (LL6)						
Light	2.86	1.38562	0.43972	0.19197	0.511673±25	a
VI. Juvinas						
ALIQ-1	1.24	5.5245	1.7848	0.19543	0.511804±19	a

[a]Sample spiked with ^{150}Nd and ^{147}Sm tracers. Data normalized to $^{146}Nd/^{142}Nd = 0.636151$ and $^{148}Sm/^{154}Sm = 0.49419$. Concentrations calculated using $^{142}Nd/^{144}Nd = 1.138266$, $^{145}Nd/^{144}Nd = 0.348968$, $^{146}Nd/^{144}Nd = 0.724109$, $^{148}Nd/^{144}Nd = 0.243079$, $^{150}Nd/^{144}Nd = 0.238581$ (McCulloch and Wasserburg, 1978a) and an atomic weight of 144.24 for Nd. For Sm we used an atomic weight of 150.35 and the isotopic composition reported by Russ et al. (1971) and Russ (1974); $^{144}Sm/^{154}Sm = 0.13516$, $^{147}Sm/^{154}Sm = 0.65918$, $^{149}Sm/^{154}Sm = 0.60750$, $^{150}Sm/^{154}Sm = 0.32440$, $^{152}Sm/^{154}Sm = 1.17537$. [b]Unspiked samples normalized to $^{150}Nd/^{142}Nd = 0.2096$. [c]Reported errors are 2σ of the mean. [d]Weight of dissolved sample.

Table 2. Results for non-radiogenic Nd isotopes.[a]

Sample	ε_{142}	ε_{145}	ε_{146}	ε_{148}
I. Murchison				
#1-ALIQ-2	−0.4±0.4	+0.6±0.7	+0.5±0.7	−0.7±1.1
ALIQ-3	−0.5±0.4	−0.8±0.6	-	−1.0±0.7
#2	−0.2±0.5	+0.5±0.9	-	−0.4±1.6
II. Allende				
ALIQ-2	0.0±0.4	+0.4±0.5	0.0±0.5	+0.5±1.0
ALIQ-2	+0.1±0.6	+0.1±0.5	0.0±0.5	+0.7±0.6
III. Guareña				
	+0.3±0.4	−0.9±0.6	-	−0.3±0.9
IV. Peace River				
ALIQ-2	+0.4±0.4	+0.1±0.7	−0.6±0.7	−0.1±1.0
V. St. Severin				
Light	−0.2±0.4	+0.3±0.5	-	+0.2±1.1
VI. Juvinas				
ALIQ-1	−0.1±0.4	+0.1±0.5	-	+0.1±0.8

[a] ε-values are given as deviations in parts in 10^4 relative to the grand mean of terrestrial normals given in Table 1. Reported errors are 2σ of the mean.

Figure Captions

Fig. 1. Schematic representation of the evolution of $^{143}Nd/^{144}Nd$ with time for chondritic and achondritic parent bodies. Solid objects started to condense from the solar nebula (SN) at time T_C and accreted to parent bodies at time T_A. Subsequent to T_A a part of the parent bodies of achondrites may have differentiated at T_D into crust and depleted mantle. At times T_X subsequent to T_D, melts may be tapped from both depleted mantle (D1) and from previously undifferentiated material (D2).

Fig. 2. Sm-Nd evolution diagram for chondrite samples and Juvinas. A reference line with a slope of 4.6 AE is shown. The dashed lines represent the new values selected for average chondrites (CHUR).

Fig. 3. Histogram showing all available $^{147}Sm/^{144}Nd$ ratios (N = 61) for chondritic meteorites determined by isotope dilution methods. The ratios from previously published REE studies on chondrites (Tanaka and Masuda, 1973; Masuda et al., 1973; Nakamura, 1974; Notsu and Mabuchi, 1975; Schnetzler and Bottino, 1971; Gast et al., 1970; Evensen et al., 1978) are probably accurate to ~2%. Chondritic meteorites show a large range in $^{147}Sm/^{144}Nd$, with most of the data in the range from 0.188 to 0.206. The value selected for average chondrites of 0.1967 is close to the peak of the histogram and is shown by the arrow. The $\varepsilon_{Nd}(0)$ value calculated assuming T_C = 4.6 AE is shown on the top of the figure. It is evident from these data that a total rock isochron for chondrites may be determined.

Fig. 4. Sm-Nd evolution diagram comparing new chondrite data (black dots) and the Juvinas value with previously published data for achondrites. The points labelled L1, L2, and L3 represent three successive versions of the Juvinas total rock value by Lugmair et al. (1975, 1976) and Lugmair and Carlson (1978).

Fig. 5. The $^{143}Nd/^{144}Nd$ value in CHUR is shown as a function of age in the neighborhood of 4.6 AE. If a solid object condensed from the solar nebula at 4.6 AE ago, it would have an initial $^{143}Nd/^{144}Nd$ ratio of 0.505829. Note the shift in $^{143}Nd/^{144}Nd$ for a change in choice of age.

Fig. 6. Fractional deviations in parts in 10^4 of initial $^{143}Nd/^{144}Nd$ of Archean rocks, from evolution in the CHUR reservoir. Data for Stillwater, Great Dyke, Louis Lake batholith, Preissac Lacorne batholith, Fiskenaesset anorthosite, and Amitsoq gneiss from DePaolo and Wasserburg (1976a,b, 1979); Duffer dacite and Uivak gneiss from McCulloch (1979); Rhodesian Greenstones, Lewisian granulite and amphibolite facies gneisses, Onweracht volcanics, and Isua volcanics, from Hamilton et al. (1977, 1978, 1979a,b).

Fig. 7. Hypothetical evolution of $^{143}Nd/^{144}Nd$ for the earth (⊕) and CHUR. DM represents the average $\varepsilon_{Nd}(0)$ value for depleted mantle as determined from mid-ocean ridge basalts, and CC the average $\varepsilon_{Nd}(0)$ value for the continental crust. T_C is the time of condensation and T_A the time of accretion. The figure shows the hypothetical case where the bulk earth gets a 1.7% higher Sm/Nd ratio than that of CHUR during accretion. This results in an $\varepsilon_{Nd}(0)$ value of +2 for the bulk earth today. As discussed in the text if this is the case then it may change our interpretation of data that follow the CHUR curve.

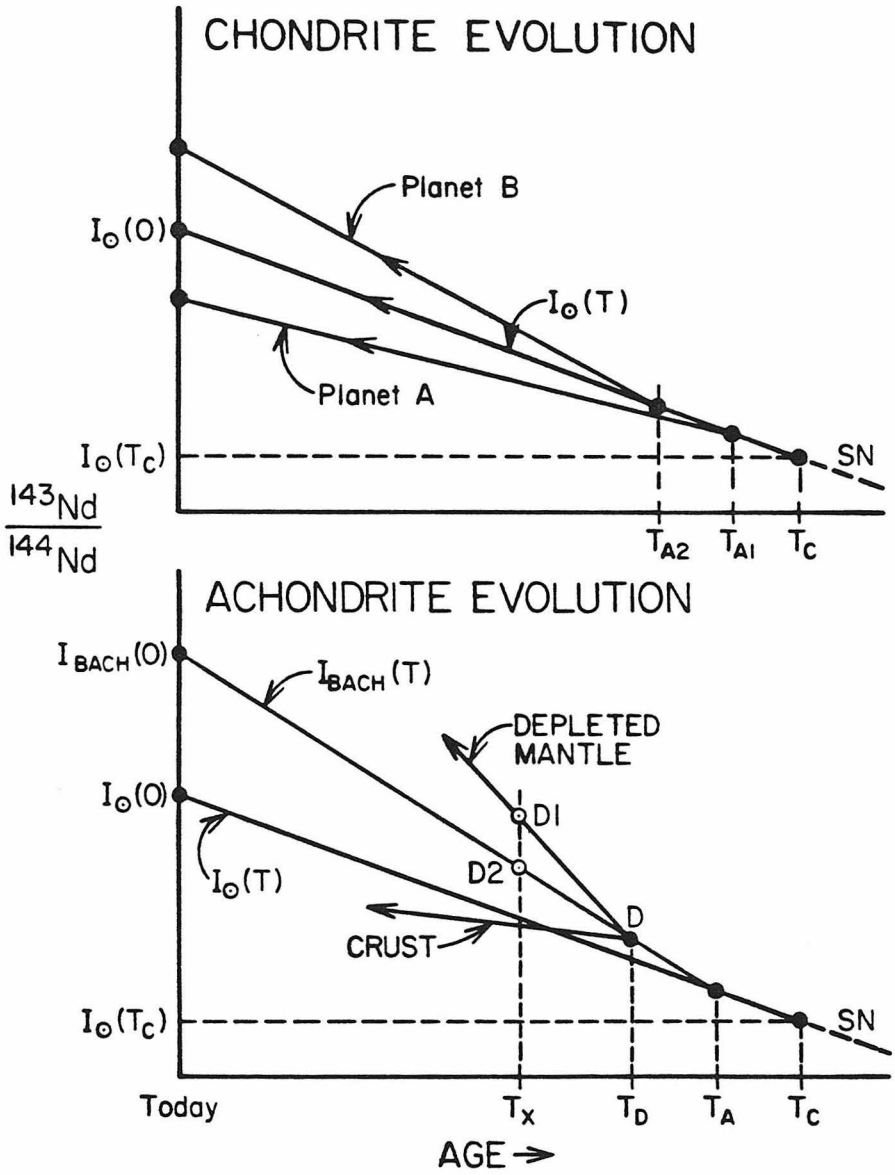
CHONDRITE EVOLUTION
Planet B
$I_\odot(0)$
$I_\odot(T)$
Planet A
$I_\odot(T_C)$
SN
$\frac{143Nd}{144Nd}$
T_{A2}
T_{A1}
T_C
ACHONDRITE EVOLUTION
$I_{BACH}(0)$
$I_{BACH}(T)$
DEPLETED MANTLE
$I_\odot(0)$
D1
D2
$I_\odot(T)$
D
CRUST
$I_\odot(T_C)$
SN
Today
T_X
T_D
T_A
T_C
AGE →

Figure 1

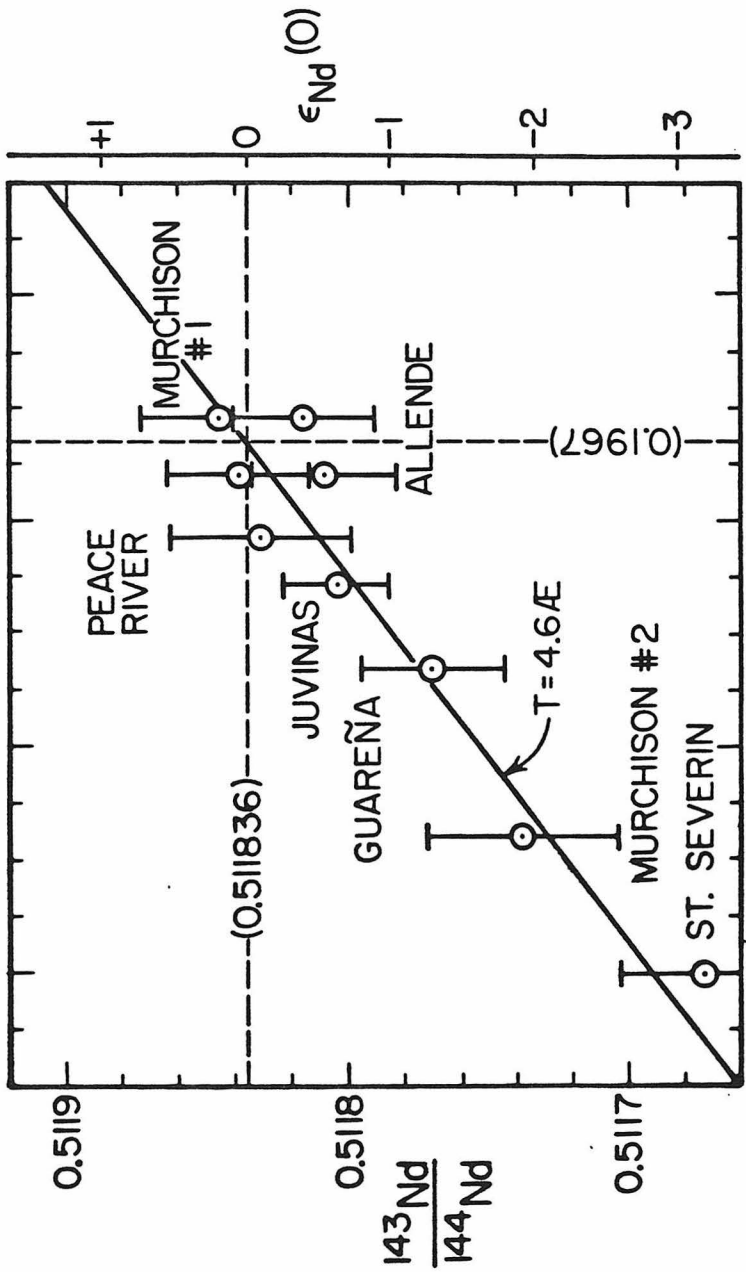
+1
0
-1
-2
-3
$\epsilon_{Nd}(0)$
MURCHISON #1
ALLENDE
PEACE RIVER
JUVINAS
GUAREÑA
T = 4.6Æ
MURCHISON #2
ST. SEVERIN
(0.1967)
(0.511836)
0.5119
0.5118
0.5117
$\frac{143Nd}{144Nd}$
0.192
0.194
0.196
0.198
$\frac{147Sm}{144Nd}$

Figure 2

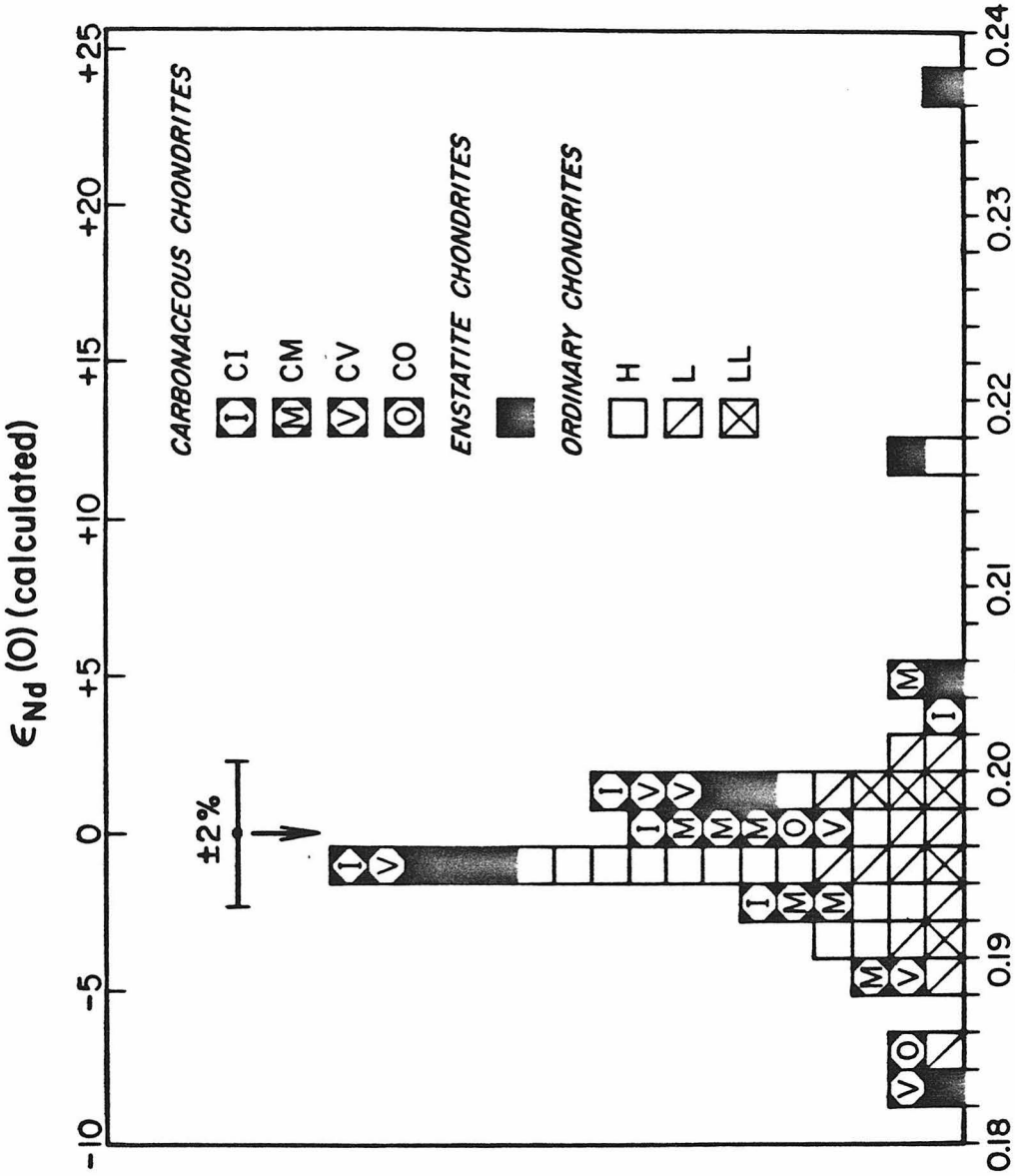
ϵ_{Nd} (0) (calculated)
+25
+20
+15
+10
+5
0
-5
-10
0.24
0.23
0.22
0.21
0.20
0.19
0.18
$^{147}Sm/^{144}Nd$ (measured)
±2%
CARBONACEOUS CHONDRITES
CI
CM
CV
CO
ENSTATITE CHONDRITES
ORDINARY CHONDRITES
H
L
LL

Figure 3

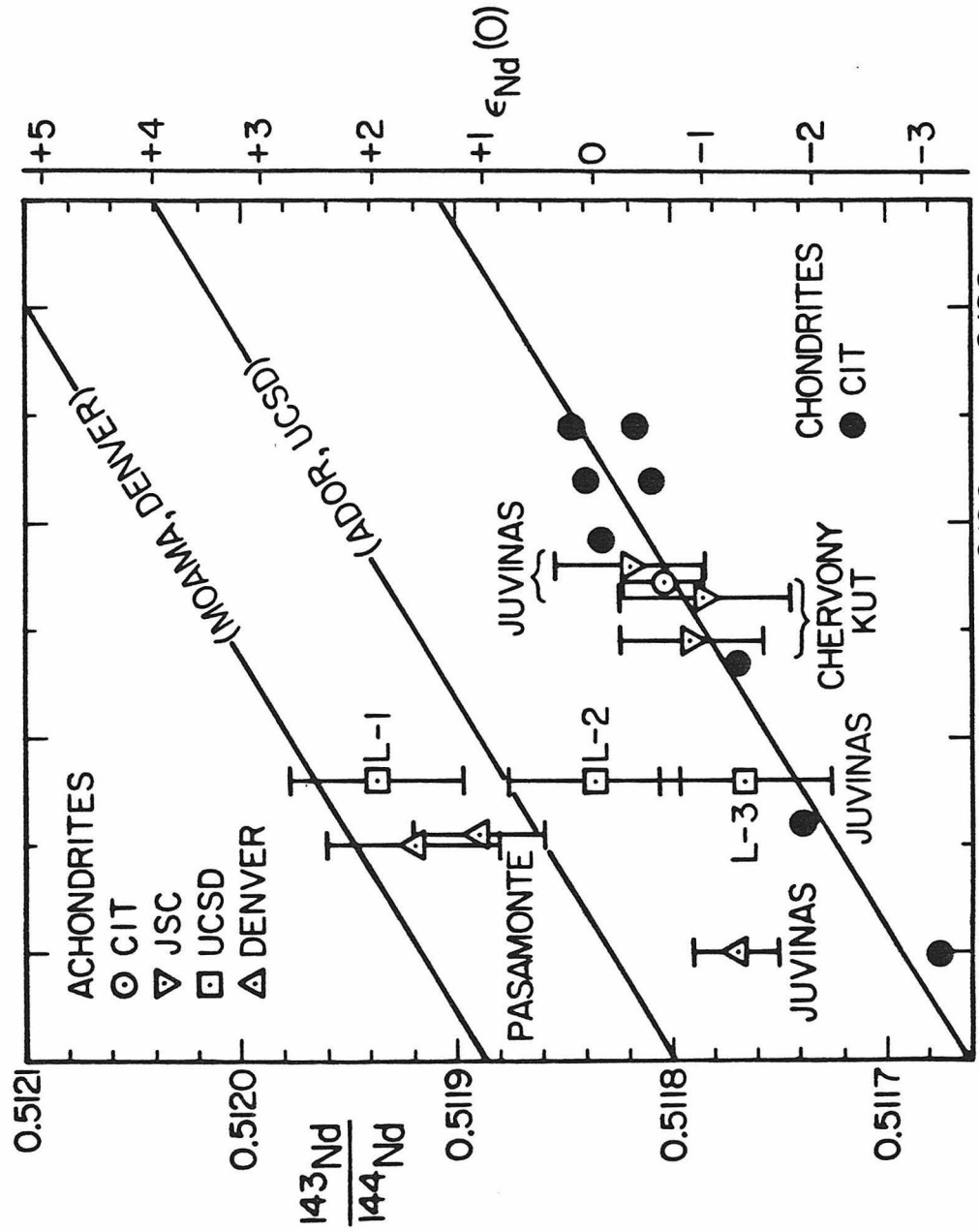
+5
+4
+3
+2
+1
0
-1
-2
-3
$\epsilon_{Nd}(0)$
0.5121
0.5120
0.5119
0.5118
0.5117
$\frac{143Nd}{144Nd}$
0.192
0.194
0.196
0.198
$\frac{147Sm}{144Nd}$
ACHONDRITES
CIT
JSC
UCSD
DENVER
(MOAMA, DENVER)
(ADOR, UCSD)
PASAMONTE
L-1
L-2
L-3
JUVINAS
JUVINAS
JUVINAS
CHERVONY KUT
CHONDRITES
CIT

Figure 4

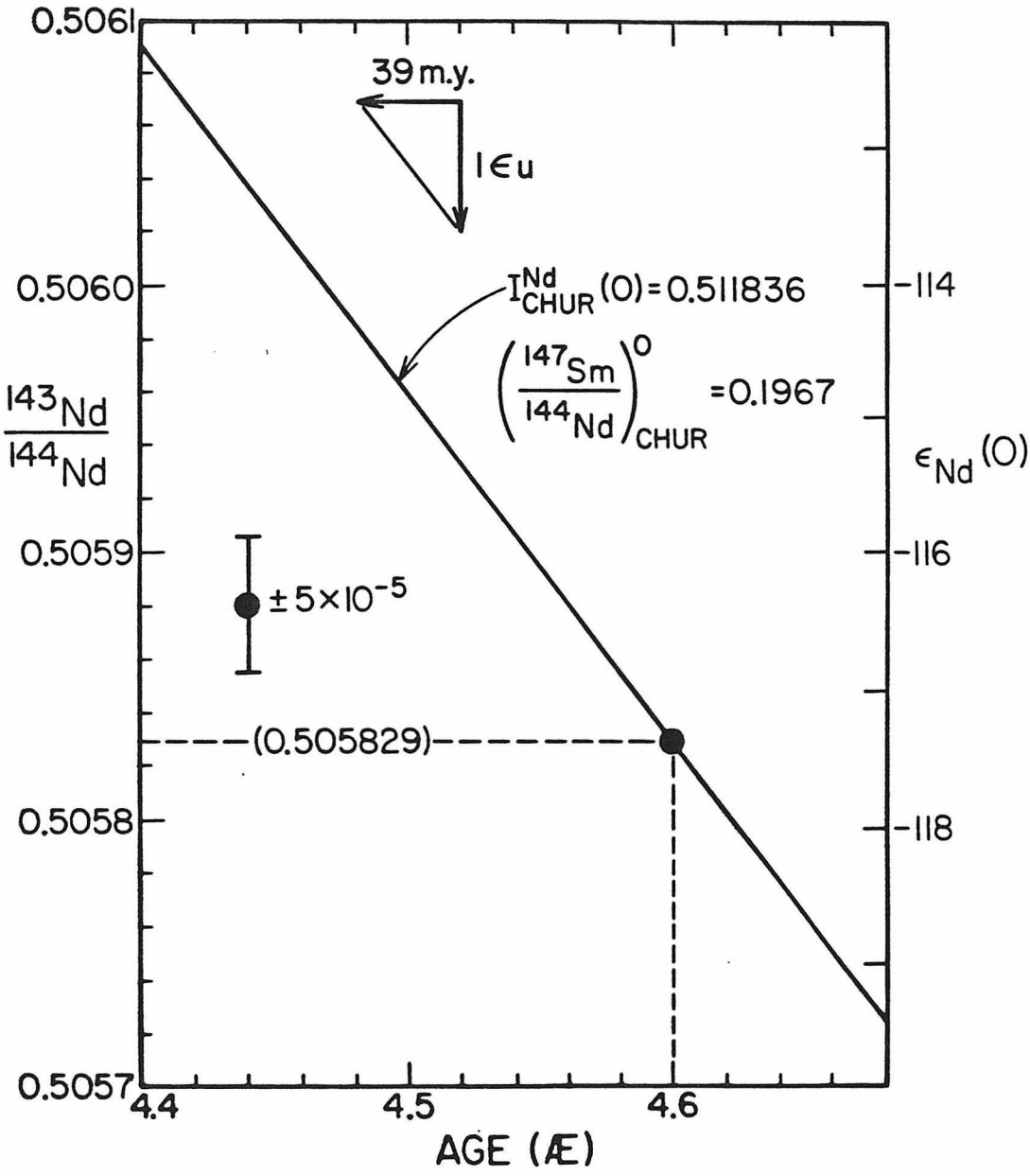
0.5061
0.5060
0.5059
0.5058
0.5057
143Nd/144Nd
39 m.y.
1 εu
I^Nd_CHUR(0) = 0.511836
(147Sm/144Nd)^0_CHUR = 0.1967
±5×10^-5
(0.505829)
114
116
118
εNd(0)
4.4
4.5
4.6
AGE (Æ)

Figure 5

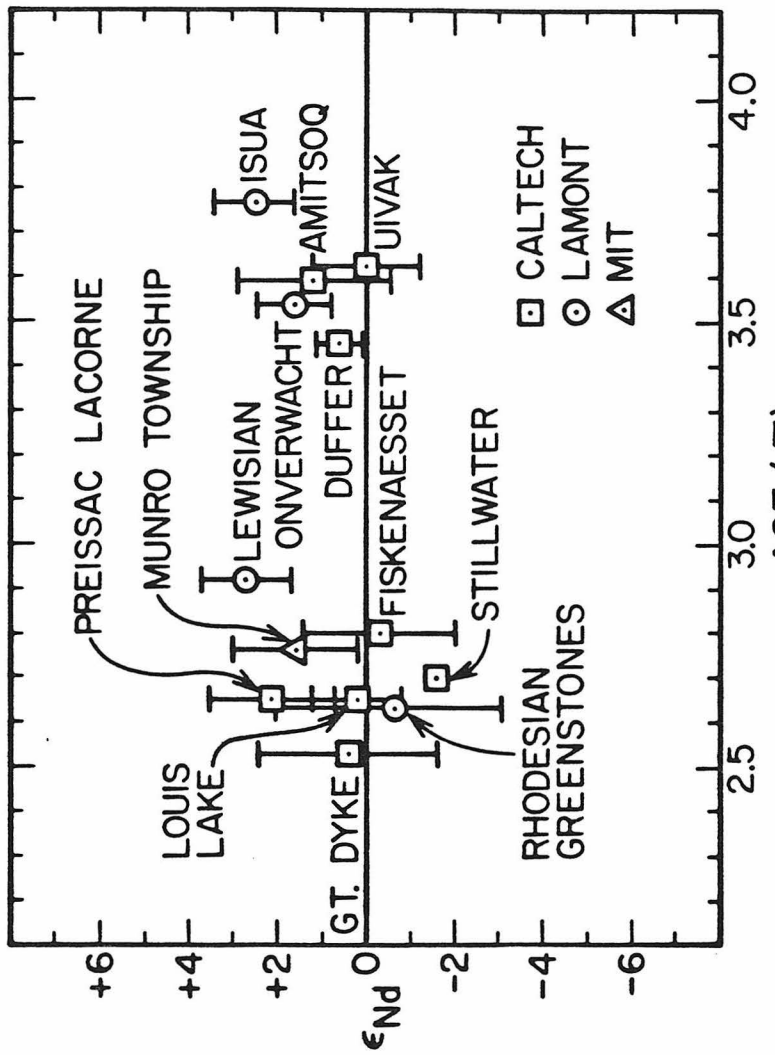
PREISSAC LACORNE
MUNRO TOWNSHIP
LEWISIAN
ONVERWACHT
ISUA
AMITSOQ
UIVAK
DUFFER
FISKENAESSET
STILLWATER
LOUIS LAKE
GT. DYKE
RHODESIAN GREENSTONES
CALTECH
LAMONT
MIT
+6
+4
+2
0
-2
-4
-6
ϵ_{Nd}
2.5
3.0
3.5
4.0
AGE (Æ)

Figure 6

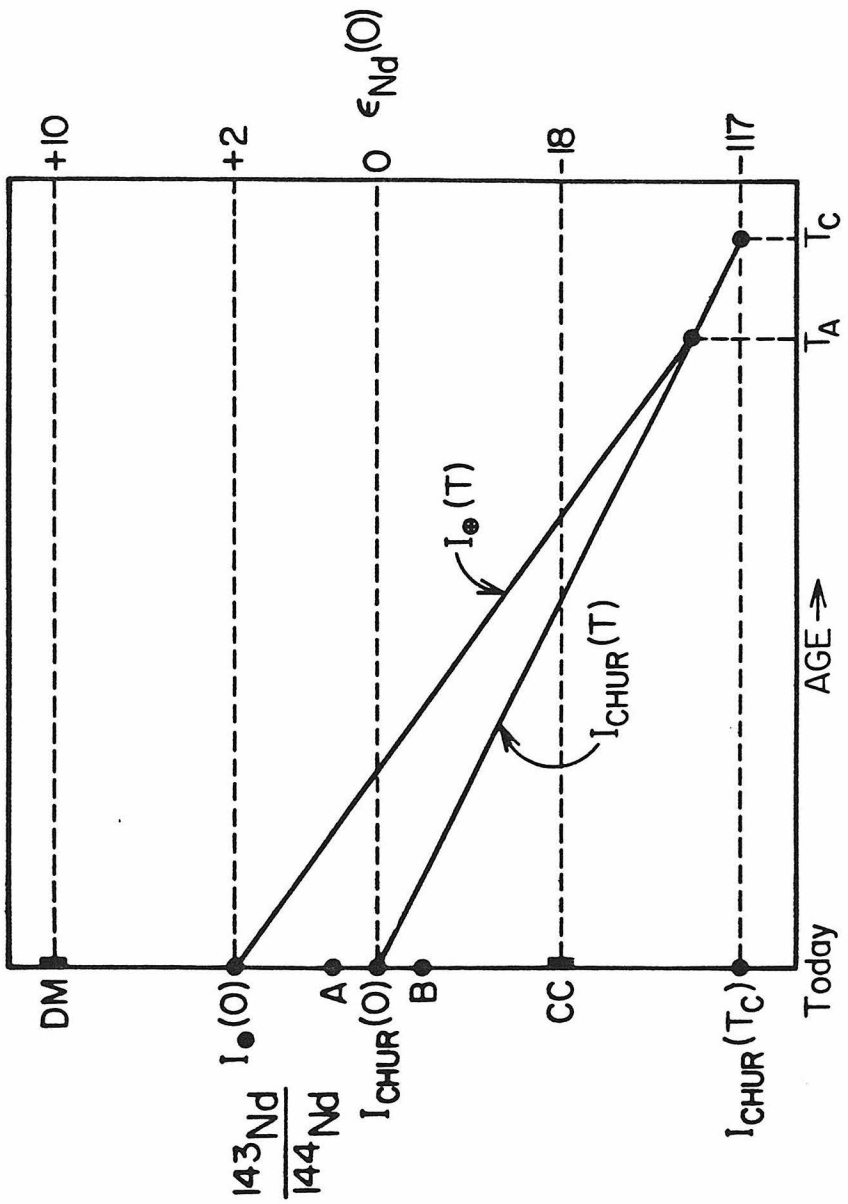
+10
+2
0
-18
-117
$\epsilon_{Nd}(0)$
T_C
T_A
$I_\bullet(T)$
$I_{CHUR}(T)$
AGE →
DM
$I_\bullet(0)$
A
$I_{CHUR}(0)$
B
CC
$I_{CHUR}(T_C)$
Today
$\frac{143Nd}{144Nd}$

Figure 7

APPENDIX 5.

INTERPRETATION OF Nd, Sr AND Pb ISOTOPE DATA FROM ARCHEAN MIGMATITES IN VESTERÅLEN, N. NORWAY

By S. B. Jacobsen and G. J. Wasserburg
The Lunatic Asylum
Division of Geological and Planetary Sciences
California Institute of Technology
Pasadena, California

In this report we discuss constraints on the time of crust formation in Vesterålen, northern Norway, and parent-daughter fractionation of Sm-Nd, Rb-Sr and U-Pb during the subsequent granulite facies metamorphism. The rocks collected at Vikan, Langøy, are heterogeneous migmatitic granulite facies gneisses with granitic neosome grading into tonalitic to dioritic palaeosome. A Rb-Sr whole-rock study by Heier and Compston (1969) demonstrated a complex thermal history with events at ∿ 2.8 b.y. and ∿ 1.8 b.y. Green and others (1972) showed that adjacent amphibolite facies gneisses have REE distribution patterns similar to the granulite facies gneisses, whereas Heier and Thoresen (1971) demonstrated that the granulite facies rocks have been depleted in Rb, U, and Th relative to the amphibolite facies rocks. Taylor (1975) reported a Pb-Pb whole-rock "isochron" age of 3.41 ± 0.07 b.y. and a Rb-Sr whole-rock "isochron" of 2.30 ± 0.15 b.y. with a high initial $^{87}Sr/^{86}Sr$ of 0.7126 for the migmatites at Vikan. He interpreted the Pb-Pb age as the time of migmatite formation and the Rb-Sr age as the time of a granulite facies metamorphism resulting in Rb-depletion and argued that the U-Pb system was not disturbed during granulite facies metamorphism. In an attempt to solve this conflict, we analyzed these rocks for Sm and Nd isotopes because the limited available data indicated that the REE did not fractionate during the granulite facies metamorphism. From previous studies, however (Heier and Compston, 1969; Griffin and others, 1978), it seems firmly established that a period of granulite facies metamorphism took place ∿ 1.8 b.y. ago.

Approach: We assume that the major REE-fractionation for crustal rocks occurs during their derivation from a mantle reservoir. The mantle reservoir used as a reference for the Sm-Nd system (CHUR) has a chondritic Sm/Nd ratio with $(^{147}Sm/^{144}Nd)^{\circ}_{CHUR} = 0.1936$ and $^{143}Nd/^{144}Nd$ ratio of 0.511836 today (De Paolo and Wasserburg, 1976a). The reference reservoir for Rb-Sr (UR) has $(^{87}Rb/^{86}Sr)^{\circ}_{UR} = 0.0839$ and $^{87}Sr/^{86}Sr = 0.7045$ today (De Paolo and Wasserburg, 1976b). These reference reservoirs may be representative of the bulk Earth. Model ages T^{Nd}_{CHUR} and T^{Sr}_{UR} can be calculated relative to these reference reservoirs and date the time in the past at which $^{143}Nd/^{144}Nd$ or $^{87}Sr/^{86}Sr$ ratios in the samples were identical to those in the reference reservoirs CHUR and UR, respectively. All Archean rocks that have been measured so far have initial $^{143}Nd/^{144}Nd$ ratios very close to CHUR (De Paolo and Wasserburg, 1976a, b; Hamilton and others, 1977). Further, McCulloch and Wasserburg (1978) have shown that for Canadian Shield composites $T^{Nd}_{CHUR} \simeq T^{Sr}_{UR}$ for samples ranging in age from ∿ 1.0 to 2.7 b.y.

Results: Sm-Nd and Rb-Sr data on one dioritic and one granitic gneiss sample from Vikan are given in table 1. Their $^{147}Sm/^{144}Nd$ ratios are much lower than chondritic and also lower than the average crustal ratio of 0.11. The T^{Nd}_{CHUR} model ages of both rocks are identical at 2.6 b.y. within analytical error although their Sm/Nd ratios are different by ∿ 20 percent. This suggests that Sm-Nd did not fractionate during the much later granulite facies metamorphism. These model ages provide the best estimate for the time of formation of the protoliths of the migmatites. We will use the more precise model age of the granitic sample ($T^{Nd}_{CHUR} = 2.64 \pm 0.02$ b.y.) in the following model calculations for the Rb-Sr and U-Pb systems.

Taylor (1975) obtained a fairly good linear array of data points in a Rb-Sr evolution diagram for these rocks; some scatter about the best-fit line, however, suggests a disturbed Rb-Sr system. We present two additional analyses from the same locality in table 1. Both of these plot far from Taylor's Rb-Sr isochron. Further, all points plot to the left

of a T_{UR}^{Sr} = 2.64 b.y. reference isochron which suggests Rb-depletion significantly later than the time of formation of the protoliths of the migmatites.

Table 1.--Analytical results and model ages

Rb-Sr	$^{87}Rb/^{86}Sr$	$^{87}Sr/^{86}Sr$	T_{UR}^{Sr} [2]
Dioritic granulite---	0.0368·3	0.70890·8	-7.06·0.18
Granitic granulite---	2.01 ±1	0.79026±6	3.13±0.02

Sm-Nd	$^{147}Sm/^{144}Nd$	$^{143}Nd/^{144}Nd$ [1]	T_{CHUR}^{Nd} [2]
Dioritic granulite---	0.10332±5	0.510316±46	2.55±0.08
Granitic granulite---	0.08602±3	0.509961±16	2.64±0.02

[1]Normalized to $^{146}Nd/^{142}Nd$ = 0.636151.
[2]Decay constants $\lambda(^{147}Sm)$ = 0.00654 x 10^{9} yr^{-1}; $\lambda(^{87}Rb)$ = 0.0139 x 10^{9} yr^{-1}.

Discussion: The Pb-Pb and Rb-Sr data by Taylor (1975) and our Rb-Sr data for the gneisses at Vikan display significant scatter and neither age nor initial Sr or Pb isotopic ratios can be precisely determined from these data. Taylor excluded three data points from the Pb-Pb "isochron" regression analysis and even then the analytical errors of some of the remaining points would have to be expanded by a factor of seven for all the data to fall on the isochron. Although there is no evidence for Rb or U depletion in the amphibolite-facies migmatites, the Rb-Sr data by Heier and Compston (1969) imply that the Rb-Sr whole-rock systems have been significantly disturbed but still indicate an age of ∿ 2.5 b.y. Thus, it seems doubtful that further Rb-Sr and Pb-Pb total rock analyses of either the amphibolite or the granulite facies migmatites will help to define the age of this gneiss complex more precisely.

If we accept the model age obtained from the Sm-Nd data, then the Pb and Sr isotope data can be well explained in terms of a two-stage model with the time of formation of these crustal rocks at T_X = 2.64 b.y. and the time of granulite facies metamorphism at T_M = 1.8 b.y. Choosing α_I = 13.896 and β_I = 14.836 as initial lead from the normal growth curve of Gancarz and Wasserburg (1977)--essentially that of Doe and Stacey (1974)--at 2.64 b.y., we can then calculate a μ_1 value for the time interval from T_X to T_M (stage 1) and a μ_2 value for the time interval T_M to 0 (stage 2). The U/Pb fractionation factor at T_M is then given by $F_{U/Pb}$ = μ_2/μ_1 and from the data of Taylor (1975) we calculate an average $F_{U/Pb}$ ∿ 0.25, which compares well with the average $(U/Pb)_G/(U/Pb)_A$ of ∿ 0.36 (G = granulite facies, A = amphibolite facies) calculated from the U-Pb data of Heier and Thoresen (1971) for these migmatites. Similarly, by using the $^{87}Sr/^{86}Sr$ value in UR at 2.64 b.y. of 0.70136 we can calculate an average Rb-Sr fractionation factor $F_{Rb/Sr}$ = $(Rb/Sr)_2/(Rb/Sr)_1$ at T_M of ∿ 0.46. From the concentration data of Heier and Thoresen (1971) we obtain $(K/Rb)_A/(K/Rb)_G$ ∿ 0.47. It thus appears that both concentration data and isotopic data are well explained by assuming a bulk loss of U and Rb from the granulite facies gneisses. If this two-stage model is approximately correct, then the isotopic data require this loss to have occurred at ∿ 1.8 b.y. This is one of the rare cases where granulite facies metamorphism postdates rock formation by as much as 0.8 b.y.

We further note that the average $F_{U/Pb}$ and $F_{Rb/Sr}$ vary systematically with the mineralogy or major-element composition of the gneisses at Vikan.

	$F_{U/Pb}$	$F_{Rb/Sr}$
Granitic granulites----------	0.15	0.7
Granodioritic-tonalitic granulites----------	0.4	0.25
Dioritic granulites----------	0.5	0.15

Taylor (1975) obtained the apparently erroneous old Pb-Pb age (3.41 b.y.) by forcing his data into a model with a first stage covering the time between the origin of the earth and 3.41 b.y. and a second stage extending from this age to the present. The very low μ-values of the granulite facies gneisses today (mainly in the range ∿ 1 to 3) imply that their Pb isotope composition has changed much less since 1.8 b.y. than in the time interval from 2.64 to 1.8 b.y. when the μ-values averaged ∿13. Thus, the isochron that was produced in the time interval from 2.64 to 1.8 b.y. has mainly been preserved and only been slightly shifted to the right in a α-β diagram.

Our results strongly suggest that total-rock Rb-Sr and Pb-Pb data have to be interpreted with great care for granulite facies gneisses. Complex Rb-Sr and U-Pb systematics displayed by granulite facies gneisses may, however, be resolved by ages obtained with independent methods and can be used to trace U/Pb and Rb/Sr fractionations during high-grade metamorphism. For migmatite complexes T_{CHUR}^{Nd} model ages appear to provide the best time constraints for the formation of the protoliths as the dominating REE-fractionation will be associated with this event rather than with subsequent metamorphic events. If a granulite facies metamorphism occurred long after the time of crust formation, then in general we may expect $T_{UR}^{Sr} > T_{CHUR}^{Nd}$.

We conclude that the interpretation presented by Taylor (1975) for a very ancient crustal component in the Archean terrane of Vesterålen is not valid. Instead this terrane appears to be part of the worldwide crustal-forming event at 2.6 b.y. The possibility that very ancient crustal segments may really be present in other areas of the Fennoscandian Shield must remain the subject of future investigations.

De Paolo, D. J., and Wasserburg, G. J., 1976a, Nd isotopic variations and petrogenetic models: Geophysical Research Letters, v. 3, p. 249-252.

_____ 1976b, Inferences about magma sources and mantle structure from variations of $^{143}Nd/^{144}Nd$: Geophysical Research Letters, v. 3, p. 743-746.

Doe, B. R., and Stacey, J. S., 1974, The application of lead isotopes to the problem of ore genesis and ore prospect evaluation; a review: Economic Geology, v. 69, p. 757-776.

Gancarz, A. J., and Wasserburg, G. J., 1977, Initial Pb of the Amitsoq gneiss, West Greenland, and implications for the age of the earth: Geochimica Cosmochimica Acta, v. 41, p. 1283-1301.

Green, T. H., Brunfelt, A. O., and Heier, K. S., 1972, Rare-earth element distribution and K/Rb ratios in granulites, mangerites and anorthosites, Lofoten-Vesterålen, Norway: Geochimica Cosmochimica Acta, v. 36, p. 241-257.

Griffin, W. L., Taylor, P. N., Hakkinen, J. W., Heier, K. S., Iden, I. K., Krogh, E. J., Malm, O., Olsen, K. I., Ormassen, D. E., and Tveten, E., (in press), Crustal evolution in Lofoten-Vesterålen, Norway; 3500-400 m.y. B.P.: Journal of the Geological Society of London.

Hamilton, P. J., O'Nions, R. K., and Evensen, N. M., 1977, Sm-Nd dating of Archean basic and ultrabasic volcanics: Earth and Planetary Science Letters, v. 36, p. 263-268.

Heier, K. S., and Compston, W., 1969, Interpretation of Rb-Sr age patterns in high-grade metamorphic rocks, North Norway: Norsk Geologisk Tidsskrift, v. 49, p. 257-283.

Heier, K. S. and Thoresen, K., 1971, Geochemistry of high grade metamorphic rocks, Lofoten-Vesterålen, North Norway: Geochimica Cosmochimica Acta, v. 35, p. 89-99.

McCulloch, M. T., and Wasserburg, G. J., (in press), Sm-Nd and Rb-Sr chronology of continental crust formation: Science.

Taylor, P. N., 1975, An early Precambrian age for migmatitic gneisses from Vikan: Bø, Vesterålen, North Norway: Earth and Planetary Science Letters, v. 27, p. 35-42.

APPENDIX 6.

Nd AND Sr ISOTOPIC STUDY OF THE PERMIAN OSLO RIFT

By S. B. Jacobsen and G. J. Wasserburg
The Lunatic Asylum
Division of Geological and Planetary Sciences
Caltech, Pasadena, California 91125

We report measurements of initial $^{143}Nd/^{144}Nd$ and $^{87}Sr/^{86}Sr$ on volcanic and plutonic rocks from the Permian Oslo Rift to evaluate models of magma genesis in this continental riftzone. In addition we report data on the local Precambrian basement in order to decide whether this could be the source for any of the Oslo igneous rocks and to evaluate effects of crustal contamination or mixing with anatectic melts.

A likely source for the magmatic rocks in the rift is a body of dense material extending along the entire length of the Oslo Rift at the base of the crust (Ramberg 1976). While the major part of this lower crustal body may be gabbro, the block probably also includes significant amounts of ultramafic rocks. The presence of a large gabbroic magma chamber would probably also cause significant melting of the lower crust. Ramberg has interpreted this deep crustal magma chamber to be due to the rapid development and rise of a hot asthenospheric diapir and to discharge of basaltic material into the base of a gradually thinned crust.

Previous workers that have studied the variation of initial Sr in the volcanic and plutonic rocks of the Oslo Rift (Heier and Compston, 1969; Sundvoll, 1977) have concluded that these can be explained without postulating any contamination by country rock, and that an observed increase in initial $^{87}Ar/^{86}Sr$ in the more differentiated products can be accounted for by an increase in Rb/Sr ratio with time in a fractionating magma chamber. They further conclude that the magma source is restricted to the upper mantle or the lower crust.

Sm-Nd and Rb-Sr systematics: Initial $^{143}Nd/^{144}Nd$ and $^{87}Sr/^{86}Sr$ of a rock of age T are expressed as fractional deviations in parts in 10^4 from the values in a uniform reference reservoir at time T and denoted ε_{Nd} and ε_{Sr} respectively. The reference reservoir used for Nd (CHUR) has a chondritic Sm/Nd ratio with $(^{147}Sm/^{144}Nd)^0_{CHUR}$ = 0.1936 and $^{143}Nd/^{144}Nd$ = 0.511836 today (DePaolo and Wasserburg, 1976a). The reference reservoir for Sr (UR) has $(^{87}Rb/^{86}Sr)^0_{UR}$ = 0.0839 (Rb/Sr = 0.029) and $^{87}Sr/^{86}Sr$ = 0.7045 today (DePaolo and Wasserburg, 1976b). These reference reservoirs for Nd and Sr are thought to be close approximations to the bulk earth values. A major problem in the interpretation of variations in initial Sr, Pb, and Nd data has been to decide whether

the variations are due to longterm heterogeneities in the mantle sources or to recent mixing of crustal and mantle material. Measurements of young basaltic rocks from oceanic and continental regions have shown that ε_{Nd} and ε_{Sr} are strongly correlated for samples with $\varepsilon_{Sr} < +10$ (DePaolo and Wasserburg, 1976b; O'Nions and others, 1977). This correlation appears to be characteristic of mantle reservoirs and may provide a reference line against which effects due to crust-mantle mixing processes can be evaluated and separated from the variations due to longterm mantle heterogeneity.

Results: Nd isotopic data on twelve Oslo Rift samples are shown in figure 1. All samples have ε_{Nd} lying in the relatively narrow range from -1 to +4. These values are distinct from the bulk of the MOR basalts, ocean island basalts, and island arc rocks but overlap with the bulk of continental flood basalts and fill in the gap between ocean island basalts and continental flood basalts. The Oslo Rift is a mildly alkaline province with sodic alkaline rocks. The ε_{Nd} values are very different from those of potassic alkaline rocks (fig. 1). The ε_{Sr} values on the same samples show a much larger range from -15 to +33. The data plot on both sides of the ε_{Nd} - ε_{Sr} correlation line and show no immediate relation to it. From the ε_{Nd} data we conclude that the source materials of these rocks must have time-integrated REE patterns that range from approximately chondritic to slightly light REE-depleted. The strong light REE-enrichment observed in these alkaline rocks by Neumann and others (1977) must, therefore, result from fractionation during recent magmatic processes. It is clear from the ε_{Nd} data that none of the rocks could have formed by anatexis of either upper or lower continental crustal materials. This includes such felsic rocks as syenite, trachyte, biotite granite, and peralkaline granite.

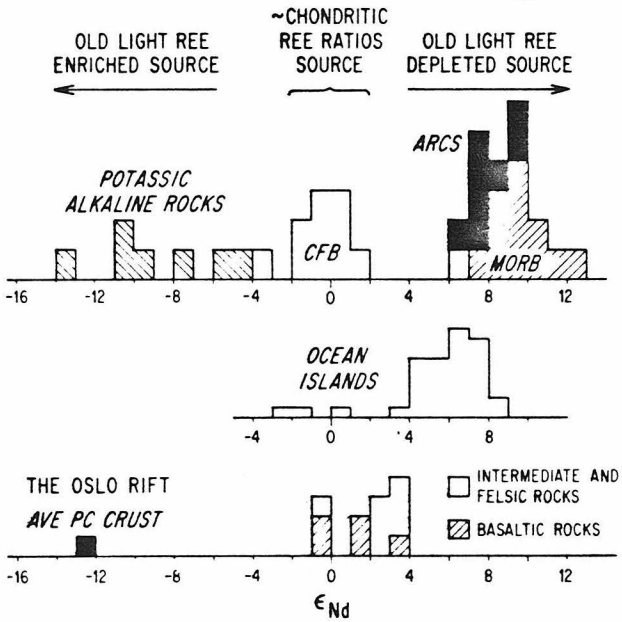

Figure 1.--Histogram of ε_{Nd} values for the igneous rocks in the Oslo Rift compared with histograms of ε_{Nd} values for young basalt samples and inferred REE pattern of their parental reservoirs. Also shown in the ε_{Nd} value measured today of a composite sample of the Precambrian basement in the Oslo Rift. Data on continental flood basalts (CFB), oceanic island basalts, mid-ocean ridge basalts (MORB), island arcs (ARCS) and continental potassic alkaline rocks from DePaolo and Wasserburg (1976a, b, 1977), O'Nions and others (1977), Richard, Shimizu, and Allegre (1976), and Carter and others (1978).

Two samples from the Skien basalt series of ankaramites, nephelinites, and basanites that represent the earliest volcanism in the rift have $\varepsilon_{Nd} = +1.5$ and $\varepsilon_{Sr} \sim -15$. They plot further to the left of the ε_{Nd} - ε_{Sr} correlation line than any other terrestrial rocks that have been measured so far.

One explanation for this may be interaction with old lower crustal materials, as low-SiO_2 magmas seem to have a very strong tendency to interact with the quartz-bearing crustal rocks (Turi and Taylor, 1976). However, this would require an extremely Rb-depleted lower crust with a low Sr/Nd ratio. Alternatively they may have been derived from some special mantle reservoir.

One ankaramite from the subsequent alkali-olivine basalt volcanism further north (Holmestrand basalt series) had $\varepsilon_{Nd} = +3$ and $\varepsilon_{Sr} = +20$. This was followed by tholeiitic volcanism in the northern part of the rift (Kolsås basalt member) and two samples give $\varepsilon_{Nd} = -0.7$ and $\varepsilon_{Sr} \sim +18$. They thus plot on a trend typical for continental tholeiitic flood basalts. This trend extrapolates back to the correlation lines at $\varepsilon_{Nd} \approx 0$ and $\varepsilon_{Sr} \approx 0$ and thus indicates a chondritic source with respect to the REE elements. This trend has been interpreted by DePaolo and Wasserburg (1977) to be due to contamination of tholeiitic magmas to varying degree at shallow levels in the crust.

Intermediate volcanic and plutonic rocks have $\varepsilon_{Nd} \sim +3$ to +4 and $\varepsilon_{Sr} \simeq -8$ to -5 and the felsic members have $\varepsilon_{Nd} \sim +3$ to -1 and $\varepsilon_{Sr} \sim 0$ to +33. They all plot to the right of the ε_{Nd} - ε_{Sr} correlation line and suggest that small amounts of crustal contamination may be important in the genesis of these rocks. The composition of the local Precambrian basement in Permian time was $\varepsilon_{Nd} \sim -10$ and $\varepsilon_{Sr} \sim +160$. The dashed line in figure 2 shows the shape of a mixing curve with the monzonitic magmas and the Precambrian basement as end members. The curve was calculated from the Sr and Nd isotopic compositions and concentrations measured for the end members. Variable contamination could probably in part account for the great variety of differentiation trends observed from major- and

trace-element studies of these rocks (Neumann, 1976; Neumann and others, 1977). If crustal contamination is the reason for the variability in the Sr and Nd isotopic composition for the intermediate and felsic rocks, then the uncontaminated parent magmas must have had $\varepsilon_{Nd} > +4$ and $\varepsilon_{Sr} < -10$.

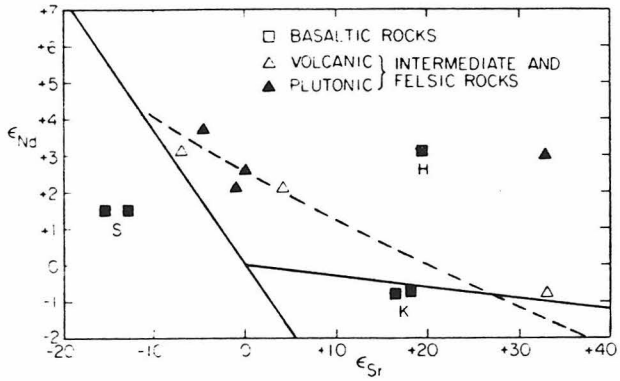

Figure 2.--ε_{Nd} versus ε_{Sr} for rocks from the Oslo Rift. The ε_{Nd} - ε_{Sr} correlation line for young oceanic and continental basalts with $\varepsilon_{Sr} < +10$ is shown. Also shown is a trend with a different slope defined by some continental tholeiitic flood basalts with $\varepsilon_{Sr} > 0$ (DePaolo and Wasserburg, 1977). Dashed curve is a mixing curve with monzonitic magmas and local Precambrian basement as end members. S = nephelinite and ankaramite from the Skien basalt series; H = ankaramite from the Holmestrand basalt series; K = two tholeiite samples from the Kolsås basalt member.

Discussion: The data presented here show that current magma models for this rift zone are oversimplifications. It seems clear that most of the igneous rocks in the Oslo Rift must have been derived from a mantle source with $\varepsilon_{Nd} > +4$. The possibility of crustal contamination makes it difficult to use the isotopic data to put detailed constraints on the mantle sources of these rocks. However, the data suggest that three different sources should be considered: 1) one that is the source of alkali-olivine basalts and intermediate to felsic magmas, 2) one that is the source of nephelinites and ankaramites in the Skien area, and 3) one that is the source of the tholeiitic basalts. The fact that tholeiitic and alkalic rocks alternate in the volcanic series indicates that both tholeiitic and alkalic basaltic magma chambers occurred within the lower crust at the same time. The alkalic magmas are, however, volumetrically the most important.

In this study of ε_{Nd} and ε_{Sr} variations in a continental rift zone, we have attempted to sort out effects due to crustal contamination and thus obtain information about the mantle sources. This was done by using previously established rules for variations of ε_{Nd} and ε_{Sr} in mantle sources. The data base for ε_{Nd} - ε_{Sr} systematics is, however, still small and our understanding of the principles governing these rules is at present inadequate.

Carter, S. R., Evensen, N. M., Hamilton, P. J., and O'Nions, R. K., 1978, Continental volcanics derived from enriched and depleted source regions; Nd- and Sr-isotope evidence: Earth and Planetary Science Letters, v. 37, p. 401-408.

DePaolo, D. J., and Wasserburg, G. J., 1976a, Nd isotopic variations and petrogenetic models: Geophysical Research Letters, v. 3, p. 249-252.

___1976b, Inferences about magma sources and mantle structure from variations of $^{143}Nd/^{144}Nd$: Geophysical Research Letters, v. 3, p. 743-746.

___1977, The sources of island arcs as indicated by Nd and Sr isotope studies: Geophysical Research Letters, v. 4, p. 465-468.

Heier, K. S., and Compston, W., 1969, Rb-Sr isotopic studies of the plutonic rocks of the Oslo Region: Lithos, v. 2, p. 133-145.

Neumann, E. -R., 1976, Compositional relations among pyroxenes, amphiboles and other mafic phases in the Oslo Region plutonic rocks: Lithos, v. 9, p. 85-109.

Neumann, E. -R., Brunfelt, A. O., and Finstad, K. G., 1977, Rare earth elements in some igneous rocks of the Oslo rift, Norway: Lithos, v. 10, p. 311-319.

O'Nions, R. K., Hamilton, P. J., and Evensen, N. M., 1977, Variations in $^{143}Nd/^{144}Nd$ and $^{87}Sr/^{86}Sr$ ratios in oceanic basalts: Earth and Planetary Science Letters, v. 34, p. 13-22.

Ramberg, I. B., 1976, Gravity interpretation of the Oslo Graben and associated igneous rocks: Norges Geologiske Undersokelse, v. 325, p. 1-194.

Richard, P., Shimizu, N., and Allegre, C. J., 1976, $^{143}Nd/^{146}Nd$, a natural tracer; An application to oceanic basalts: Earth and Planetary Science Letters, v. 31, p. 269-278.

Sundvoll, B., 1977, Rb-Sr-relationships in the Oslo igneous rocks: News from the Oslo region research group, v. 6, p. 60.

Turi, B., and Taylor, H. P., 1976, Oxygen isotope studies of potassic volcanic rocks of the Roman province, central Italy: Contributions to Mineralogy and Petrology, v. 55, p. 1-31.

APPENDIX 7.

Stein B. Jacobsen and G. J. Wasserburg, The Lunatic Asylum, Division of Geological and Planetary Sciences, Calif. Inst. Tech., Pasadena, CA.

EARTH DIFFERENTIATION MODELS, THE MEAN AGE OF MANTLE AND CRUSTAL RESERVOIRS.

The evolution of mantle and crustal reservoirs (j) is discussed in terms of two simple transport models for arbitrary rates of crustal growth. In Model I continents (j=3) are derived by melt extraction from undepleted mantle (j=1) and the residue form a depleted mantle (j=2) which today is the source of MORB. In Model II new additions to continents (3) are derived from a mantle (2) which is being depleted through time by partial melting. The transport equations have been solved for stable (s), radioactive (r) and daughter (d) isotopes for arbitrary mass growth curves $M_j(\tau)$. We assume equilibrium partial melting so the enrichment (d_i) of a species i in the melt relative to the source is given by $d_i=[1/(F+D_i(1-F)]$ where F=degree of melting and D_i = bulk distribution coefficient. Let $N_{i,j}$ denote the number of species i in j. The solutions for Model I are

$\varepsilon^*_{d,j}(\tau)=Q^*_d(\tau)[f_j^{r/s}/M_j(\tau)]\int_o^\tau M_j(\xi)\exp[\lambda(\tau-\xi)]d\xi$ where $Q^*_d(\tau)=10^4\lambda\left[\frac{N_{r,1}(\tau)}{N_{d,1}(\tau)}\right]$, $f_3^{r/s}=(d_r/d_s)-1$ and $f_2^{r/s}=(D_r d_r/D_s d_s)-1$. The mean age $\bar{\tau}_{s,j}$ of stable isotopes is equal to the mean age of the mass of j; $\bar{\tau}_{M,j}=\int_o^\tau[M_j(\xi)/M_j(\tau)]d\xi$. For longlived isotopes ($\lambda^{-1}\gg 4.5$ AE) $\varepsilon^*_{d,j}=Q^*_d f_j^{r/s}\bar{\tau}_{M,j}$ where $Q^*_d\simeq$ constant. Knowledge of $\varepsilon^*_{d,j}$ and $f_j^{r/s}$ at a single point in time fixes $\bar{\tau}_{M,j}$. The mean age shows the relationship $(d\bar{\tau}/d\tau)=1-\bar{\tau}(d\ln M/d\tau)$ so if $M_j(\tau)$ is known $\varepsilon^*_{d,j}(\tau)$ is known. For Model II the concentrations are functions of time and we obtain

$\varepsilon^*_{d,2}(\tau)=Q^*_d(\tau)\int_o^\tau f_2^{r/s}(\xi)\exp[\lambda(\tau-\xi)]d\xi=\varepsilon^*_{d,3}(\tau)[f_2^{r/s}(\tau)/f_3^{r/s}(\tau)]$,

$f_2^{r/s}(\tau)=\left[\frac{M_2(\tau)}{M_2(0)}\right]^{(d_r-d_s)}-1=f_3^{r/s}(\tau)\left\{1-\left[\frac{M_2(\tau)}{M_2(0)}\right]^{(-d_s)}\right\}$ and $M_2(\tau)+M_3(\tau)=M_2(0)$.

Define $\bar{\tau}_{r/s}\equiv\int_o^\tau[f_2^{r/s}(\xi)/f_2^{r/s}(\tau)]d\xi$ then for longlived isotopes we have $\varepsilon^*_{d,j}(\tau)=Q^*_d f_j^{r/s}(\tau)\bar{\tau}_{r/s}$ where $\bar{\tau}_{r/s}$ is the time required to generate $\varepsilon^*_{d,j}$ with the present value of $f_j^{r/s}$. Note that $\bar{\tau}_{r/s}$ depends on the parent daughter system and is in general different from $\bar{\tau}_{M,3}$. The difference is given by

$\bar{\tau}_{r/s}-\bar{\tau}_{M,3}\approx\frac{d_r-d_s}{2M_3(\tau)M_2(0)}\int_o^\tau M_3(\xi)[M_3(\tau)-M_3(\xi)]d\xi$ for small $[(d_r-d_s)/M_2(0)]$.

Decay systems with small (d_r-d_s) may be used to estimate $\bar{\tau}_{M,3}$. Available Sm-Nd and Rb-Sr data were used to evaluate these models and yield $\bar{\tau}_{M,3}$ of 1.8 AE for Model I and 1.5 AE for Model II. Both models indicate that the rate of growth of the continents for the last 0.5 AE is much less than the average growth rate. Therefore most of the crust probably formed from 0.5 AE to 3 AE ago. Search for old crustal rocks by direct dating has established a low abundance of $\sim$3.6 AE old crustal rocks and the apparent absence of much older rocks at the surface. An alternative way of looking for old crust is to look at the residue in the mantle after crust formation. The depleted mantle gives a young $\bar{\tau}_{M,3}$ and this implies either that the early crust was destroyed by rapid refluxing into the mantle in the

period from 4.5 AE to 3.6 AE ago or that very little early crust ever formed. Both models show that the continents were only formed from $\sim 30\%$ of the total mantle leaving 70% of the mantle as undepleted. For Model I the trace element concentrations in new additions to the crust is constant and the isotopic values are those of the undepleted mantle in agreement with Nd isotopic studies. The correlation between ε_{Nd} and ε_{Sr} for young basalts can be explained with Model I by mixing of magmas but it cannot in any simple way be explained by Model II. Model II implies that new additions to the continents have the isotopic characteristics of depleted mantle and that the concentration of Rb, U, and Ba in newly added material have changed by a factor of ~ 10 through time for which there is no evidence. The analytical expressions derived permit calculations of simple earth models with great facility without requiring heavy calculations.

Stein B. Jacobsen and G. J. Wasserburg, The Lunatic Asylum, Division of Geological and Planetary Sciences, Calif. Inst. of Tech., Pasadena, CA.

Nd AND Sr ISOTOPIC COMPOSITION OF EARLY PALEOZOIC OCEANIC CRUST AND MANTLE AND THE EVOLUTION OF THE SOURCE OF MID-OCEAN RIDGE BASALTS

Initial Nd, Sr, and Pb isotopic compositions are available on very young ($\sim$0 AE) mid-ocean ridge basalts (MORB) and give information on the isotopic composition of the present-day oceanic mantle. To better understand the time evolution of the source of MORB we have undertaken a study of the initial Nd and Sr isotopic composition of the oldest well preserved ophiolite, the Bay of Islands Complex. Two Sm-Nd internal isochrons for pyroxene-gabbros give well-defined ages of 508±6 m.y. and 501±13 m.y. with identical initial $^{143}Nd/^{144}Nd$ of $\varepsilon_{Nd} = +7.7$ and $\varepsilon_{Nd} = +7.5$. This age agrees with a previously determined U-Pb age (504 m.y.) on zircons from the trondhjemite and shows the usefulness of the Sm-Nd method for dating basic rocks in ophiolites. This time refers to the time of crystallization as a part of the Proto-Atlantic oceanic crust. The time of obduction occurred $\sim$35 m.y. later as indicated by published K-Ar ages. All other total rock samples lie on these isochrons except one two-pyroxene gabbro which gives $\varepsilon_{Nd} = +6.5\pm0.4$. The initial $^{87}Sr/^{86}Sr$ obtained on a pyroxene-gabbro is $\varepsilon_{Sr} = -19.3\pm0.3$. However, the initial $^{87}Sr/^{86}Sr$ within the different phases of the complex is found to be highly variable ($\sim$37 ε-units) and shows the effect of seawater alteration. The isotopic and trace element data demonstrate a clear oceanic affinity of this complex consistent with earlier interpretations made on the basis of structure and geochemistry and suggests that high ε_{Nd}-reservoirs are sources of oceanic crust through the Phanerozoic. The ε_{Nd} values are somewhat smaller (by $\sim$2.5 ε-units) than for typical present-day MORB ($\varepsilon_{Nd} = +10$). This is the shift we would expect for the oceanic mantle (with $f^{Sm/Nd} \approx 0.22$) over the past 0.5 AE in terms of simple mantle evolution models. For a model with a single differentiation event at time T_D to produce the depleted mantle we have at a time T subsequent to T_D that

$$\varepsilon_{Nd}(T) = Q_{Nd}\, f^{Sm/Nd}(T_D - T) \quad ; \quad Q_{Nd} = 24.74\ AE^{-1}$$

$$\varepsilon_{Sr}(T) = Q_{Sr}\, f^{Rb/Sr}(T_D - T) \quad ; \quad Q_{Sr} = 16.70\ AE^{-1}$$

Sm-Nd and Rb-Sr isotopic data for MORB give $(T_D - T) \approx 1.8$ AE at T = 0 AE. Similarly for the Bay of Islands Complex we get $(T_D - T) \approx 1.3$ AE at T = 0.5 AE, so $T_D \approx 1.8$ AE for two points in time. This is similar to proposed differentiation ages from "mantle isochrons." This age is, however, interpreted as the mean age of the MORB source and does not refer to a unique event. The total time for producing this source by a uniform process would be on the order of 2 x 1.8 AE = 3.6 AE. Rapid mixing in the oceanic mantle is indicated for at least the past 1.0 AE. The major distinction between oceanic basalts ($\varepsilon_{Nd} \approx +10$) and continental basalts ($\varepsilon_{Nd} \approx 0$) sources observed in recent rocks is preserved through the Phanerozoic and may be used to identify old obducted oceanic segments on continental blocks.

APPENDIX 9.

THE ISOTOPIC SIGNATURE OF OCEANIC CRUST AND MANTLE AND THE IDENTIFICATION OF MELTS DERIVED FROM SUBDUCTED OCEANIC PLATES

Stein B.Jacobsen and G. J. Wasserburg, The Lunatic Asylum, Division of Geological and Planetary Sciences, Calif. Inst. of Tech., Pasadena, CA

The oceanic mantle has distinctive LIL element patterns and high $f^{Sm/Nd}$ and low $f^{Rb/Sr}$ values. This is the reason for the observed present-day isotopic abundances of $\varepsilon_{Nd} = +10$ and $\varepsilon_{Sr} = -27$ in the oceanic mantle. These values are clearly distinct from the sources of continental crustal materials. The oceanic mantle is residual material left after previous continent forming events and has developed over $\sim$3.6 AE. Newly formed crust at ocean ridges reflects these isotopic characteristics; however, much of the observed elemental fractionation patterns in oceanic crust is due to recent magmatic fractionation. The upper oceanic crust is an important sink for seawater Sr due to hydrothermal alteration at the ocean floor. This gives the upper oceanic crust positive ε_{Sr}-values up to +20. The lower oceanic crust mainly preserves its low ε_{Sr}-values. Because of the very low $f^{Rb/Sr}$ of -0.9, changes in $^{87}Sr/^{86}Sr$ due to decay are insignificant. In contrast, the oceanic crust shows a large range in $f^{Sm/Nd}$ from $\sim$0 to +0.6 so variations in $^{143}Nd/^{144}Nd$ of $\sim$3 ε-units may develop due to decay during plate motion over 200 m.y. but ε_{Nd} is not changed by alteration. This distinctive isotopic signature of oceanic crust and mantle is preserved through the Phanerozoic. Melts derived from subducted oceanic crust must reflect these characteristics, which are very different from the isotopic signature of subducted sediments or old continental crust ($\varepsilon_{Nd} = -10$ to -20; $\varepsilon_{Sr} = +65$ to $+200$). Island arc magmas appear to be dominated by melting of upper oceanic crust. Magmas derived by melting of subducted oceanic plates along continental margin magmatic arcs are emplaced through older continental crust and subducted sediments so we would expect to see blends of these different source materials in the magmas . This is in general agreement with the large range in ε_{Sr}, ε_{Nd} in this type of magma.

APPENDIX 10.

MANTLE-CRUST TRANSPORT MODELS AND THE MEAN AGE OF MANTLE AND CRUSTAL RESERVOIRS

JACOBSEN, Stein B. and WASSERBURG, G. J.; The Lunatic Asylum, Division of Geological and Planetary Sciences, California Institute of Technology, Pasadena, CA 91125

Crustal evolution may be traced by looking at the depleted residue left in the mantle after crust-forming events. Mantle and crust evolution is discussed in terms of two models. In Model I continents (j=3) are derived by melt extraction from undepleted mantle (j=1) and the residue is isolated to form depleted mantle (j=2). In Model II, continents are derived from a mantle (2) which is depleted through time by repeated extraction of melts. Transport equations were solved for stable (s), radioactive (r) and daughter (d) isotopes for arbitrary mass growth curves $M_j(\tau)$. The enrichment factor of a radioactive isotope to a stable isotope relative to that in 1 is callled $f_j^{r/s}$. For longlived isotopes ($\lambda^{-1} \gg 4.5$ AE) for Model I, $\varepsilon^*_{d,j} = Q^*_d \bar{\tau}_{M,j} f_j^{r/s}$ where $\bar{\tau}_{M,j} = \int_o^\tau [M_j(\xi)/M_j(\tau)]d\xi$ is the mean age of the mass of j. In Model II we have $\varepsilon^*_{d,j}(\tau) = Q^*_d f_j^{r/s}(\tau)\bar{\tau}_{r/s}$ where $\bar{\tau}_{r/s} \equiv \int_o^\tau [f_2^{r/s}(\xi)/f_2^{r/s}(\tau)]d\xi$ is different from $\bar{\tau}_{M,3}$. Both Sm-Nd and Rb-Sr data yield $\bar{\tau}_{M,3}$ of 1.8 AE (Model I) and 1.5 AE (Model II). This young $\bar{\tau}_{M,3}$ implies that early crust was destroyed by rapid fluxing into the mantle from 4.5 AE to 3.6 AE ago or that very little early crust ever formed. Both models show that the continents were only formed from ∿30% of the total mantle. For Model I the trace element concentrations in new additions to the crust are constant, whereas in Model II they change markedly for K, Rb, U and Ba. The correlation between ε_{Nd} and ε_{Sr} for young basalts can be explained with Model I by mixing but it cannot be explained simply by Model II. Simple solutions for feedback for crust to the mantle will also be presented.

APPENDIX 11.

Sm-Nd ISOTOPIC SYSTEMATICS OF CHONDRITES. S.B. Jacobsen and G.J. Wasserburg, The Lunatic Asylum, Div. of Geol., Caltech, Pasadena, CA 91125

We present Sm-Nd results for two carbonaceous chondrites (Murchison and Allende), two ordinary chondrites (Peace River and Guareña), and one achondrite (Juvinas). Our purpose is to obtain an estimate of the average "solar" system values for $^{147}Sm/^{144}Nd$ and $^{143}Nd/^{144}Nd$ using chondrite samples. The first serious meteorite measurements were made by Lugmair, et al.[1], who chose a eucrite (Juvinas) which had a $^{147}Sm/^{144}Nd$ isotope ratio close to the average chondritic value and crystallized ~4.5 AE ago. Lugmair, et al.[2] used the Juvinas values as an approximation to chondritic Sm-Nd evolution. No serious attempt has been made yet to measure both $^{143}Nd/^{144}Nd$ and $^{147}Sm/^{144}Nd$ in chondrites. The determination of the solar values depends on whether the solar nebula was initially isotopically homogeneous for the elements of interest and whether we have samples of material which is chemically unfractionated in Sm relative to Nd. The refractory lithophile elements Si, Mg, and Cr show a factor of two fractionation relative to Al in chondritic materials which is most likely due to fractional condensation. The extent to which such processes have fractionated Sm relative to Nd is not known, but must be less than 10% as isotope dilution measurements of REE patterns in chondrites indicate a total range of $^{147}Sm/^{144}Nd$ from 0.188 to 0.206. The averages of the individual chondrite classes C, E, H, L, and LL show a smaller range in $^{147}Sm/^{144}Nd$, from 0.194 to 0.199[3,4,5]. The CI1 chondrites have a special significance as their chemical composition compares very closely with the solar abundances of the condensable elements. They do, however, show a 6% range in $^{147}Sm/^{144}Nd$ (0.192 to 0.204) so a unique value cannot be obtained from these objects. The average values of individual chondrite classes are the same as the less precisely known solar value of $(^{147}Sm/^{144}Nd)_{\odot}$ = 0.195[6]. Much of the variation must be due to sample heterogeneity rather than differences between the parent bodies as different total rock samples of a single meteorite may show a variation comparable to the total range in chondrites. The evolution of chondritic meteorite parent bodies is shown schematically in Fig.1; at time T_C, solid objects condense from the solar nebula (SN). Planet A accretes at time T_{A1} with an Sm/Nd ratio lower than the solar value and Planet B accretes at time T_{A2} with Sm/Nd higher than the solar value. The acronym CHUR ("chondritic uniform reservoir") is used for a bulk planet with $^{147}Sm/^{144}Nd$ and $^{143}Nd/^{144}Nd$ isotopic ratios the same as in average chondrites. The Sm-Nd results were obtained using previously published procedures (Table 1 and Fig.2). All non-radiogenic isotope ratios for Nd were found to lie within ±0.5 ε units of terrestrial and lunar samples measured in this laboratory. There are thus no isotopic anomalies in Nd for bulk chondrites. The data are shown on a Sm-Nd evolution diagram. If all chondrites are isochronous from an isotopically uniform source, they should today lie on a line (slope ~4.6 AE - see ref. line in Fig.2). The present-day range in these chondrites is only 2 ε units in $^{143}Nd/^{144}Nd$ and 2% in $^{147}Sm/^{144}Nd$. A variety of chondrites and the achondrite Juvinas lie within ±0.5 ε units of the reference line shown. This conclusion is insensitive to the particular choice of age in a plausible neighborhood of 4.6 AE. As there is variation in the Sm/Nd ratio between chondrite samples, there is no unique way of picking a set of values for $^{143}Nd/^{144}Nd$ and $^{147}Sm/^{144}Nd$ as representing the true "solar" ratios. Note that the precision

with which the CHUR evolution should be known corresponds to an uncertainty in the $^{147}Sm/^{144}Nd$ ratio for CHUR of $\sim 3‰$. A single set of reference values for $^{143}Nd/^{144}Nd$ and $^{147}Sm/^{144}Nd$ today must be consistent with the data array in Fig.2. The approach used here will be to define the present-day "solar" reference values. We have chosen the modern value $I^{Nd}_{CHUR}(0) = 0.511836$ for $^{143}Nd/^{144}Nd$, which is the currently used value for CHUR from the revised data of Lugmair, et al.[7]. The corresponding self-consistent $^{147}Sm/^{144}Nd$ ratio on the reference isochron is 0.1967, and is very close to the average values for chondrites discussed earlier. The $^{147}Sm/^{144}Nd$ chosen here is 1.6% higher than that of Lugmair, et al.[7]. This yields an initial $I^{Nd}_{CHUR}(T_C)$ at 4.6 AE which is 1.8 ε units below the earlier data and will consequently change the growth curve and model ages. Based on the data reported here and the extensive tracer calibrations carried out in this laboratory, we believe that the new values given here are sufficiently reliable to justify their use and may be used as the basis for calculating the CHUR curve. Previously published data on achondrites that fall in the neighborhood of our new data on chondrites and Juvinas are shown (Fig. 3). The Juvinas data of Lugmair [1,2](L1) is about 3.8 ε units above our reference line. A revised value (L2) with the same Sm/Nd ratio was reported by Lugmair, et al.[7] and is 1.9 ε units above our reference line. Recently Lugmair and Carlson [8] reported a 1.4 ε unit reduction in their measured $^{143}Nd/^{144}Nd$ for their laboratory standard. They chose, however, to correct their new data to be compatible with their previously published data. Their current Juvinas value (L3) as measured is 1.4 ε unit lower and as shown in Fig.3, this value is within error of our data array for chondrites. The values obtained by Nakamura, et al.[9] for Juvinas plot distinctly above our data array. Recently Nyquist, et al.[10] published data on Juvinas which agree with the $^{143}Nd/^{144}Nd$ of L3 by Lugmair and the value by Nakamura, et al.[9] but with a significantly higher $^{147}Sm/^{144}Nd$ ratio. Data on Juvinas by Nyquist, et al.[10] and the data obtained independently by us agree to within 1‰ for $^{147}Sm/^{144}Nd$ and 0.3 ε units for $^{143}Nd/^{144}Nd$. It would appear that the $^{143}Nd/^{144}Nd$ of Nakamura, et al.[9] and the revised data (L3) of Lugmair and Carlson [8] are consistent with the $^{143}Nd/^{144}Nd$ obtained by Nyquist, et al.[10] and by us, but their $^{147}Sm/^{144}Nd$ ratios are significantly lower and suggest an error in tracer calibrations by these workers. The data for Pasamonte [11] and the isochrons of Moama [12], and ADOR [13] also lie significantly above our reference line (Fig.3). It is clear that there is either major Sm/Nd fractionation in achondrite parent bodies in the very early solar system or that the isotopic data or Sm/Nd ratios of the USGS and UCSD laboratories are subject to some errors. The actual cause of these discrepancies must be resolved before one may safely use data from different laboratories. Although the initial Nd and age of chondrites are not sufficiently well known, we may in principle pick any set of self-consistent initial $^{143}Nd/^{144}Nd$ ratio, age, and $^{147}Sm/^{144}Nd$ ratio that plot on the CHUR curve as reference values to describe the CHUR evolution curve instead of the present-day values we are using. We may pick the values as $T_C = 4.6$ AE and $I^{Nd}_{\odot}(T_C) = 0.505829$ which are compatible with the new CHUR curve. There is no a priori basis for assuming that the bulk moon precisely follows the CHUR evolution curve. We have no young samples from the moon so it is difficult to get a good time-integrated $^{147}Sm/^{144}Nd$ value for the moon. In addition, there is clear

evidence of early lunar differentiation which resulted in large Sm/Nd fractionation in lunar magmas [14]. Assuming that CHUR is representative of lunar Sm-Nd evolution, we may calculate T^{Nd}_{CHUR} model ages relative to the CHUR evolution curve. Lunar highland rocks have $f^{Sm/Nd} \approx -0.1$ and for such samples, it is not possible to determine precise T^{Nd}_{CHUR} model ages as they will be very sensitive to analytical uncertainties and to small shifts in the CHUR evolution line [15]. The new CHUR values changes the T^{Nd}_{CHUR} model ages of Oberli, et al. [15] to ~0.5 AE younger values thus being more in agreement with Rb-Sr and U-Pb data on the same samples. The revised CHUR evolution curve reported here does not alter the basic conclusion of other workers that a variety of terrestrial crustal rocks follow the evolution of a reservoir with a chondritic Sm/Nd ratio. However, the ~3.8 AE old Isua volcanics [16] now plot distinctly above the CHUR curve by 2.5±1.0 ε units. Such a shift implies that the source of the Isua volcanics was residual mantle material that was involved in crust-forming events at least 4.2 AE ago. For typical continental crustal rocks with $f^{Sm/Nd} \approx -0.4$, the new model parameters will only cause small changes in previously published T^{Nd}_{CHUR} model ages.

REF.: 1.EPSL 27(1975)79; 2.Proc. 6th(1975)1419; 3.GCA 37(1973)239; 4.GCA 38 (1974)757; 5.GCA 42(1978)1199; 6.Science 191(1976)1223; 7.Proc. 7th(1976)2009; 8.Proc. 9th(1978)689; 9.Proc. 7th(1976)2309; 10.Proc. 10th(1979); 11.EPSL 37 (1977)1; 12.Proc. 9th(1978)1115; 13.EPSL 35(1977)273; 14.Proc. 8th(1977)1639; 15.Lunar Sci. IX(1978)832; 16.Nature 272(1978)41. Div.Contrib.No.3387(341).

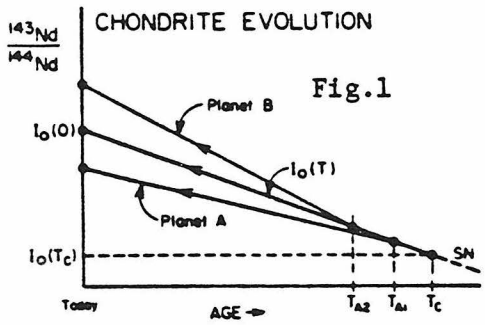

Fig.1

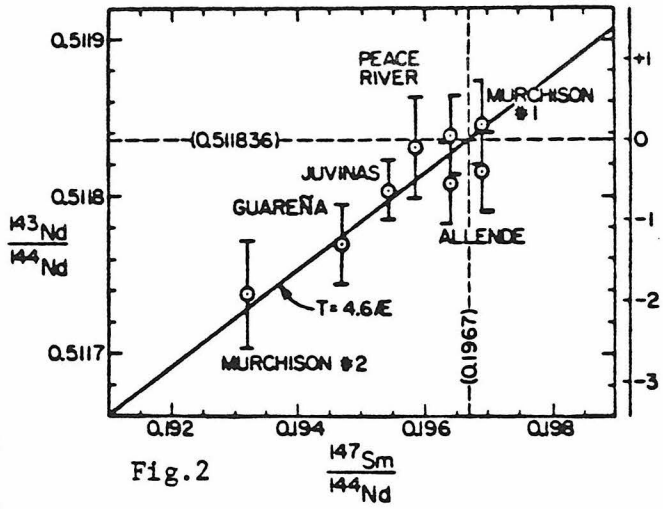

Fig.2

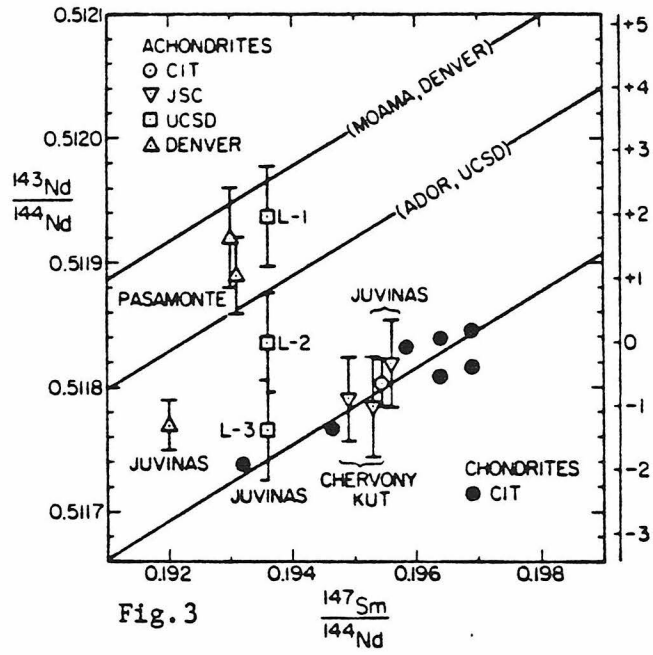

Fig.3

Table 1. Sm-Nd isotopic results.

Sample	$\frac{147Sm}{144Nd}$	$\frac{143Nd}{144Nd}$
Murchison #1	0.19693	0.511845±29
	0.19691	0.511816±25
Murchison #2	0.19320	0.511738±34
Allende	0.19639	0.511802±26
	-	0.511839±25
Peace River	0.19584	0.511831±32
Guareña	0.19468	0.511769±24
Juvinas	0.19543	0.511804±19

Data normalized to $^{150}Nd/^{142}Nd$ = 0.2096. Errors are 2σ of the mean. The uncertainty in the $^{147}Sm/^{144}Nd$ ratio is 0.05%.

Fig.1. Schematic representation of the evolution of $^{143}Nd/^{144}Nd$ with time for chondrite parent bodies. Solid objects began to condense from the solar nebula (SN) at time T_C and accreted to parent bodies at time T_A and T_{A2}.

Fig.2. Sm-Nd evolution diagram for chondrite samples and Juvinas. A reference line with a slope of 4.6 AE is shown. The dashed lines represent the new present day values selected for average chondrites (CHUR). The $\varepsilon_{Nd}(0)$ values are given on the right side of the diagram.

Fig.3. Sm-Nd evolution diagram comparing our new chondrite data (black dots) with our new Juvinas value and previous data for achondrites. The points labelled L1, L2, L3 represent three successive revisions of the Juvinas total rock value by Lugmair, et al. [1,7,8]. The $\varepsilon_{Nd}(0)$ values are given on the right side of the diagram.